NASA TECHNICAL MEMORANDUM

NASA TM X-2815

C.2

NASA TM X-2815

EFFECTS OF SIMULATED DAMAGE ON STABILITY AND CONTROL CHARACTERISTICS OF A FIXED-WING TWIN-VERTICAL-TAIL FIGHTER MODEL AT MACH NUMBERS FROM 2.50 TO 4.63

by Milton Lamb

Langley Research Center
Hampton, Va. 23665

NATIONAL AERONAUTICS AND SPACE ADMINISTRATION • WASHINGTON, D. C. • NOVEMBER 1973

1. Report No.	2. Government Accession No.	3. Recipient's Catalog No.
NASA TM X-2815		

4. Title and Subtitle	5. Report Date
EFFECTS OF SIMULATED DAMAGE ON STABILITY AND CONTROL CHARACTERISTICS OF A FIXED-WING TWIN-VERTICAL-TAIL FIGHTER MODEL AT MACH NUMBERS FROM 2.50 TO 4.63 (U)	November 1973
	6. Performing Organization Code
7. Author(s)	8. Performing Organization Report No.
Milton Lamb	L-8989
	10. Work Unit No.
9. Performing Organization Name and Address	760-65-03-01
NASA Langley Research Center Hampton, Va. 23665	11. Contract or Grant No.
	13. Type of Report and Period Covered
12. Sponsoring Agency Name and Address	Technical Memorandum
National Aeronautics and Space Administration Washington, D.C. 20546	14. Sponsoring Agency Code

15. Supplementary Notes

16. Abstract

An experimental investigation has been conducted in the high Mach number test section of the Langley Unitary Plan wind tunnel over the Mach number range from 2.50 to 4.63 to determine the effect of simulated damage on the longitudinal and lateral aerodynamic characteristics of a fixed-wing twin-inlet fighter model having an aft horizontal tail and twin vertical tails. Damage was simulated on the wing, horizontal tail, and one of the vertical tails. The results are presented in figure form.

17. Key Words (Suggested by Author(s))	18. Distribution Statement
Effects of simulated damage Fixed-wing twin-vertical-tail fighter model	Confi[redacted] Agencies and [redacted] Only

19. Security Classif. (of this report)	20. Security Classif. (of this page)	21. No. of Pages	22. Price
Confidential	Unclassified	125	

"NATIONAL SECURITY INFORMATION"

Unauthorized Disclosure Subject to Criminal Sanctions.

CONFIDENTIAL CLASSIFIED
BY Henry A. Fedziuk
Security Classification Officer, NASA LaRC
SUBJECT TO GENERAL DECLASSIFICATION SCHEDULE OF EXECUTIVE ORDER 11652 AUTOMATICALLY DOWNGRADED AT TWO YEAR INTERVALS AND DECLASSIFIED ON DEC 31 1979

EFFECTS OF SIMULATED DAMAGE ON STABILITY AND CONTROL CHARACTERISTICS OF A FIXED-WING TWIN-VERTICAL-TAIL FIGHTER MODEL AT MACH NUMBERS FROM 2.50 TO 4.63*

By Milton Lamb
Langley Research Center

SUMMARY

An experimental investigation has been conducted in the high Mach number test section of the Langley Unitary Plan wind tunnel over the Mach number range from 2.50 to 4.63 to determine the effect of simulated damage on the longitudinal and lateral aerodynamic characteristics of a fixed-wing twin-inlet fighter model having an aft horizontal tail and twin vertical tails. Damage was simulated on the wing, horizontal tail, and one of the vertical tails.

The results showed that for the reference moment center used, the model remained longitudinally stable for all the damaged configurations tested. The horizontal tail remained an effective trim device and generally was capable of providing some degree of trim in pitch and roll. The rudder was effective in providing some degree of trim in yaw and roll for cases of damage to the wing or horizontal tail. The loss of the right vertical tail generally caused the model to become directionally unstable.

INTRODUCTION

As an aid in assessing the aerodynamic effects of battle damage that might be sustained by military airplanes, several wind-tunnel investigations (refs. 1 to 4) have been performed at the Langley Research Center in which damage was simulated with models by the removal of all or parts of the wing, the horizontal tail, and the vertical tail. In addition to the static aerodynamic coefficients in the supersonic speed range, some limited control effectiveness data have also been obtained. These investigations are limited to the effects of damage on static aerodynamic characteristics over a limited angle-of-attack and angle-of-sideslip range with no attempt made to trim the models about all three axes simultaneously. The investigations have a twofold purpose: (1) to serve as an aid in determining the "kill" probability for enemy airplanes and (2) to serve as an aid

*Title, Unclassified.

in determining the extent of damage that might be sustained and still allow an airplane and/or pilot to return to friendly territory or to complete a mission.

As part of these continuing investigations, tests have been made to determine the effects of simulated damage on the stability and control characteristics of a fixed-wing twin-inlet fighter model with twin vertical tails and a conventional aft horizontal tail, and the results are presented herein. Damage was simulated on the wing, horizontal tail, and one of the vertical tails. Control effectiveness data were obtained for the horizontal tail and rudder. The aerodynamic characteristics of the undamaged configuration can be found in references 5 to 7.

The tests were conducted in the high Mach number test section of the Langley Unitary Plan wind tunnel. The Mach number range was from 2.50 to 4.63. The angle-of-attack range was from about -5° to 22°, and the angle-of-sideslip range was from about -4° to 8°.

SYMBOLS

The moment reference center is located on the body axis 58.70 cm rearward of the nose of the model (21 percent $\bar{c}$). Measurements were taken in U.S. Customary Units and are given in the International System of Units. All data were reduced to coefficient form by using the reference wing area, reference wing span, and reference wing chord. (See table I.) Longitudinal characteristics are presented about the stability-axis system, and lateral-directional characteristics are presented about the body-axis system. The symbols are defined as follows:

A	aspect ratio
b	reference wing span
C_D	drag coefficient, $\frac{\text{Drag}}{qS}$
C_L	lift coefficient, $\frac{\text{Lift}}{qS}$
C_l	rolling-moment coefficient, $\frac{\text{Rolling moment}}{qSb}$
C_{l_β}	effective dihedral parameter, $\left(\frac{\Delta C_l}{\Delta \beta}\right)_{\beta=0^{\circ},3^{\circ}}$, per deg
C_m	pitching-moment coefficient, $\frac{\text{Pitching moment}}{qS\bar{c}}$

C_n yawing-moment coefficient, $\frac{\text{Yawing moment}}{qSb}$

C_{n_β} directional stability parameter, $\left(\frac{\Delta C_n}{\Delta \beta}\right)_{\beta=0^o,3^o}$, per deg

C_Y side-force coefficient, $\frac{\text{Side force}}{qS}$

C_{Y_β} side-force parameter, $\left(\frac{\Delta C_Y}{\Delta \beta}\right)_{\beta=0^o,3^o}$, per deg

$\bar{c}$ reference wing chord

c_r root chord

c_t tip chord

L/D lift-drag ratio

M free-stream Mach number

q free-stream dynamic pressure

R free-stream Reynolds number

S reference area of wing including fuselage intercept

α angle of attack, deg

β angle of sideslip, deg

δ_h deflection of horizontal tail (positive when trailing edge is down), deg

δ_r rudder deflection (positive when trailing edge is left), deg

Γ dihedral angle, deg

Λ leading-edge sweep angle, deg

Model components:

V vertical tail

W wing

APPARATUS AND METHODS

Model

A three-view drawing of the basic model is shown in figure 1, and some geometric characteristics are given in table I. The wing planform incorporated a slight break in the leading-edge sweep angle, with $\Lambda = 42^{\circ}$ on the inner panel and $\Lambda = 38^{\circ}$ on the outer panel. The wing had 4.167° of negative dihedral. The wing sections, horizontal-tail sections, and vertical-tail sections were 4-percent-thick circular arcs symmetrical about their respective chord plane. The ventral fins were made from a 0.478-cm-thick flat plate with a 20° bevel-edge angle. Provisions were made for airflow through the model, and a canopy was simulated.

Damage was simulated by removing approximately 50 percent of the exposed right-hand wing panel, the right-hand horizontal-tail panel, and the right-hand vertical tail. The damaged areas are indicated by the hatched portions in figure 1.

Tests

The tests were conducted in the high Mach number test section of the Langley Unitary Plan wind tunnel, described in reference 8. This variable-pressure, continuous-flow tunnel has an asymmetrical sliding-block nozzle that permits a continuous variation in test-section Mach number from 2.30 to 4.65.

The present tests were made over the Mach number range from 2.50 to 4.63. The Reynolds number was 9.84×10^6 per meter except for the higher angles of attack and sideslip data for Mach numbers of 2.50 and 2.86, where the Reynolds number was reduced to 6.56×10^6 per meter in order to reduce balance loads. Test conditions are given in the following table:

Mach number	Stagnation temperature, K	Stagnation pressure, kN/m^2, for –	
		$R = 9.84 \times 10^6$	$R = 6.56 \times 10^6$
2.50	339	122	81
2.86	339	148	98
3.95	353	277	---
4.63	353	379	---

The dewpoint was maintained sufficiently low to prevent measurable condensation effects in the test section. For these tests, the angle-of-attack range was approximately -5° to 22°, and the angle-of-sideslip range was approximately -4° to 8°. In order to insure boundary-layer transition to turbulent conditions, a transition strip composed of No. 40 grit was placed on the body 3.05 cm aft of the nose. The transition trips for the wings and tails were composed of No. 45 grit in 0.16-cm-wide strips placed 1.02 cm rearward of the leading edges (measured streamwise).

Measurements and Corrections

Aerodynamic forces and moments on the model were measured by means of a six-component strain-gage balance that was housed within the model. The balance was attached to a sting which was rigidly fastened to the tunnel support system. The balance-chamber pressures were measured with pressure tubes located in the vicinity of the balance.

The angles of attack were corrected for deflection of the balance and sting under load. The drag data were adjusted to correspond to free-stream static pressures at the model base by applying corrections for the balance-chamber pressure and for base-pressure values from previous tests. In addition, corrections were made for the internal-flow momentum loss. The internal-flow measurements shown in reference 5 were applied, with the measurements at a Mach number of 3.75 being used for Mach numbers of 3.95 and 4.63.

PRESENTATION OF RESULTS

The data are presented in the following figures:

DISCUSSION

The longitudinal aerodynamic characteristics for the asymmetric wing condition with various control deflections are shown in figures 2 to 4. These figures show that the loss of 50 percent of the exposed right wing results in measurable reductions in static stability level and lift-curve slope and slight reductions in zero-lift drag. However, for the reference moment center used, the model remains longitudinally stable over the entire test Mach number range, with the possible exception of Mach number 4.63 where a tendency toward neutral stability is indicated. Deflection of the horizontal tail to -20^o (fig. 2) provides sufficient tail effectiveness to sustain level flight (i.e., $C_L \approx 0.075$ for $M = 2.86$, a wing loading of 3352 N/m^2, and an altitude of 19.8 km) with 50 percent of the right wing removed. The deflection of the horizontal tail to -20^o has a destabilizing effect, as shown in figures 2(c) and (d). A comparison of figure 2 with the data of reference 7 indicates that the longitudinal control effectiveness of the tail is essentially the same for the damaged and undamaged wing configurations. As might be expected, rudder deflection (fig. 3) has little effect on the longitudinal characteristics. The differential horizontal-tail settings (fig. 4) used as roll control had little effect on the longitudinal characteristics other than a slight trim change and a small increase in drag.

Loss of the right horizontal tail (fig. 5) results in reductions in static stability level and lift-curve slope with slight reductions in zero-lift drag. The reduction in stability

level is essentially the same as that for the loss of 50 percent of the exposed right wing. The deflection of the left horizontal tail to -20° provides enough tail effectiveness to sustain level flight with the right horizontal-tail panel completely removed. The longitudinal aerodynamic characteristics for an asymmetric vertical-tail condition are shown in figure 6.

The variation of lateral aerodynamic characteristics with angle of attack for an asymmetric wing condition with various control deflections is shown in figures 7 to 9. Removal of 50 percent of the exposed right wing causes substantial increases in positive rolling moment with increasing angle of attack (fig. 7). The deflection of the horizontal tail has little effect on the lateral characteristics of the damaged wing configuration. The deflection of the rudder (fig. 8) provides essentially constant effectiveness in producing yawing moment and rolling moment over the angle-of-attack range, with the effectiveness decreasing with increasing Mach number. A comparison of figure 8 with the rudder data of reference 7 shows that the effectiveness of the rudder is about the same for the damaged and undamaged wing configurations. The differential horizontal-tail settings (fig. 9) used for roll control produce positive increments in rolling moment which are relatively constant over the angle-of-attack range for each test Mach number. The differential tail produces small negative increments in yawing moment, which deteriorate with angle of attack.

The lateral characteristics with angle of attack for the asymmetric horizontal-tail condition are shown in figure 10. Deflection of the left horizontal tail to -20° provides substantial negative increments in yawing moment and rolling moment that are essentially constant over the angle-of-attack range at each Mach number.

The lateral characteristics with angle of attack for an asymmetric vertical-tail condition are shown in figure 11. Loss of the right vertical tail causes a negative yawing moment and a positive rolling moment with increasing positive angle of attack. The deflections of the remaining left rudder produce negative increments in yawing moment, which are relatively constant over the angle-of-attack range but which decrease with increasing Mach number. The deflection of the rudder produces a small effect in rolling moment.

The sideslip characteristics at various angles of attack for the various configurations are shown in figures 12 to 20. These results were obtained to show the degree of linearity of the lateral characteristics with β since all subsequent sideslip derivatives were obtained through the angle-of-attack range from incremental measurements obtained at sideslip angles of 0° and 3°. Within this range, the variations are essentially linear; therefore, the derivative values are considered valid up to $\beta = 3^{\circ}$.

Results for the deflection of the rudder to 15° with 50-percent wing damage (fig. 14) indicate that for the reference center used, the asymmetric yaw caused by wing damage

could be trimmed at $\beta \approx 4^{\circ}$. The results of figure 16 indicate that the induced roll could be trimmed at sideslip angles of about 5° to 6° through a $\pm 10^{\circ}$ deflection of the horizontal tail.

The results of figure 18 indicate that a -20° deflection of the left horizontal tail should trim the roll caused by loss of the right horizontal tail for the angles of attack shown.

The data of figure 19 indicate that the loss of the right vertical tail results in directional instability for all test conditions with the exception of a region of very low stability at $\alpha \approx 0^{\circ}$ and $M = 2.50$.

The sideslip parameters for the various asymmetric configurations are shown in figures 21 to 25. The effects are relatively insignificant with the exception of the vertical-tail damage where, as previously noted, the loss of the right vertical tail causes the model to become directionally unstable at all Mach numbers, with the possible exception of a Mach number of 2.50 where the model exhibits essentially neutral stability at low angles of attack and for the highest angles of attack for all test Mach numbers.

CONCLUDING REMARKS

An experimental investigation has been conducted in the high Mach number test section of the Langley Unitary Plan wind tunnel over the Mach number range from 2.50 to 4.63 to determine the effect of simulated damage on the longitudinal and lateral aerodynamic characteristics of a fixed-wing twin-inlet fighter model having an aft horizontal tail and twin vertical tails. Damage was simulated on the wing, horizontal tail, and one of the vertical tails.

The results showed that for the reference moment center used, the model remained longitudinally stable for all the damaged configurations tested. The horizontal tail remained an effective trim device and generally was capable of providing some degree of trim in pitch and roll. The rudder was effective in providing some degree of trim in yaw and roll for cases of damage to the wing or horizontal tail. The loss of the right vertical tail generally caused the model to become directionally unstable.

Langley Research Center,
National Aeronautics and Space Administration,
Hampton, Va., June 15, 1973.

REFERENCES

1. Hayes, Clyde: Effects of Simulated Wing Damage on the Aerodynamic Characteristics of a Swept-Wing Airplane Model. NASA TM X-1550, 1968.

2. Blair, A. B., Jr.: Effects of Simulated Damage on Stability and Control Characteristics of a Swept-Wing Fighter Airplane at Mach 1.57 and 2.00. NASA TM X-2006, 1970.

3. Fuller, Dennis E.; and Watson, Carolyn B.: Effects of Simulated Damage on the Stability and Control Characteristics of a Delta-Wing Fighter Airplane Model at Mach Numbers of 1.41 and 2.01. NASA TM X-1750, 1969.

4. Spearman, M. Leroy; and Blair, A. B., Jr.: Wind-Tunnel Studies of Simulated Damage to Aerodynamic Surfaces of Airplanes. NASA TM X-2550, 1972.

5. Lamb, Milton; Dollyhigh, Samuel M.; and Spearman, M. Leroy: Stability and Control Characteristics at Mach 0.60 to 3.75 of a Fixed-Wing Twin-Inlet Fighter Model With an Aft Horizontal Tail and Twin Vertical Tails. NASA TM X-1790, 1969.

6. Lamb, Milton; and Spearman, M. Leroy: Additional Study of a Fixed-Wing Twin-Vertical-Tail Fighter Model Including Directional Control Characteristics and Effects of Wing and Body Modifications. NASA TM X-2117, 1970.

7. Lamb, Milton; and Spearman, M. Leroy: Additional Study of a Fixed-Wing Twin-Vertical-Tail Fighter Model Including the Effects of Wing and Vertical-Tail Modifications. NASA TM X-2619, 1972.

8. Anon.: Manual for Users of the Unitary Plan Wind Tunnel Facilities of the National Advisory Committee for Aeronautics. NACA, 1956.

TABLE I.- GEOMETRIC CHARACTERISTICS

Wing:	
b (reference wing), cm	61.36
b (test wing), cm	65.56
Λ (inner panel), deg	42
Λ (outer panel), deg	38
$\bar{c}$ (reference wing chord), cm	22.448
c_r at body intersection, cm	26.238
c_t, cm	8.41
Γ, deg	-4.167
Airfoil section	4-percent-thick circular arc
S (reference wing), cm^2	1256.1
A (reference wing)	3.01
Body station for trailing-edge intersection, cm	75.527
Horizontal tail:	
Total span, cm	40.64
c_r at body intersection, cm	11.7
c_t, cm	0
Airfoil section	4-percent-thick circular arc
Λ, deg	48.5
Vertical tail:	
Exposed span, cm	11.7
Exposed c_r, cm	22.6
c_t, cm	0
Λ, deg	61.7
Airfoil section	4-percent-thick circular arc
Miscellaneous:	
Inlet area (one duct), cm^2	19.47
Exit area (one duct), cm^2	20.99
Chamber area, cm^2	14.30
Base area (excluding chamber and exit areas), cm^2	21.32

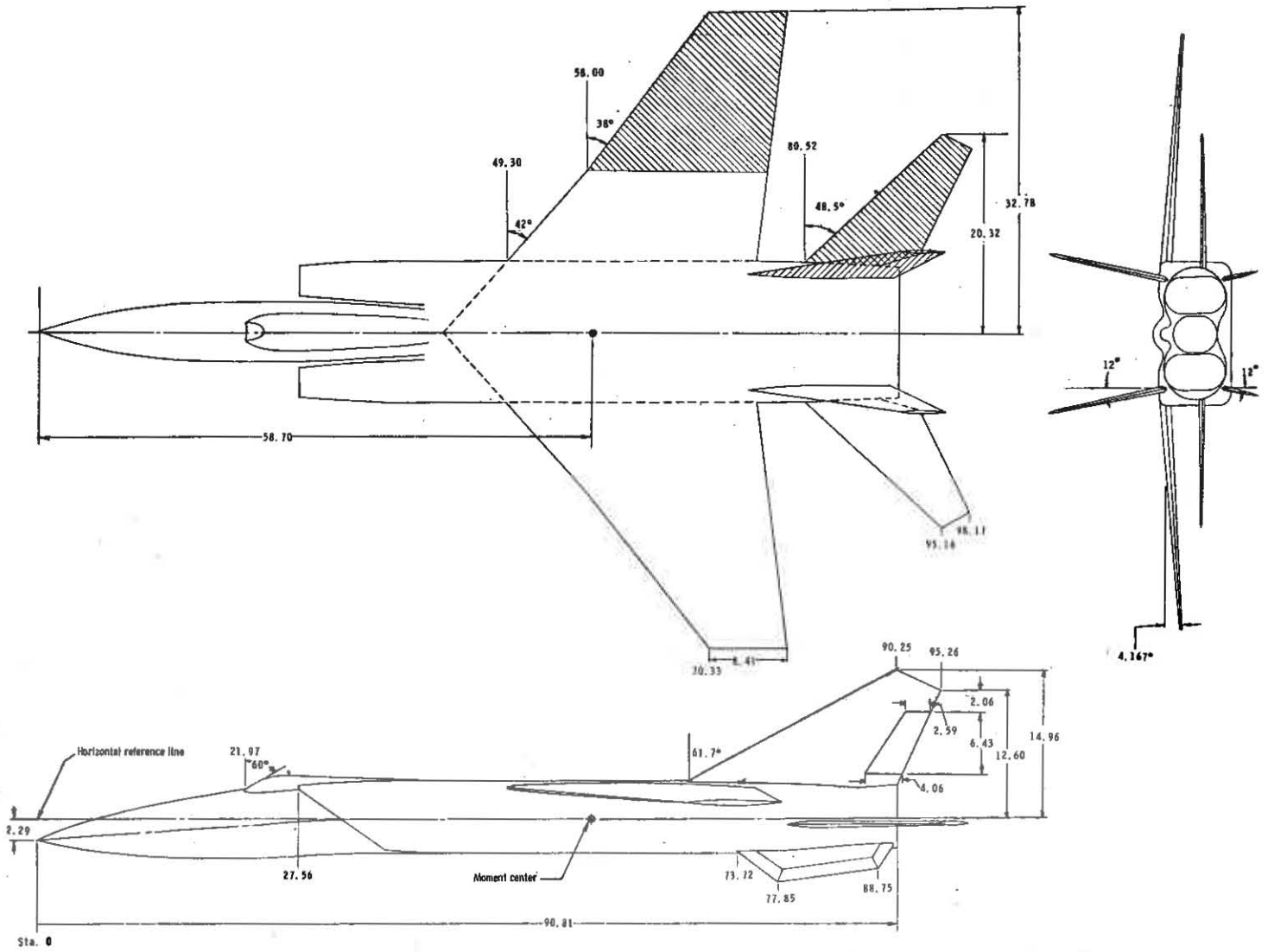

Figure 1.- Details of model. All linear dimensions are shown in centimeters.

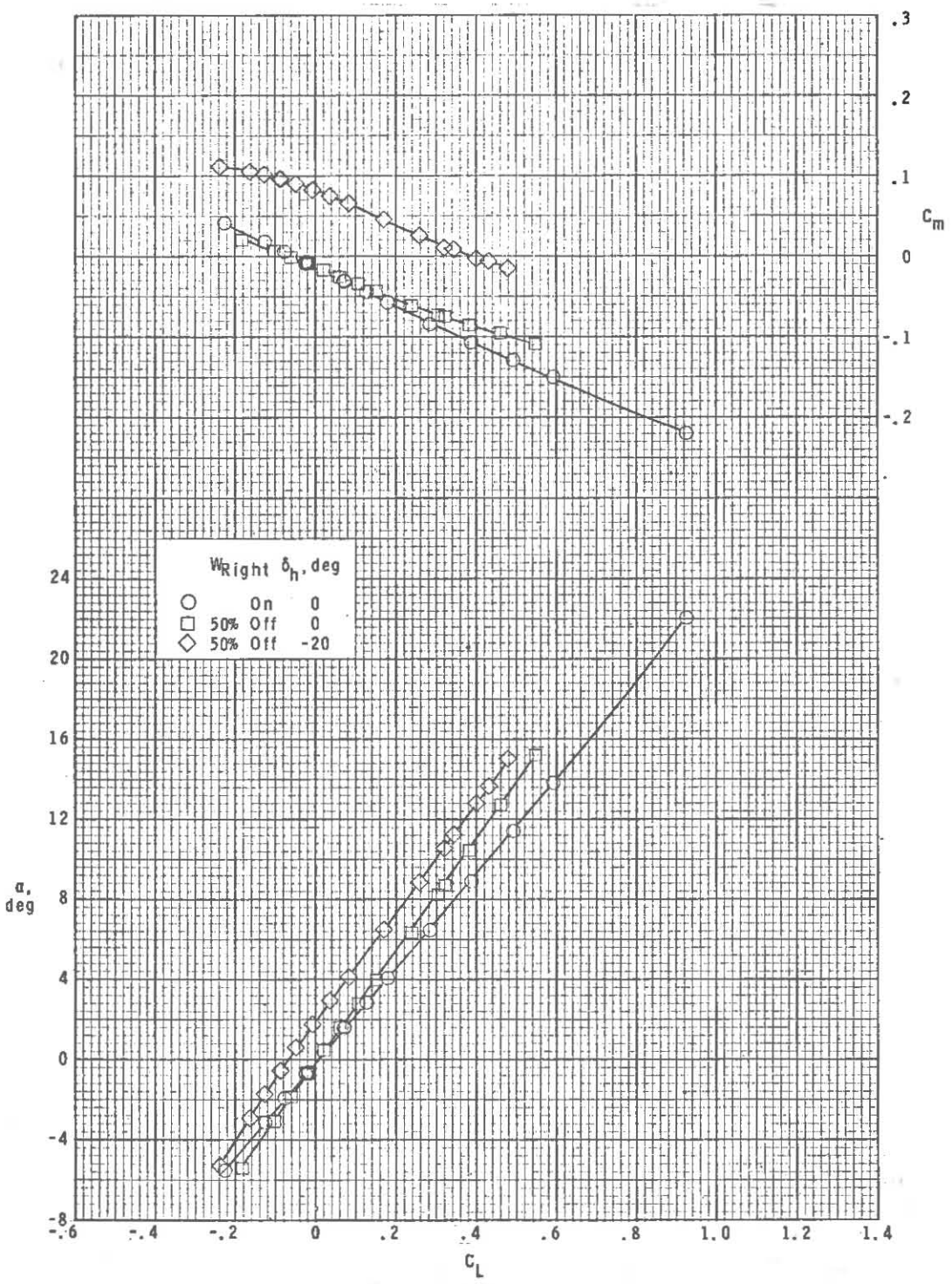

(a) M = 2.50.

Figure 2.- Longitudinal aerodynamic characteristics for asymmetric wing condition and horizontal-tail control.

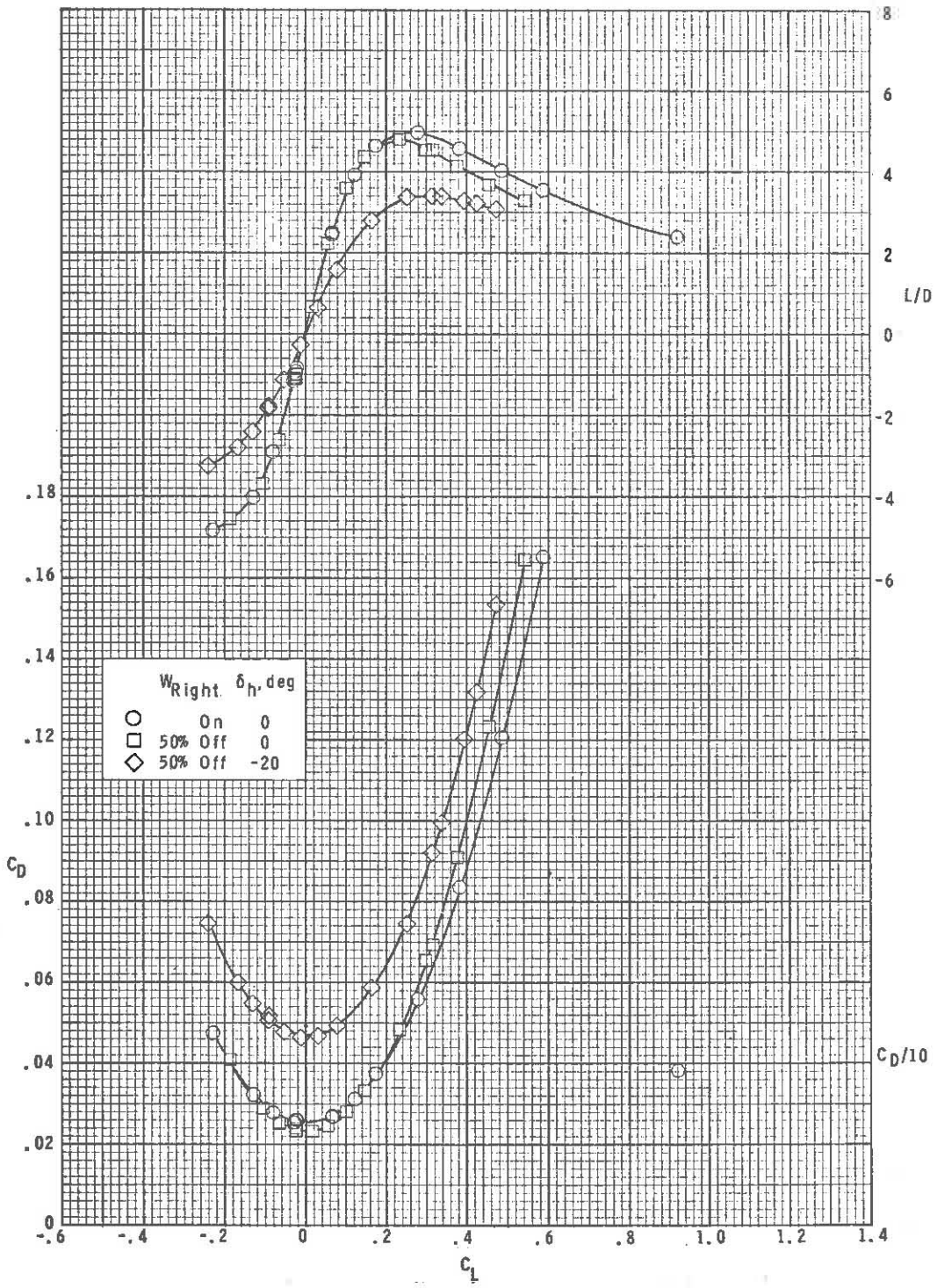

(a) Concluded.

Figure 2.- Continued.

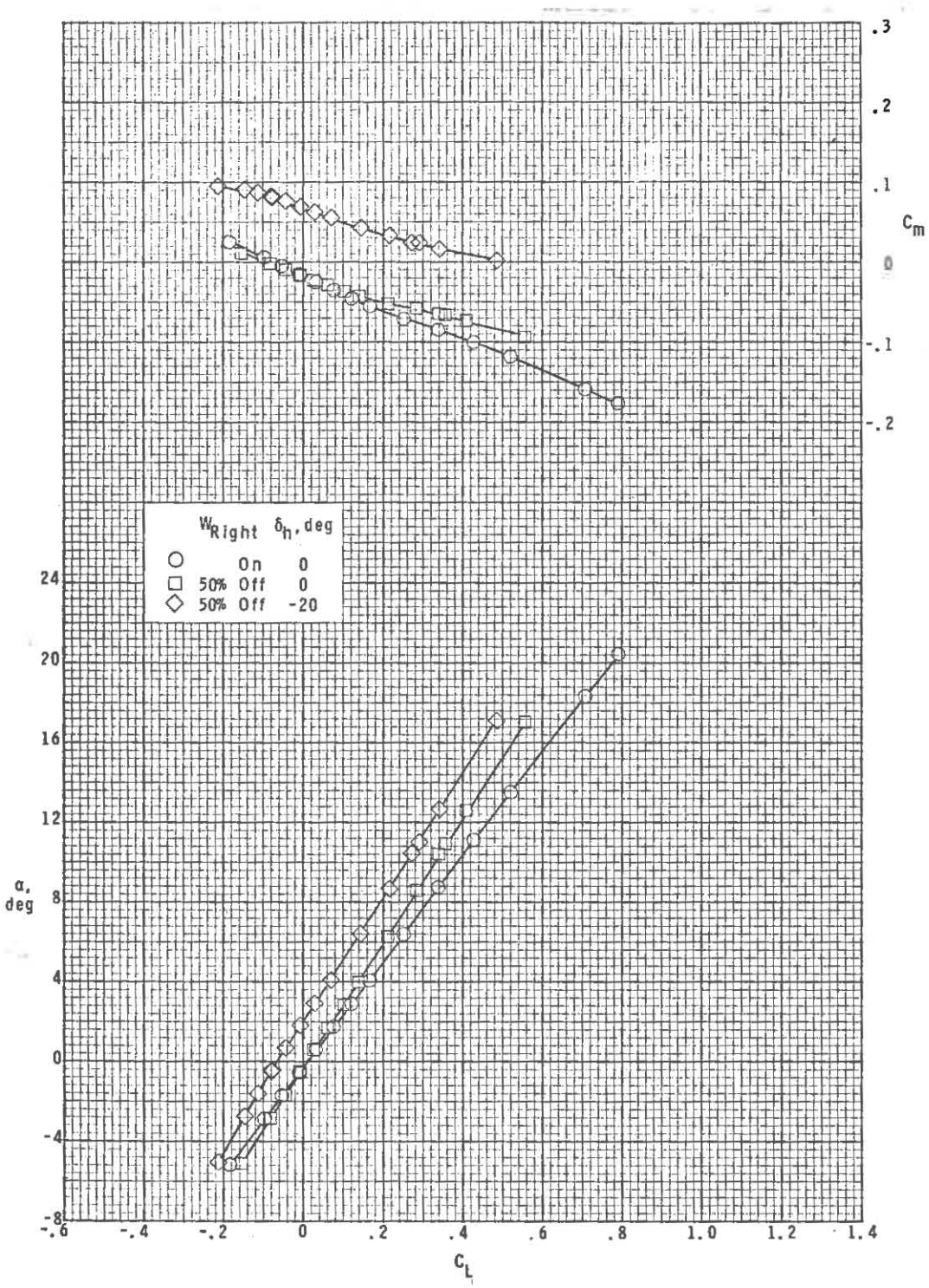

(b) M = 2.86.

Figure 2.- Continued.

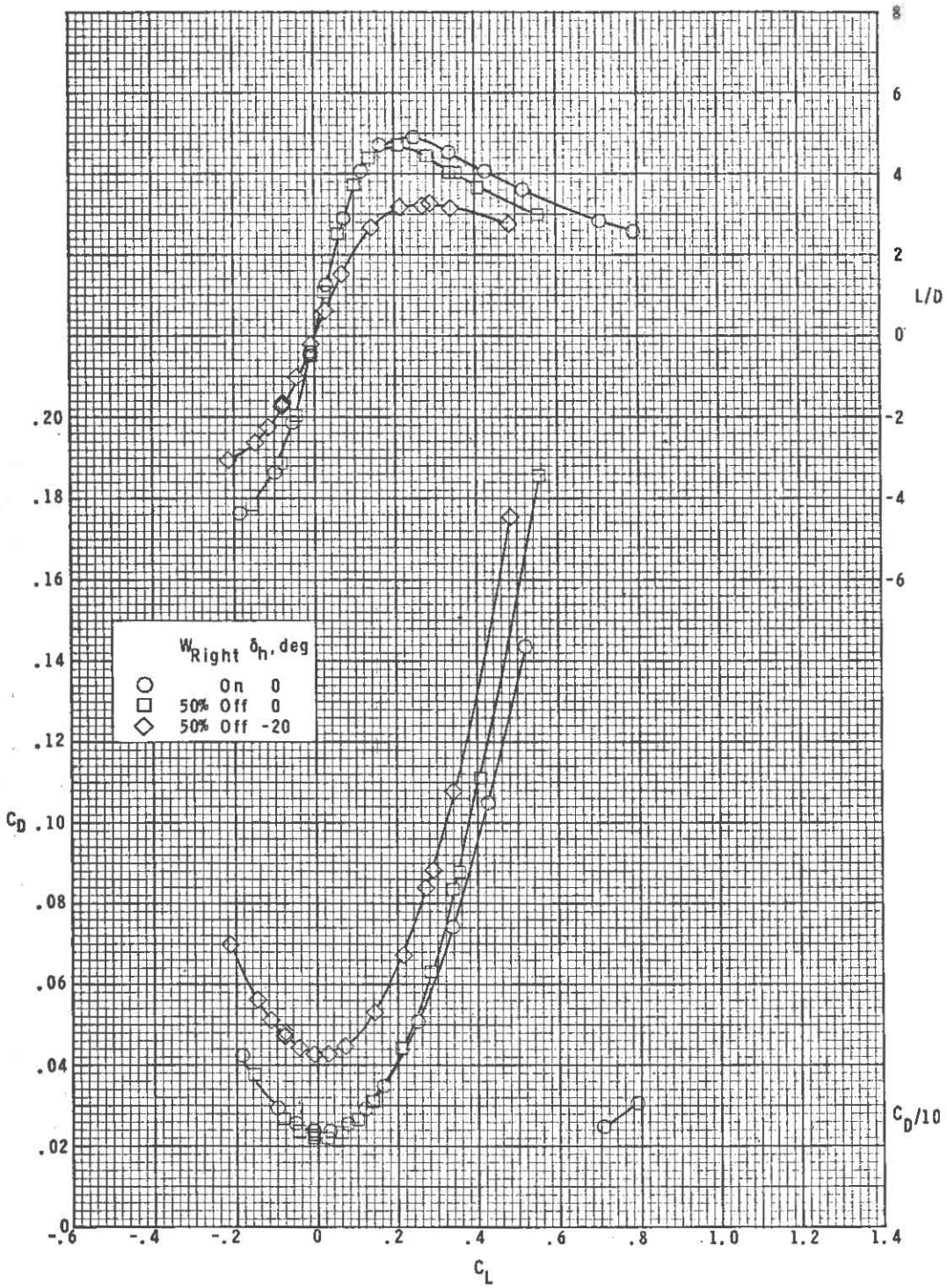

(b) Concluded.

Figure 2.- Continued.

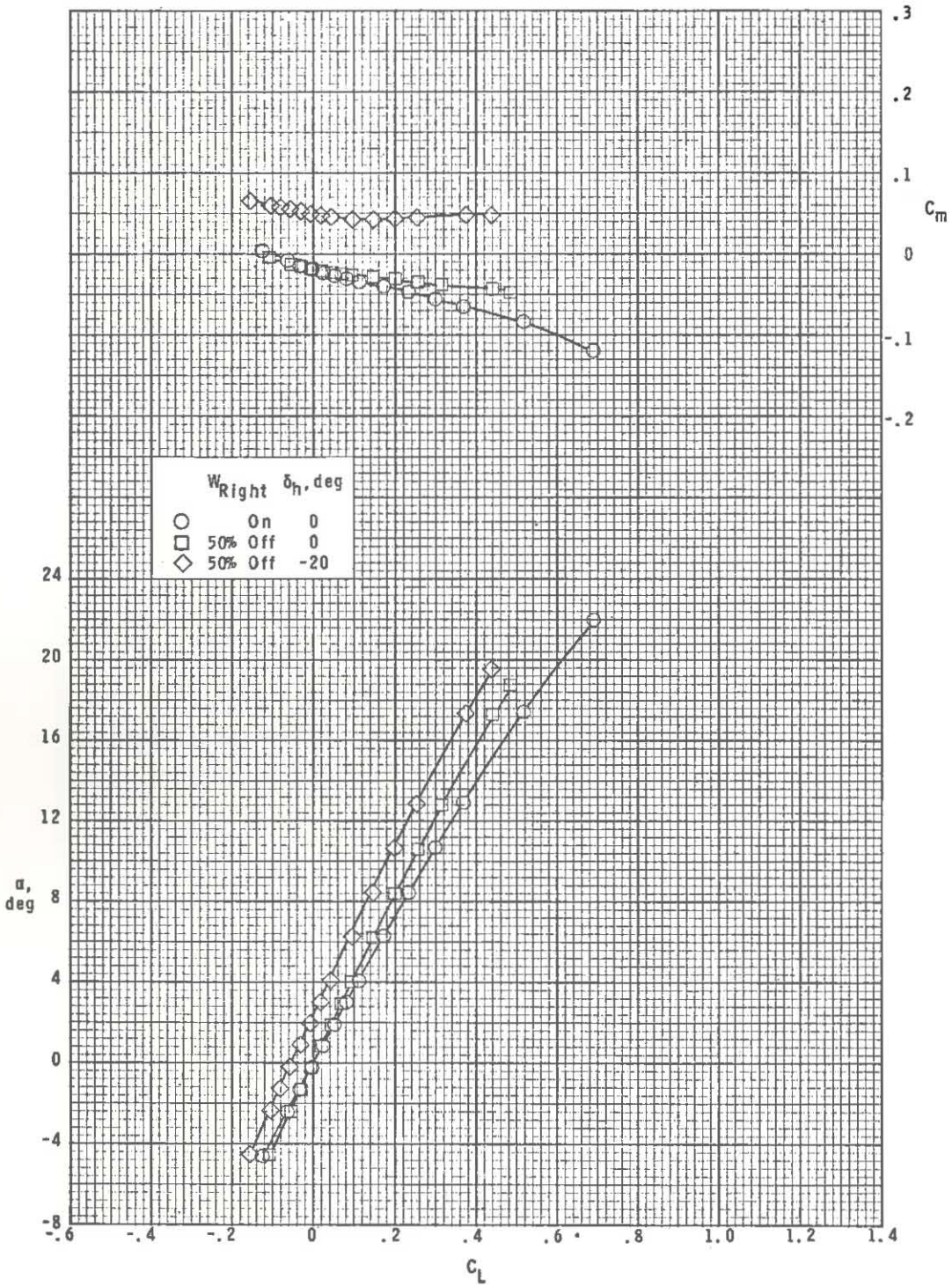

(c) M = 3.95.

Figure 2.- Continued.

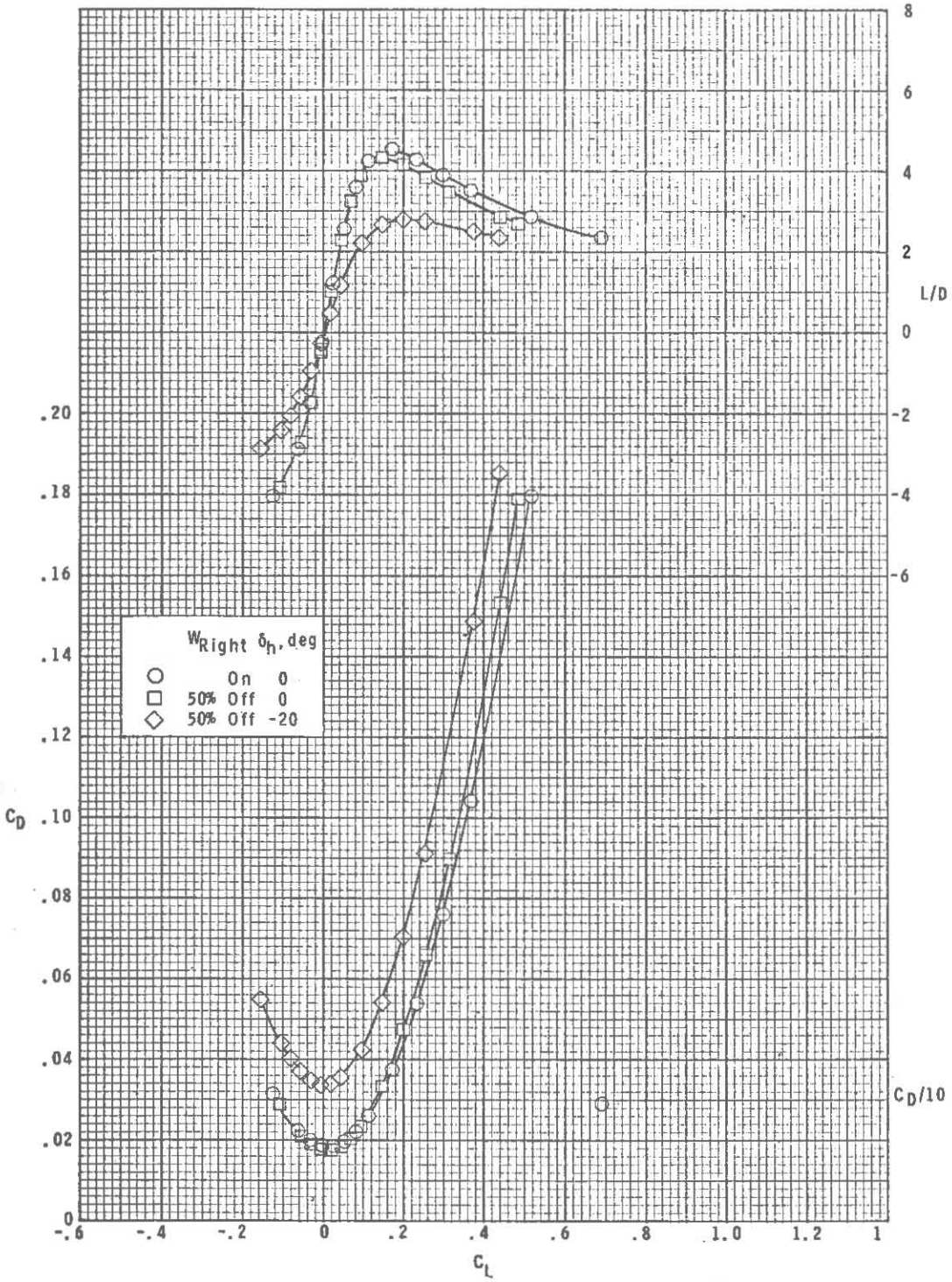

(c) Concluded.

Figure 2.- Continued.

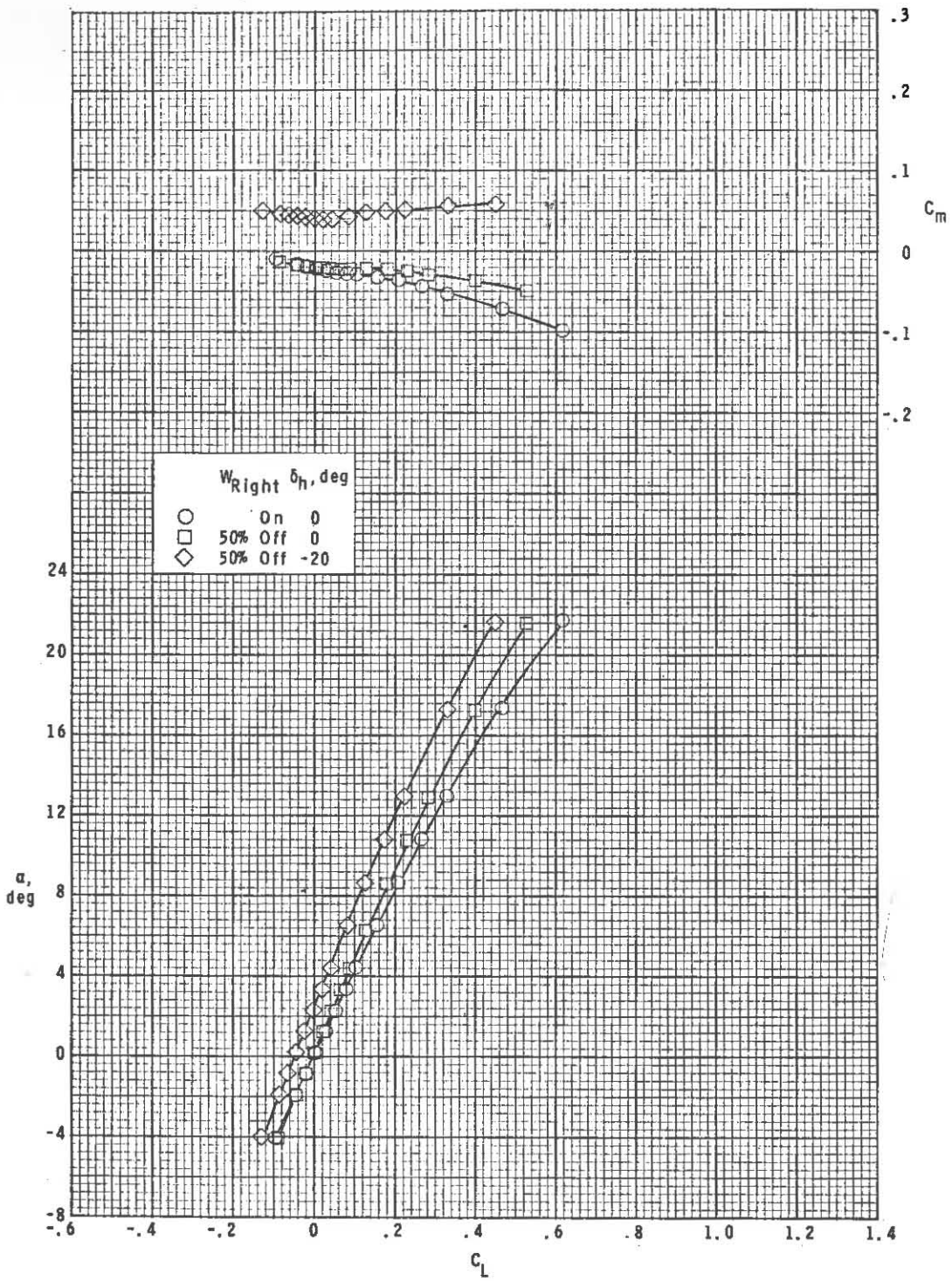

(d) M = 4.63.

Figure 2.- Continued.

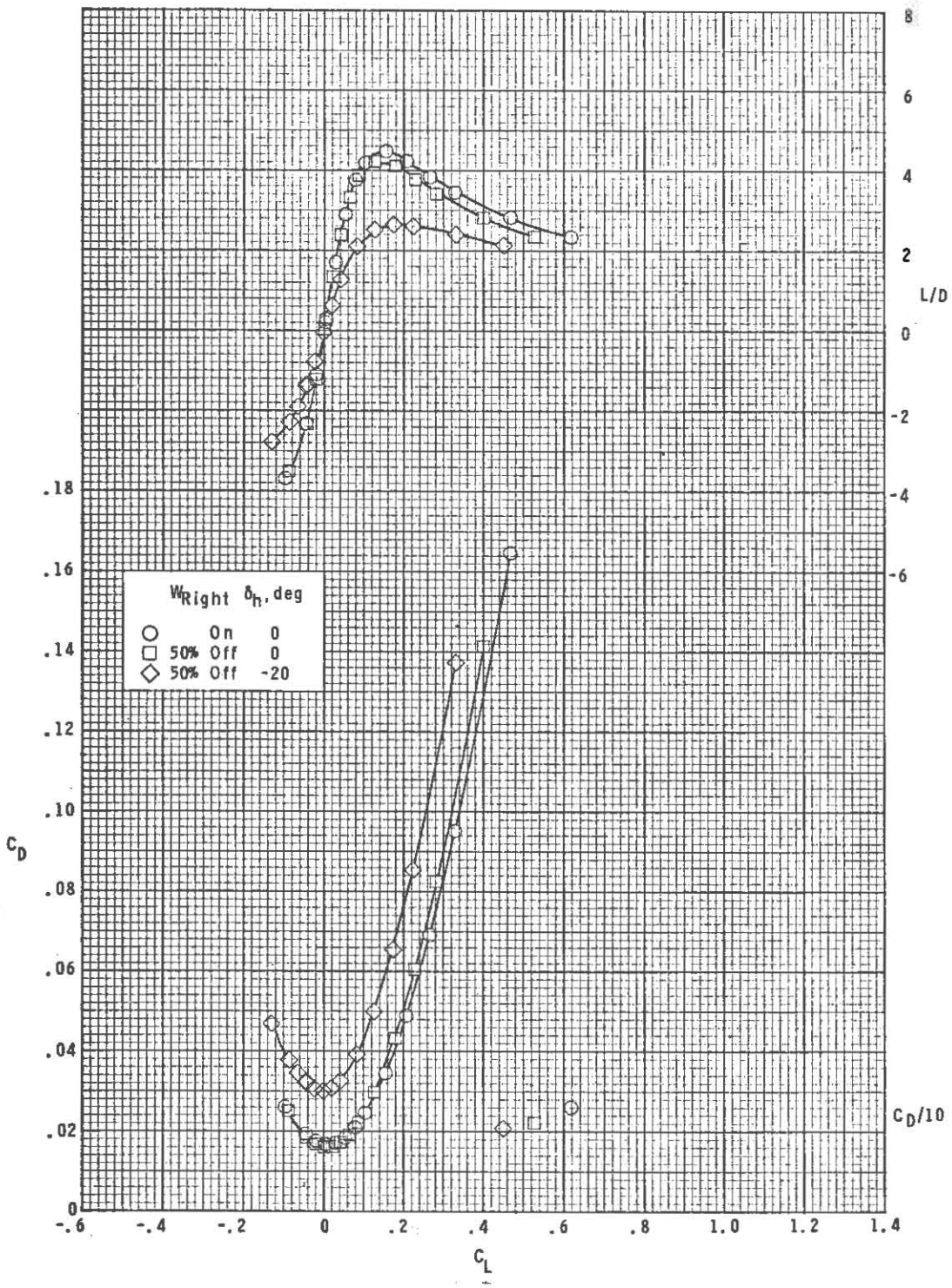

(d) Concluded.

Figure 2.- Concluded.

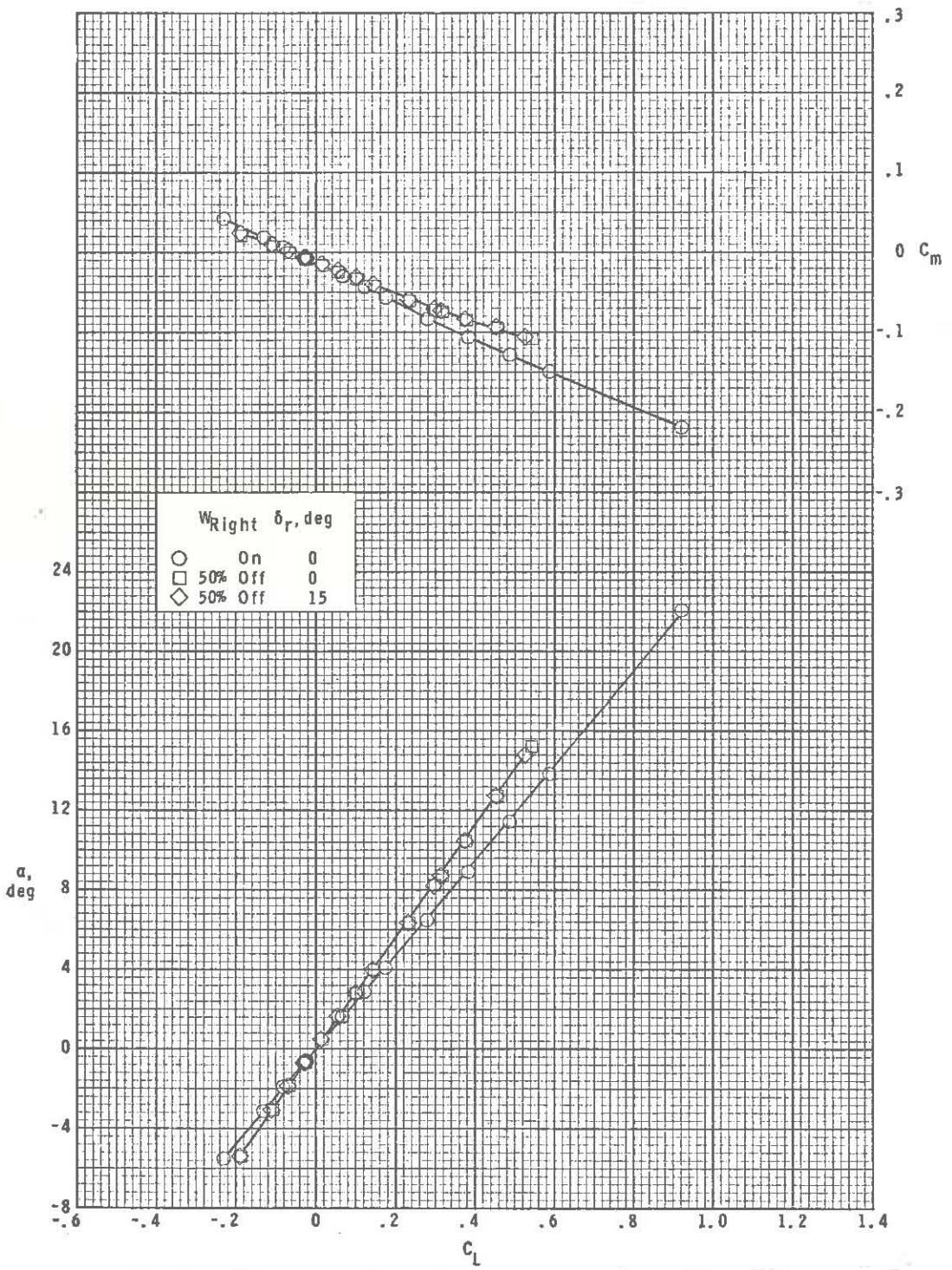

(a) M = 2.50.

Figure 3.- Longitudinal aerodynamic characteristics for asymmetric wing condition and rudder control.

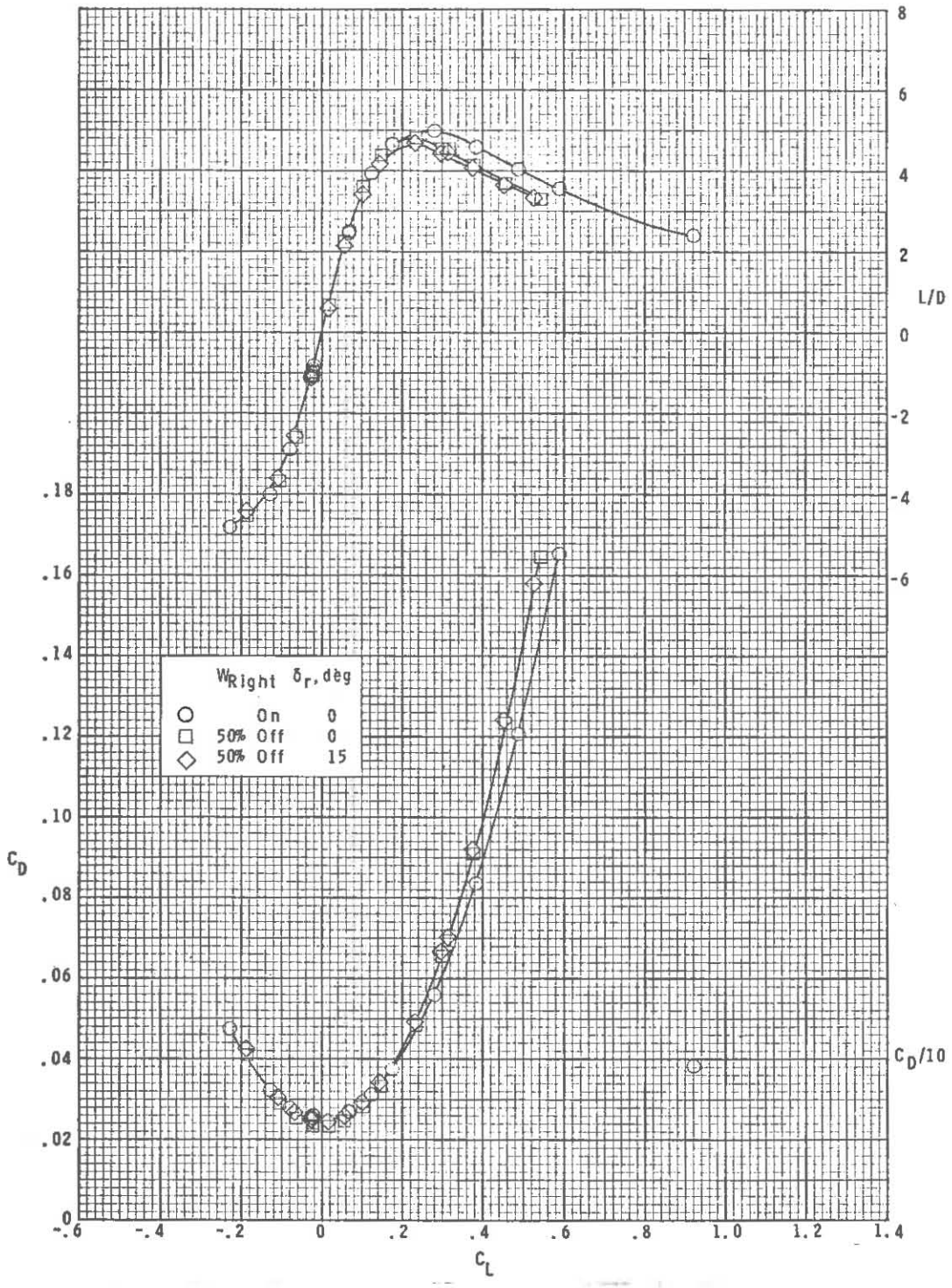

(a) Concluded.

Figure 3.- Continued.

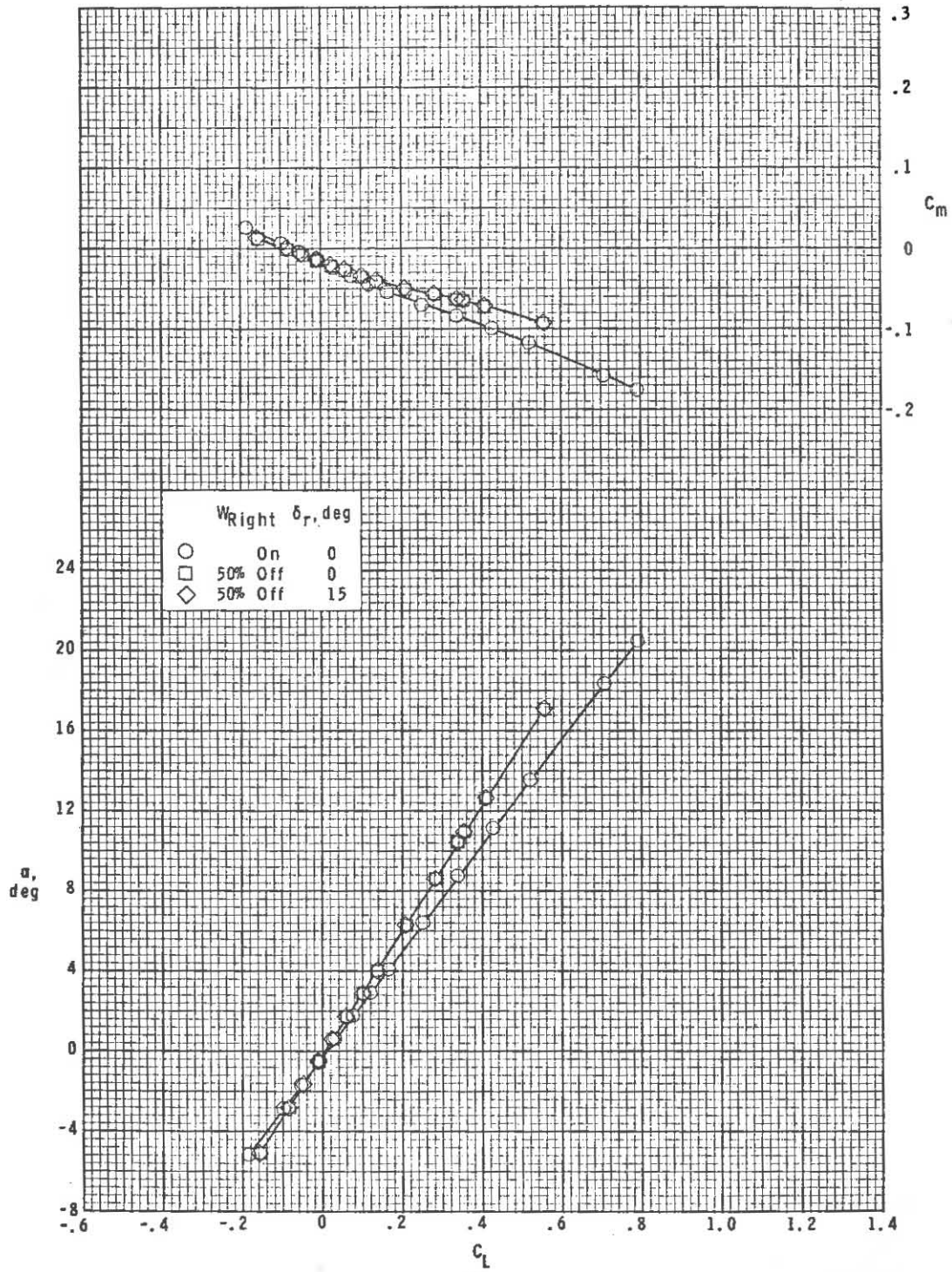

(b) M = 2.86.

Figure 3.- Continued.

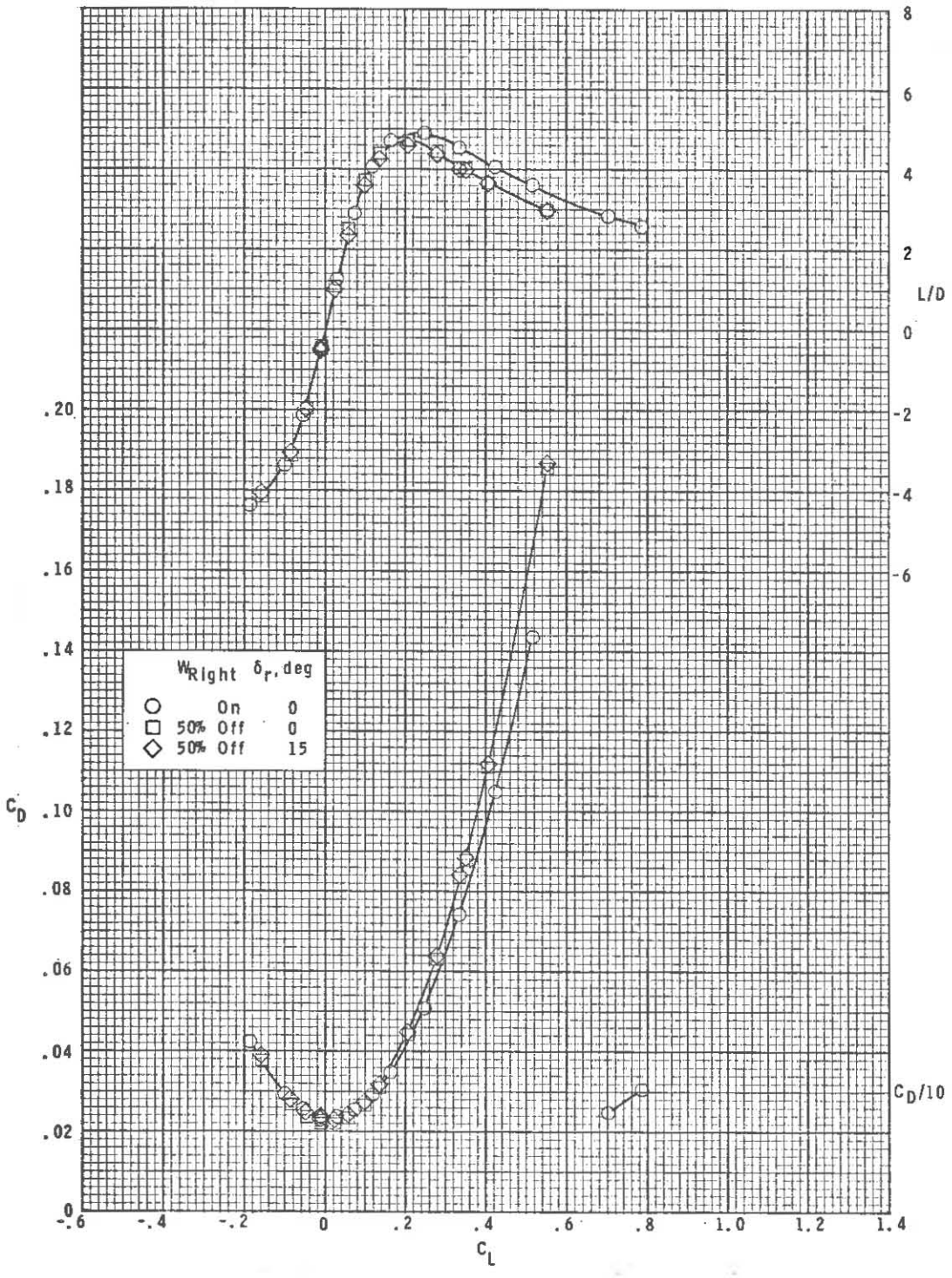

(b) Concluded.

Figure 3.- Continued.

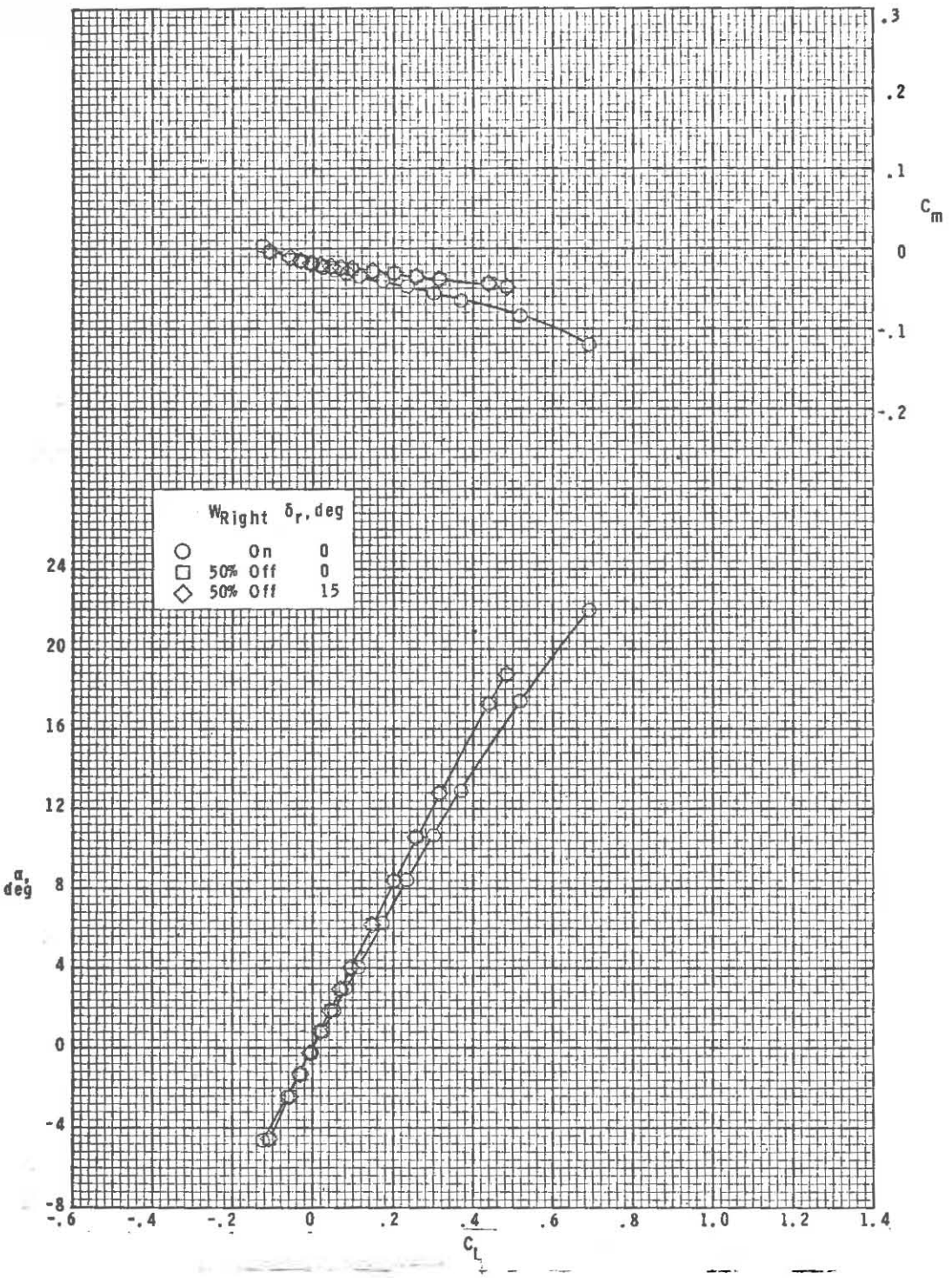

(c) M = 3.95.

Figure 3.- Continued.

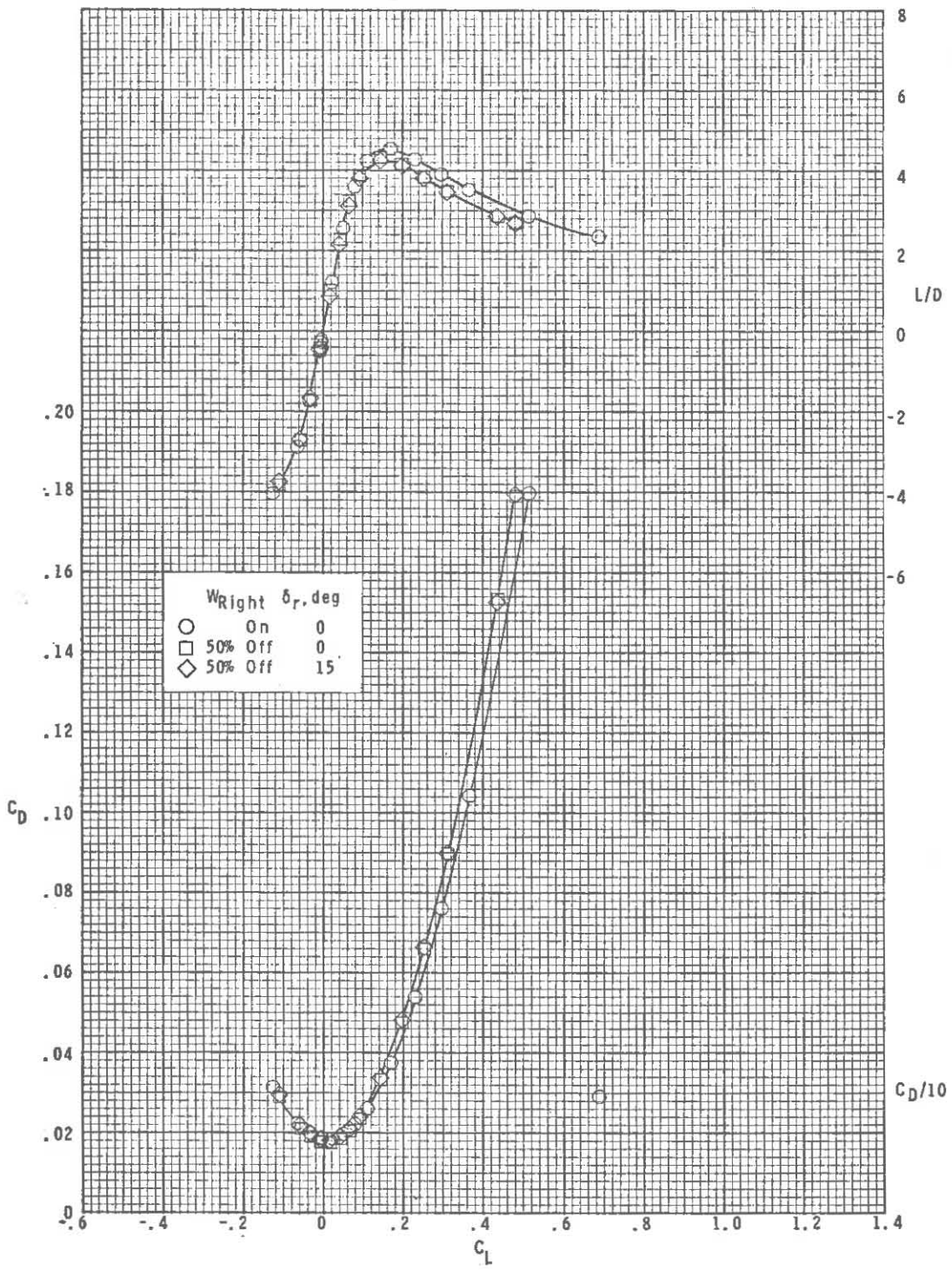

(c) Concluded.

Figure 3.- Continued.

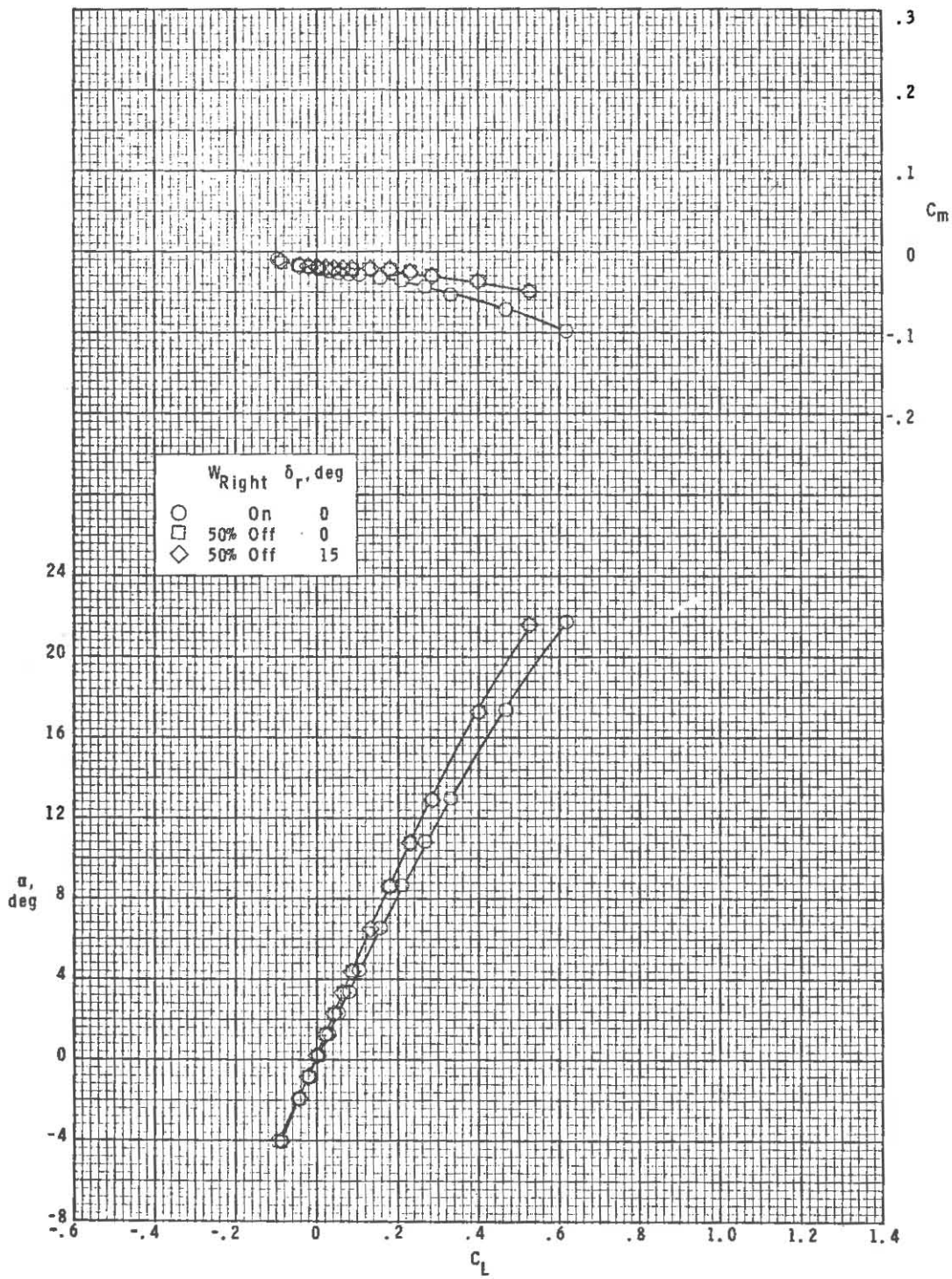

(d) M = 4.63.

Figure 3.- Continued.

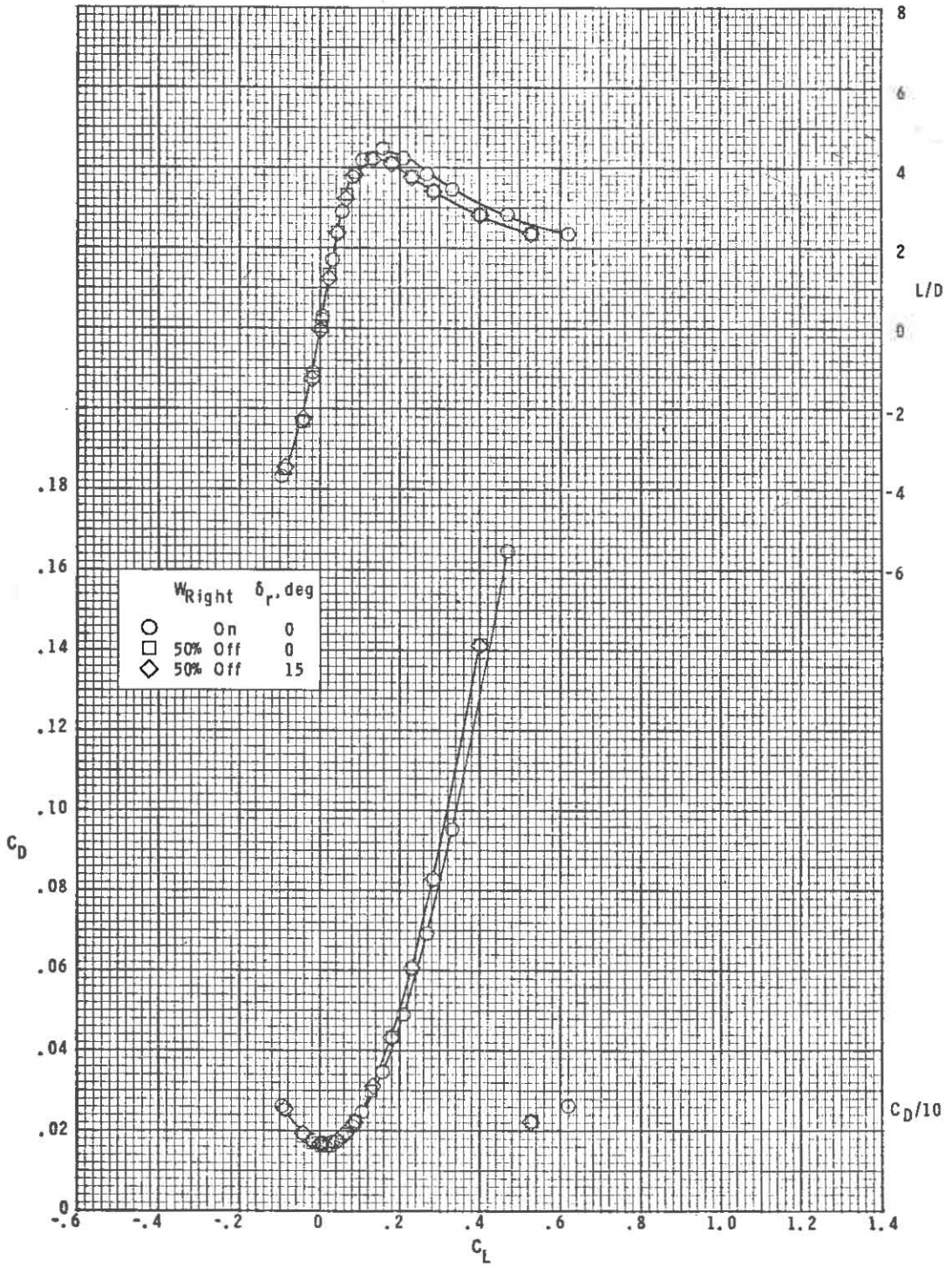

(d) Concluded.

Figure 3.- Concluded.

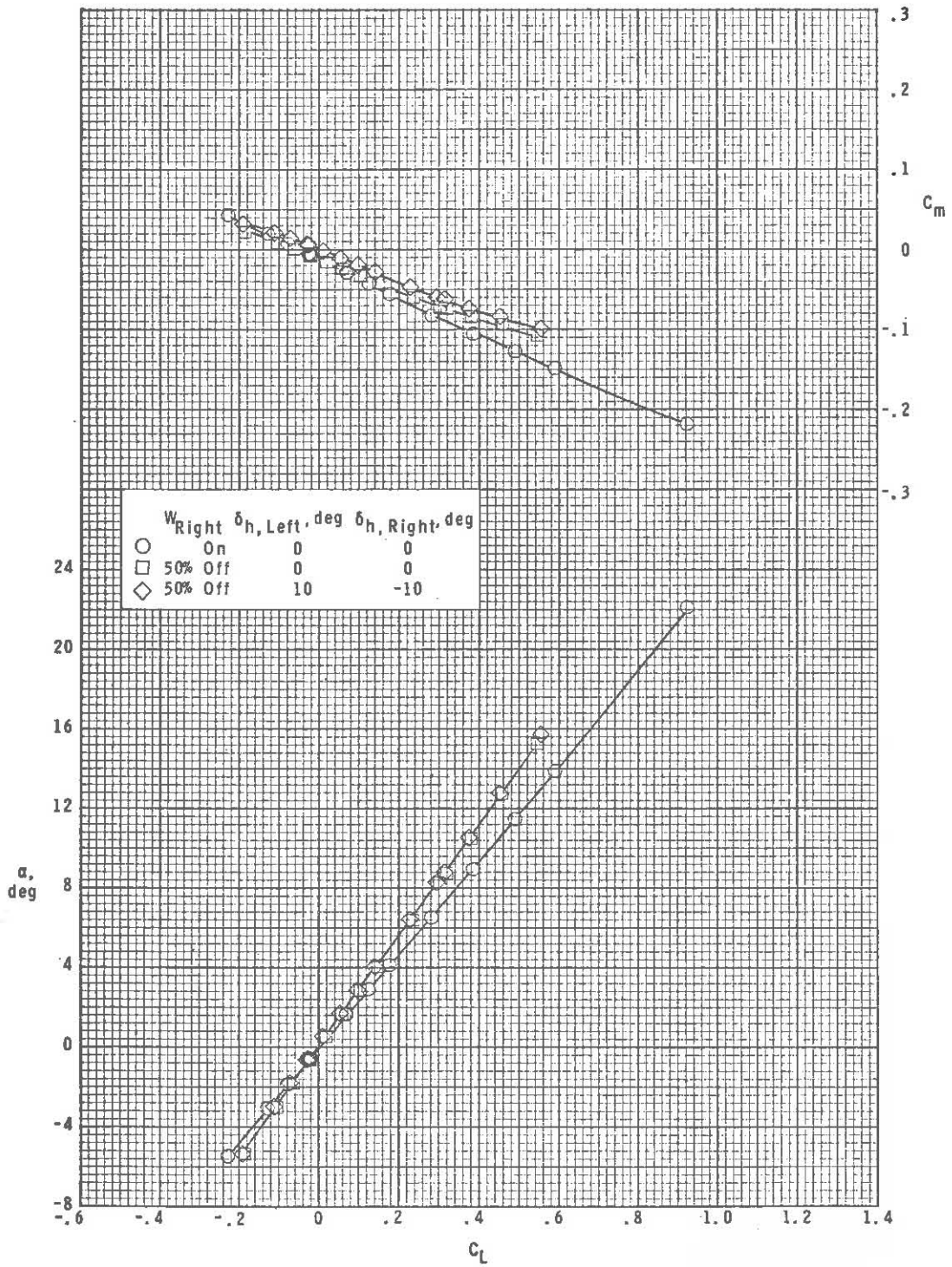

(a) M = 2.50.

Figure 4.- Longitudinal aerodynamic characteristics for asymmetric wing condition and differential horizontal-tail settings.

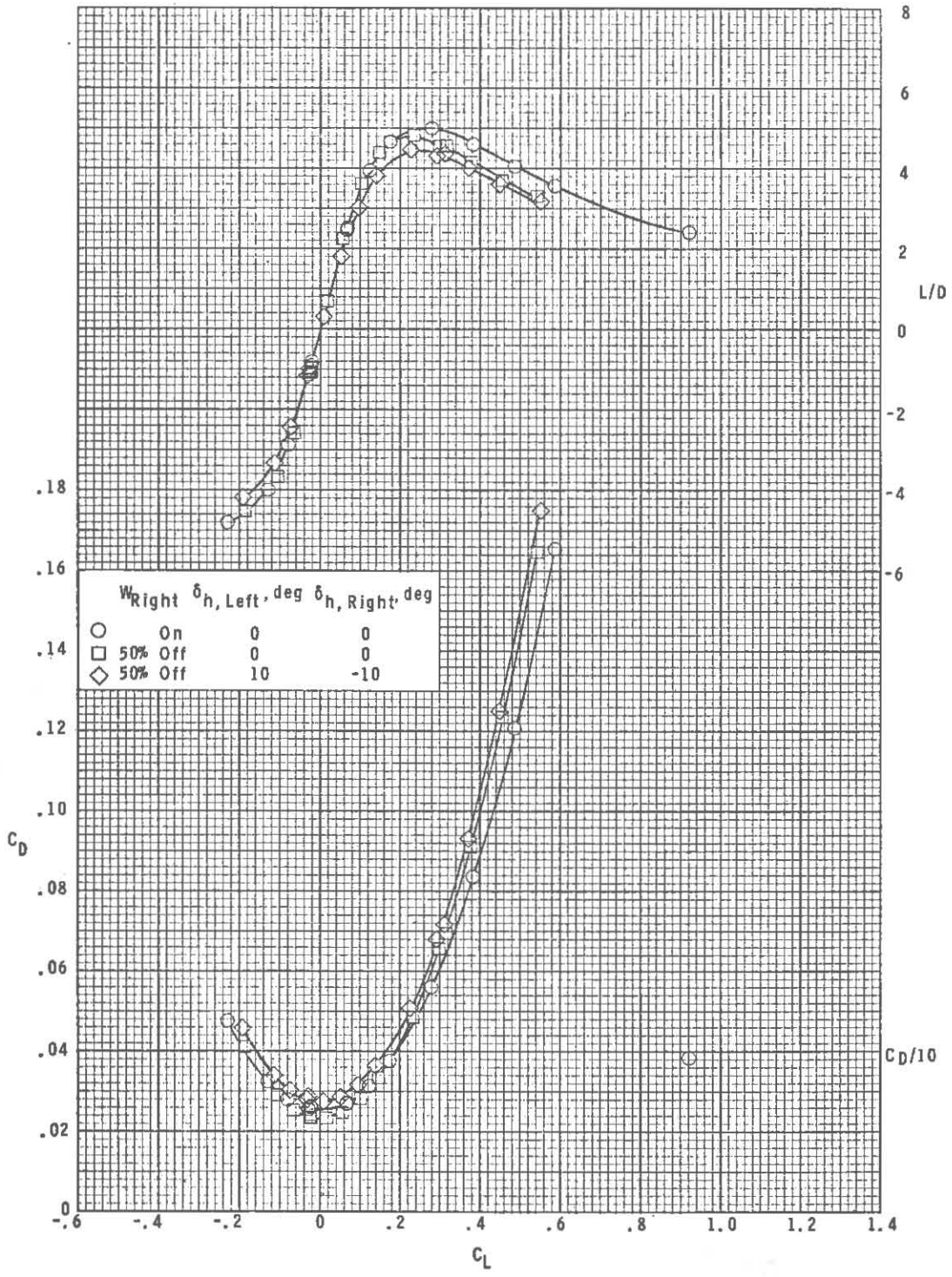

(a) Concluded.

Figure 4.- Continued.

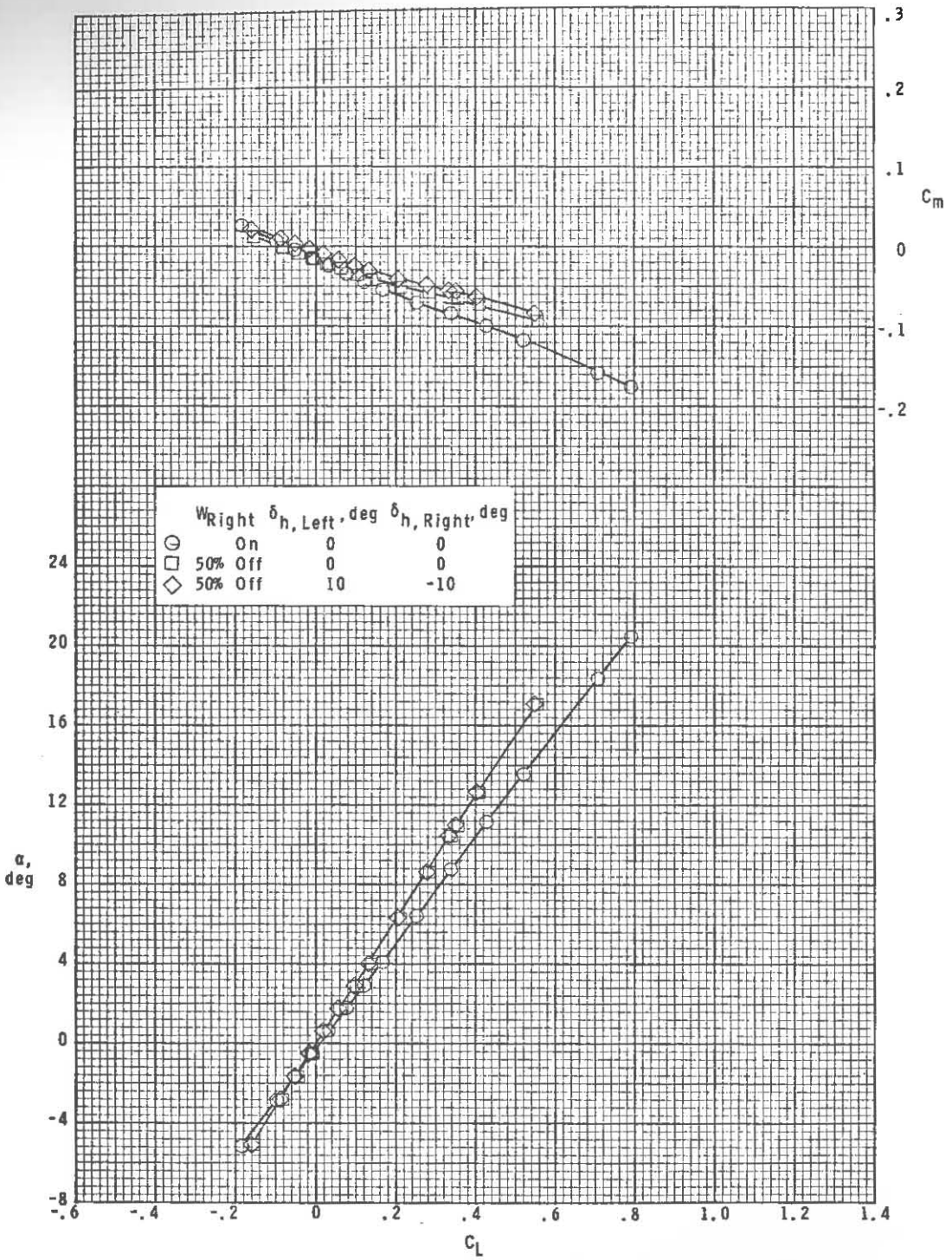

(b) M = 2.86.

Figure 4.- Continued.

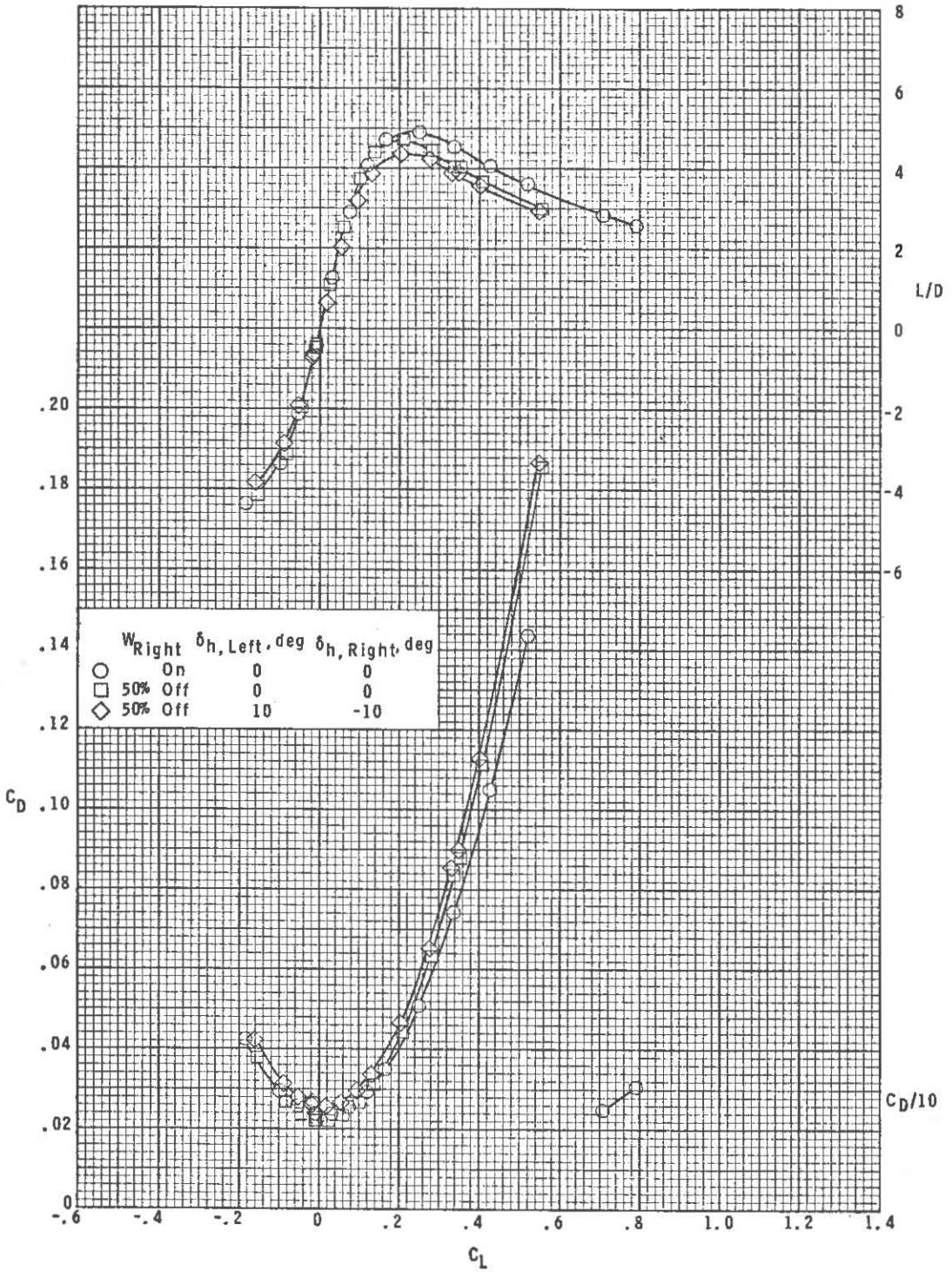

(b) Concluded.

Figure 4.- Continued.

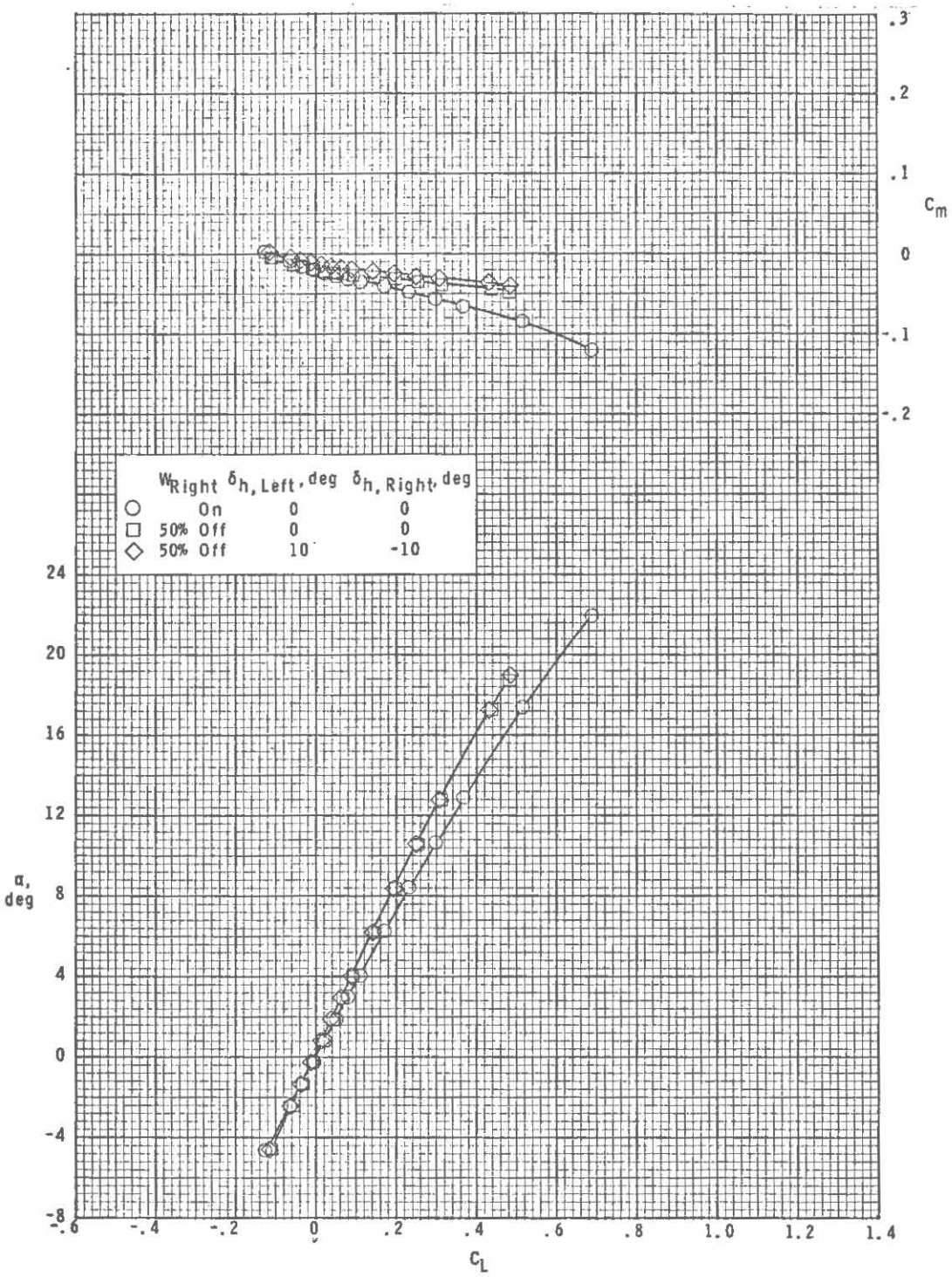

(c) M = 3.95.

Figure 4.- Continued.

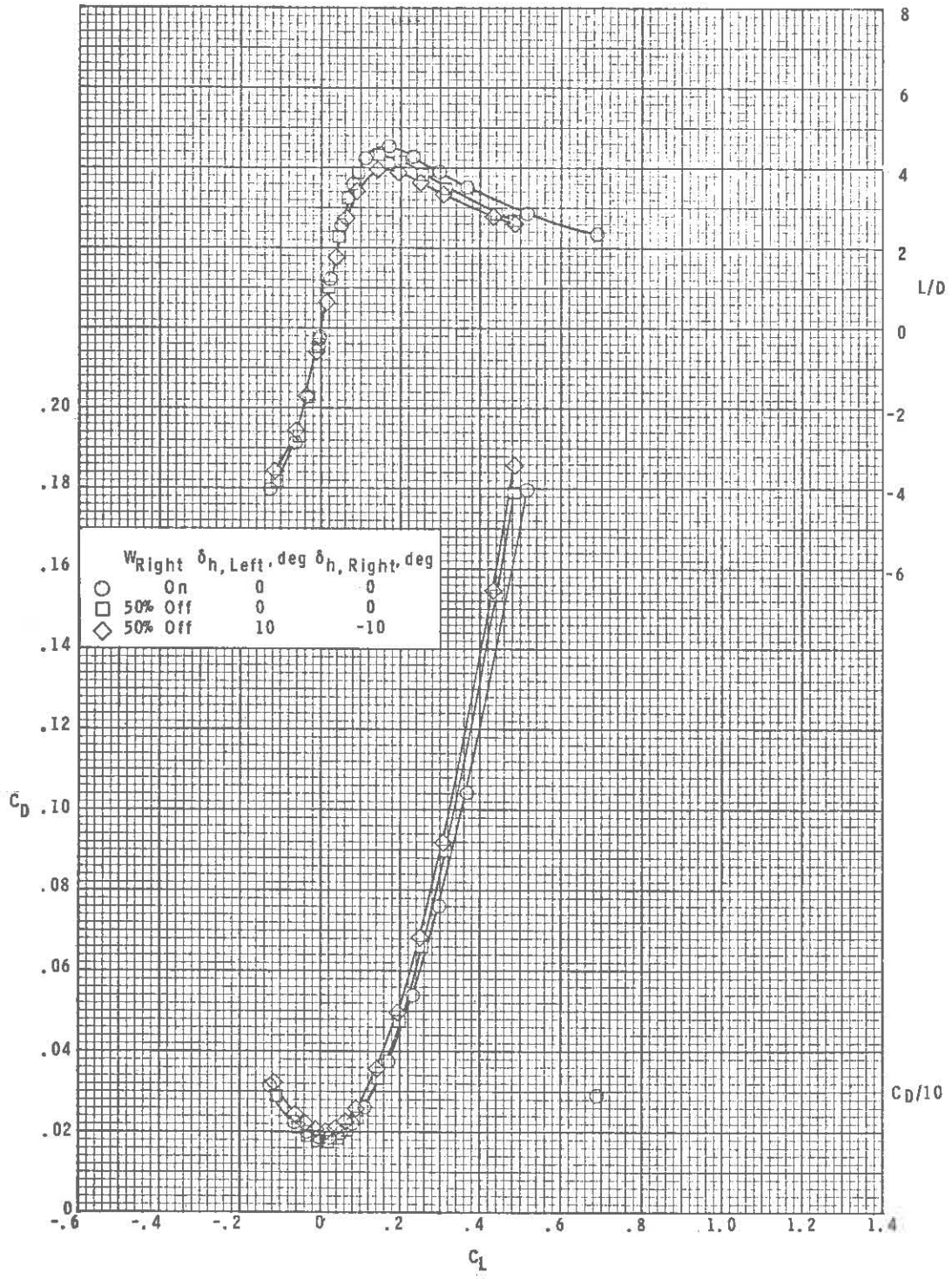

(c) Concluded.

Figure 4.- Continued.

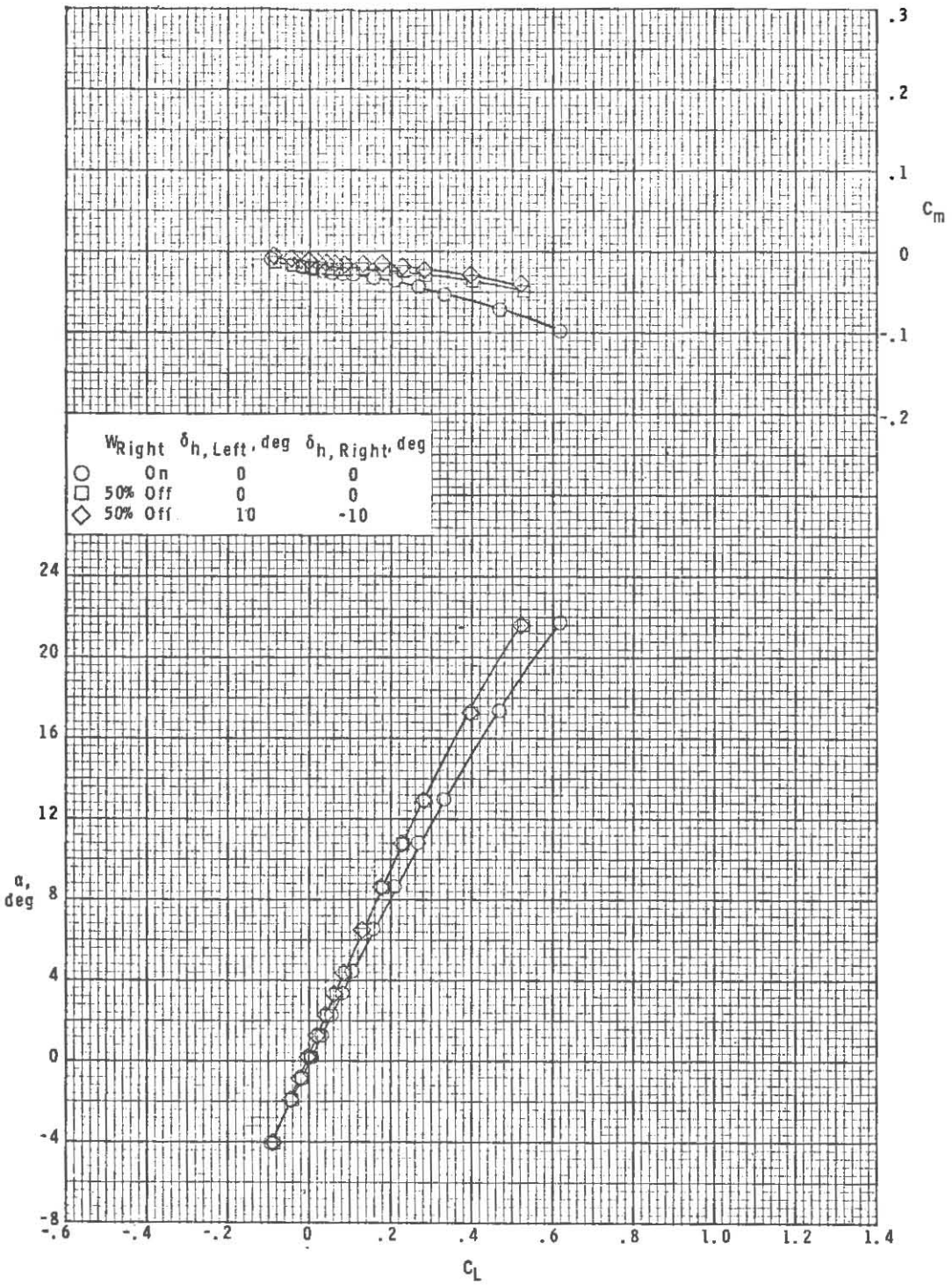

(d) M = 4.63.

Figure 4.- Continued.

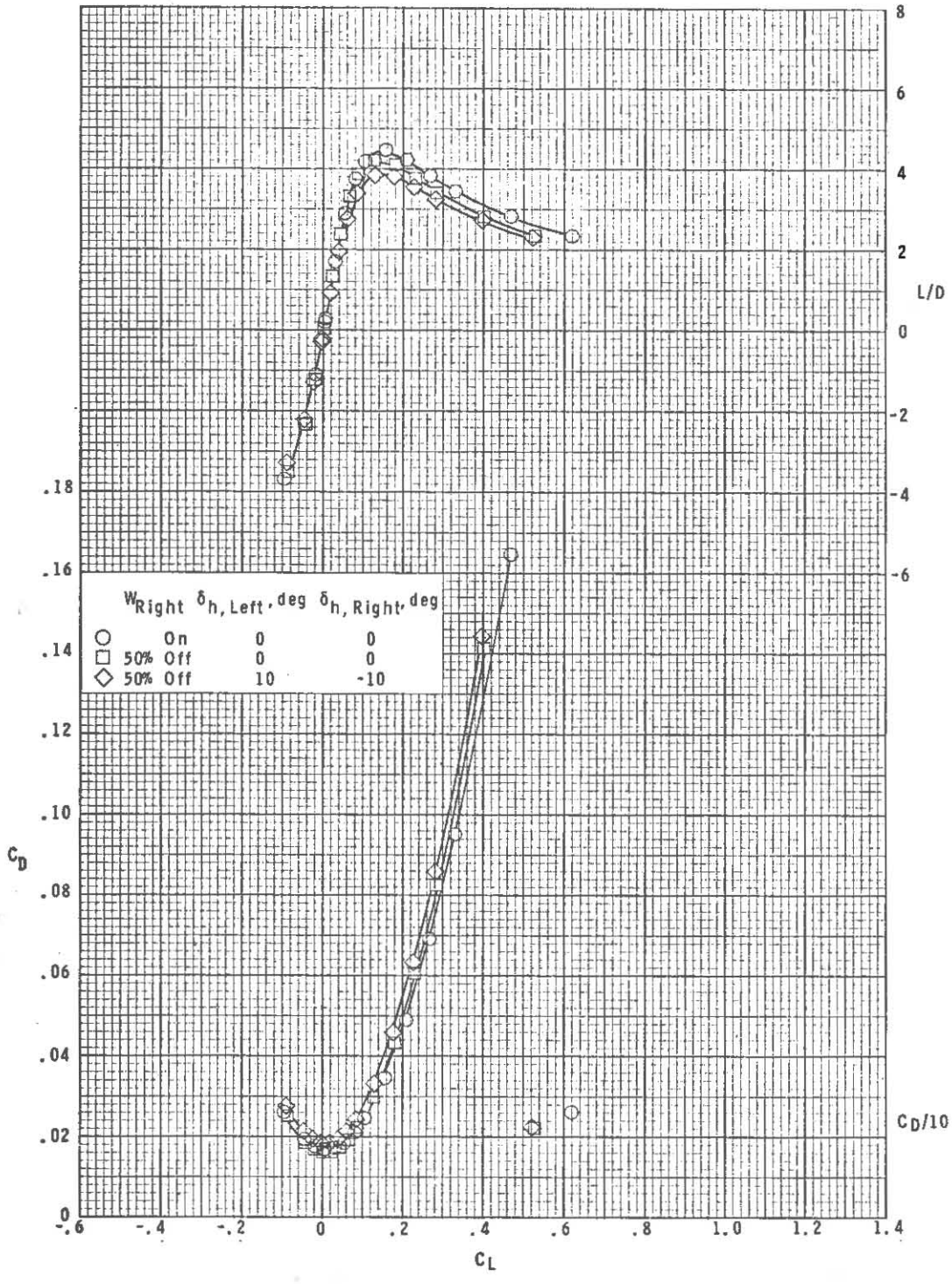

(d) Concluded.

Figure 4.- Concluded.

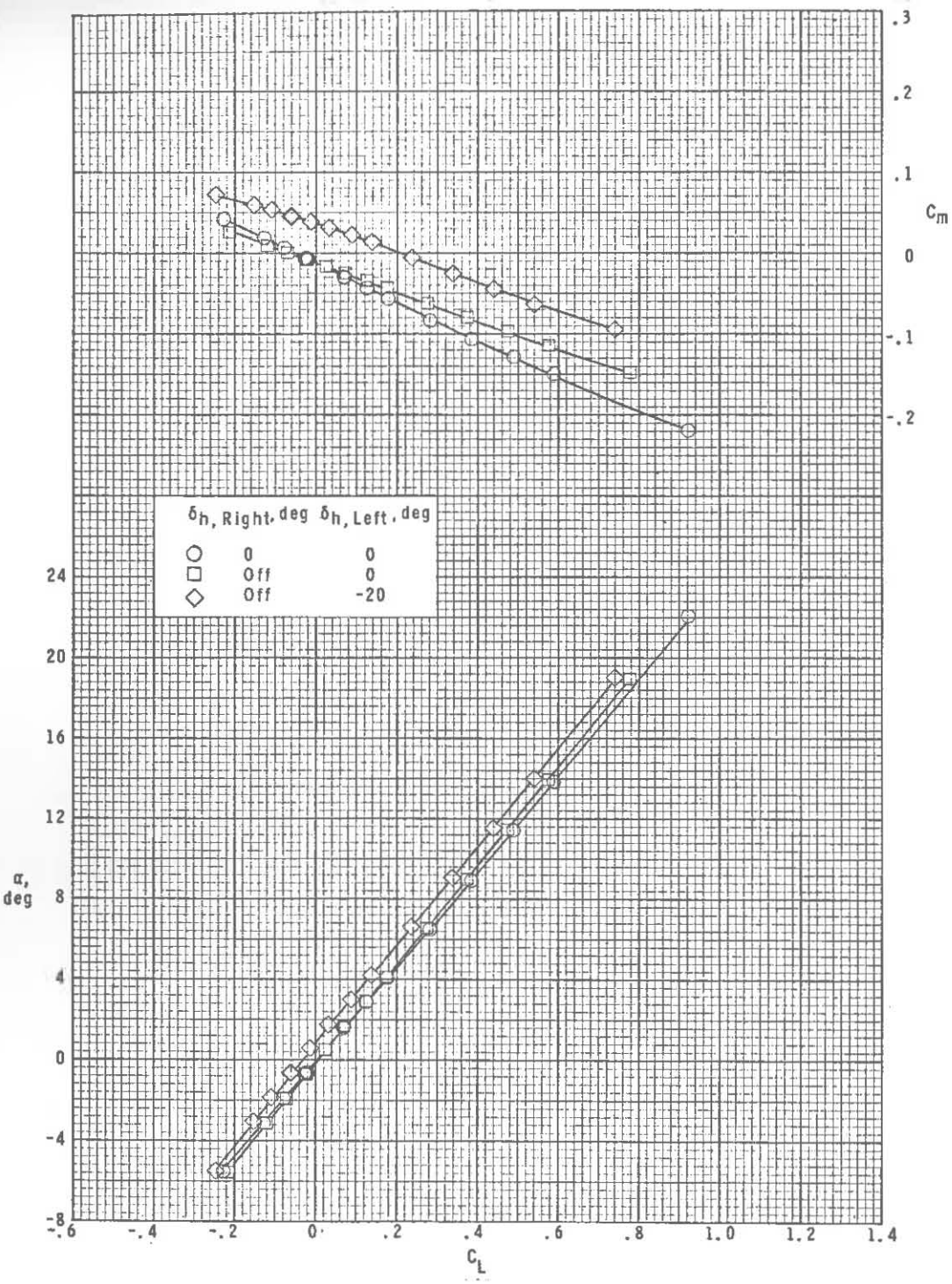

(a) M = 2.50.

Figure 5.- Longitudinal aerodynamic characteristics for asymmetric horizontal-tail condition.

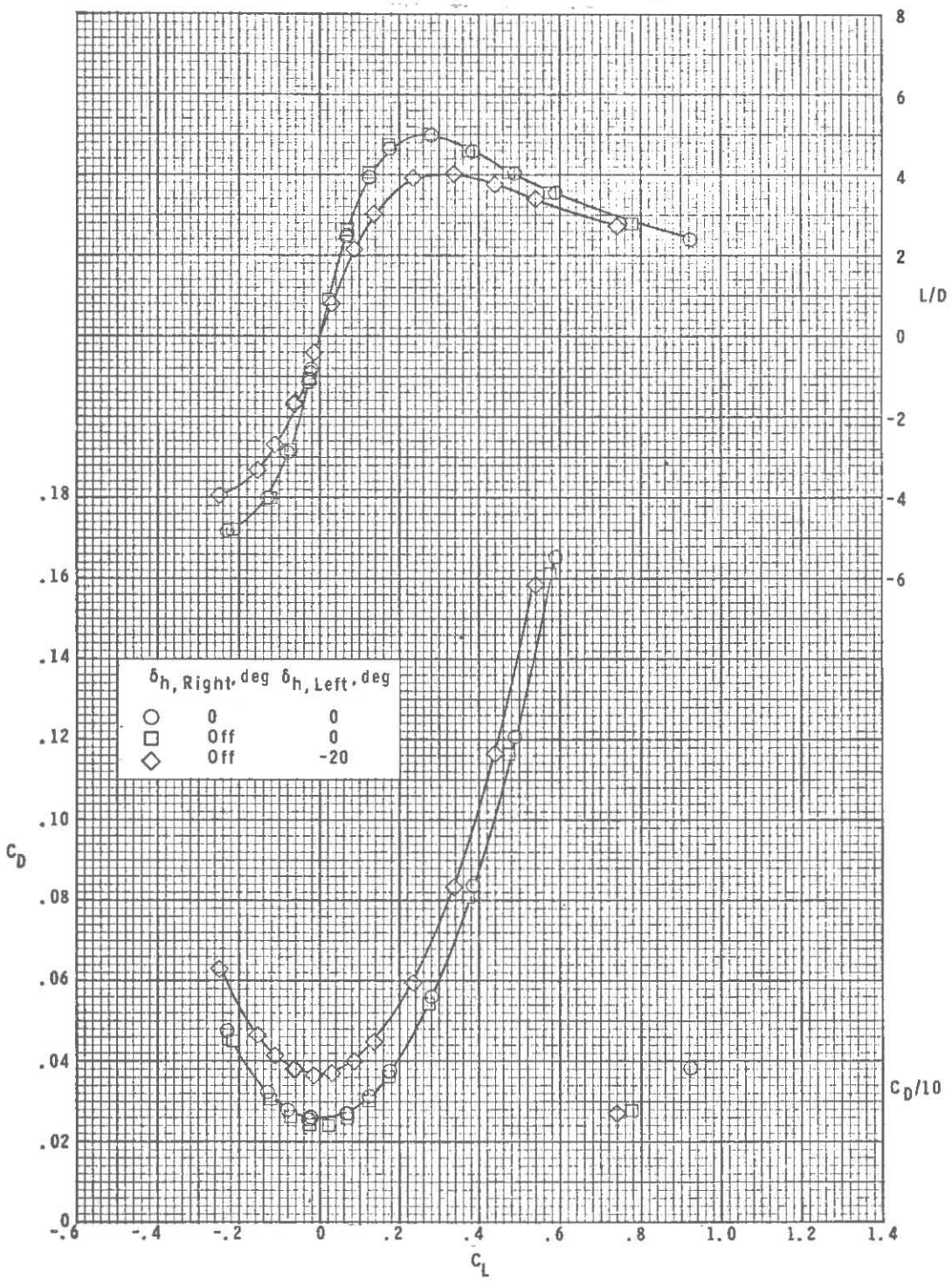

(a) Concluded.

Figure 5.- Continued.

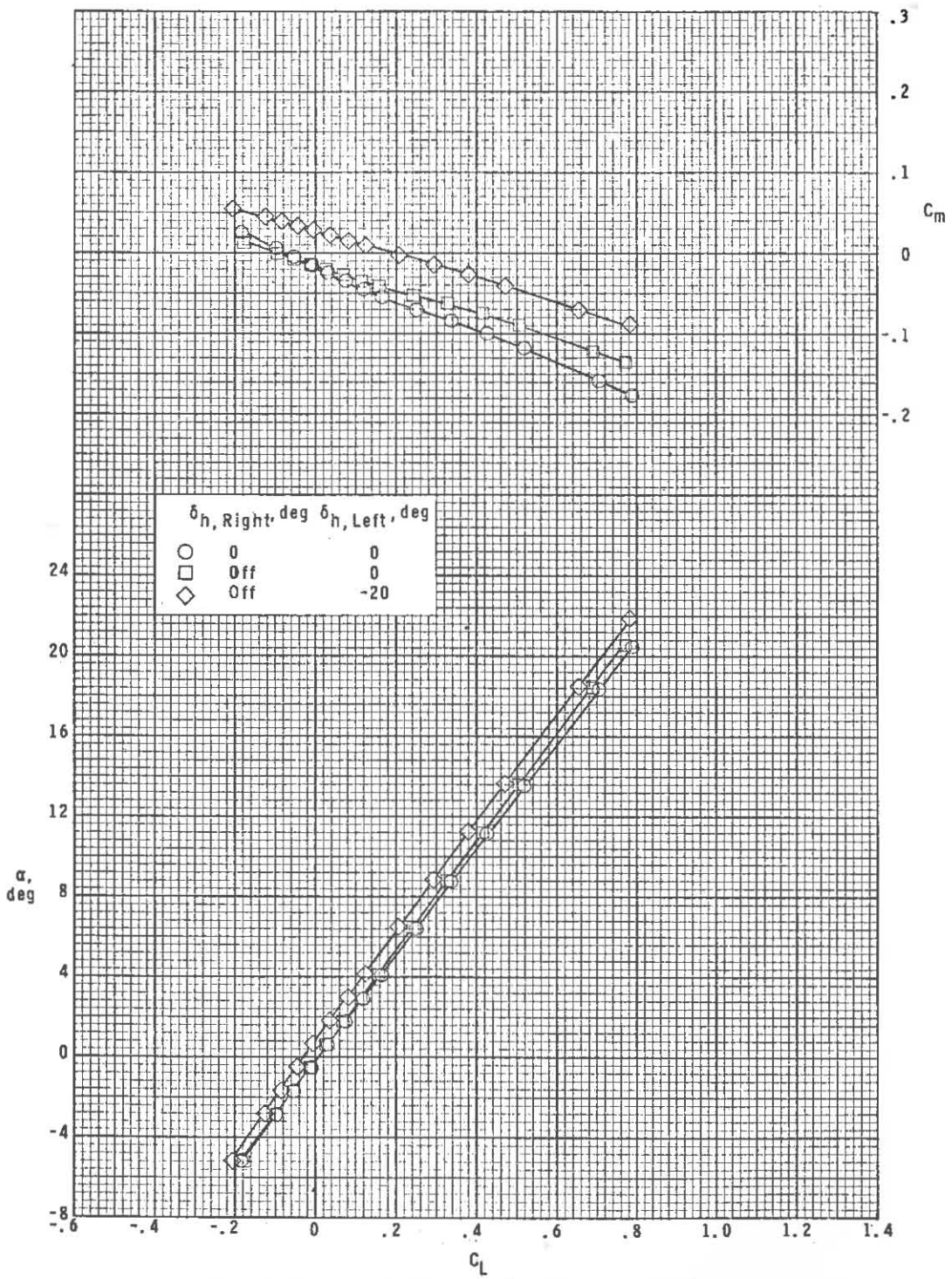

(b) M = 2.86.

Figure 5.- Continued.

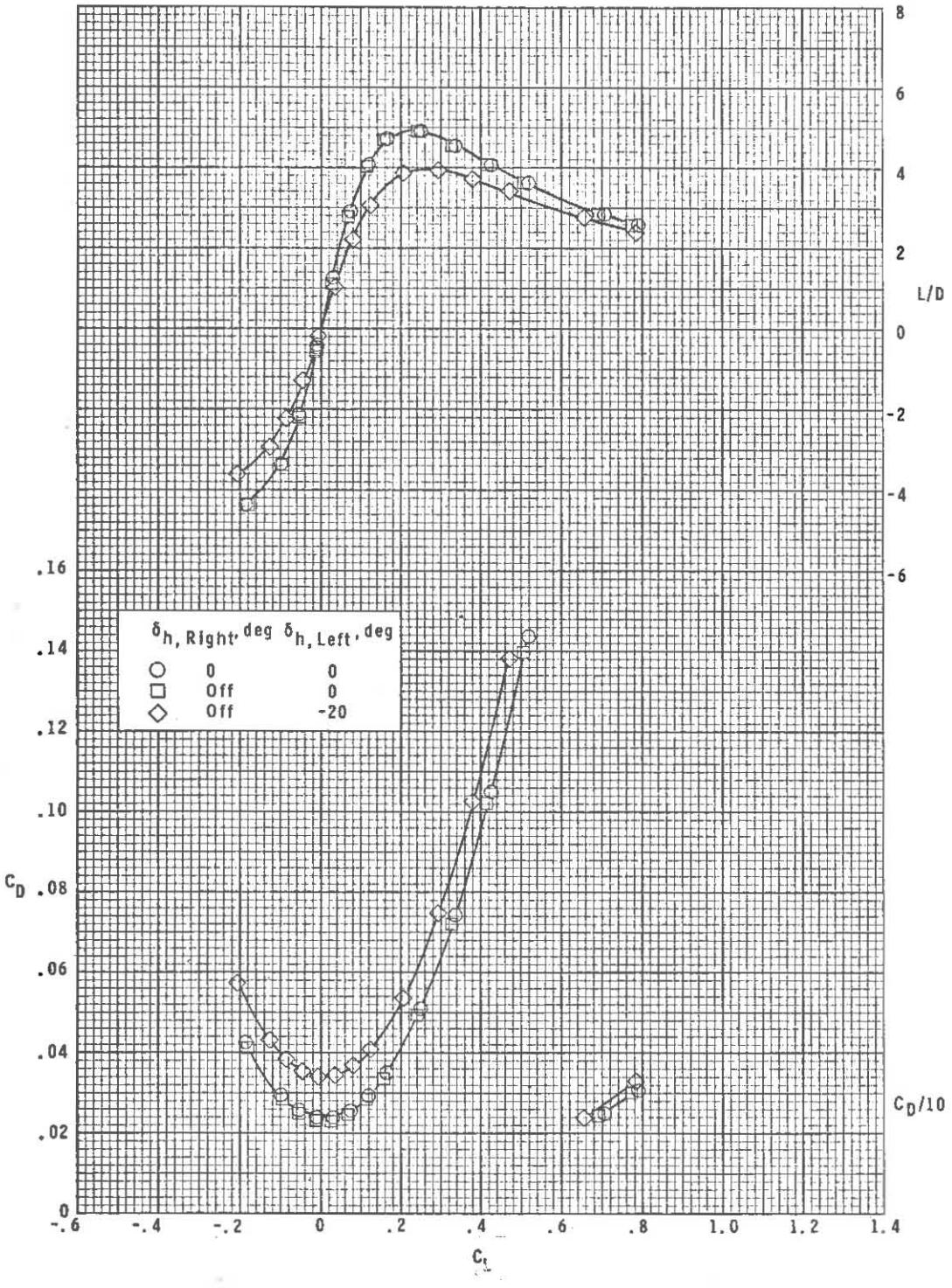

(b) Concluded.

Figure 5.- Continued.

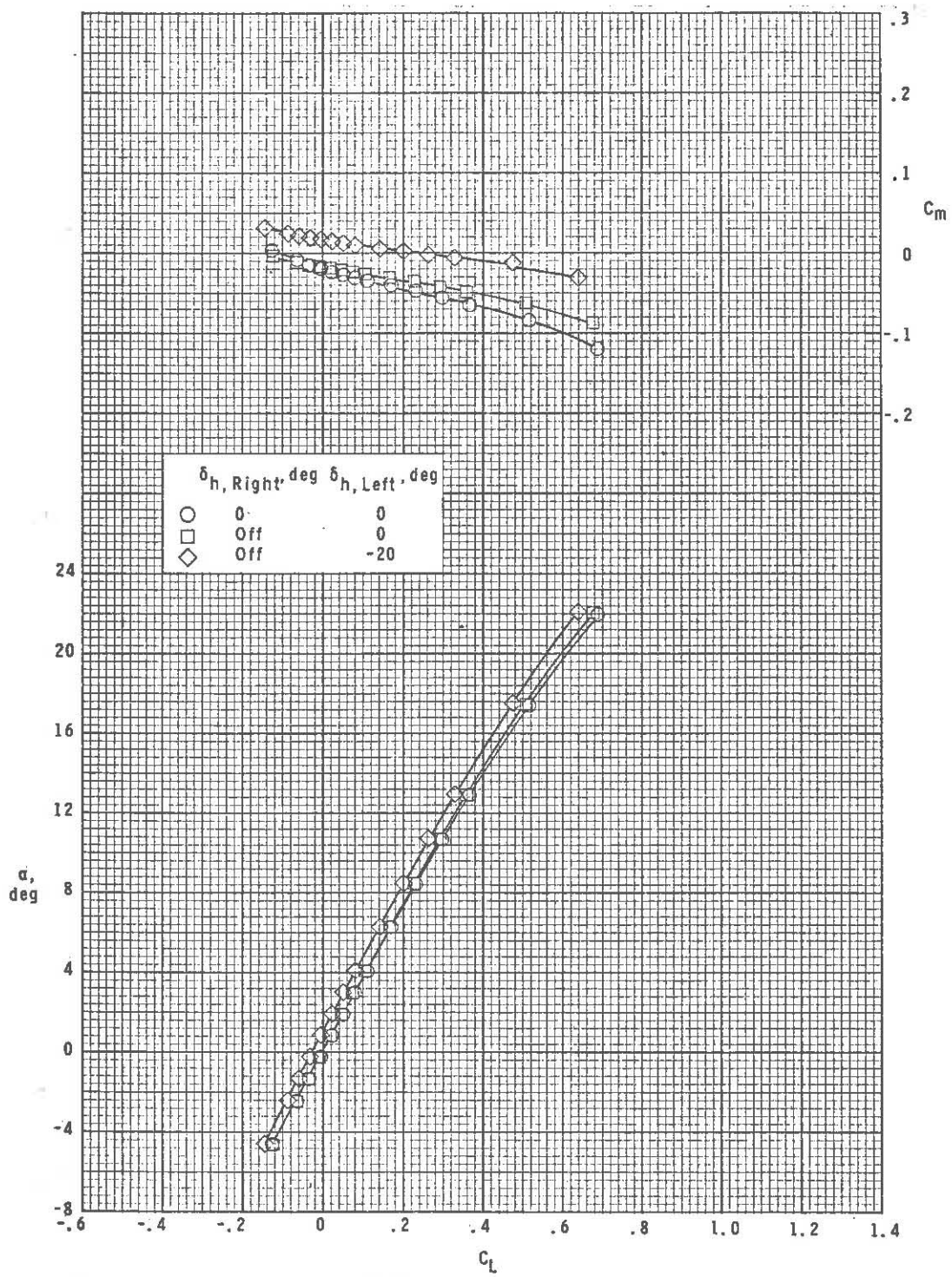

(c) M = 3.95.

Figure 5.- Continued.

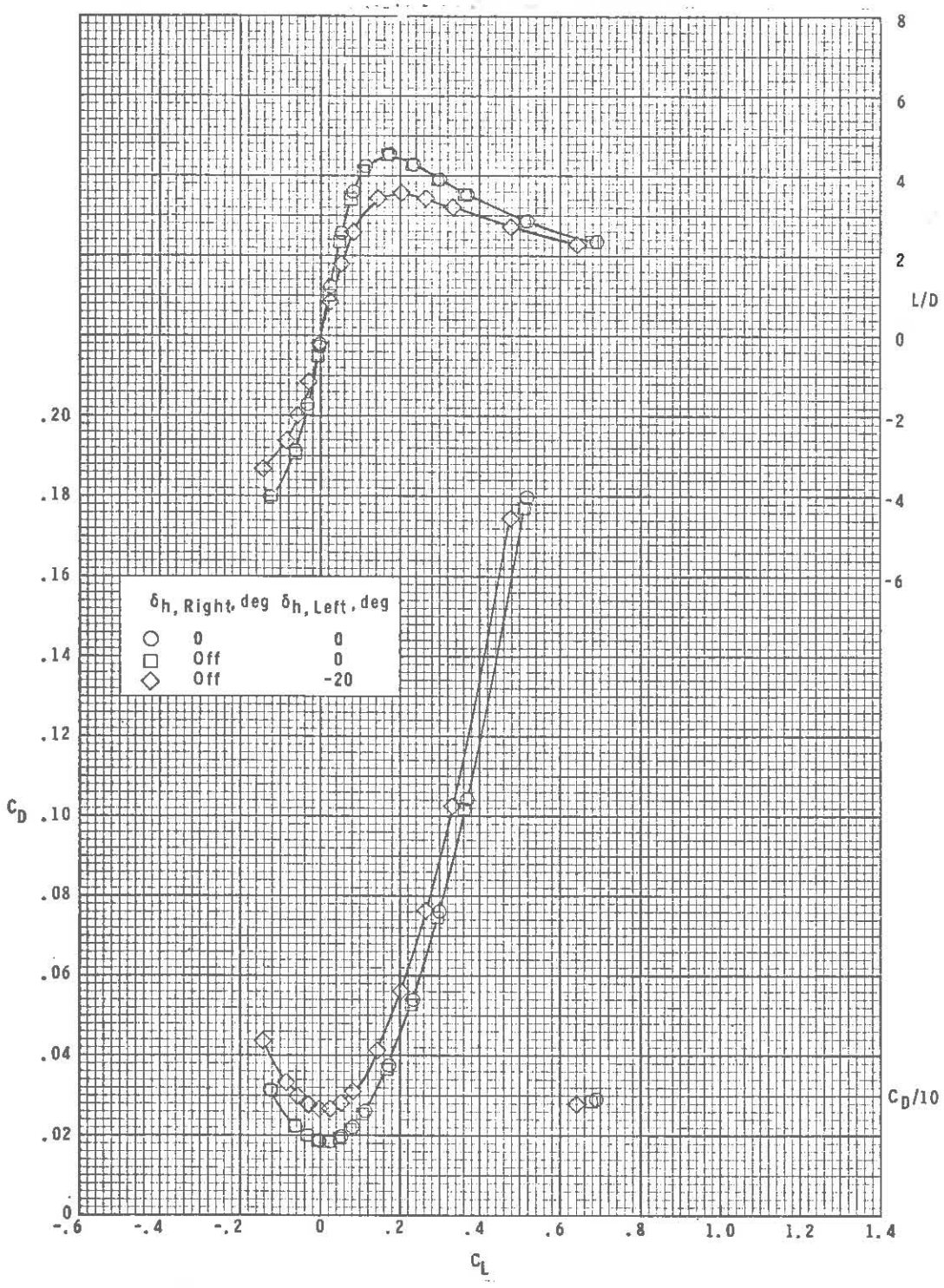

(c) Concluded.

Figure 5.- Continued.

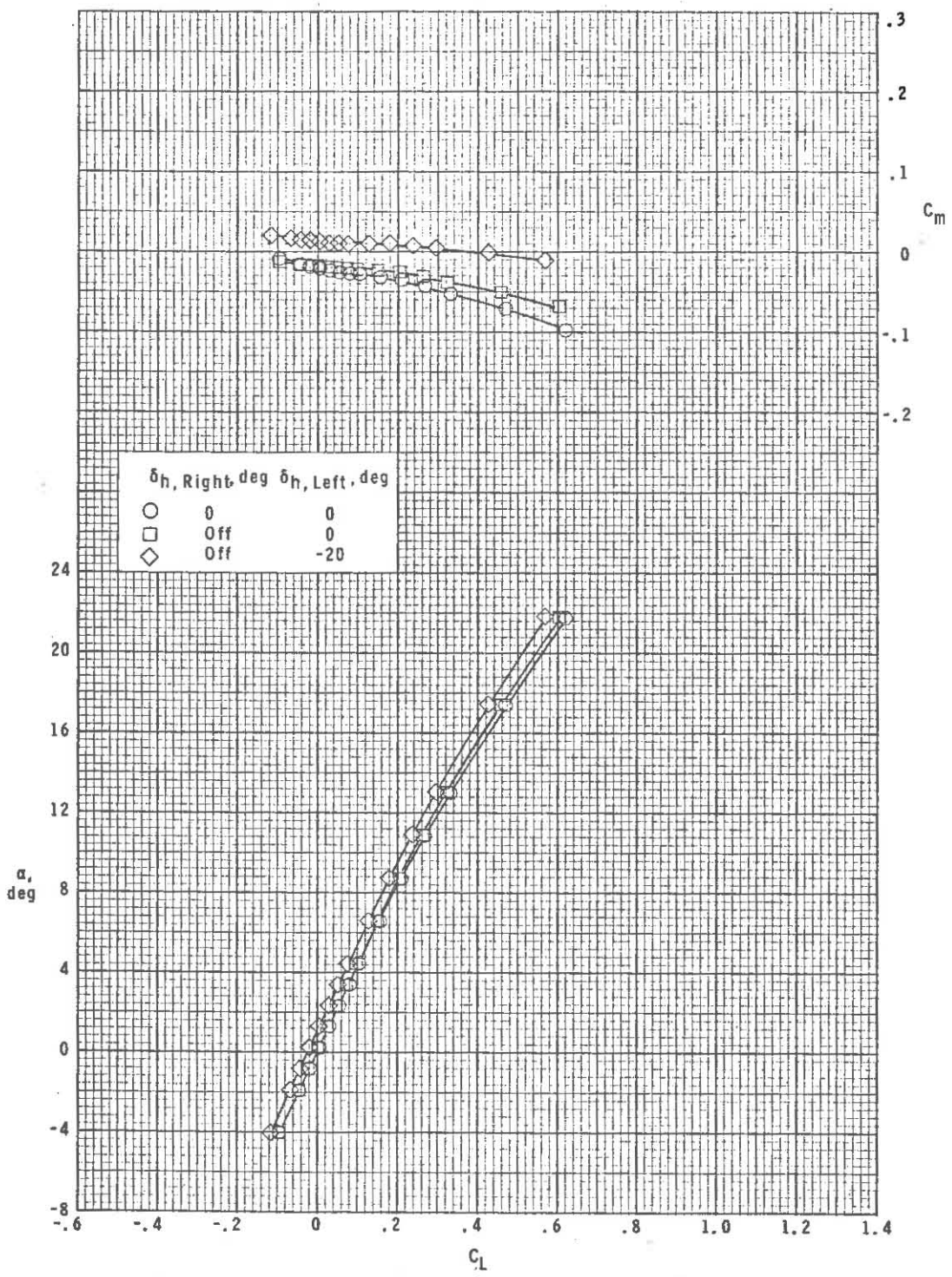

(d) M = 4.63.

Figure 5.- Continued.

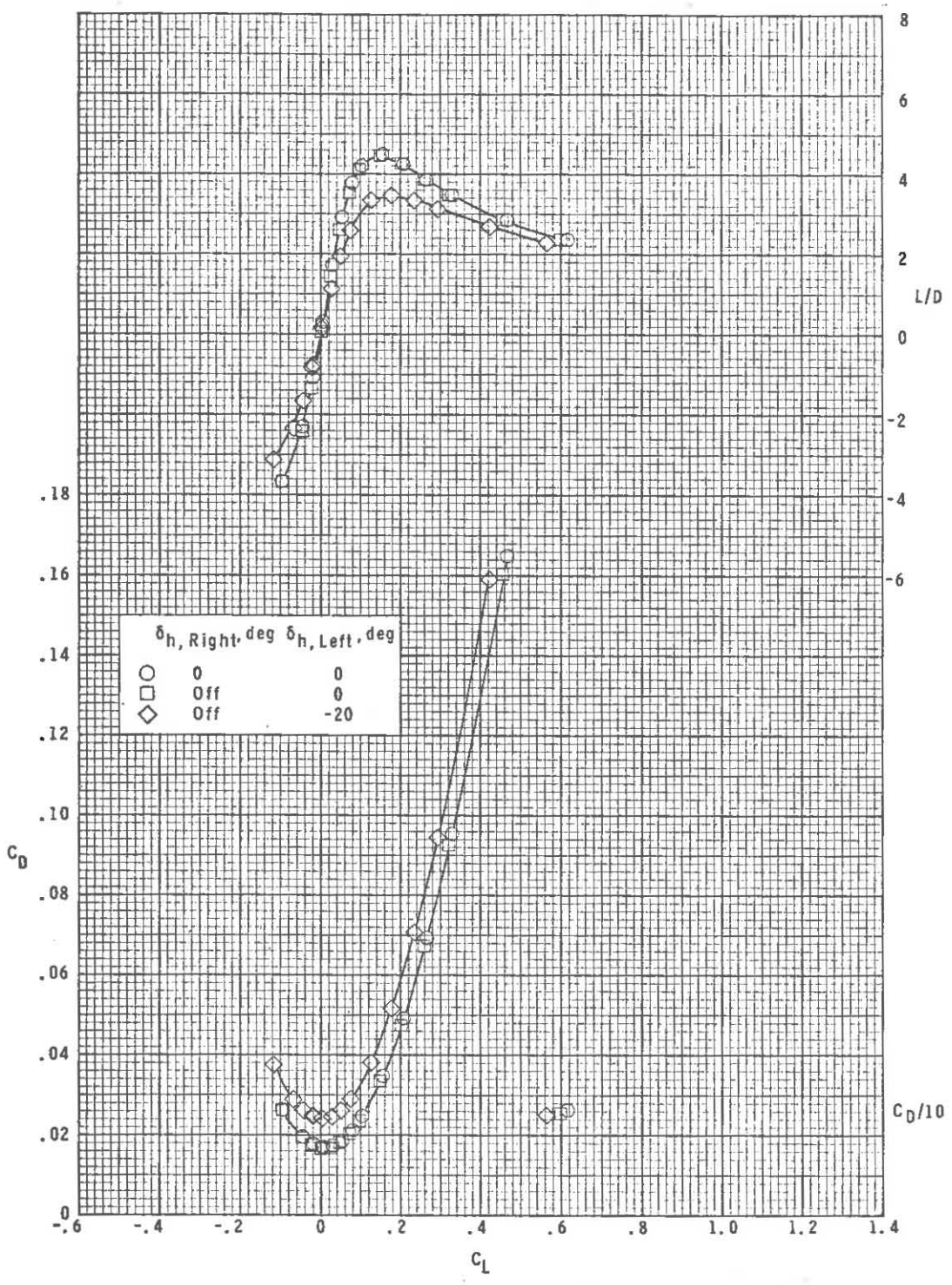

(d) Concluded.

Figure 5.- Concluded.

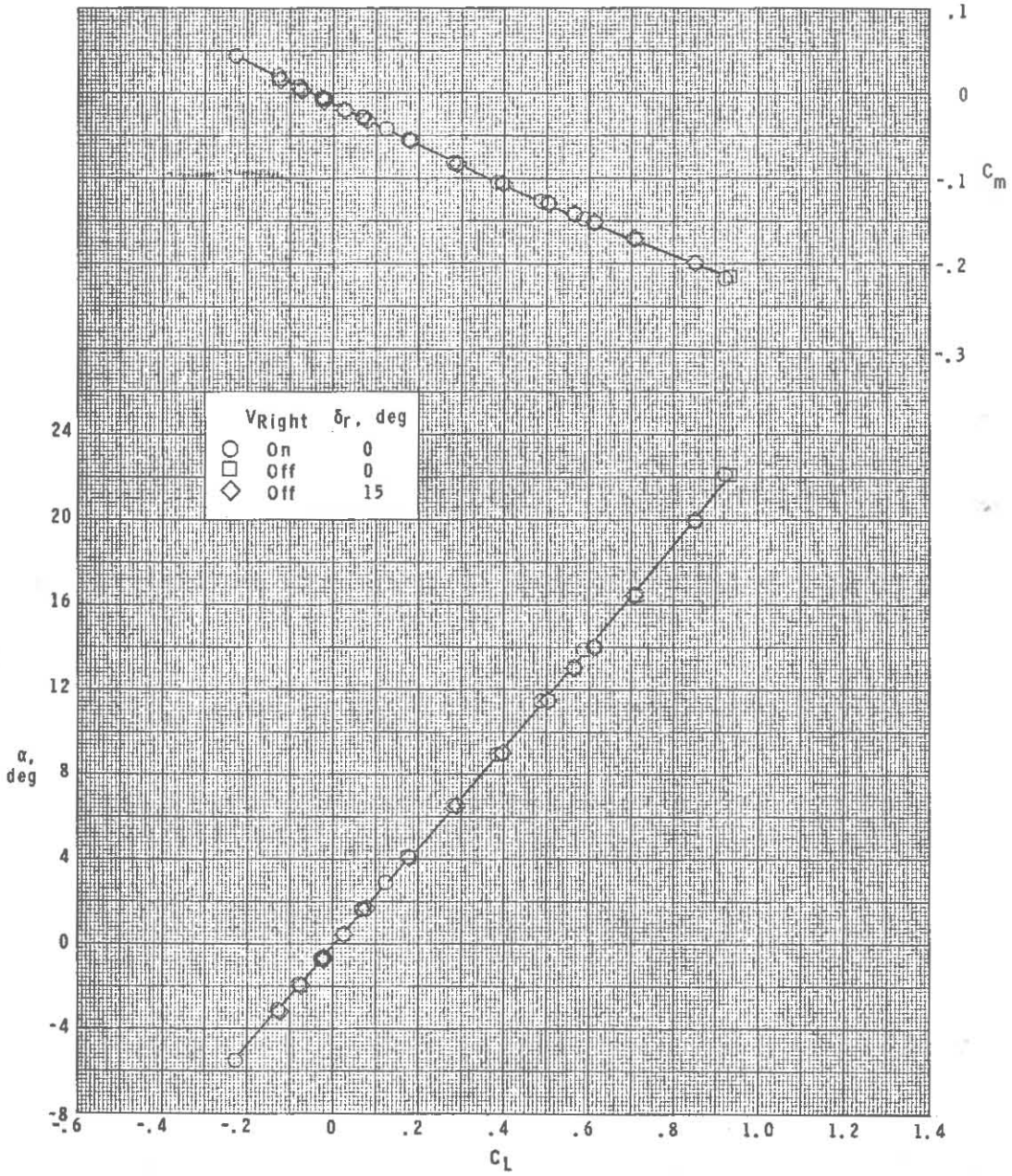

(a) M = 2.50.

Figure 6.- Longitudinal aerodynamic characteristics for asymmetric vertical-tail condition.

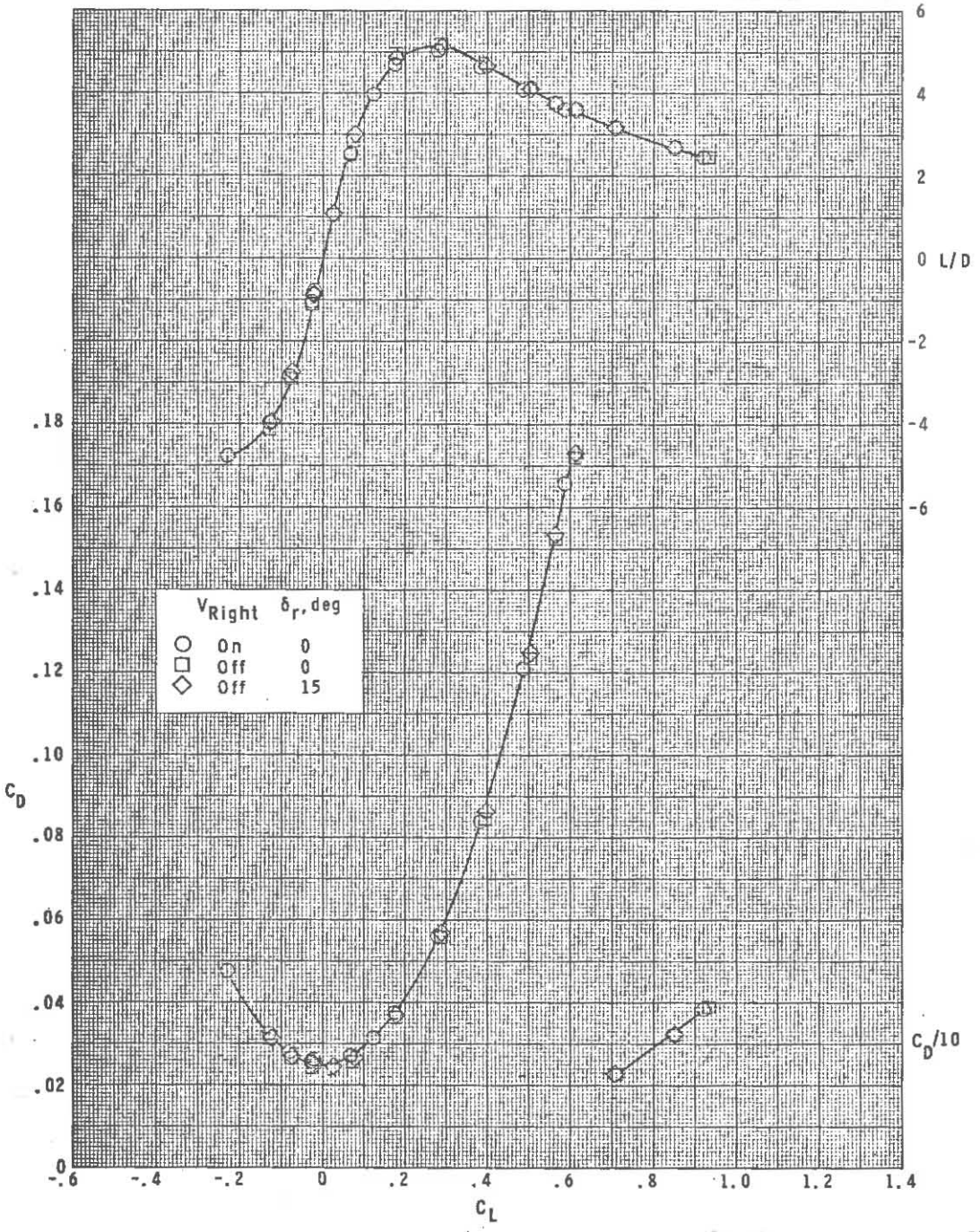

(a) Concluded.

Figure 6.- Continued.

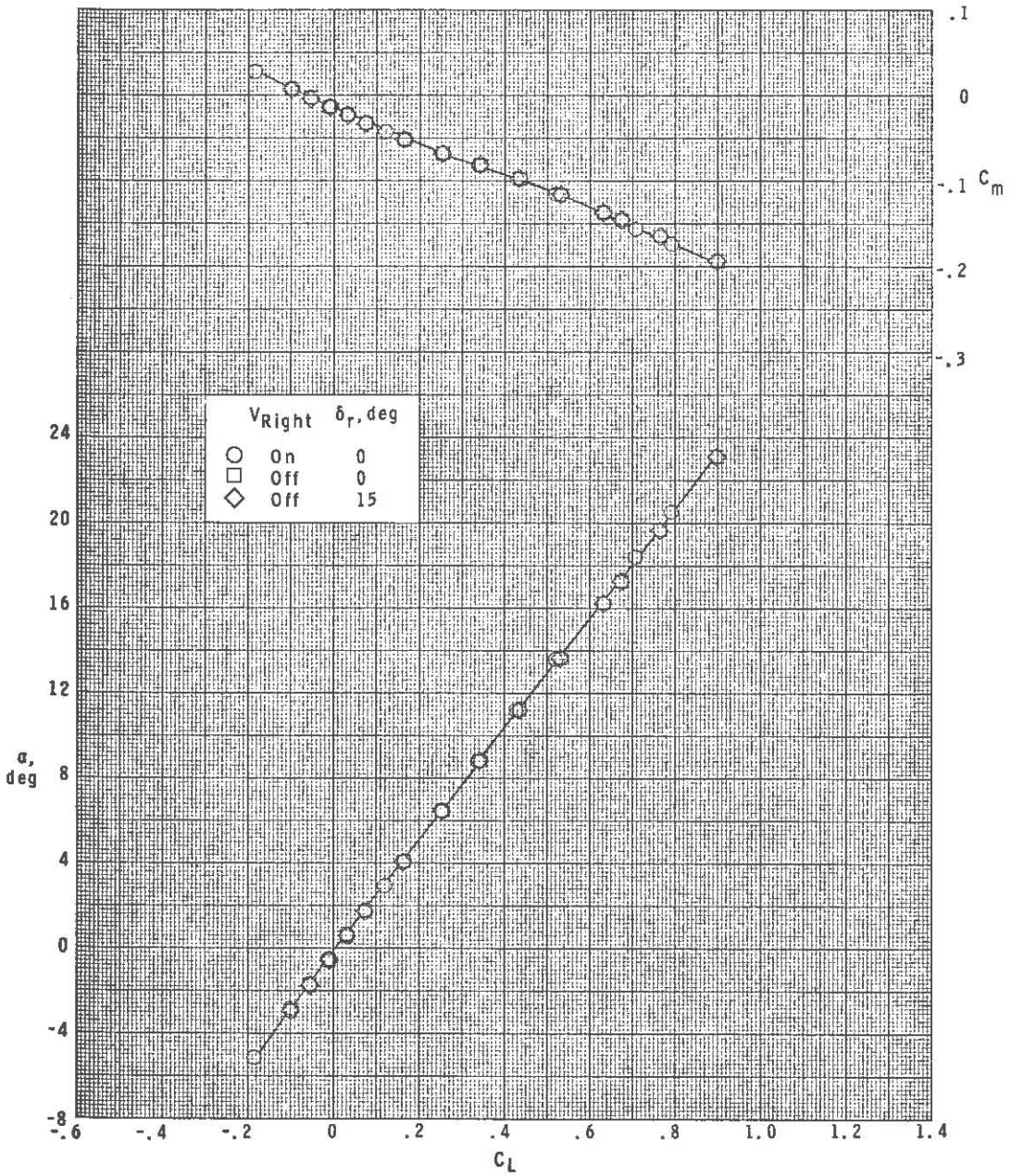

(b) M = 2.86.

Figure 6.- Continued.

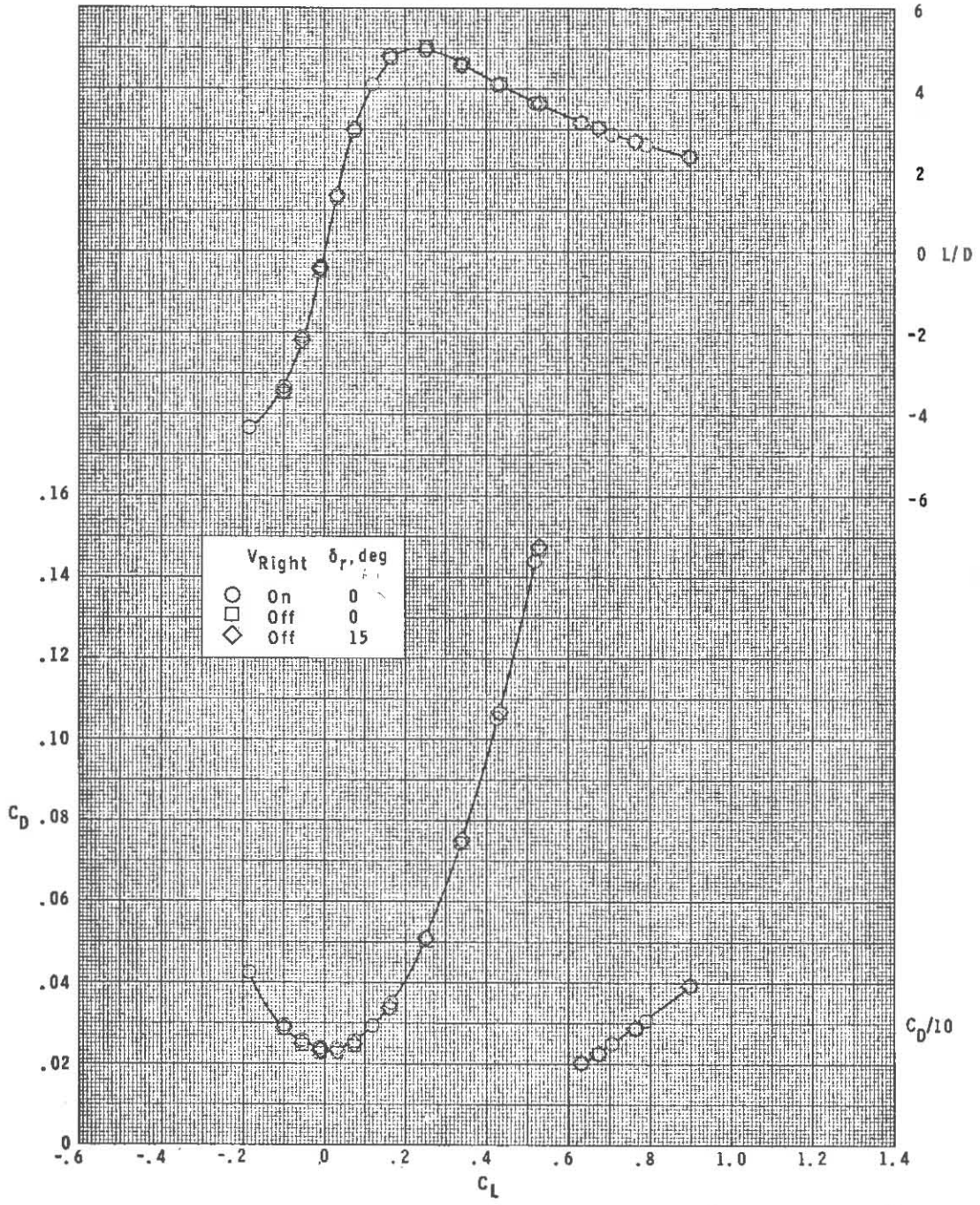

(b) Concluded.

Figure 6.- Continued.

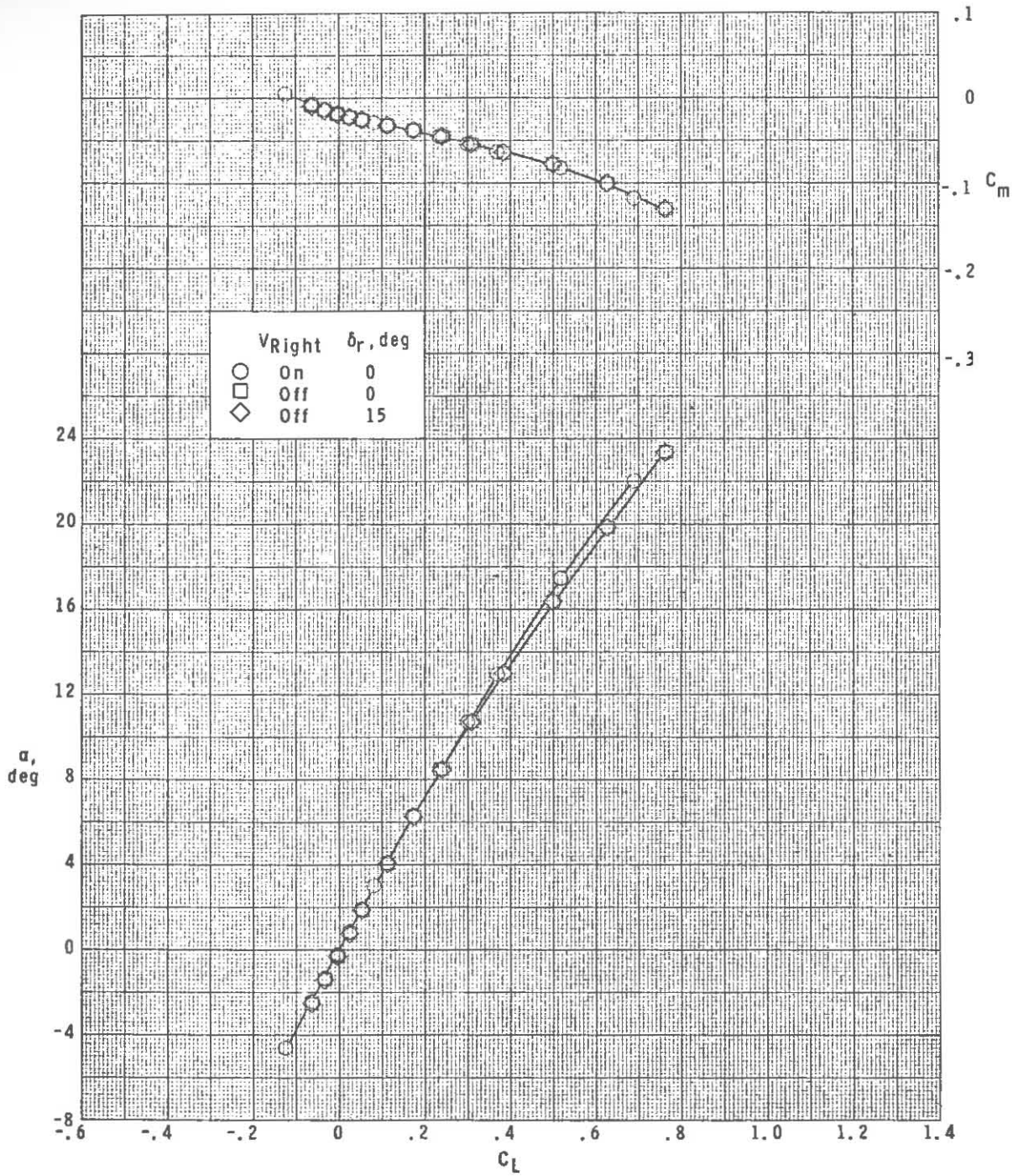

(c) M = 3.95.

Figure 6.- Continued.

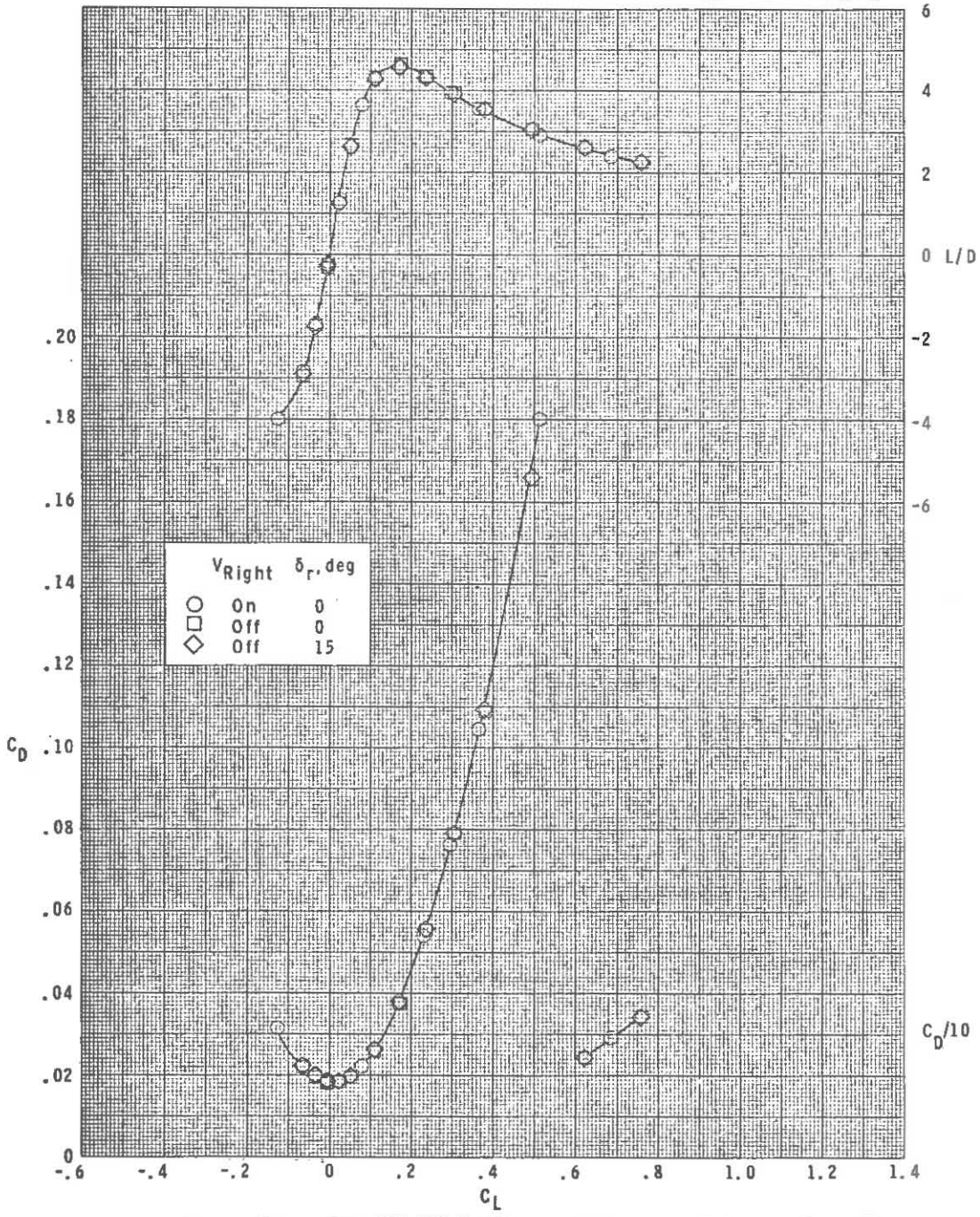

(c) Concluded.

Figure 6.- Continued.

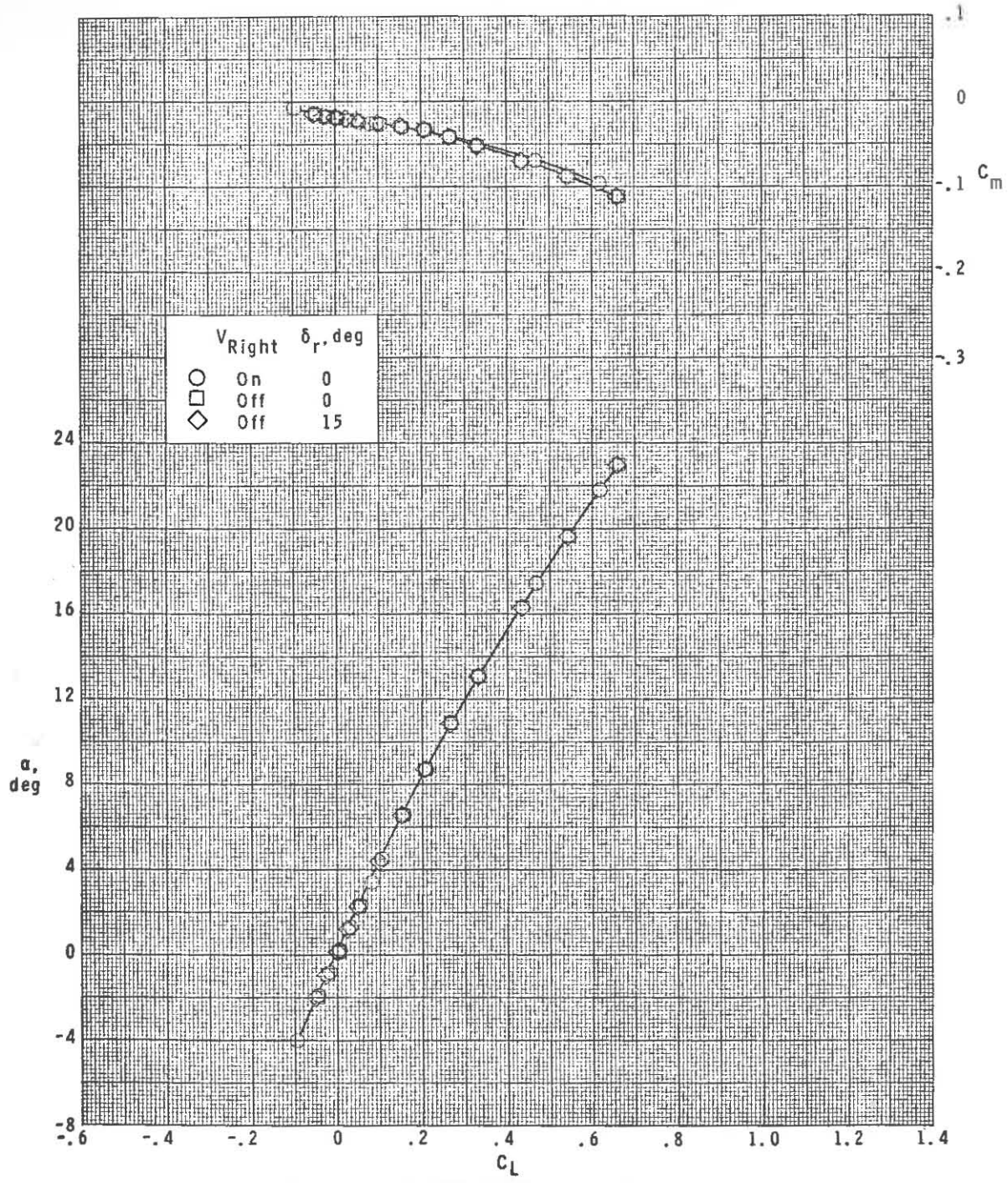

(d) M = 4.63.

Figure 6.- Continued.

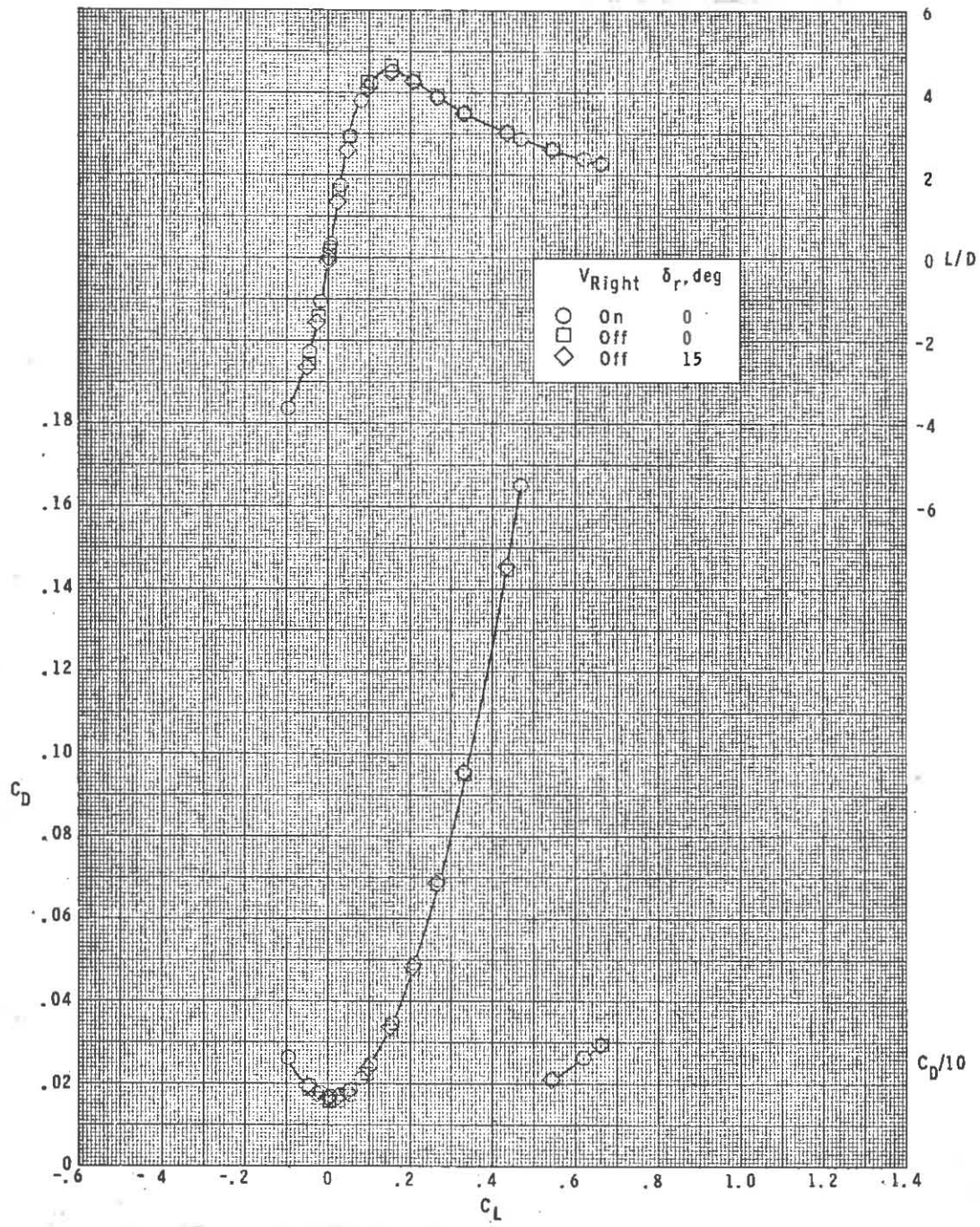

(d) Concluded.

Figure 6.- Concluded.

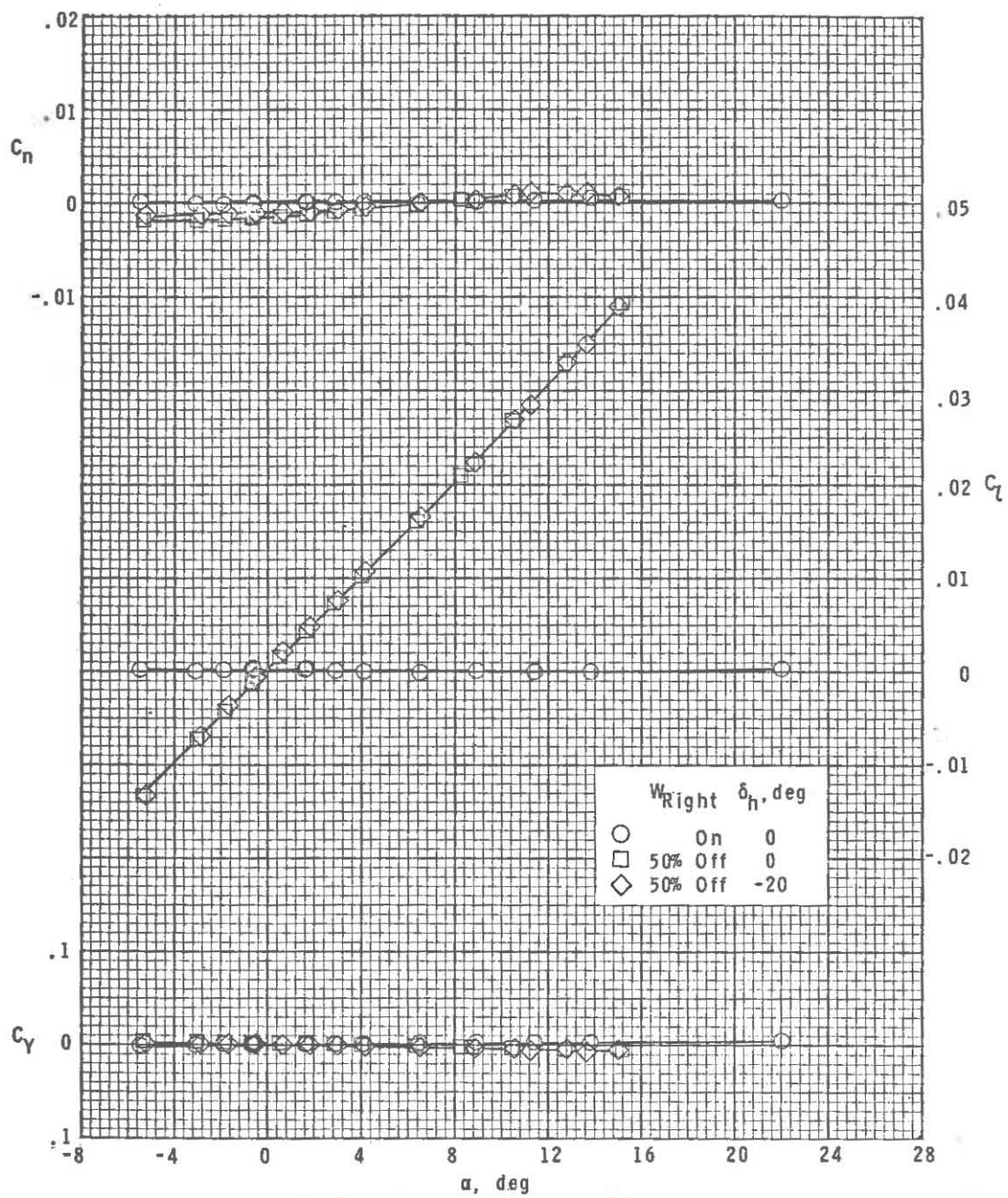

(a) M = 2.50.

Figure 7.- Variation of lateral aerodynamic characteristics with angle of attack for asymmetric wing condition and horizontal-tail control. $\beta = 0^o$.

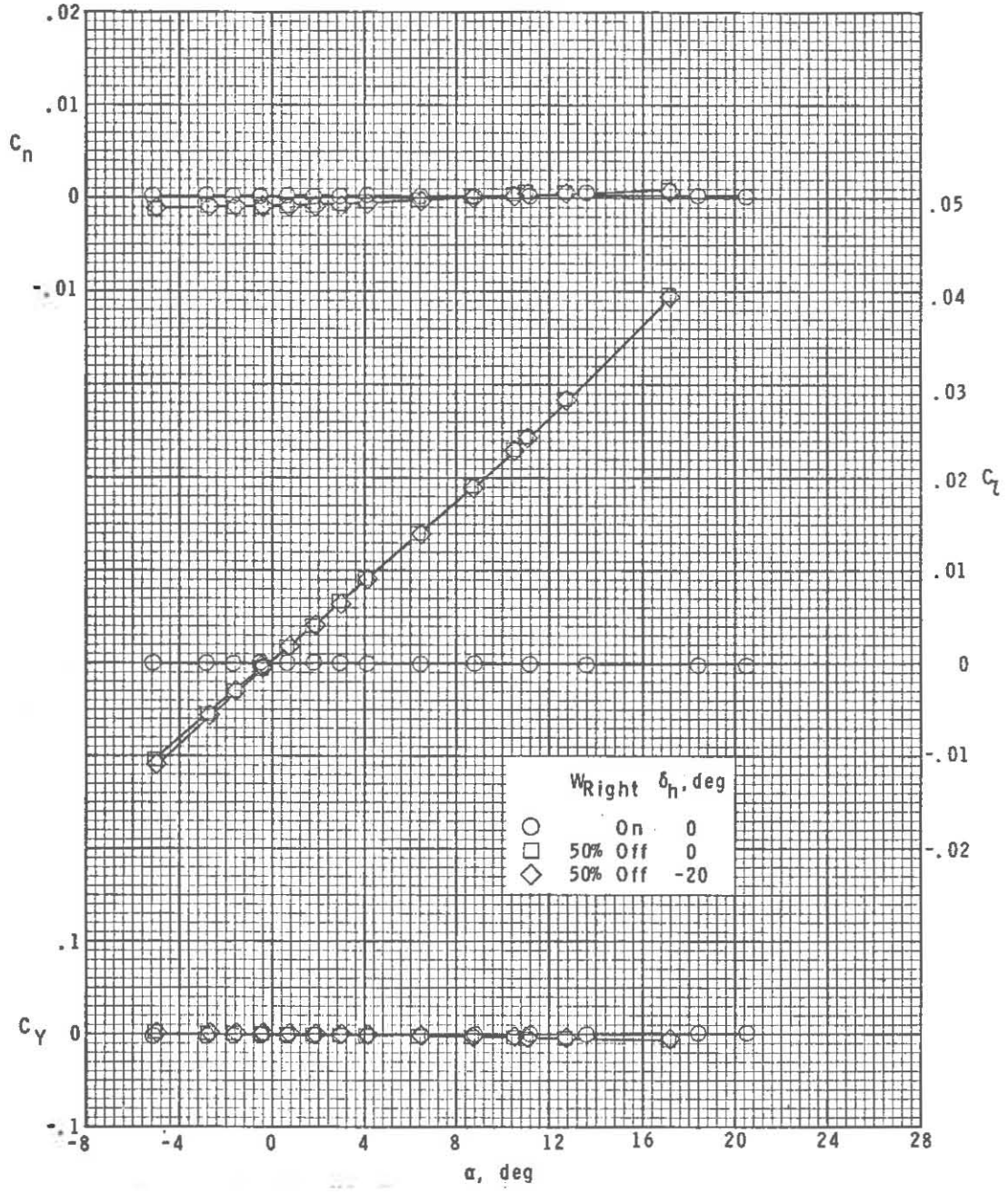

(b) M = 2.86.

Figure 7.- Continued.

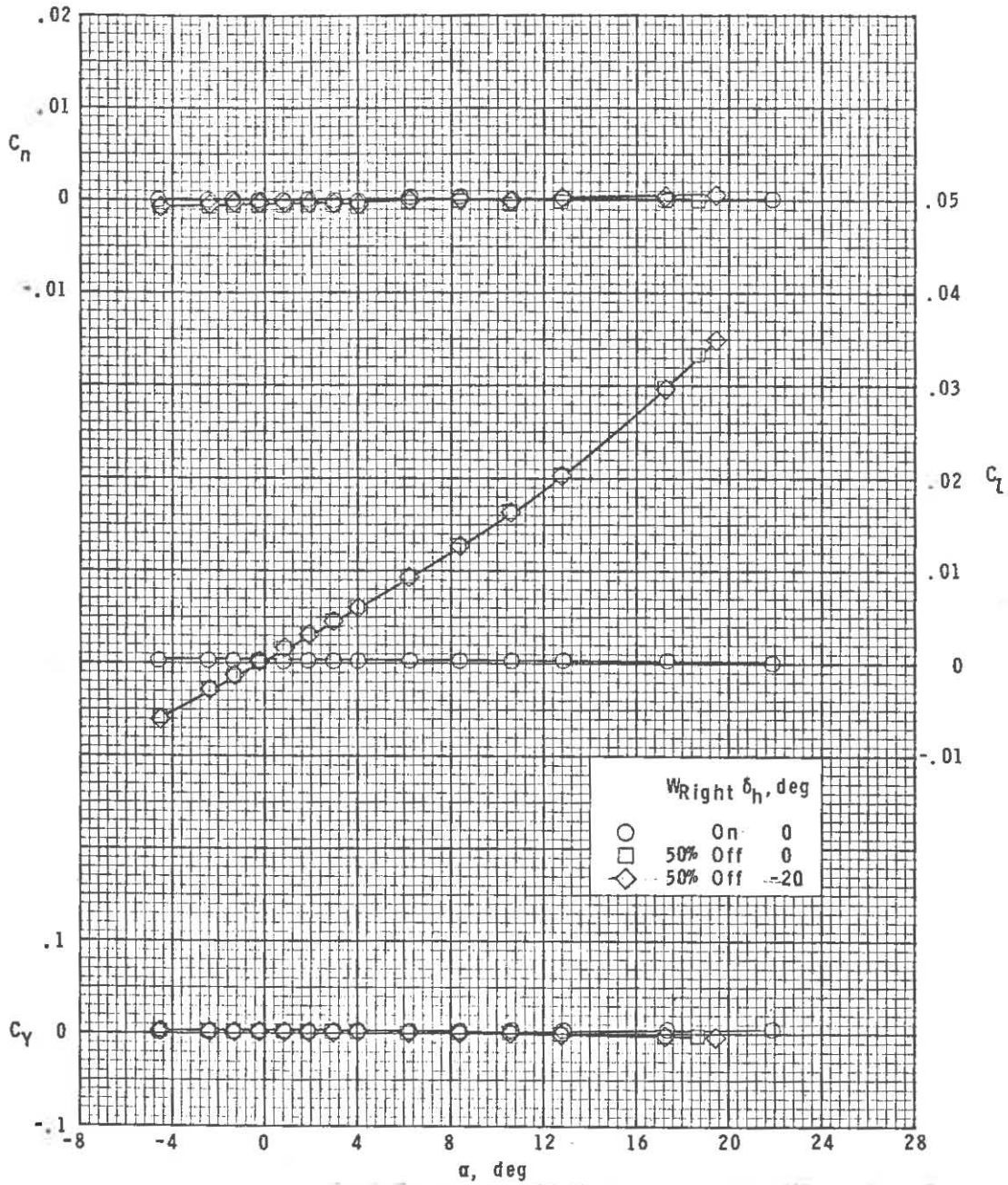

(c) M = 3.95.

Figure 7.- Continued.

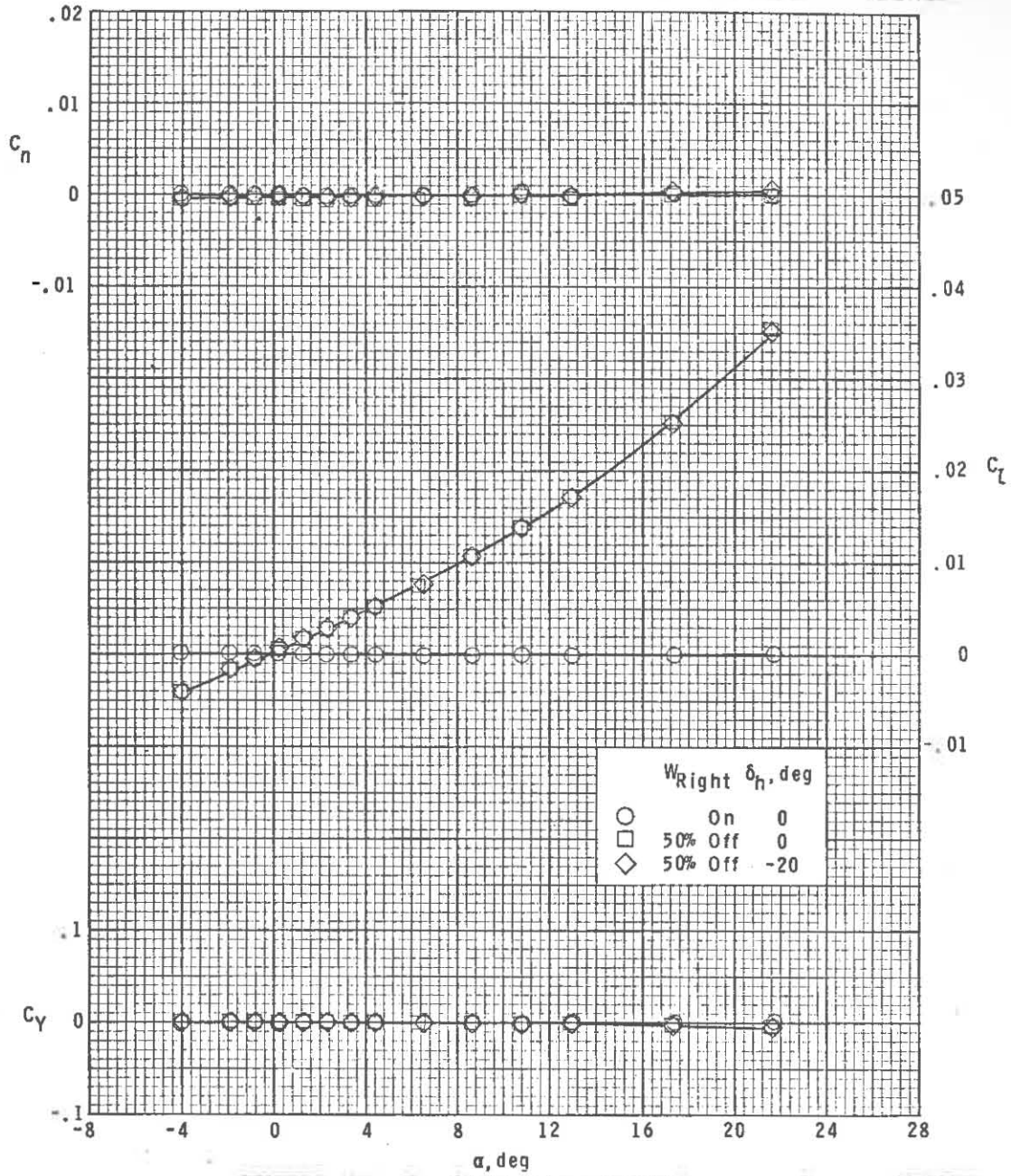

(d) M = 4.63.

Figure 7.- Concluded.

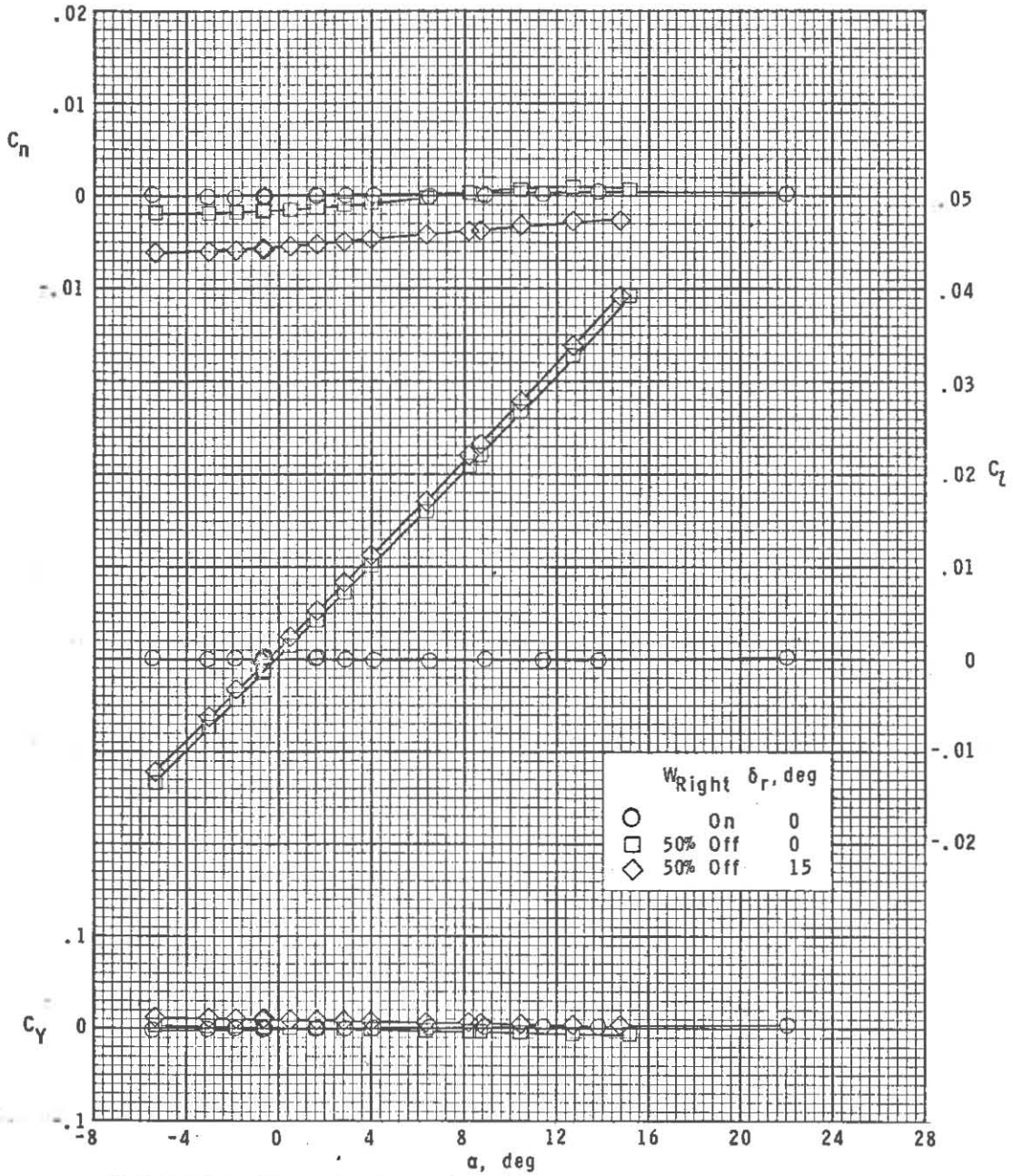

(a) M = 2.50.

Figure 8.- Variation of lateral aerodynamic characteristics with angle of attack for asymmetric wing condition and rudder control. $\beta = 0^{o}$.

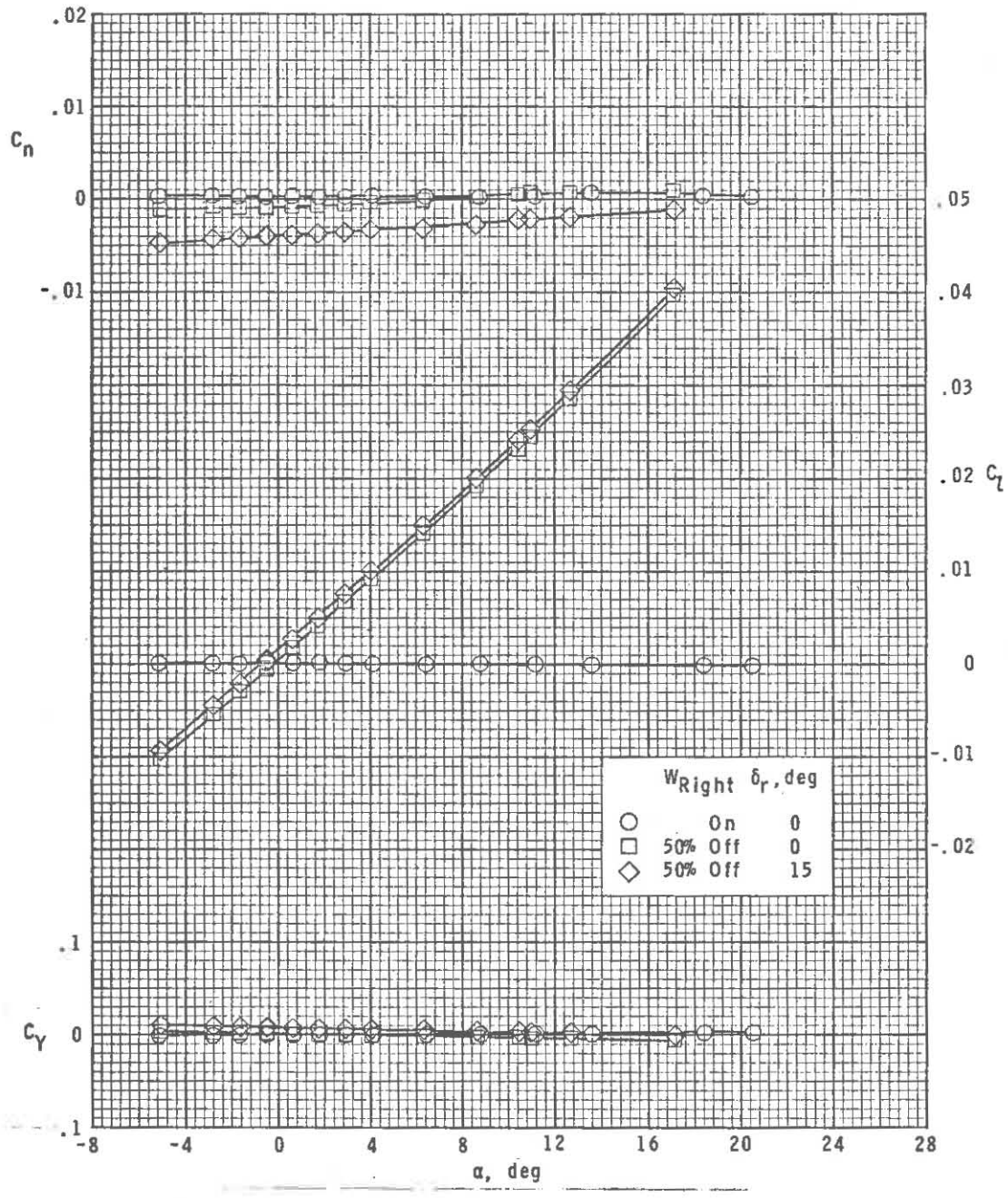

(b) M = 2.86.

Figure 8.- Continued.

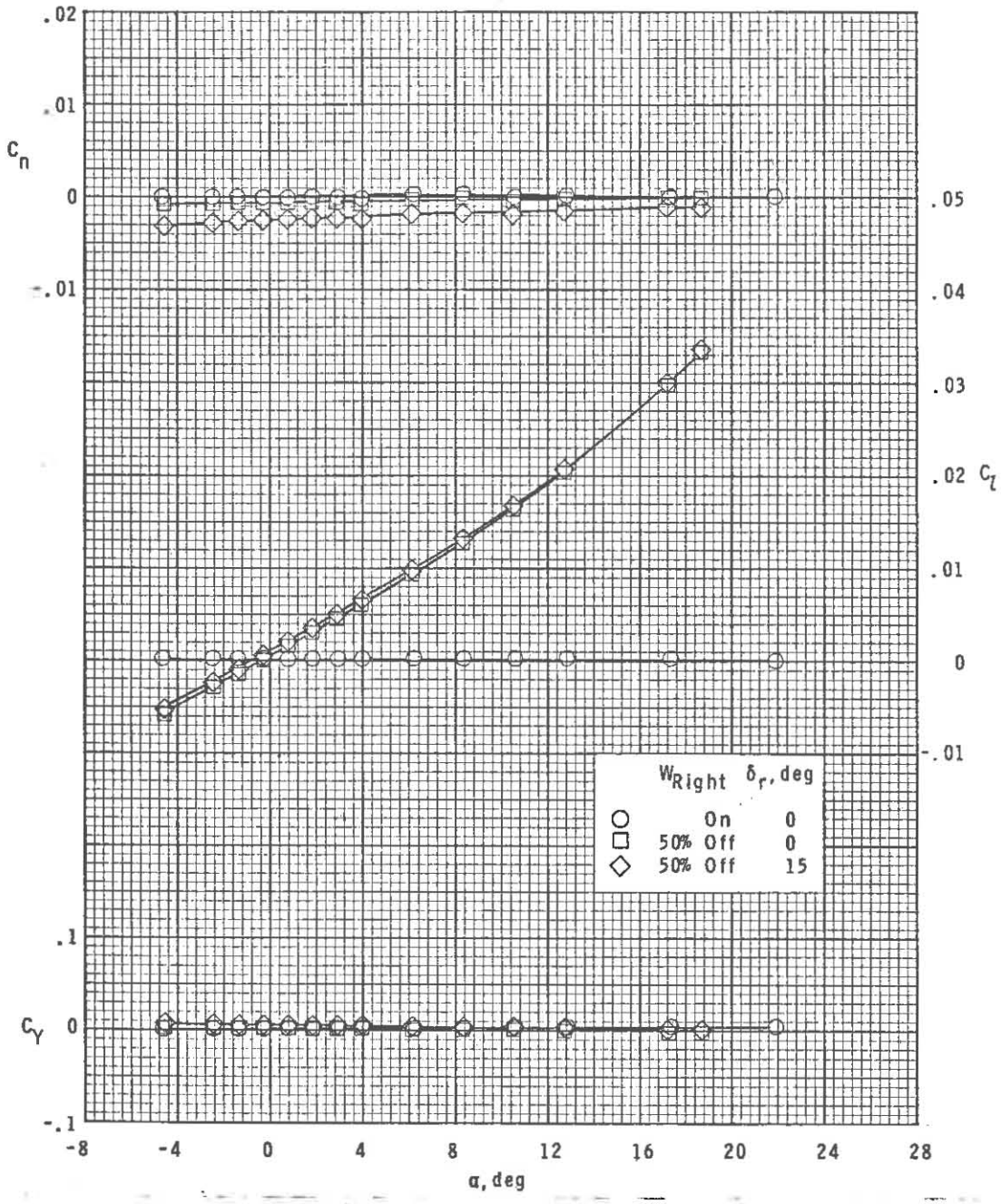

(c) M = 3.95.

Figure 8.- Continued.

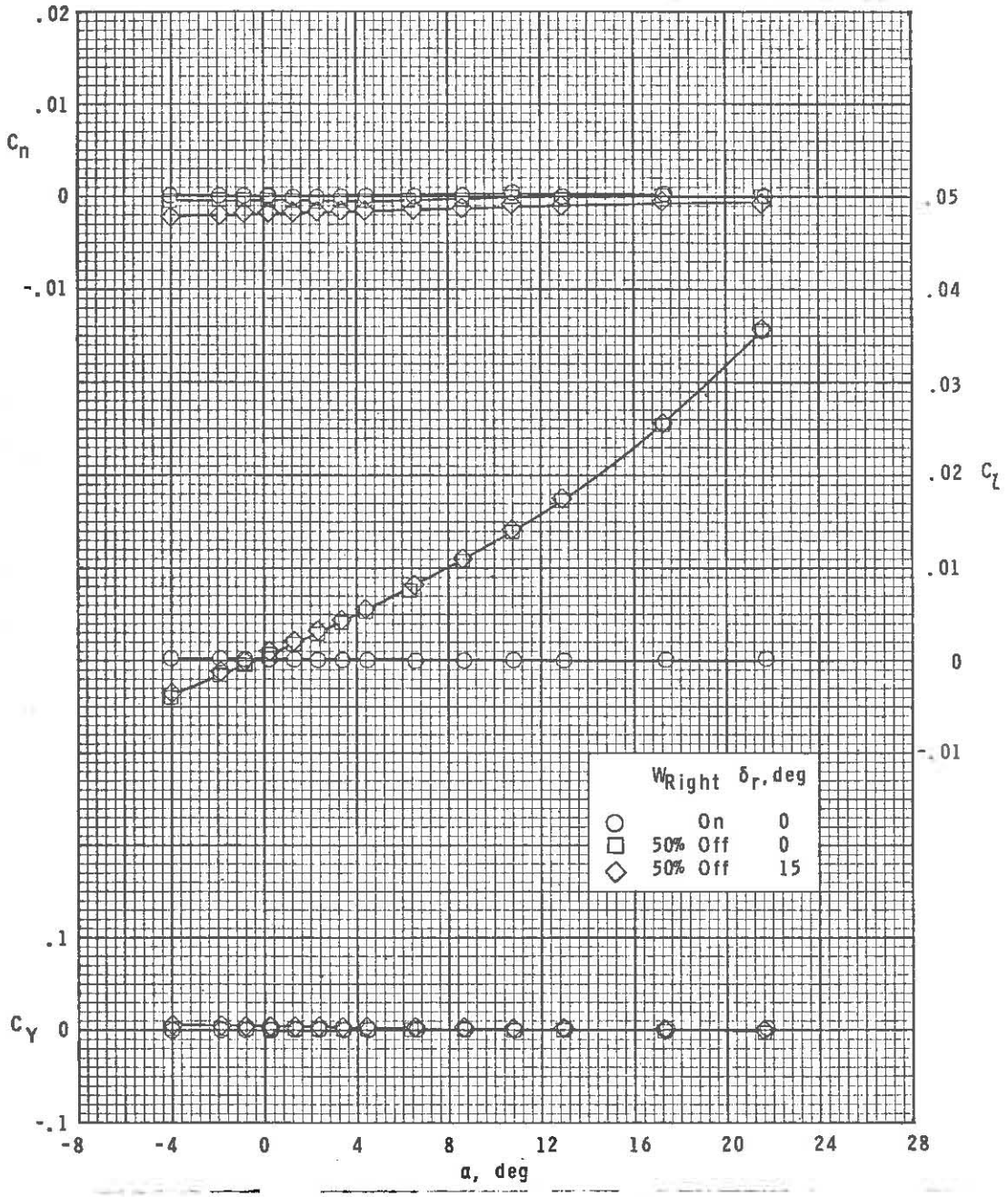

(d) M = 4.63.

Figure 8.- Concluded.

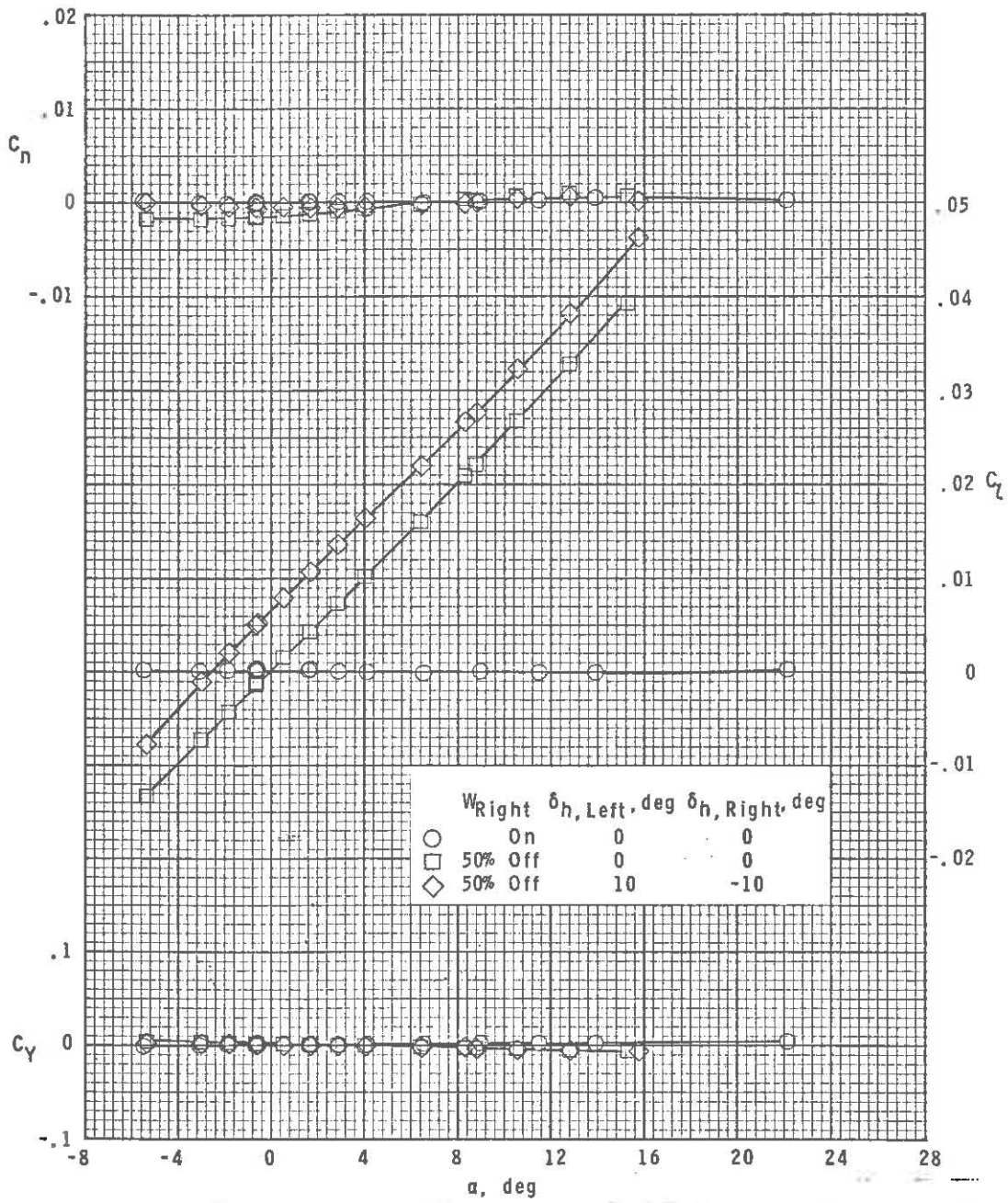

(a) M = 2.50.

Figure 9.- Variation of lateral aerodynamic characteristics with angle of attack for asymmetric wing condition and differential horizontal-tail settings. $\beta = 0^{o}$.

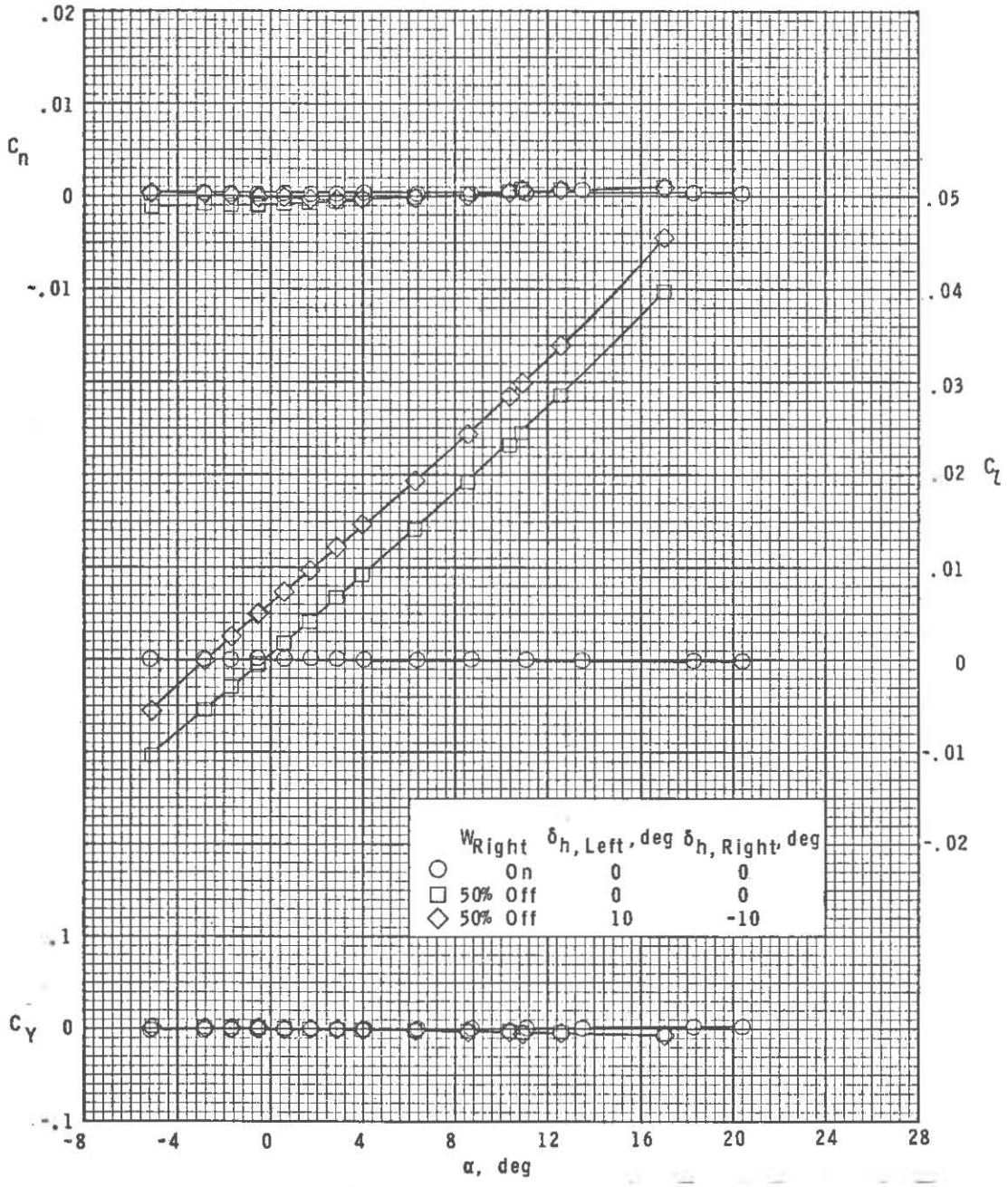

(b) M = 2.86.

Figure 9.- Continued.

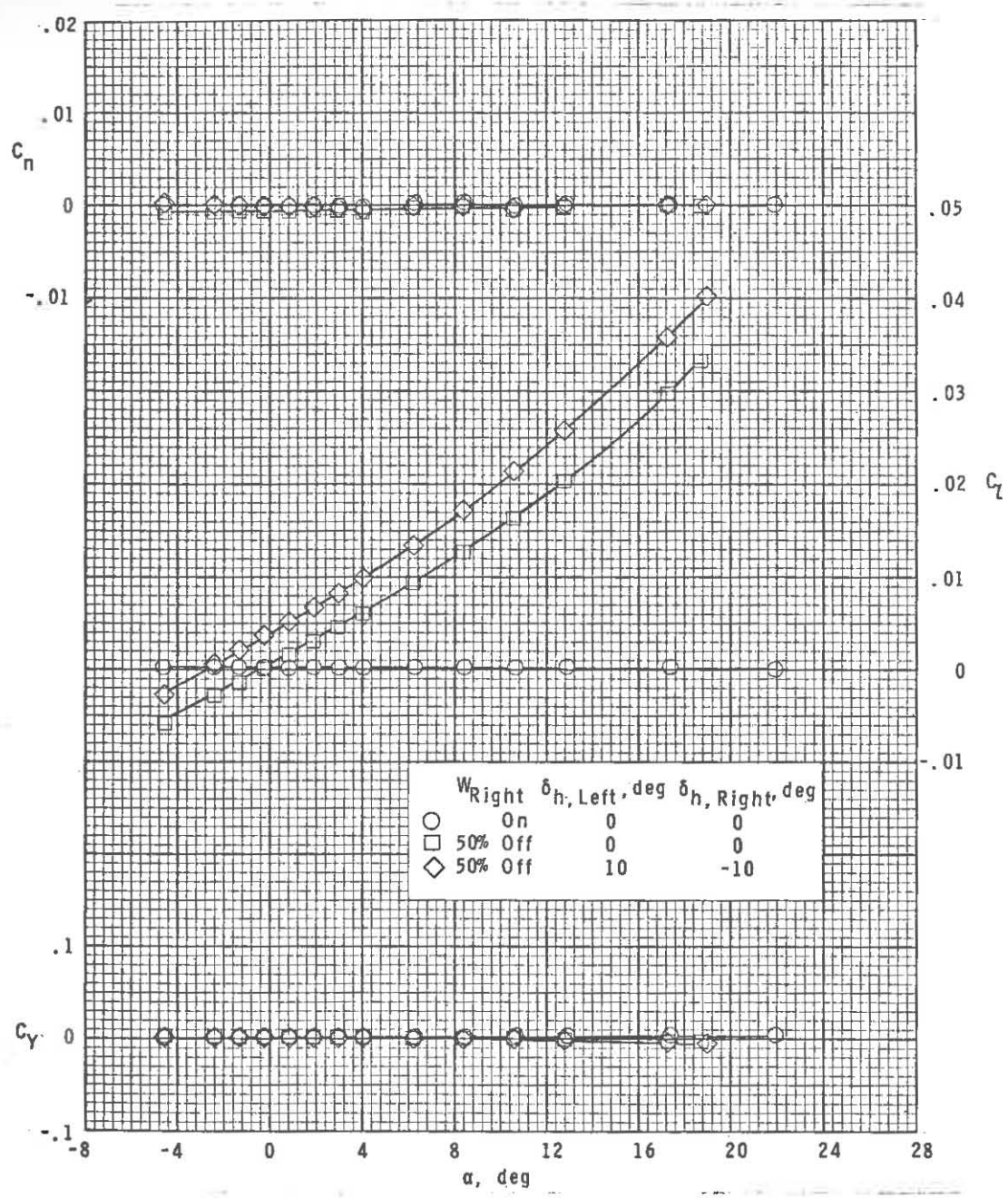

(c) M = 3.95.

Figure 9.- Continued.

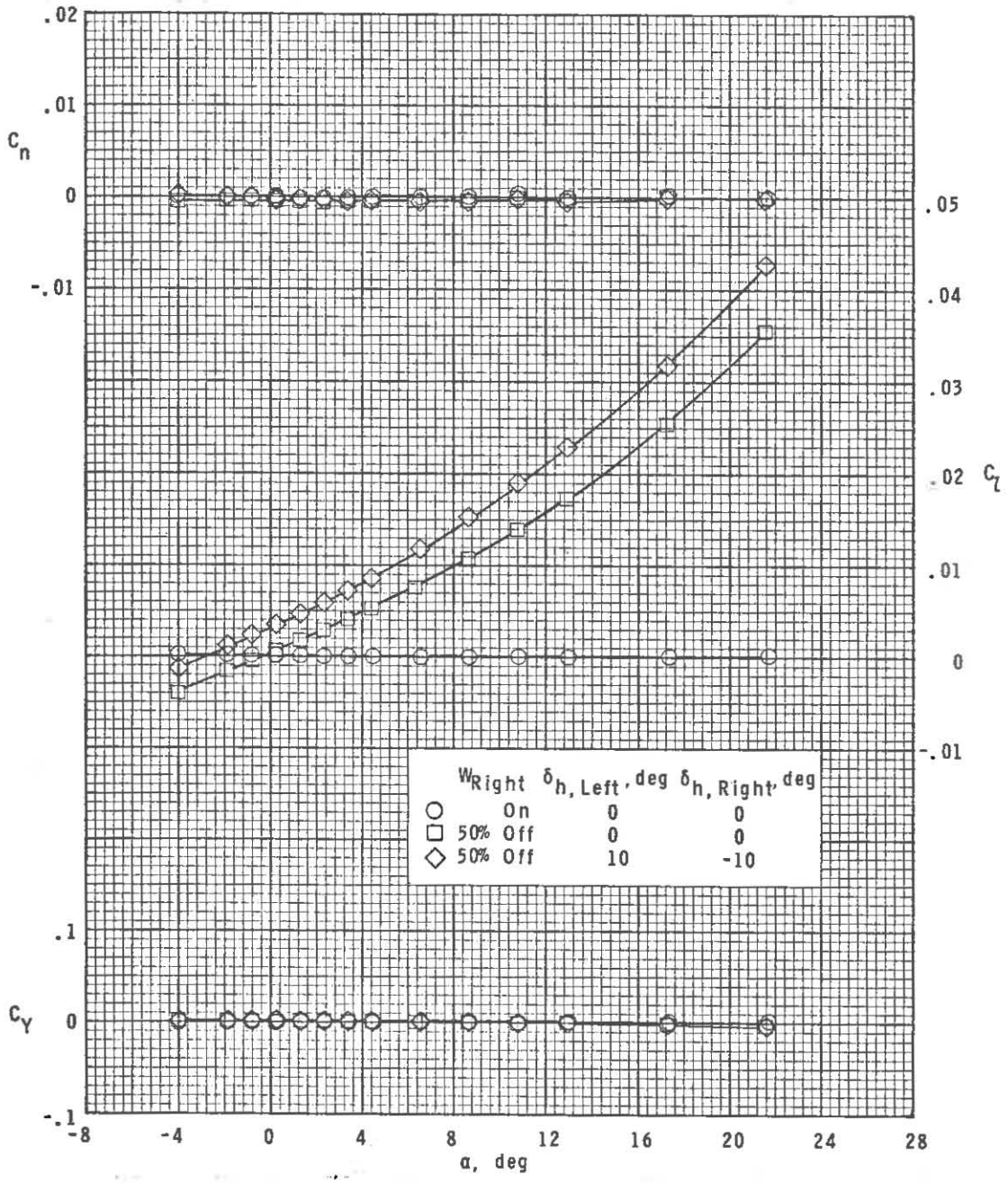

(d) M = 4.63.

Figure 9.- Concluded.

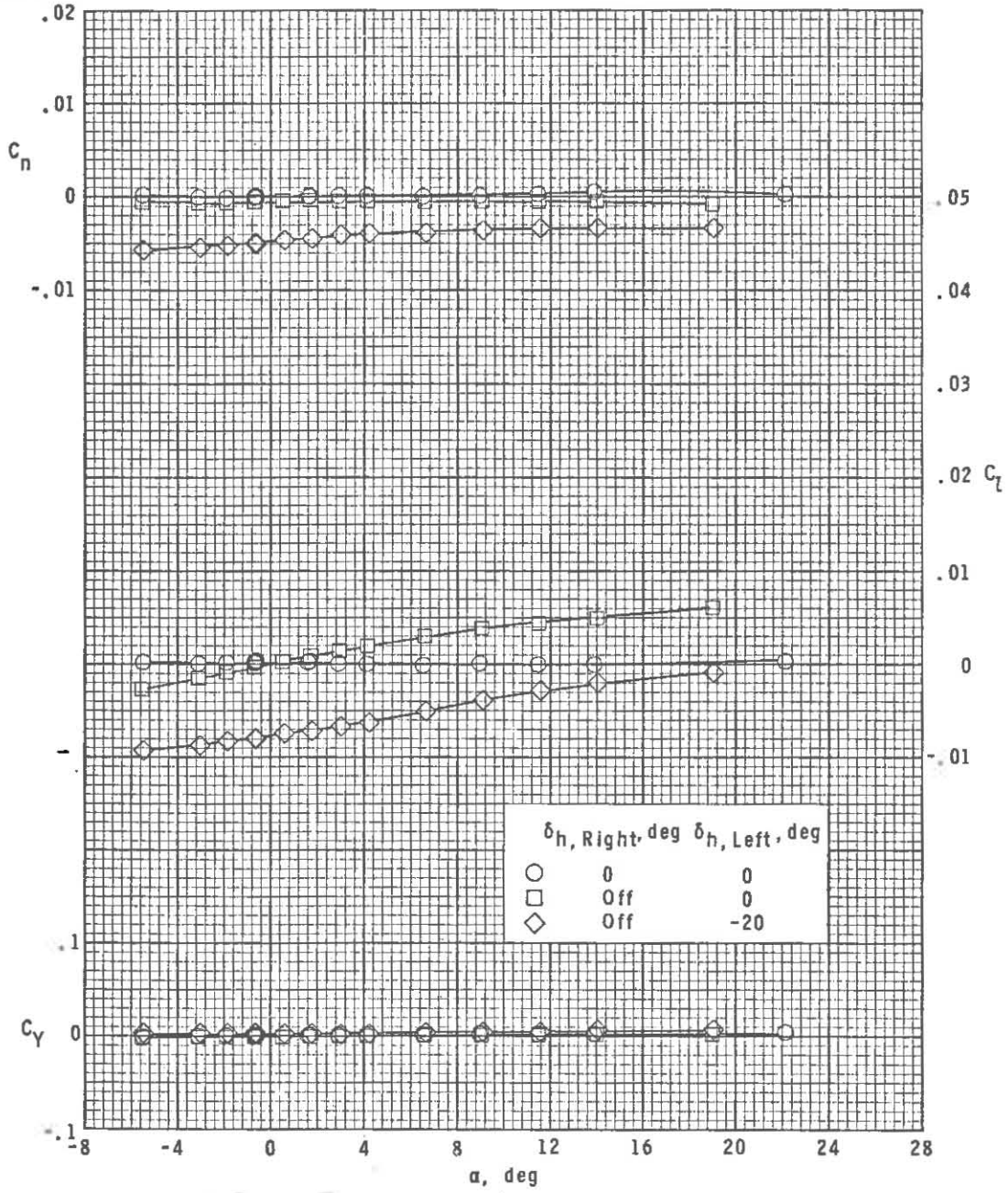

(a) M = 2.50.

Figure 10.- Variation of lateral aerodynamic characteristics with angle of attack for asymmetric horizontal-tail condition. $\beta = 0^{o}$.

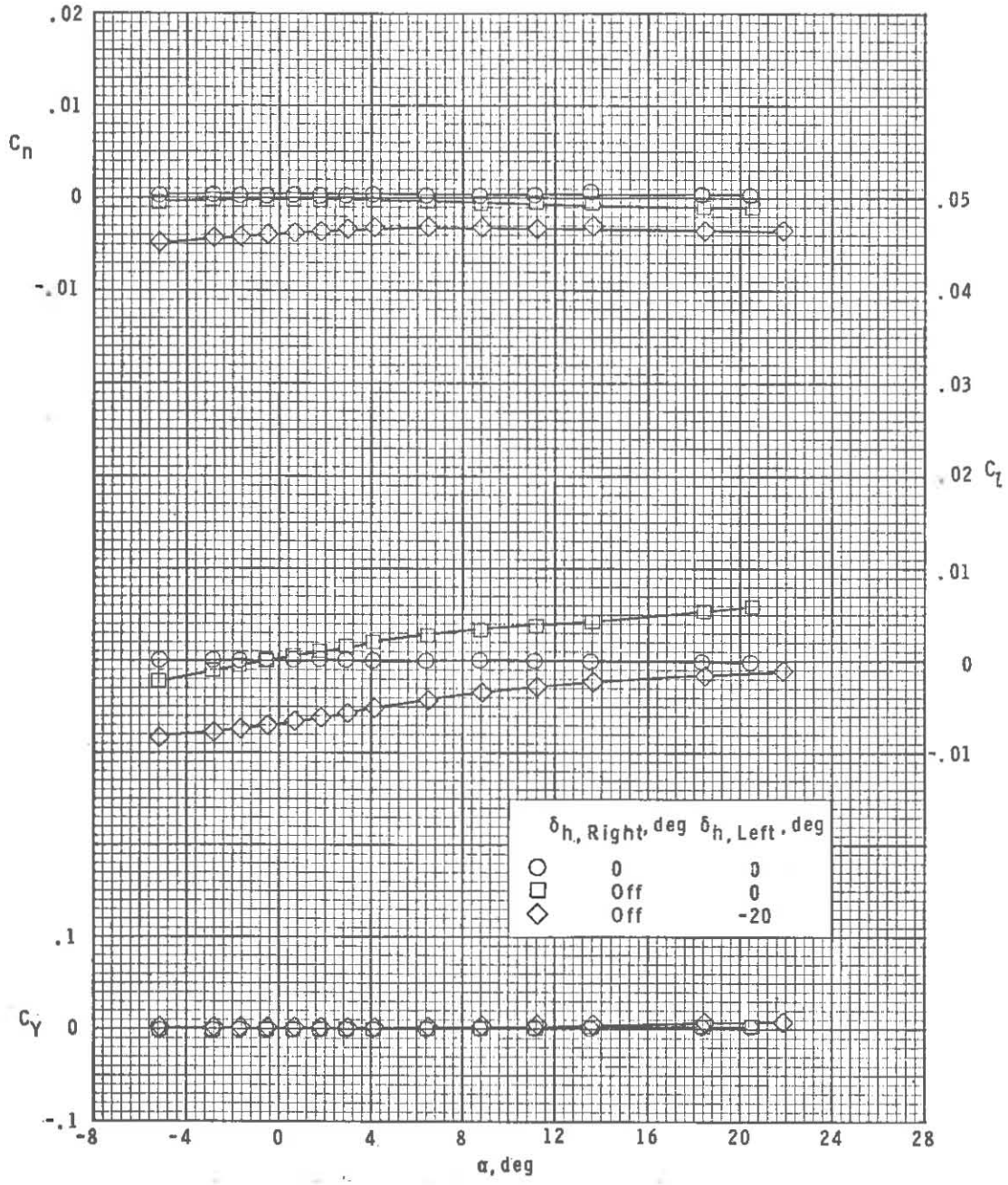

(b) M = 2.86.

Figure 10.- Continued.

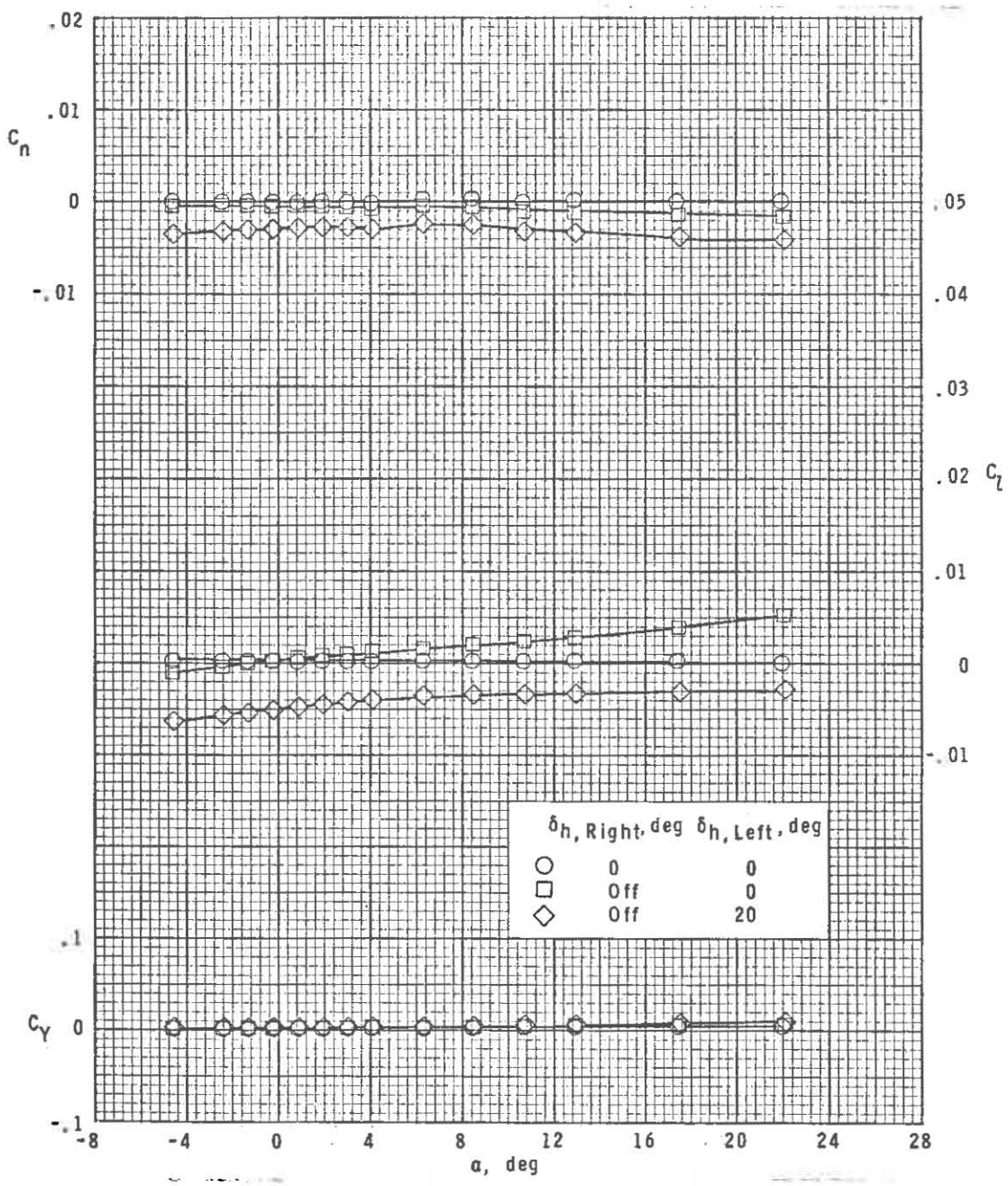

(c) M = 3.95.

Figure 10.- Continued.

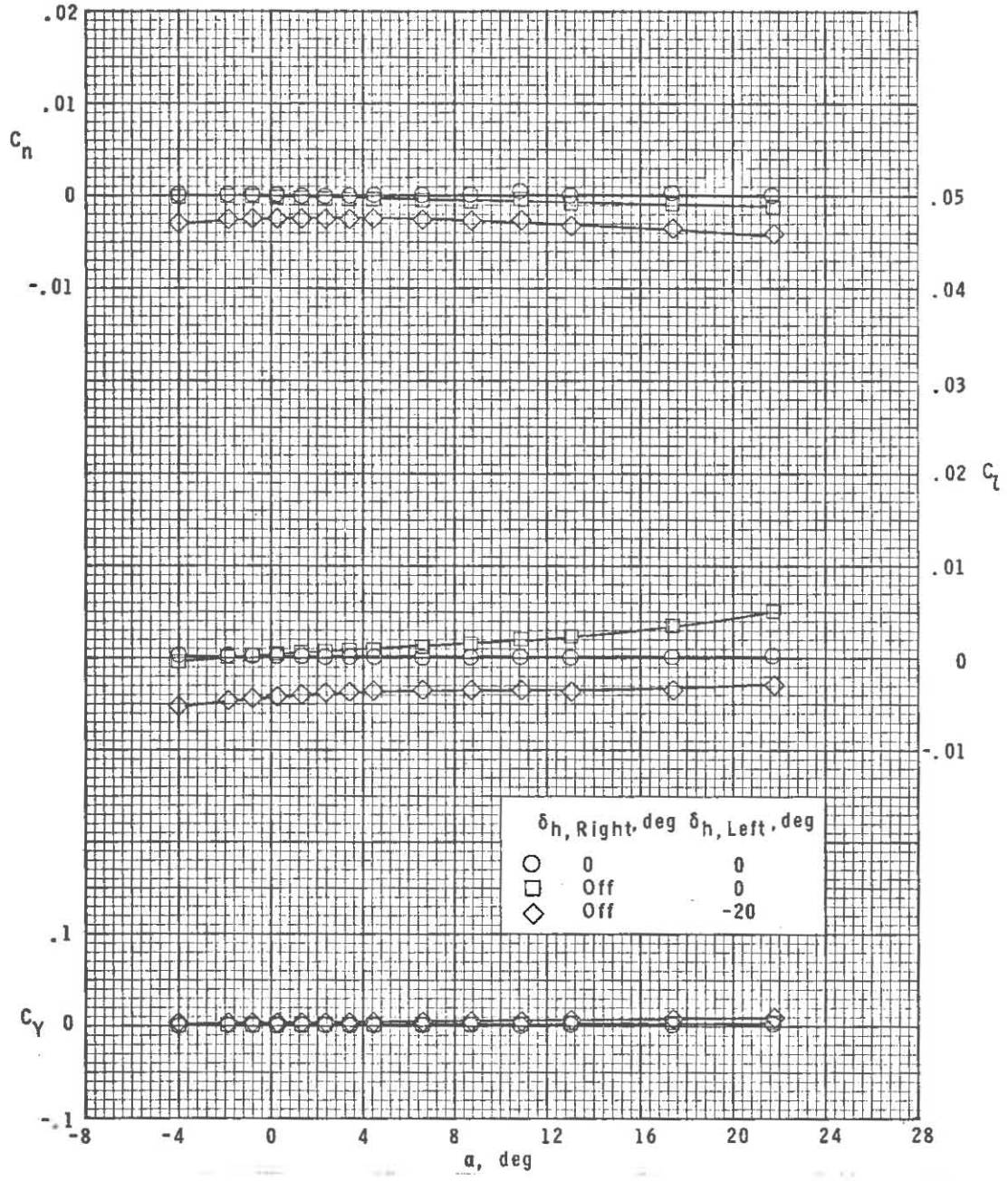

(d) M = 4.63.

Figure 10.- Concluded.

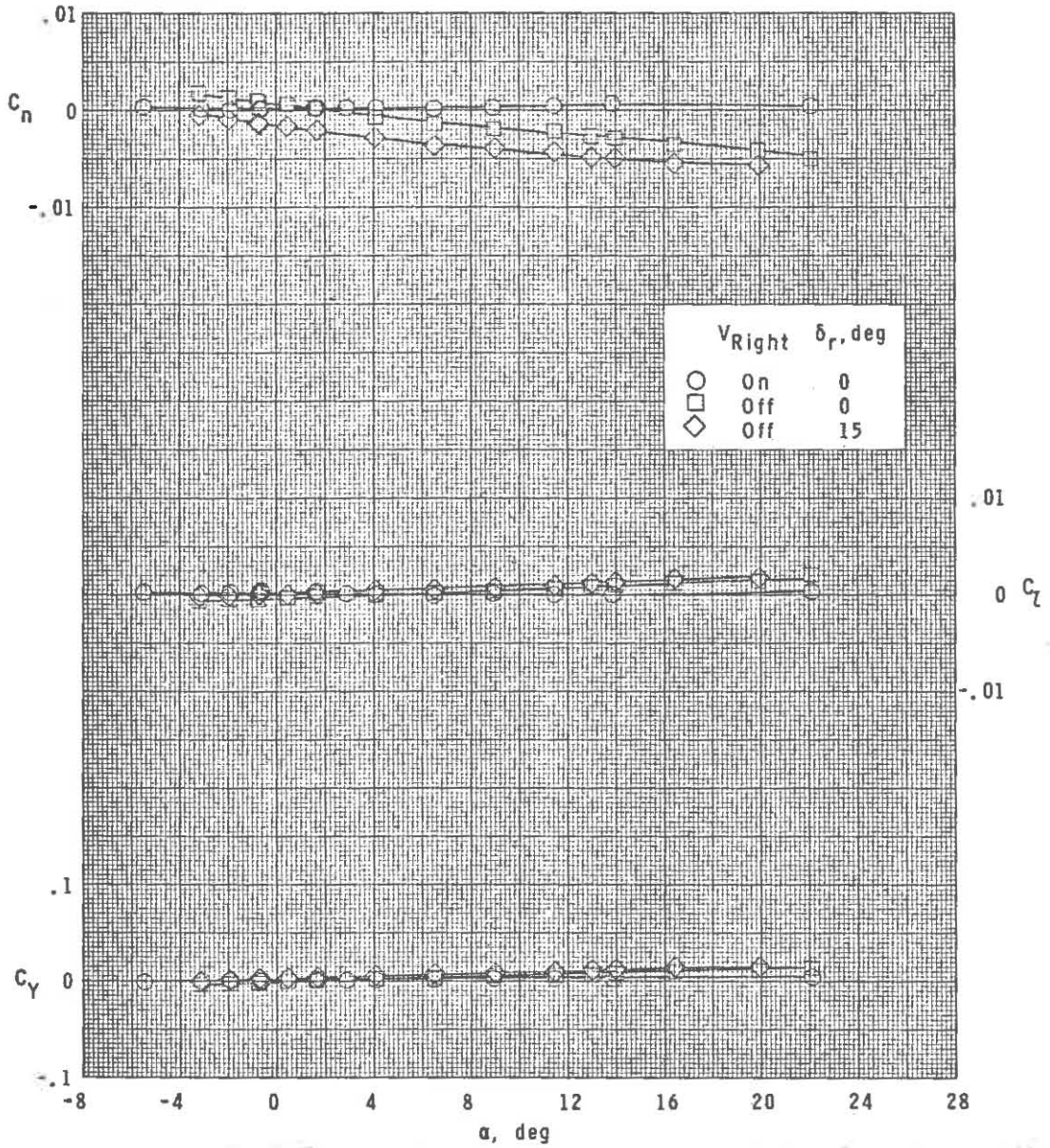

(a) M = 2.50.

Figure 11.- Variation of lateral aerodynamic characteristics with angle of attack for asymmetric vertical-tail condition. $\beta = 0^{o}$.

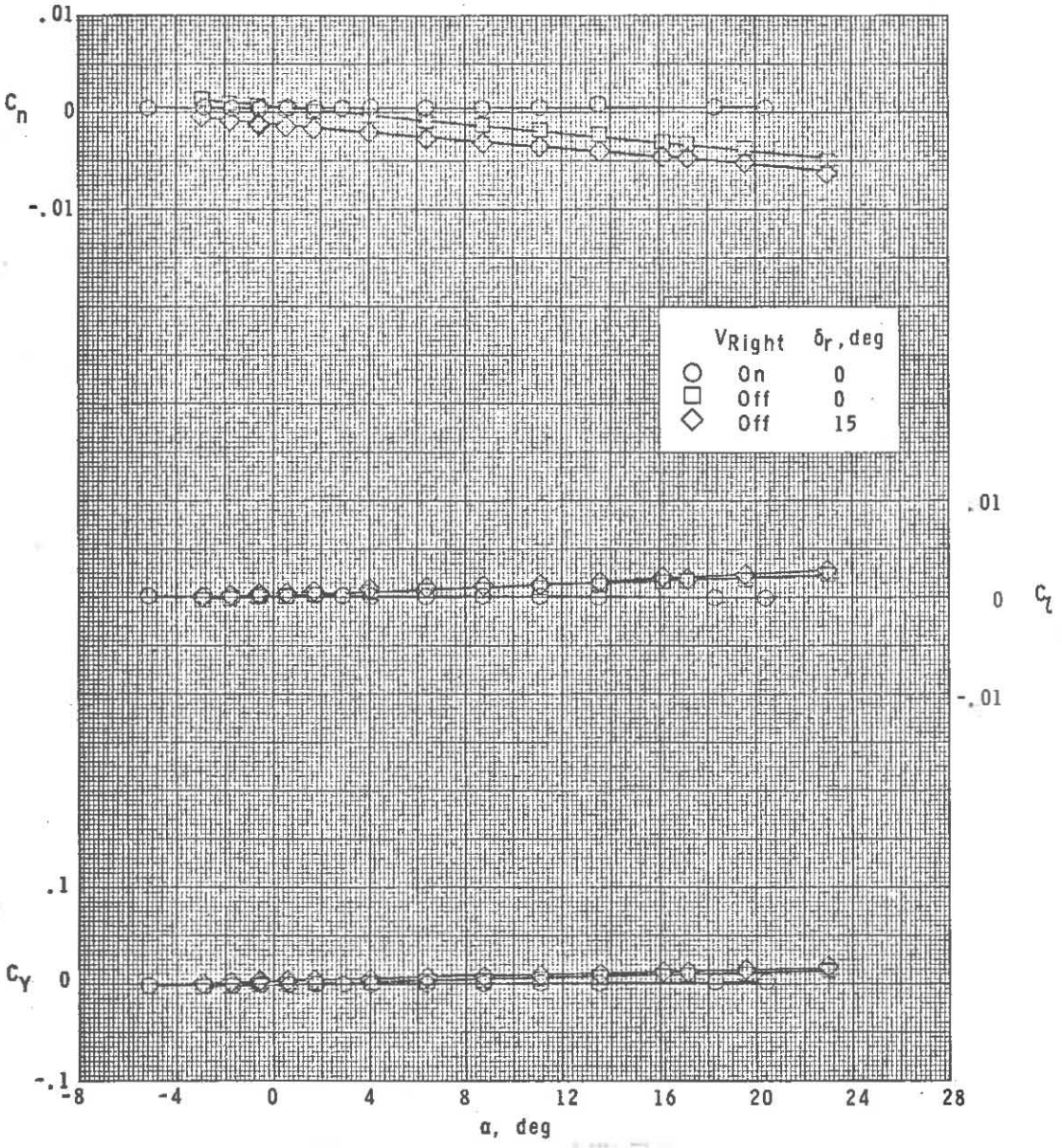

(b) M = 2.86.

Figure 11.- Continued.

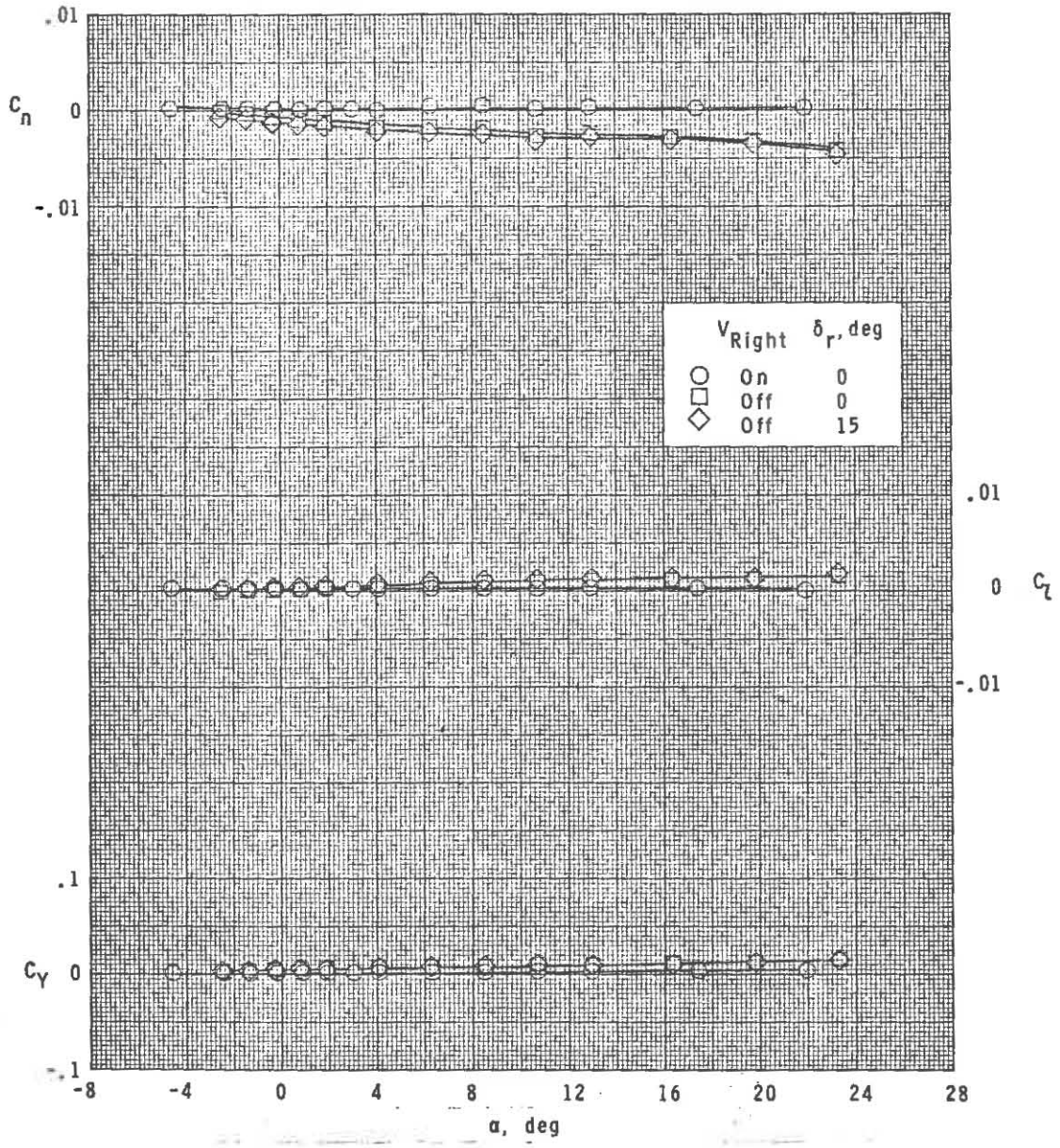

(c) M = 3.95.

Figure 11.- Continued.

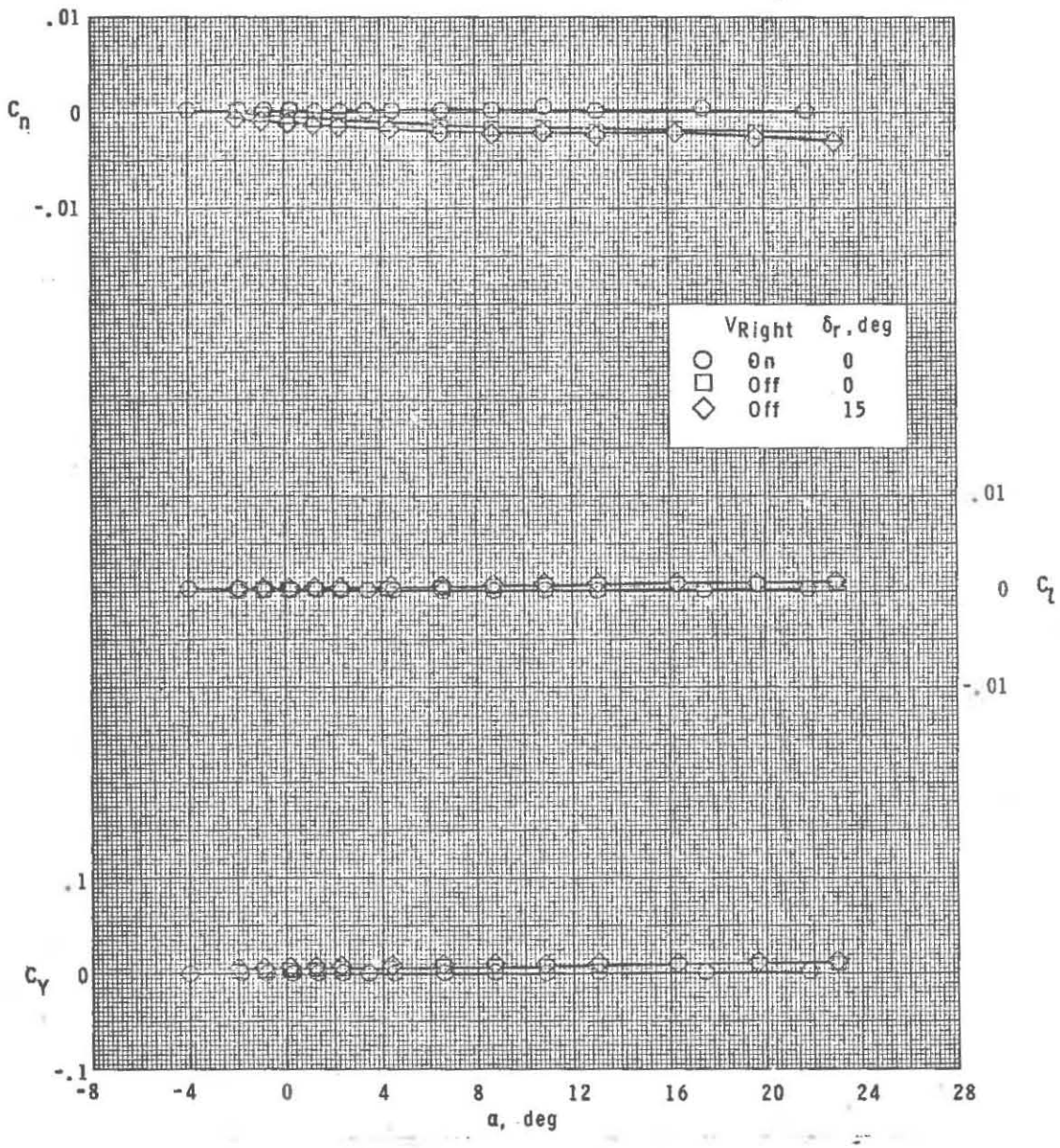

(d) M = 4.63.

Figure 11.- Concluded.

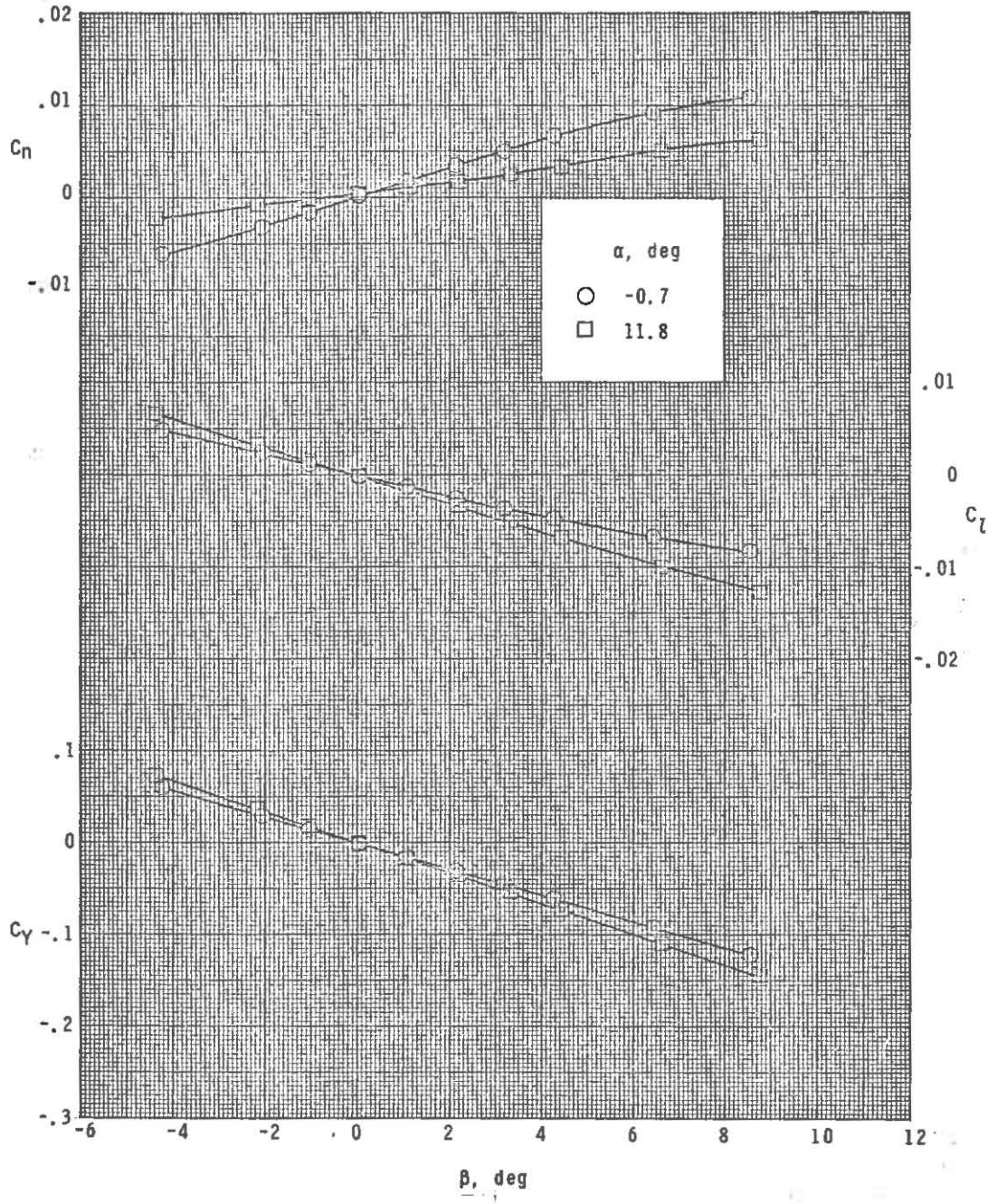

(a) M = 2.50.

Figure 12.- Sideslip characteristics at various angles of attack for complete configuration.

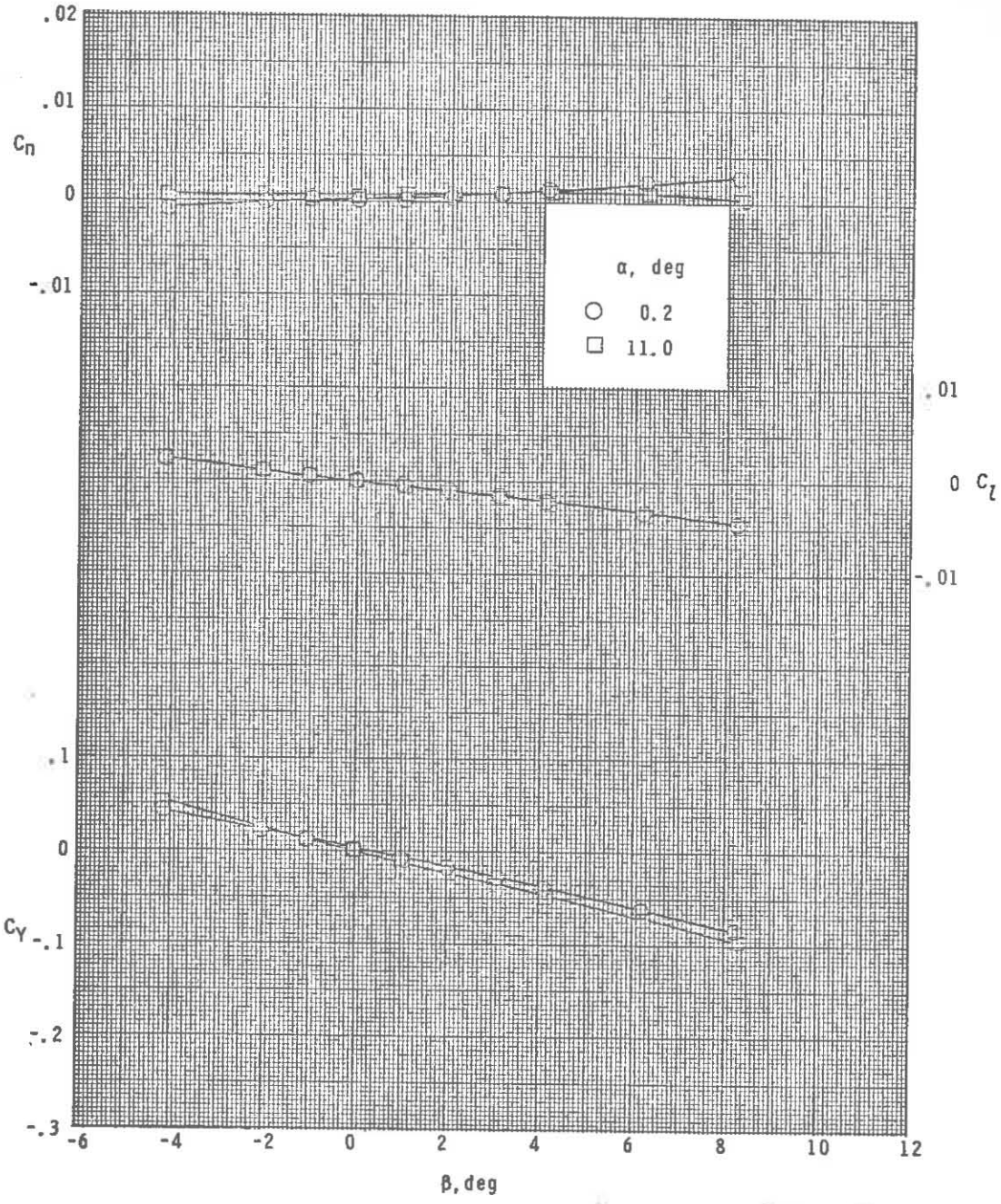

(b) M = 4.63.

Figure 12.- Concluded.

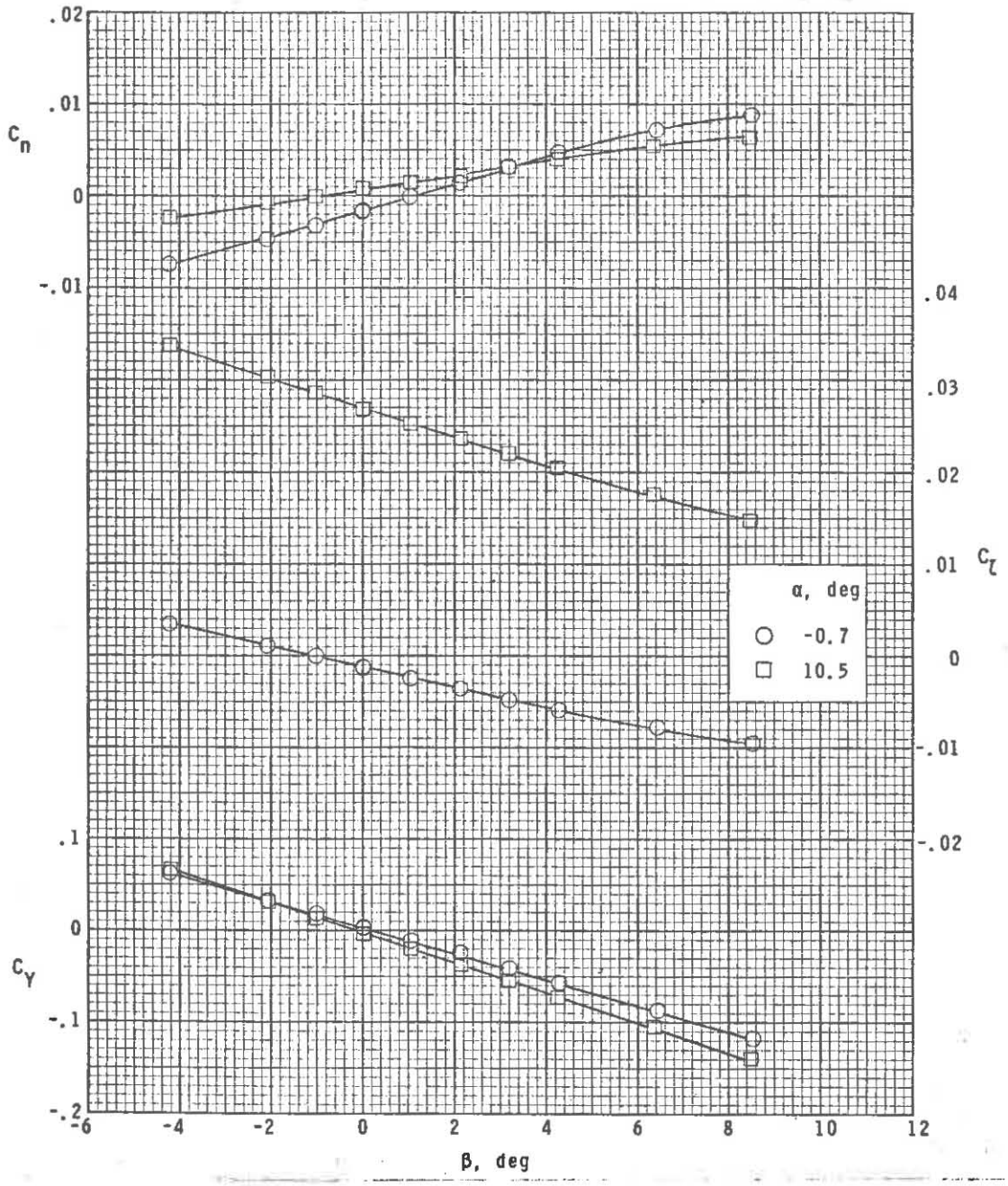

(a) M = 2.50.

Figure 13.- Sideslip characteristics at various angles of attack for 50 percent right wing off. $\delta_h = 0^o$; $\delta_r = 0^o$.

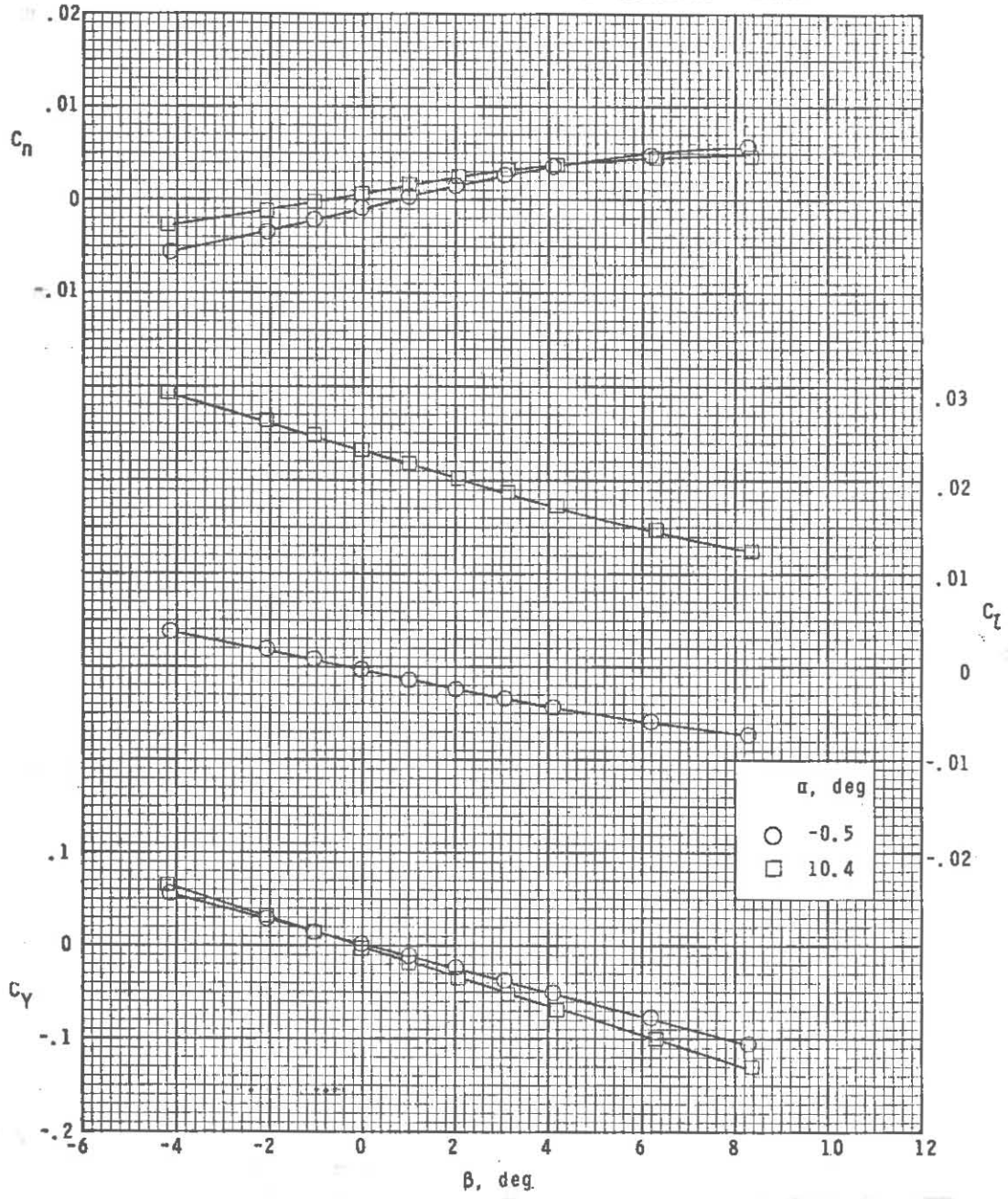

(b) M = 2.86.

Figure 13.- Continued.

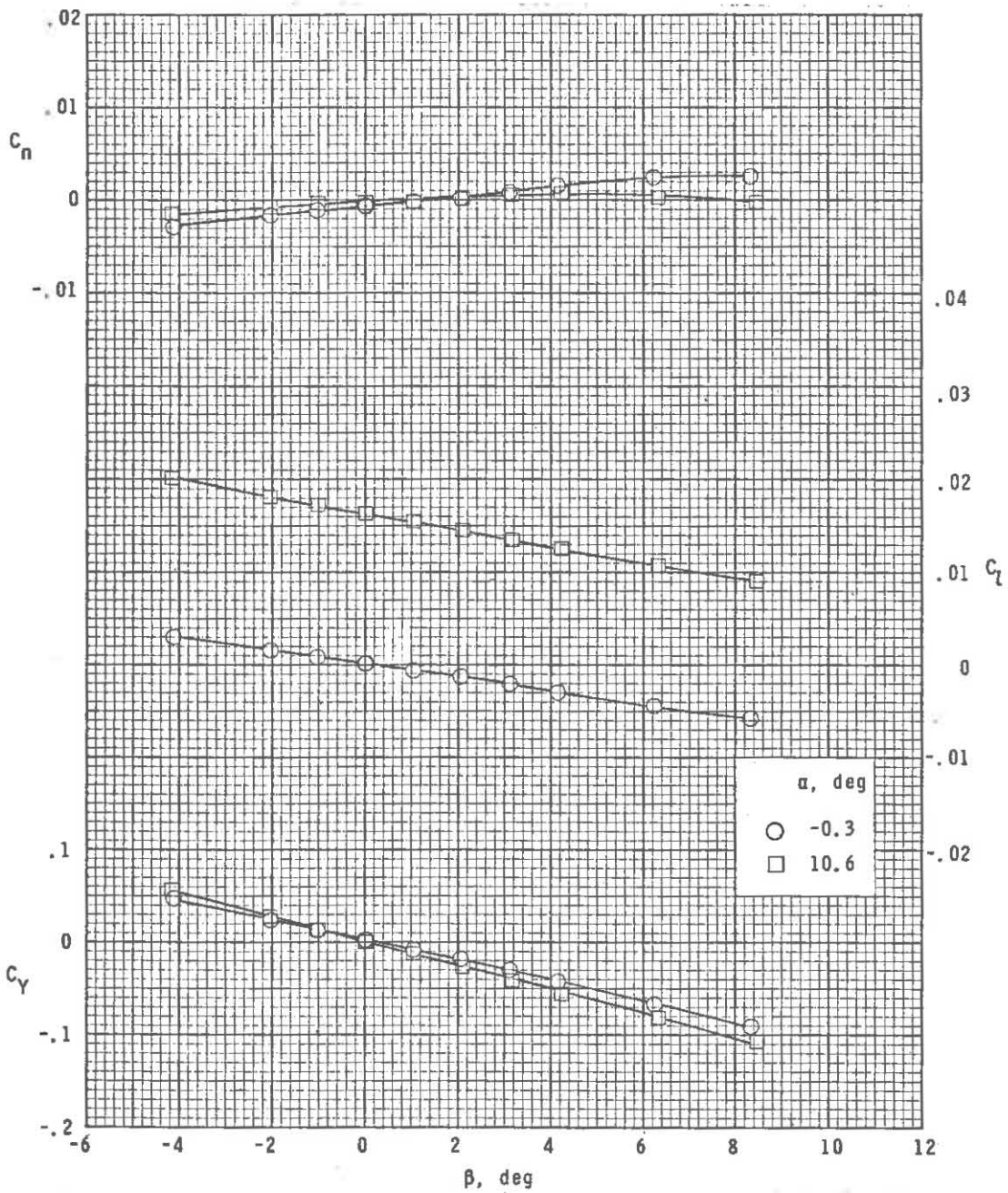

(c) M = 3.95.

Figure 13.- Continued.

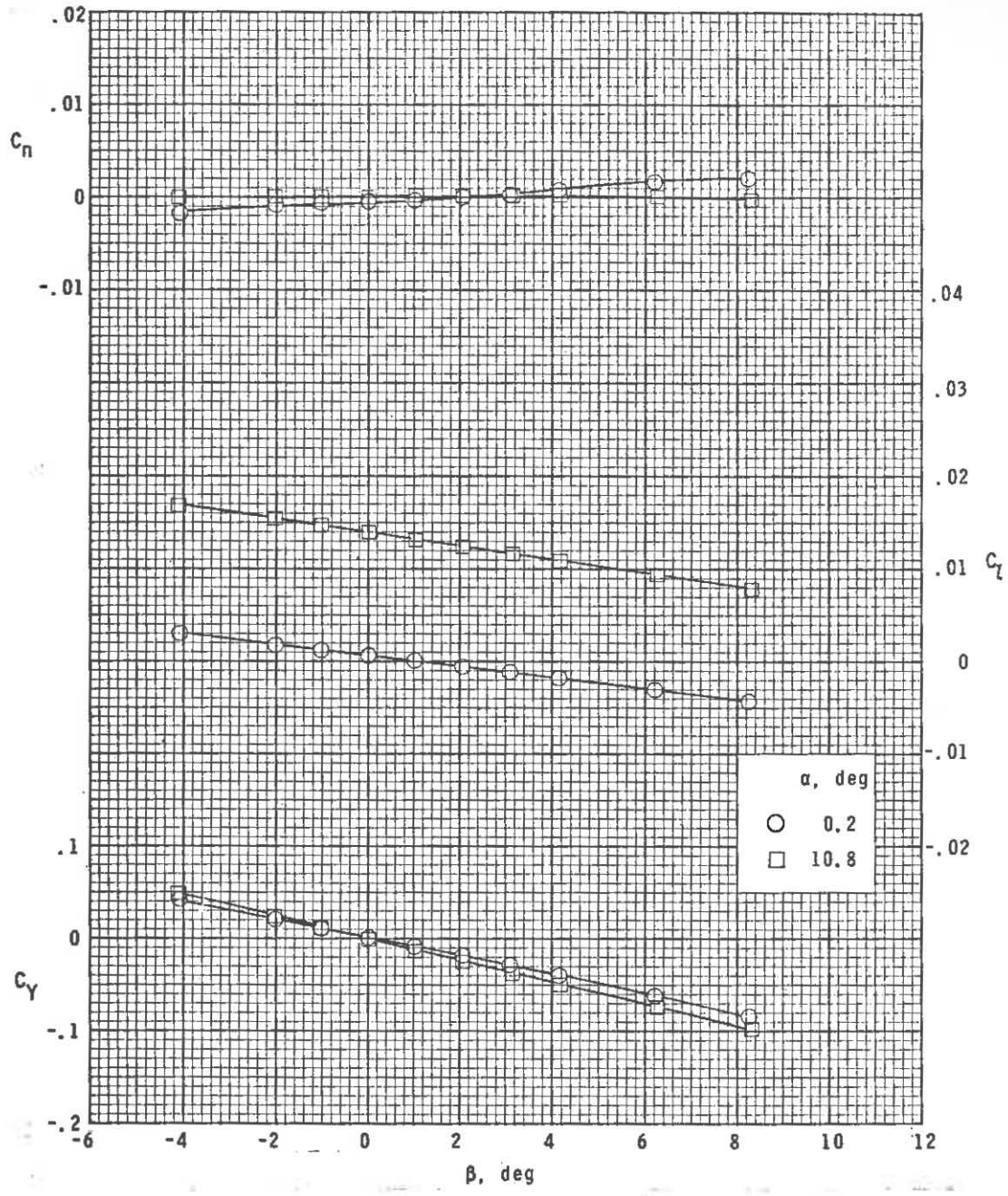

(d) M = 4.63.

Figure 13.- Concluded.

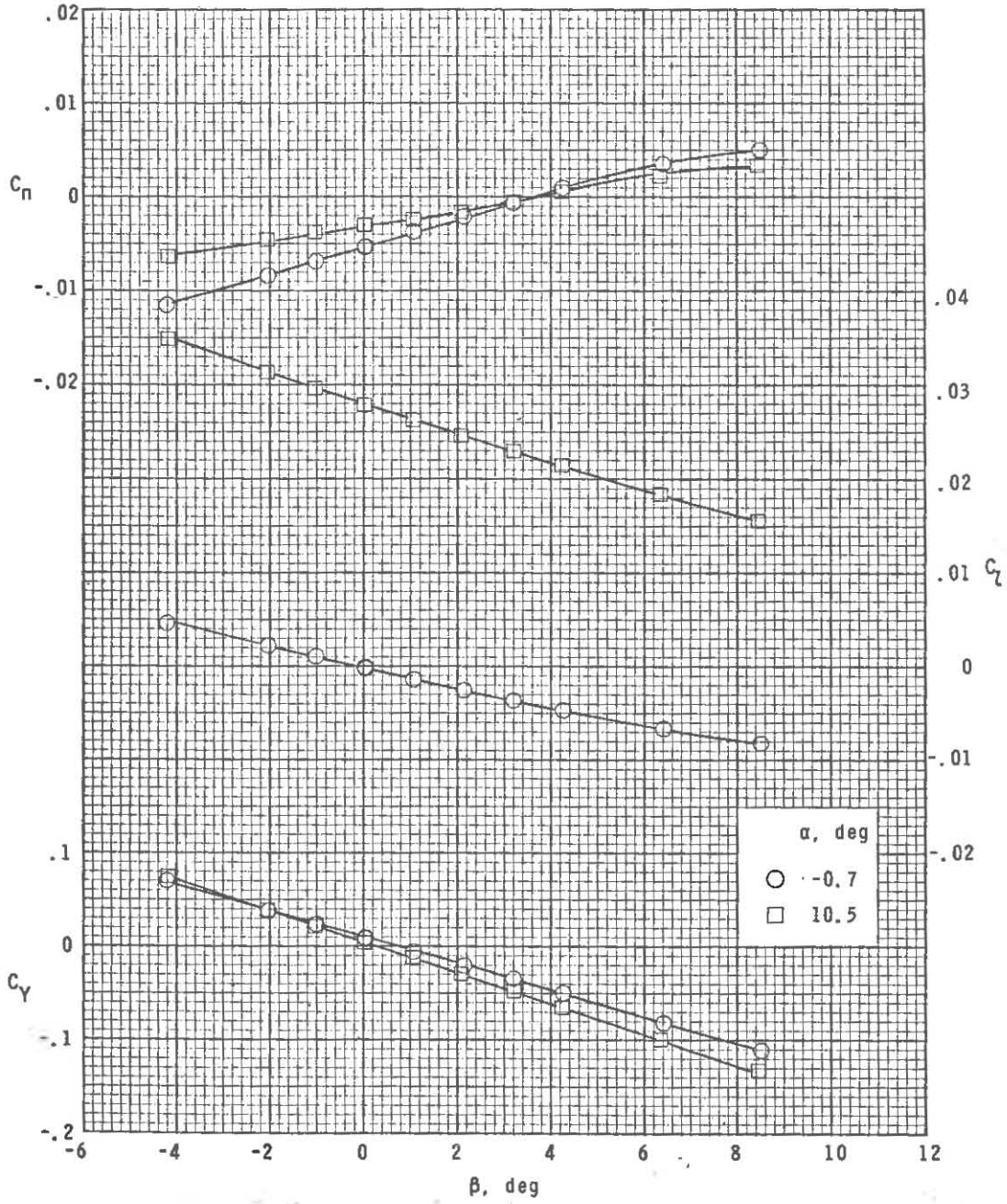

(a) M = 2.50.

Figure 14.- Sideslip characteristics at various angles of attack for 50 percent right wing off. $\delta_h = 0^o$; $\delta_r = 15^o$.

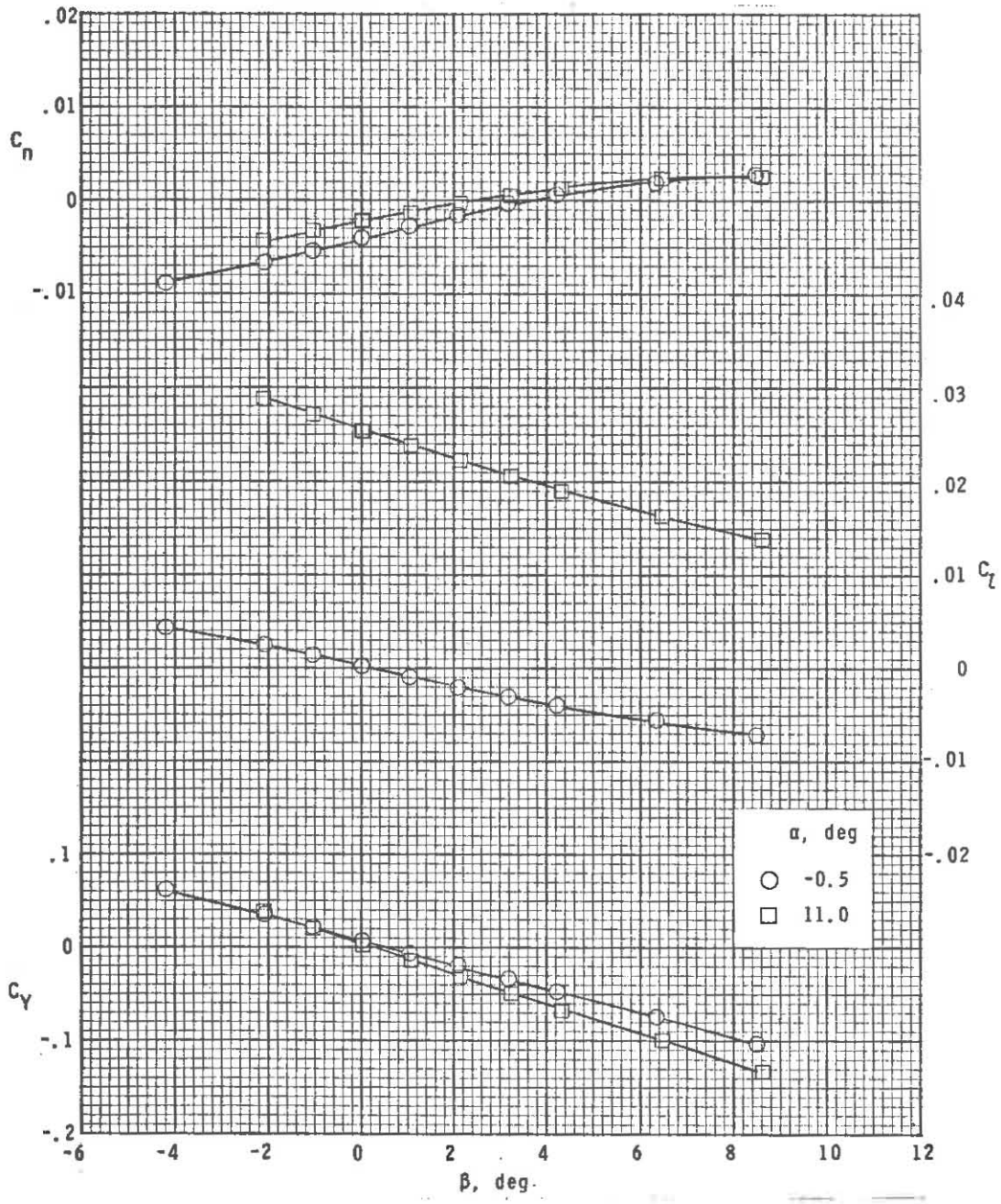

(b) M = 2.86.

Figure 14.- Continued.

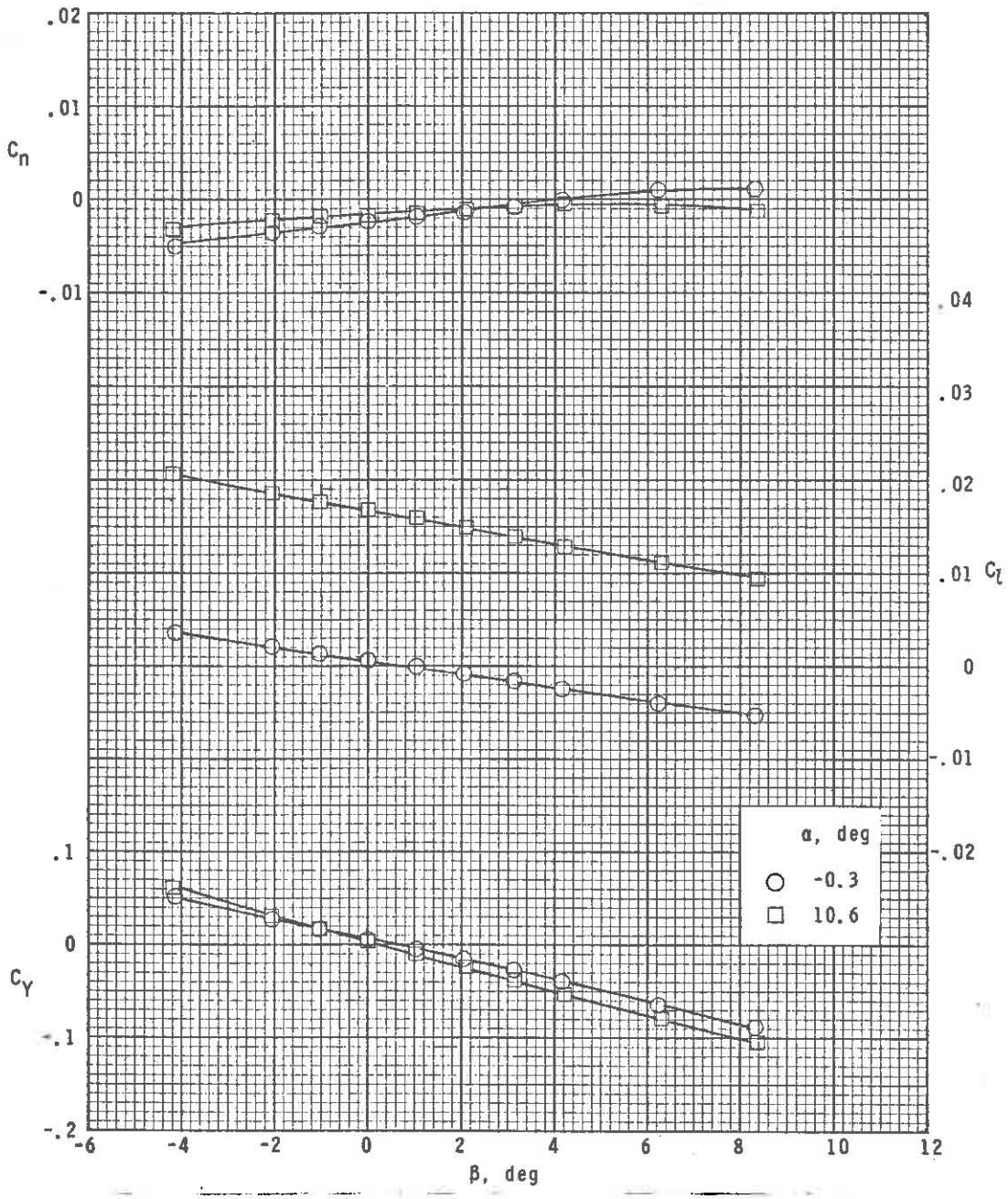

(c) M = 3.95.

Figure 14.- Continued.

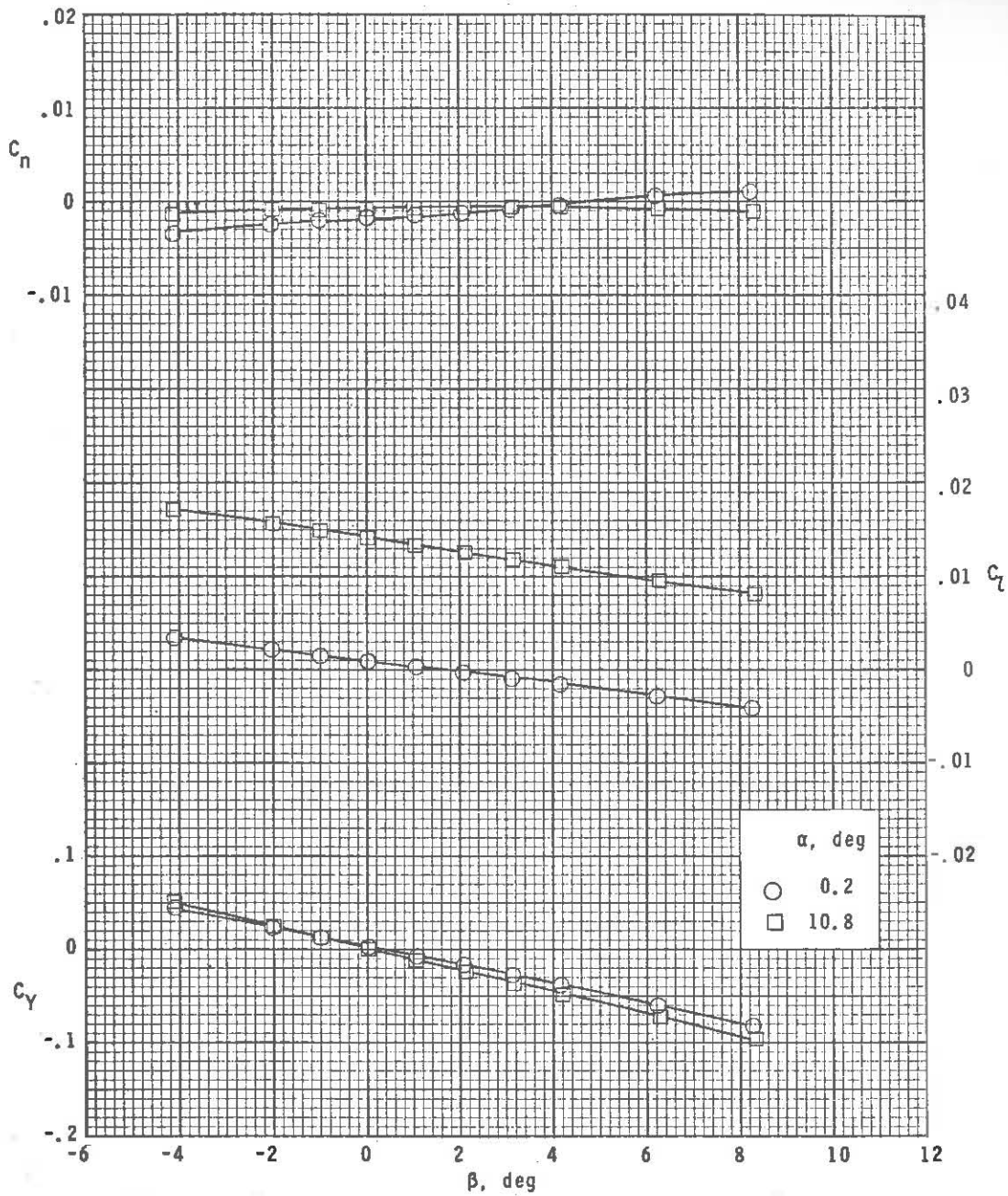

(d) M = 4.63.

Figure 14.- Concluded.

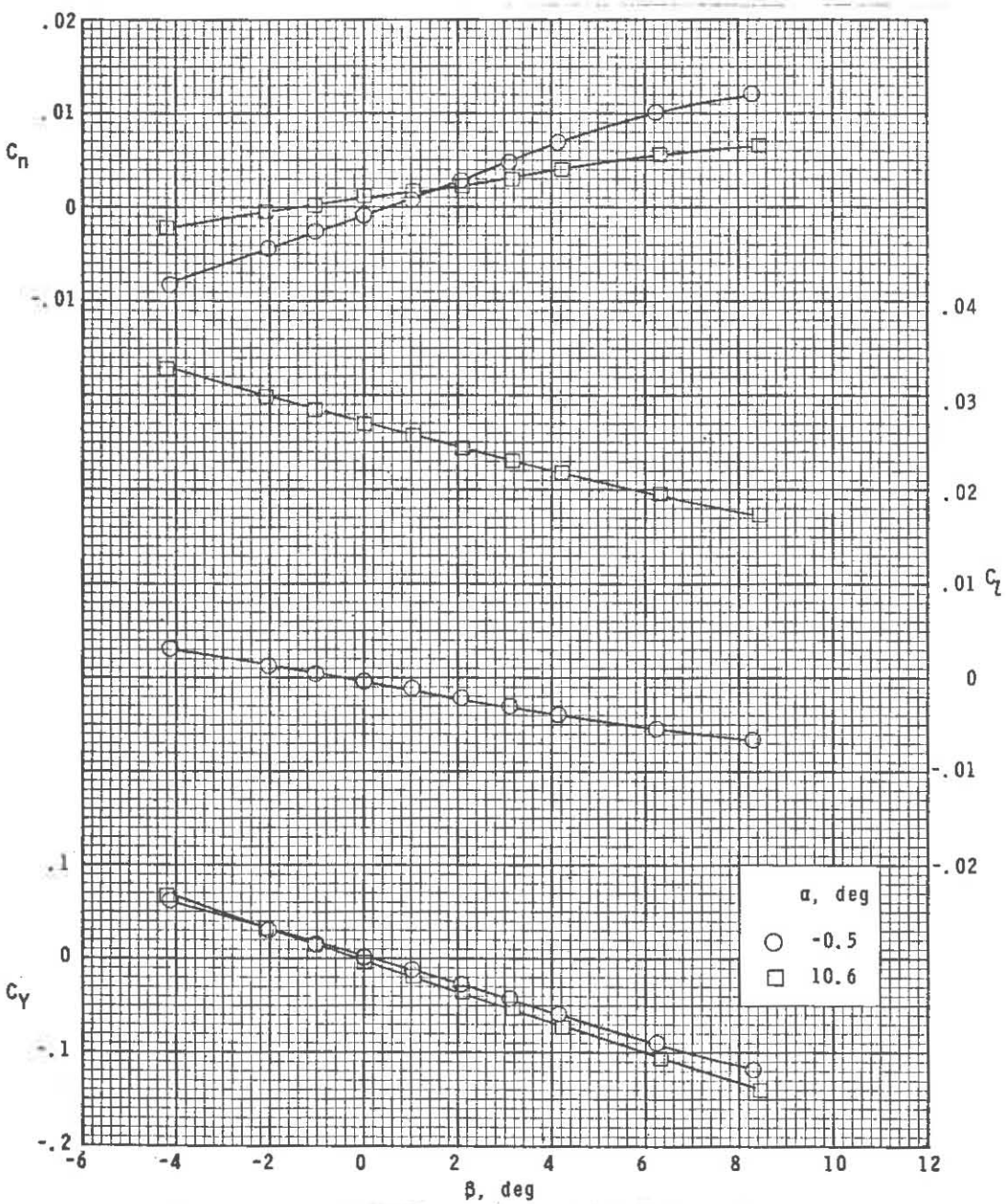

(a) M = 2.50.

Figure 15.- Sideslip characteristics at various angles of attack for 50 percent right wing off. $\delta_h = -20^o$; $\delta_r = 0^o$.

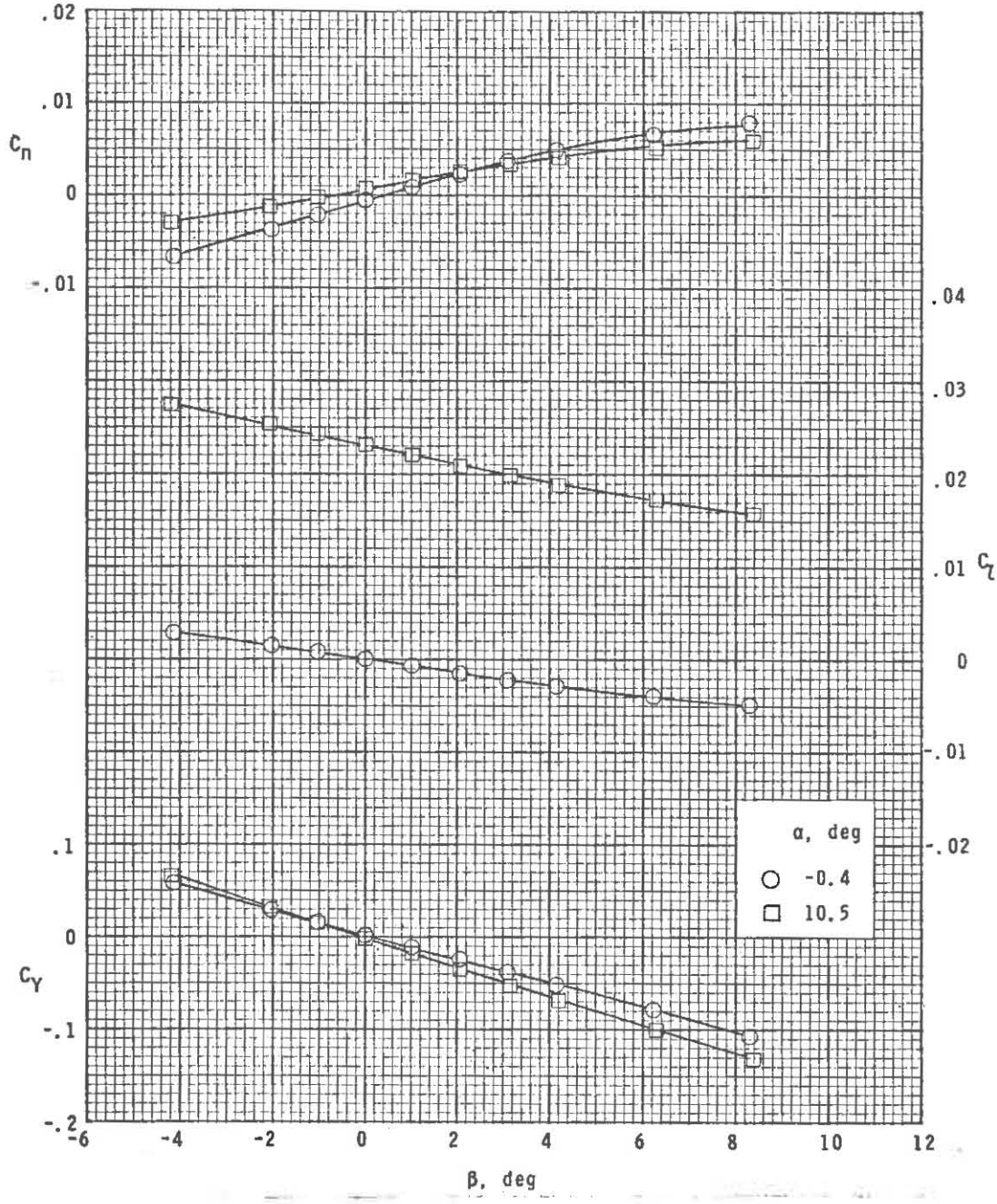

(b) M = 2.86.

Figure 15.- Continued.

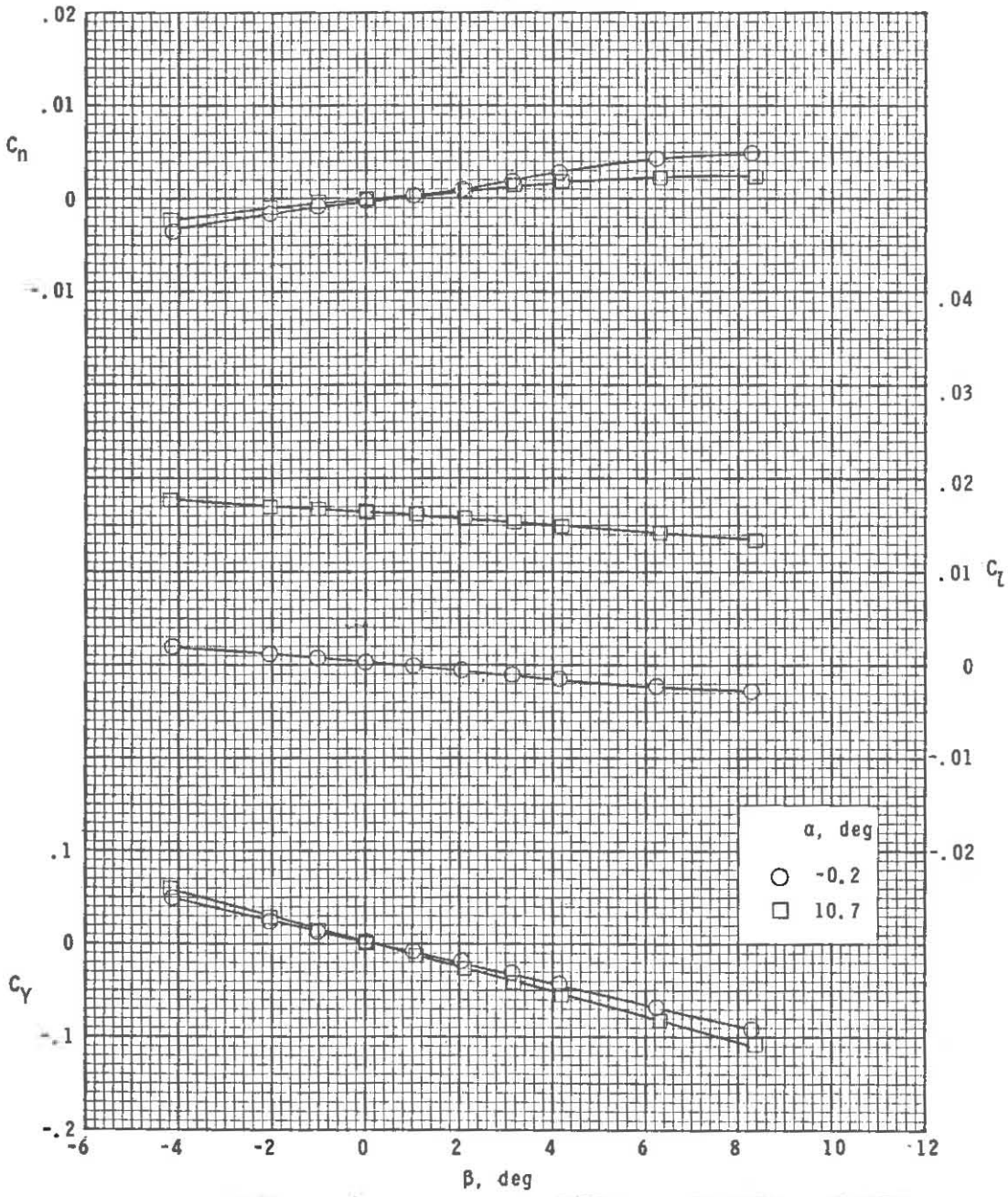

(c) M = 3.95.

Figure 15.- Continued.

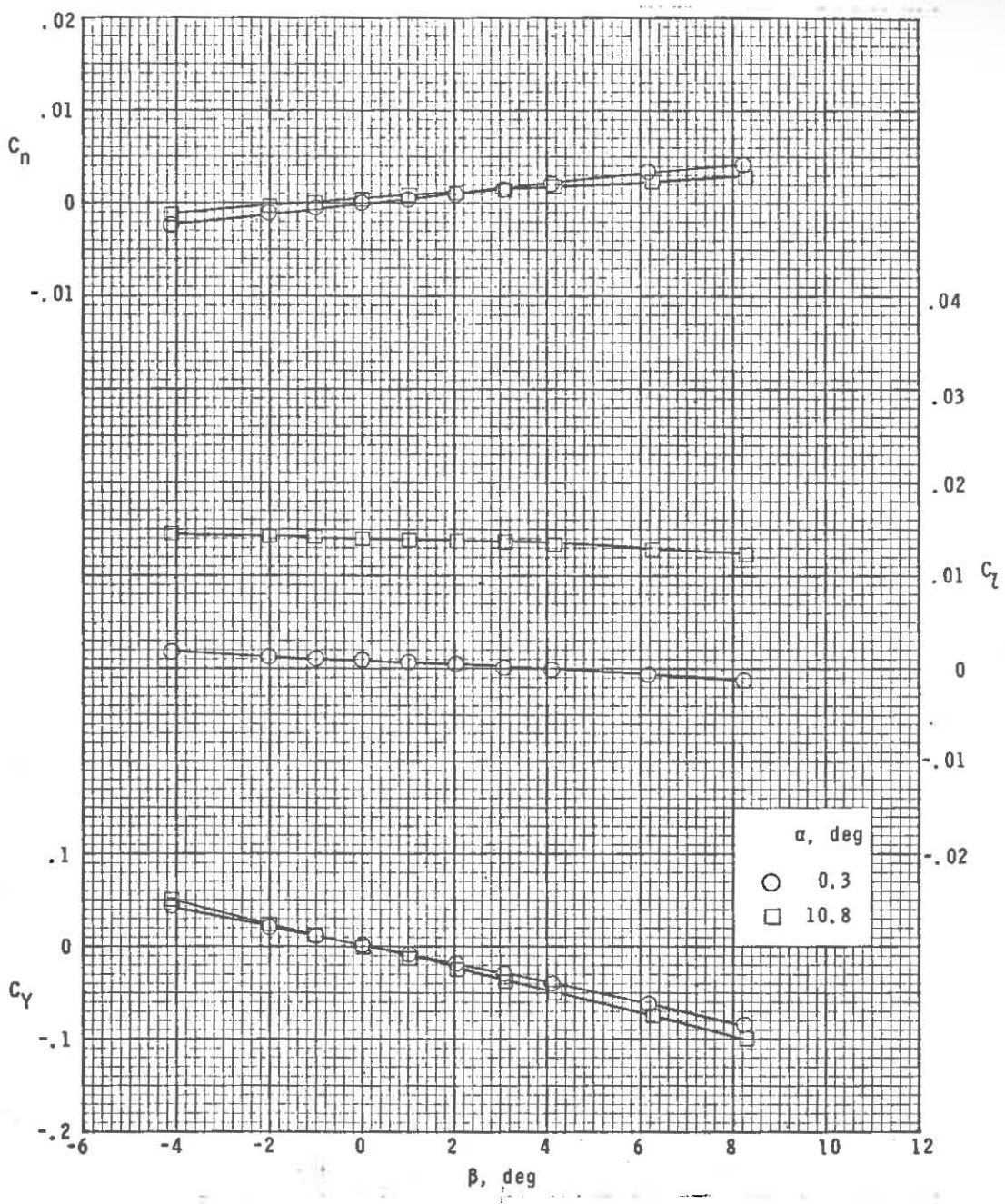

(d) M = 4.63.

Figure 15.- Concluded.

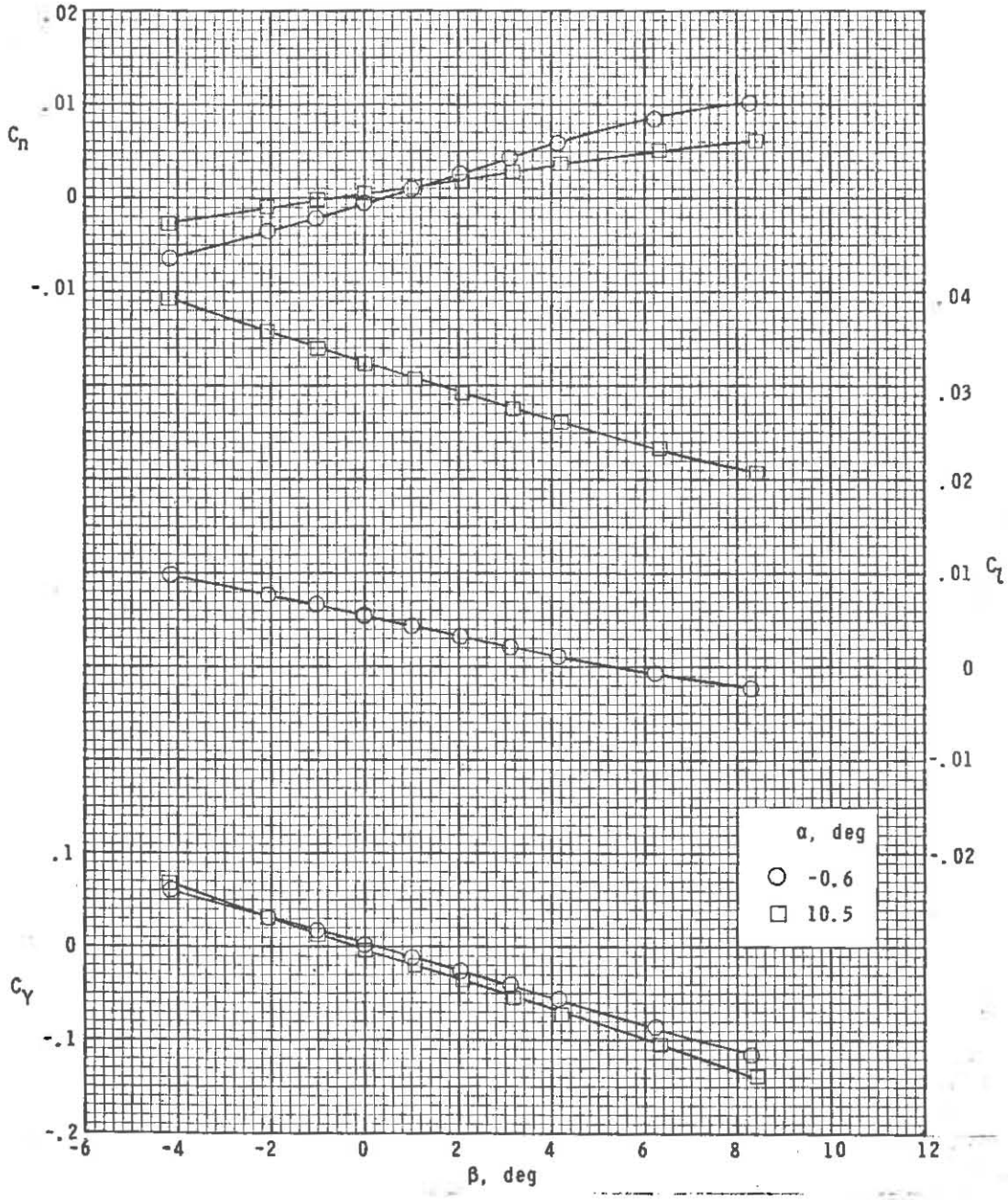

(a) M = 2.50.

Figure 16.- Sideslip characteristics at various angles of attack for 50 percent right wing off. $\delta_{h,left} = 10^o$; $\delta_{h,right} = -10^o$.

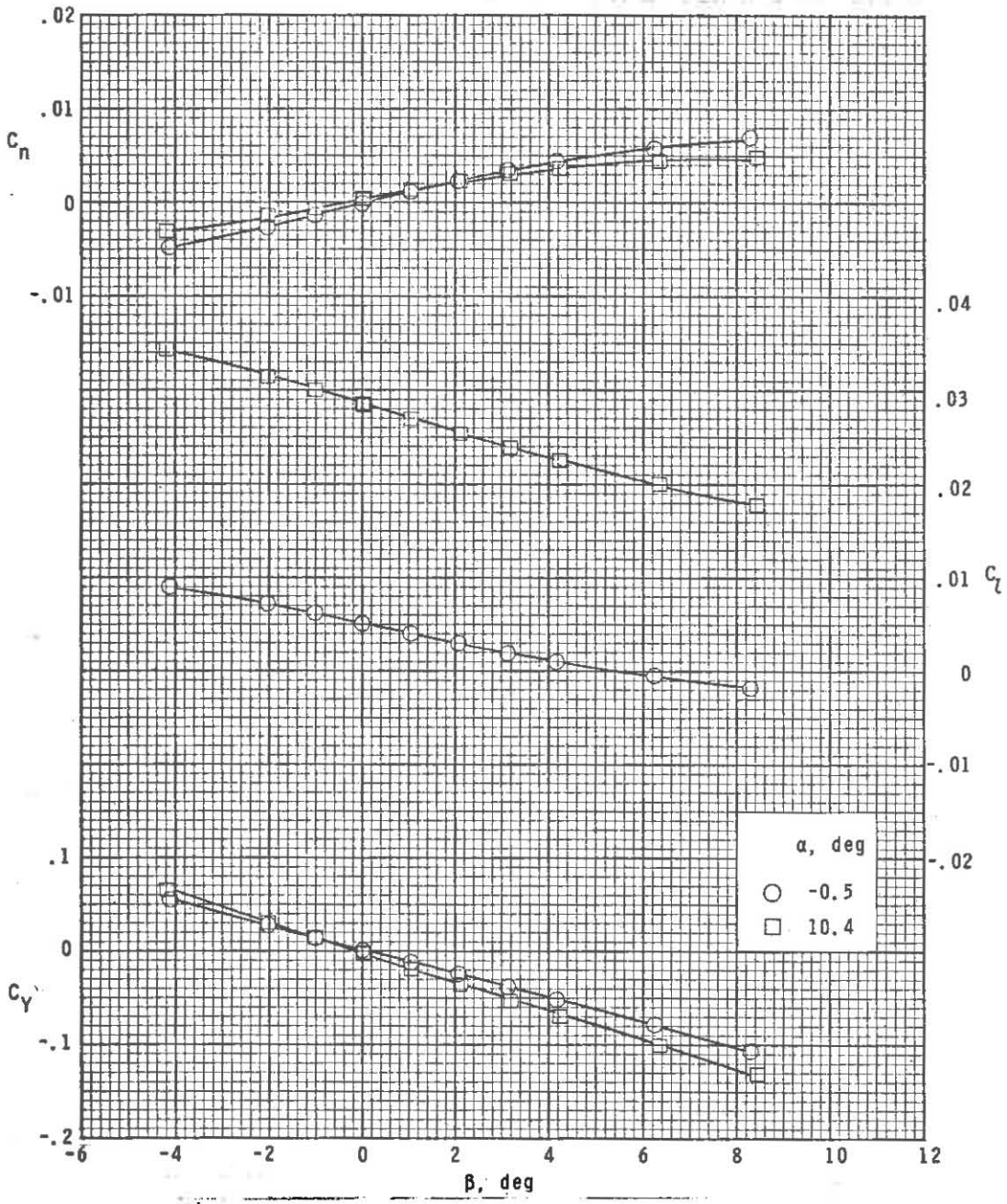

(b) M = 2.86.

Figure 16.- Continued.

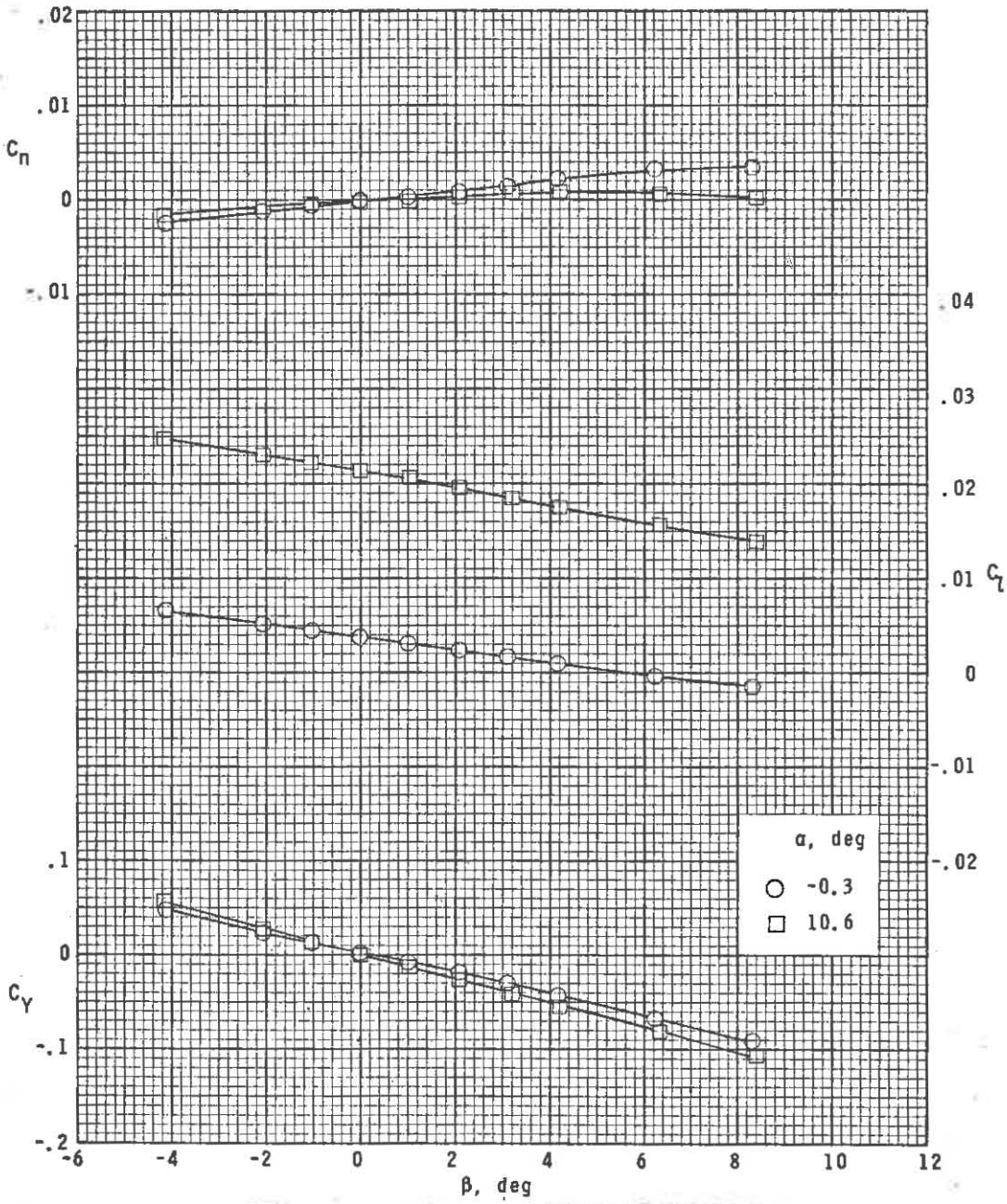

(c) M = 3.95.

Figure 16.- Continued.

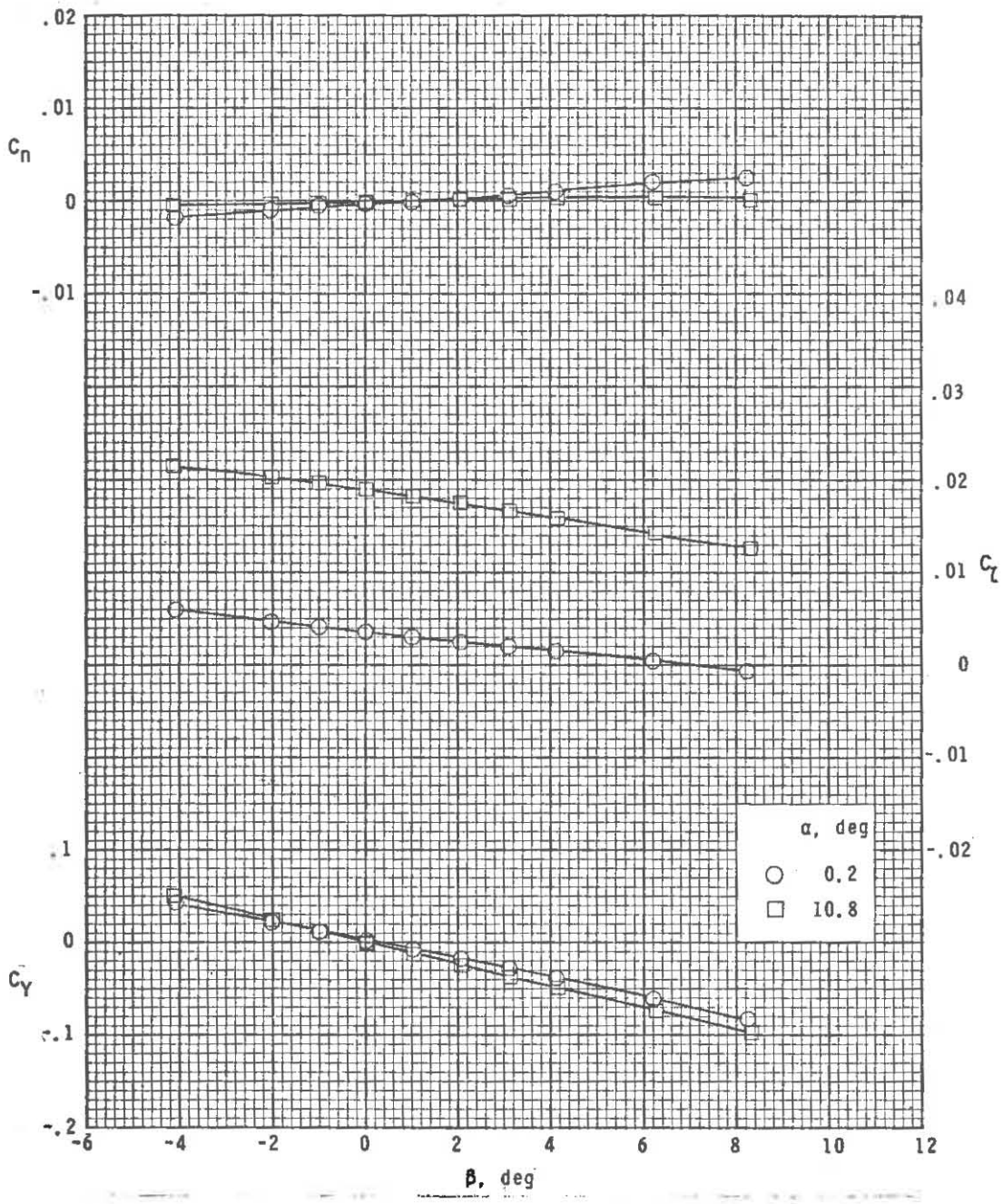

(d) M = 4.63.

Figure 16.- Concluded.

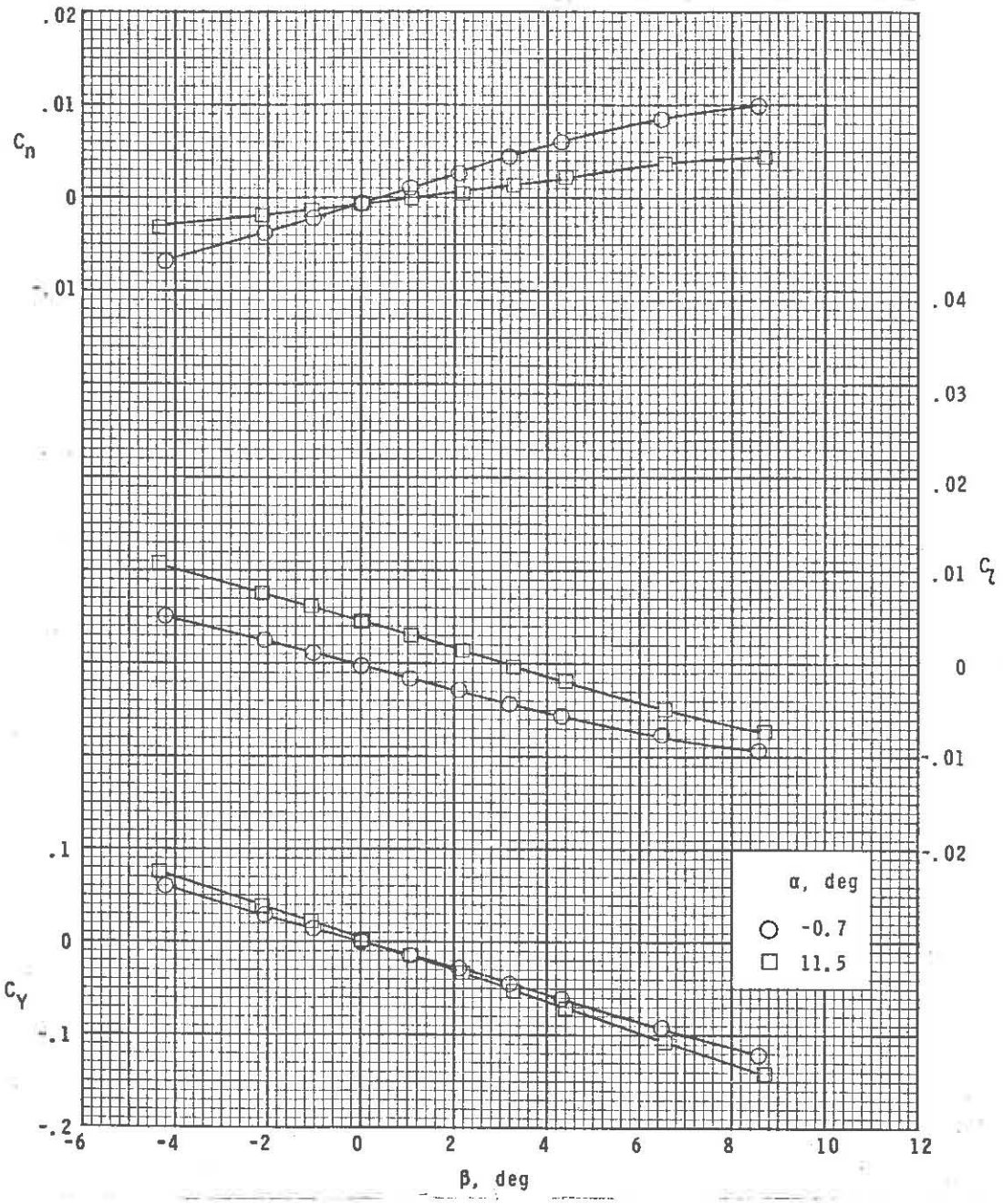

(a) M = 2.50.

Figure 17.- Sideslip characteristics at various angles of attack for right horizontal tail off. $\delta_{h,left} = 0^{o}$.

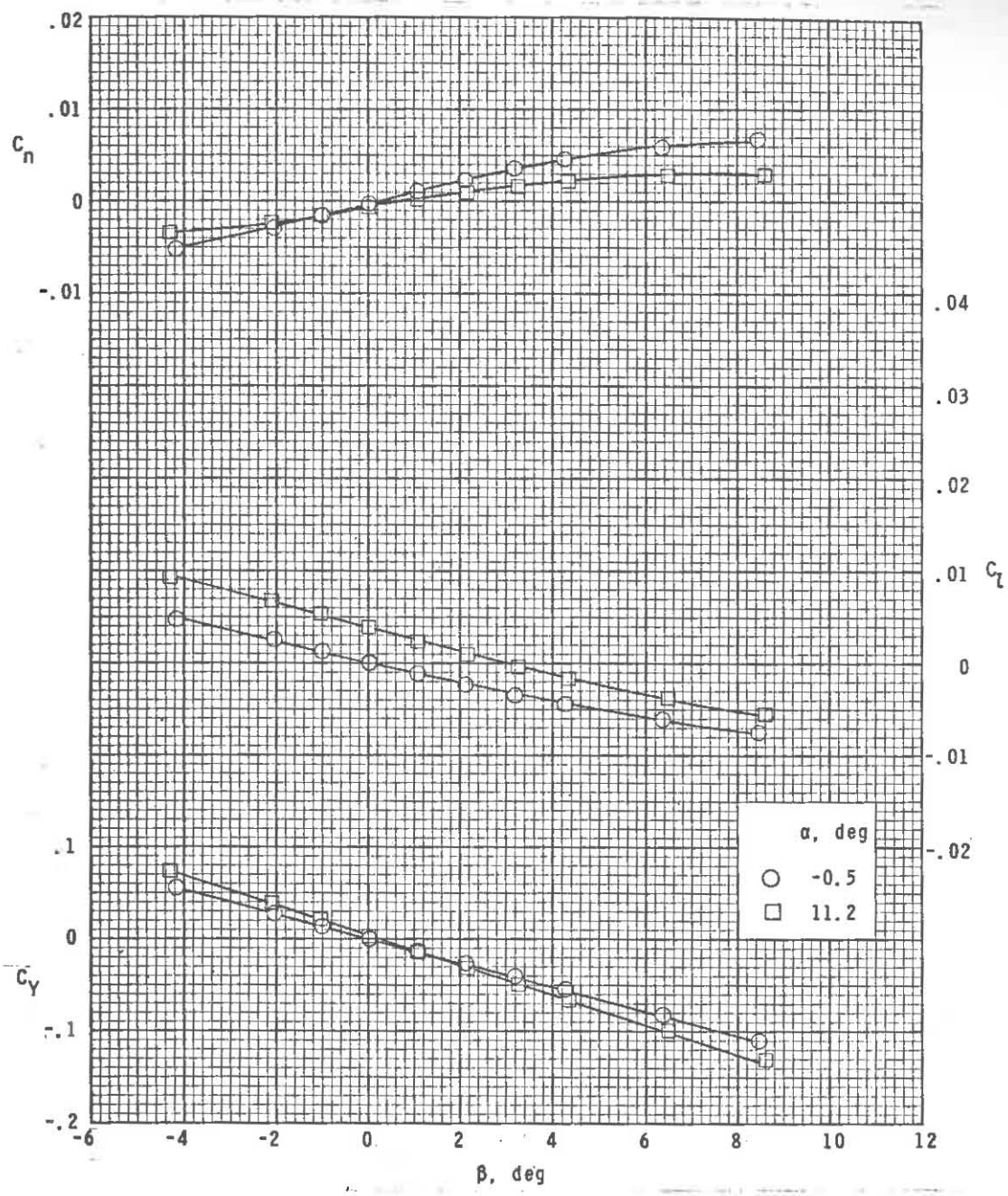

(b) M = 2.86.

Figure 17.- Continued.

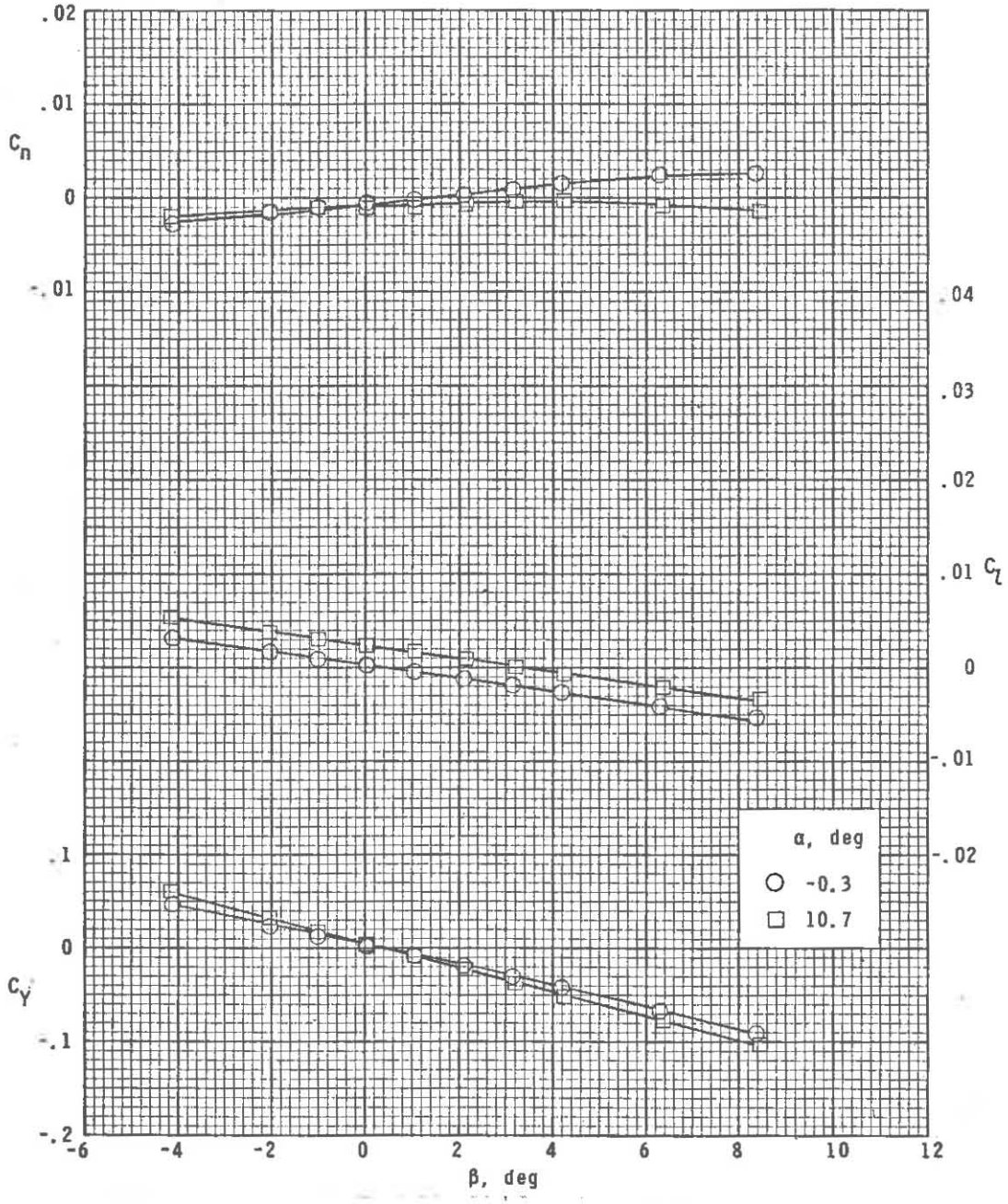

(c) M = 3.95.

Figure 17.- Continued.

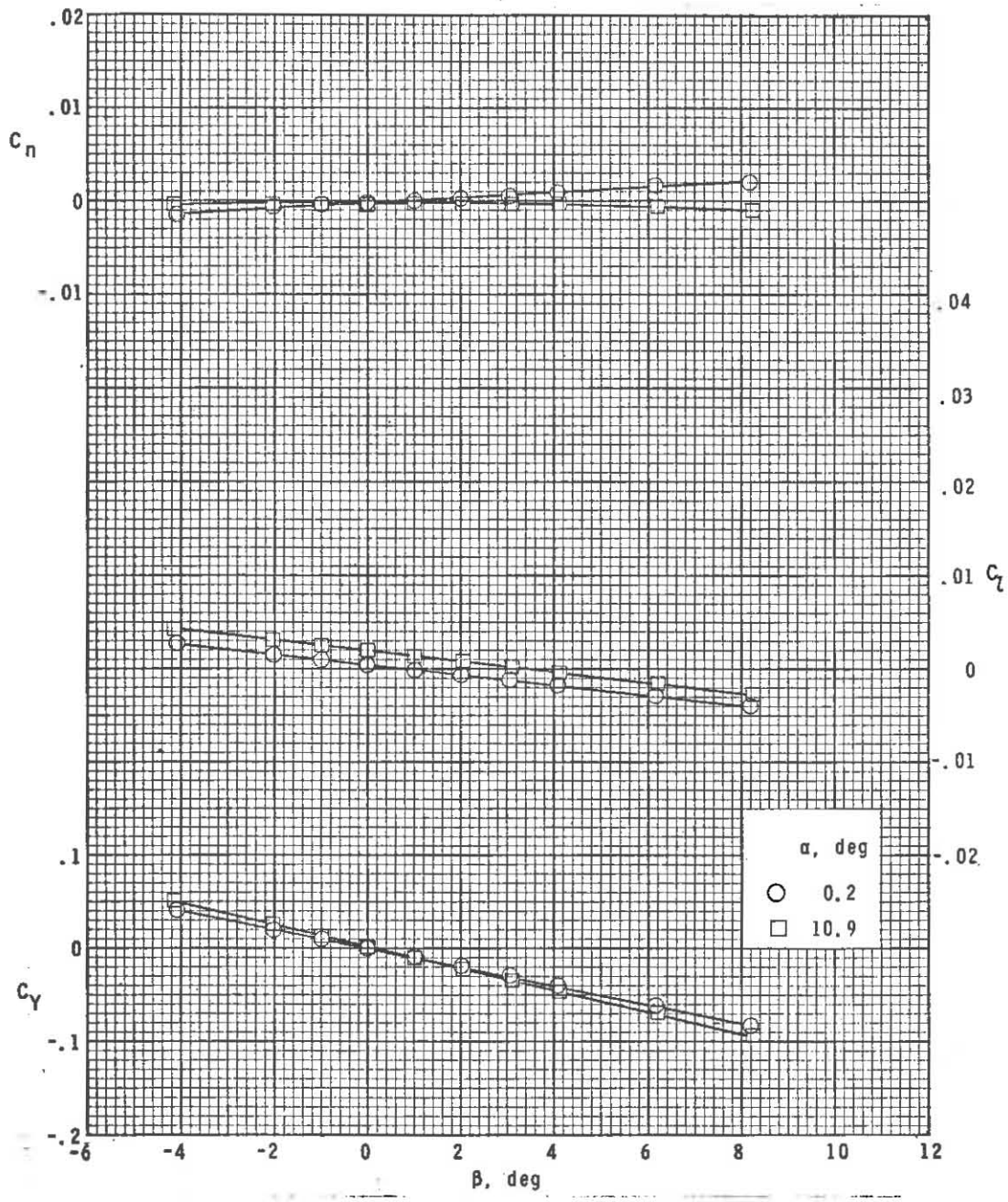

(d) M = 4.63.

Figure 17.- Concluded.

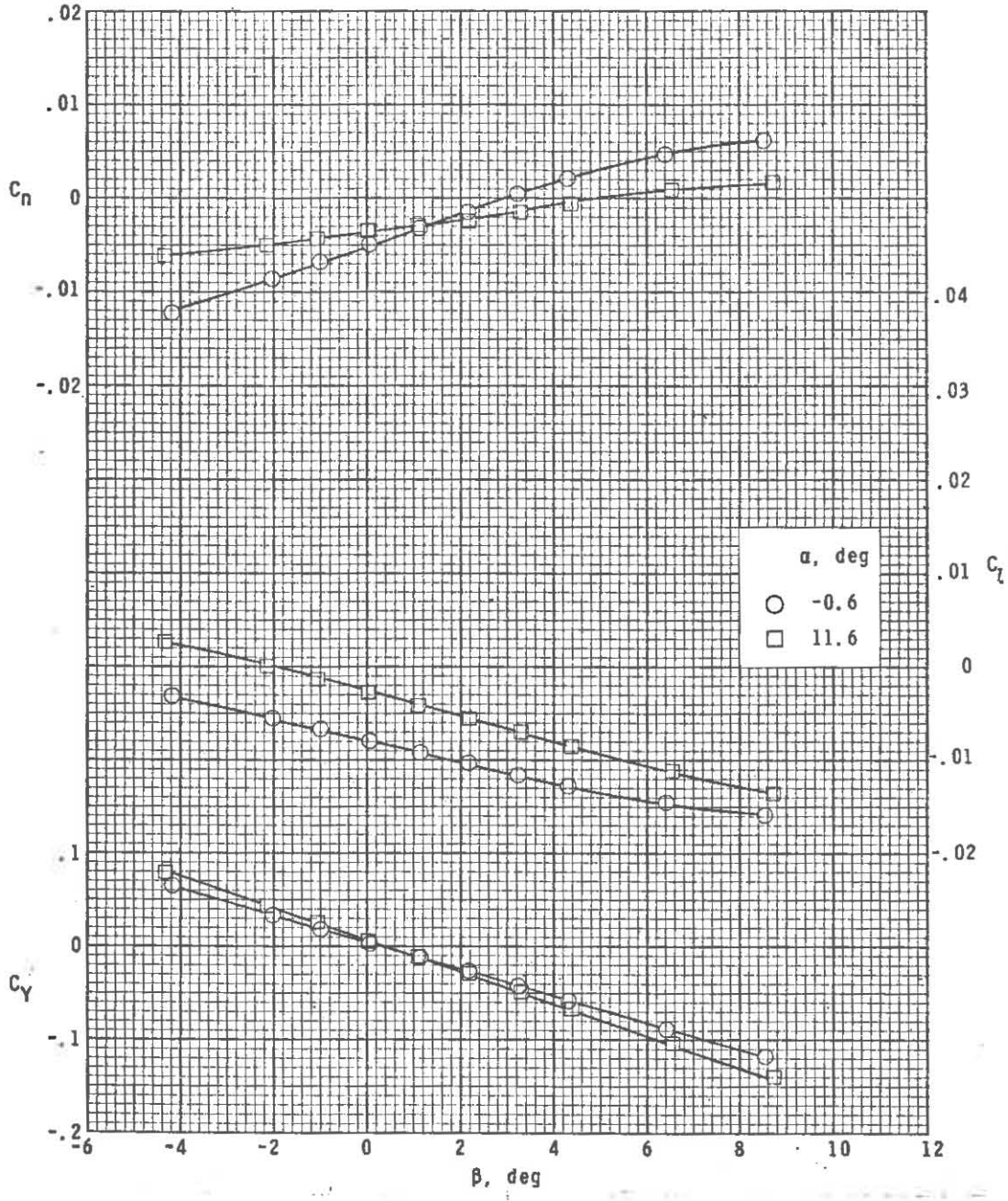

(a) M = 2.50.

Figure 18.- Sideslip characteristics at various angles of attack for right horizontal tail off. $\delta_{h,left} = -20^{o}$.

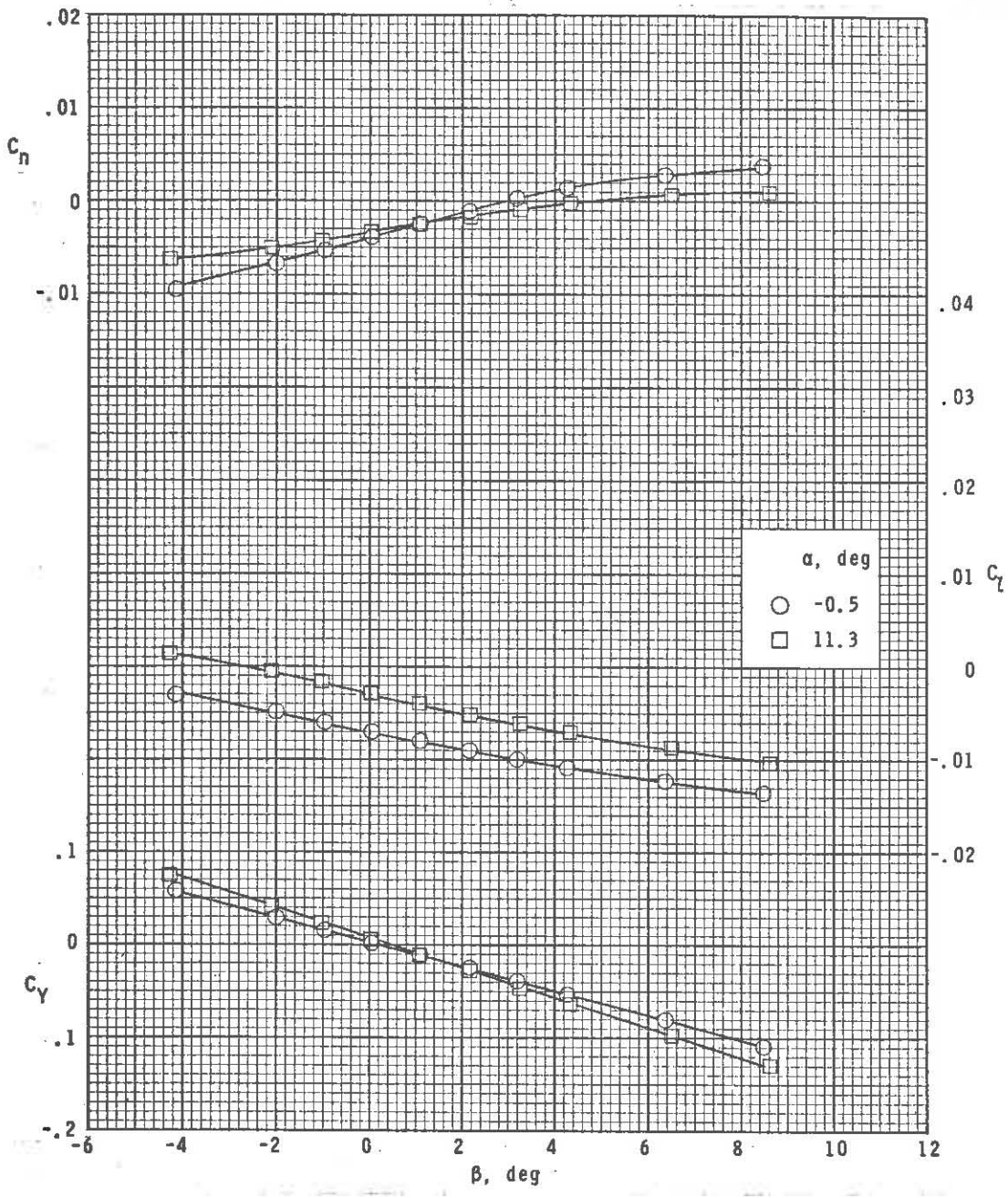

(b) M = 2.86.

Figure 18.- Continued.

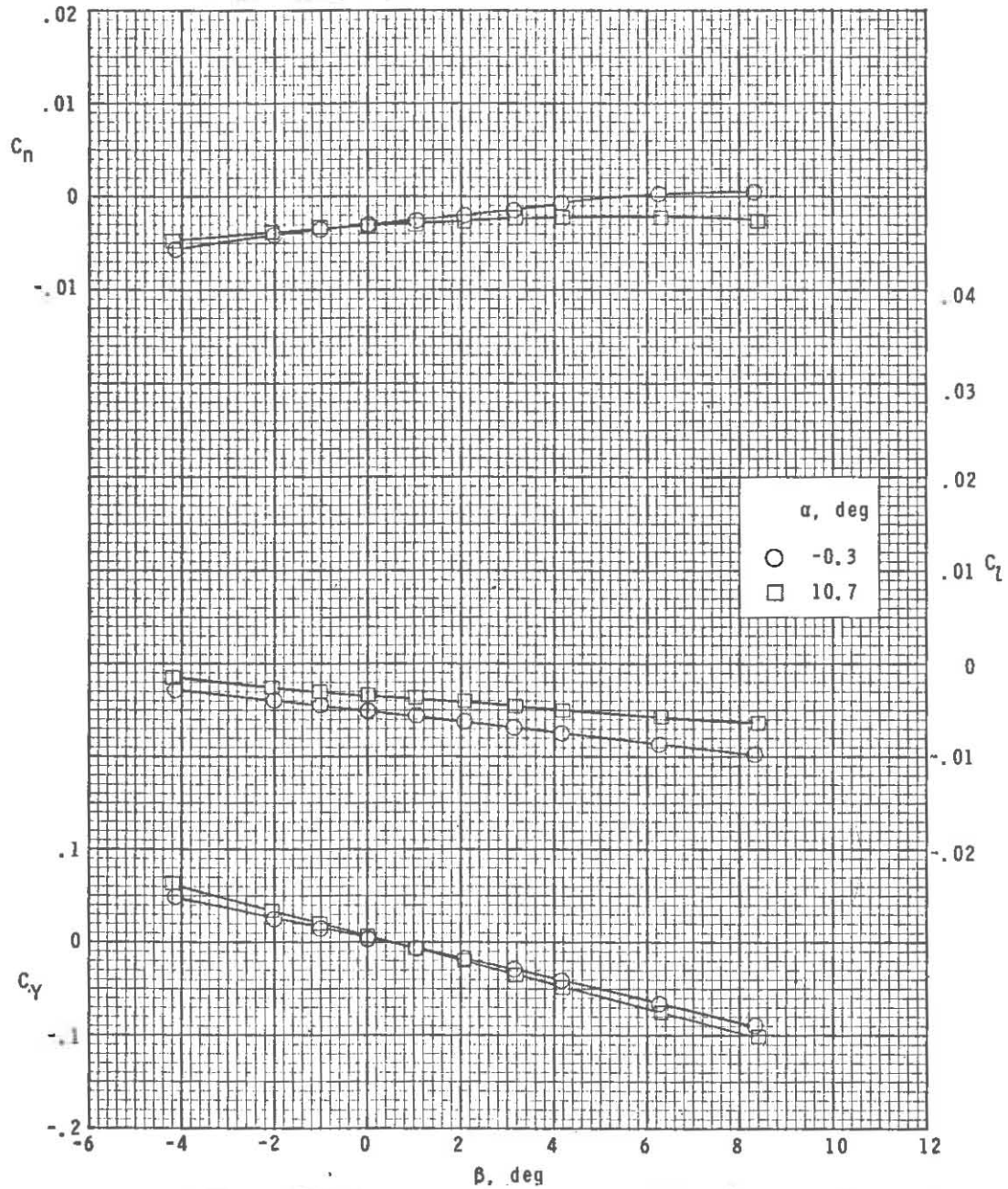

(c) M = 3.95.

Figure 18.- Continued.

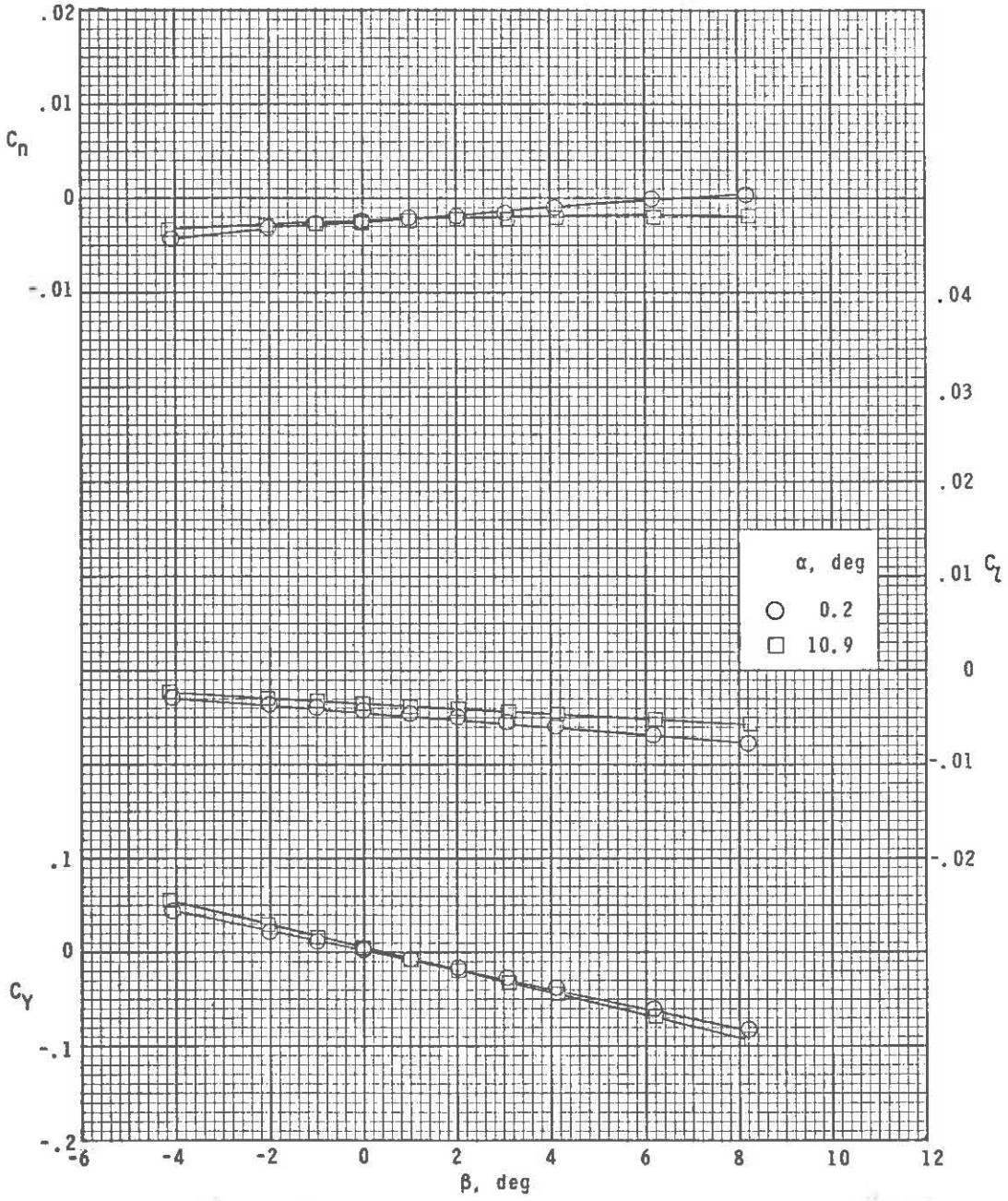

(d) M = 4.63.

Figure 18.- Concluded.

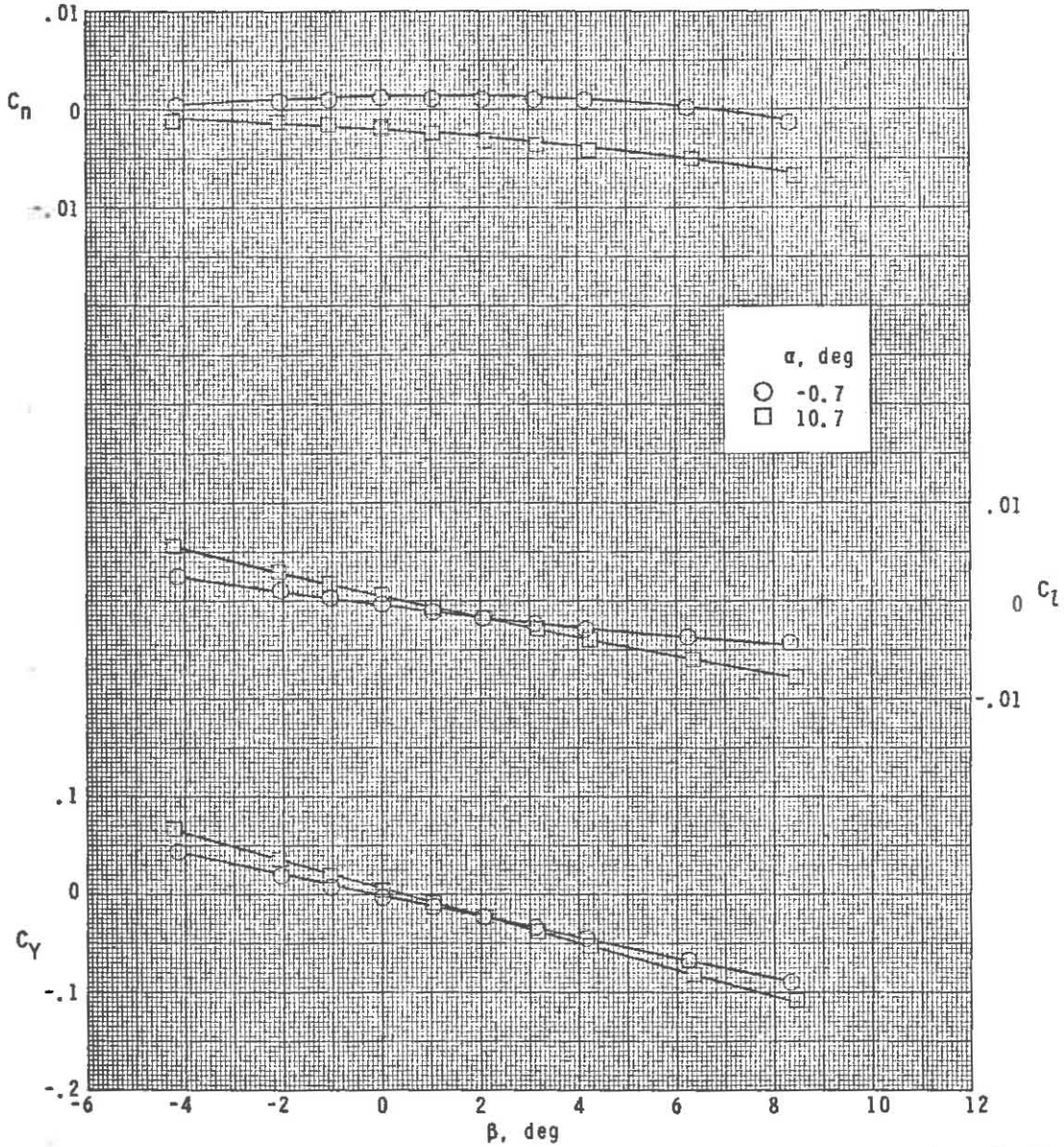

(a) M = 2.50.

Figure 19.- Sideslip characteristics at various angles of attack for right vertical tail off. $\delta_r = 0^o$.

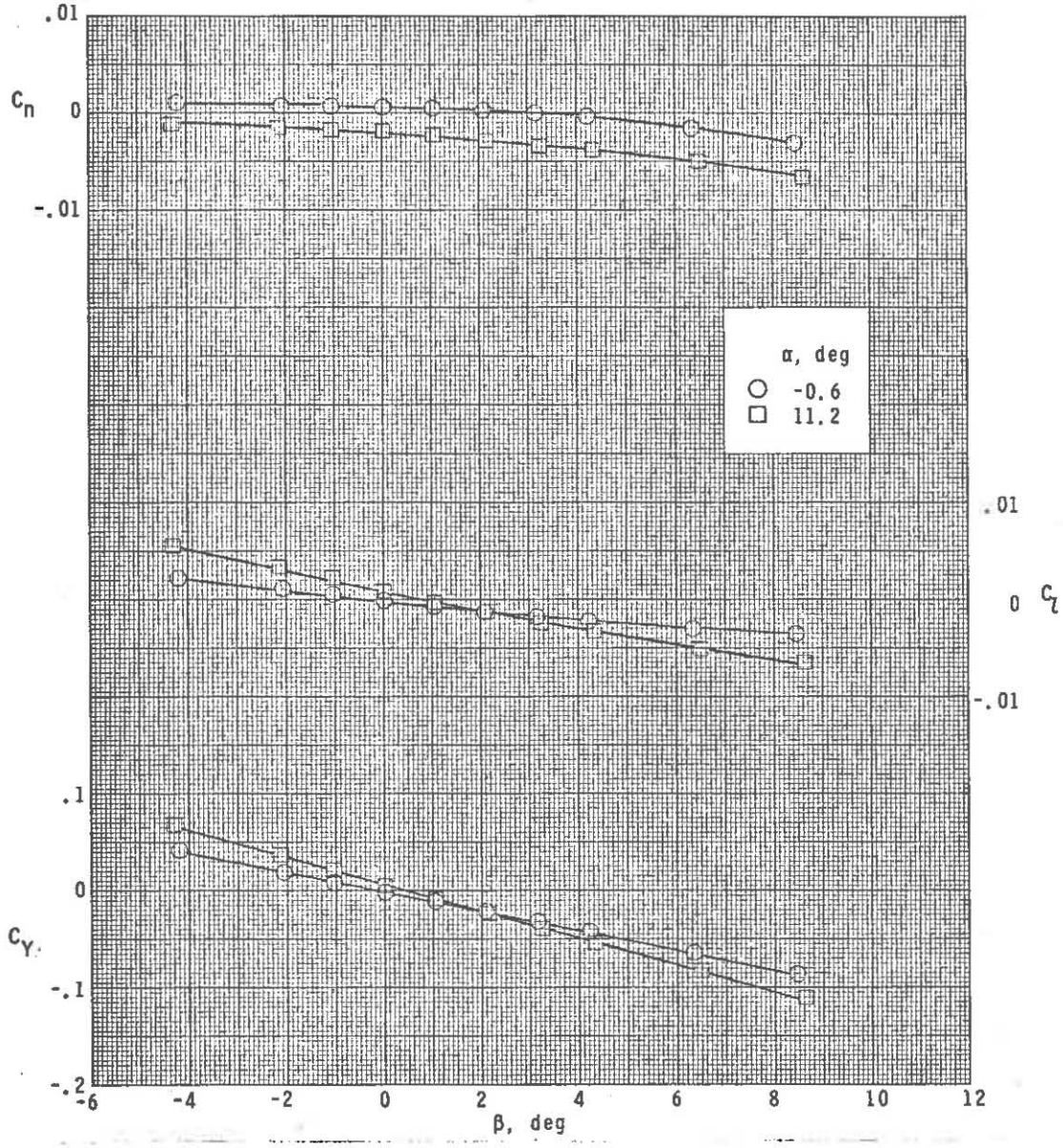

(b) M = 2.86.

Figure 19.- Continued.

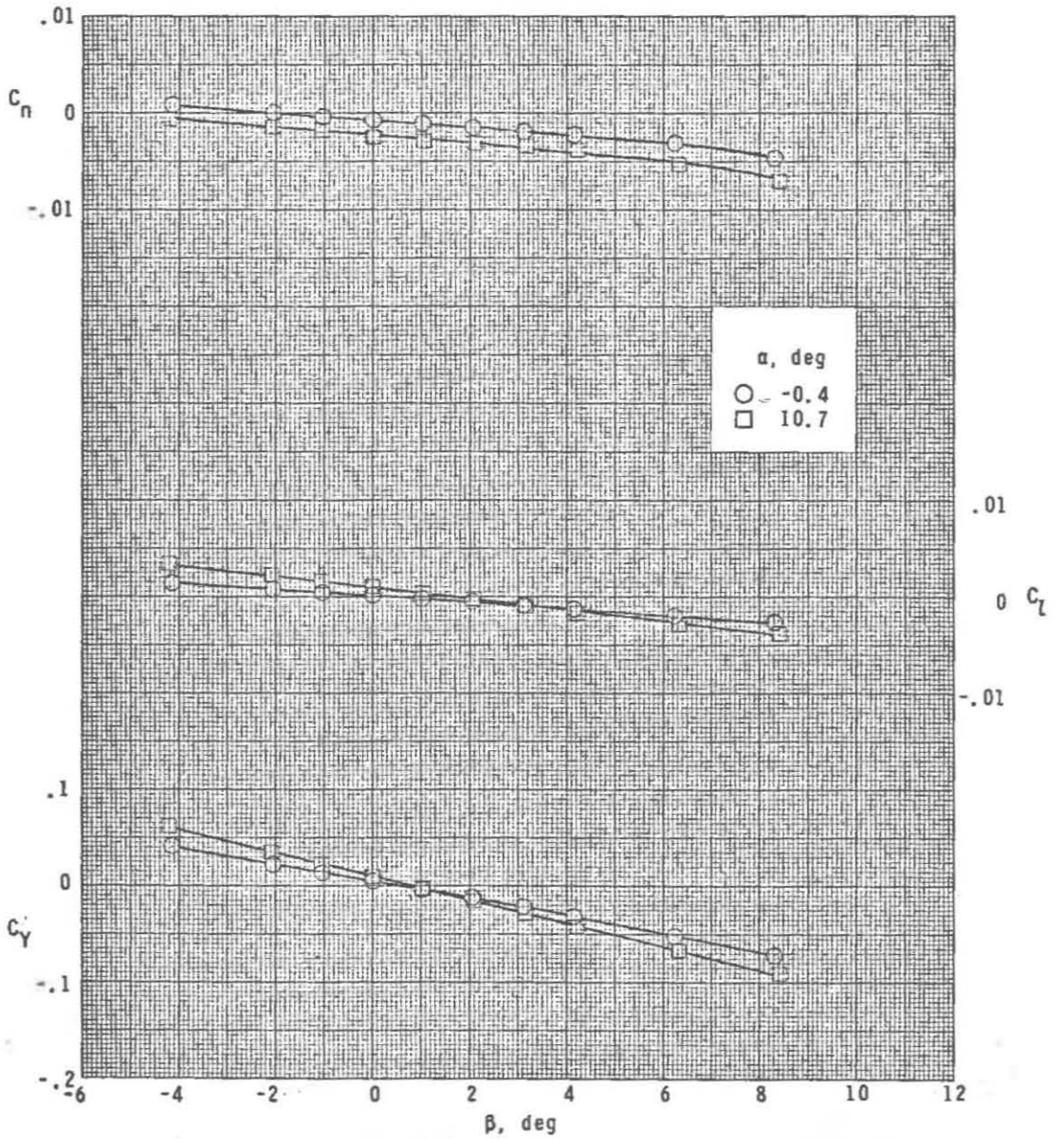

(c) M = 3.95.

Figure 19.- Continued.

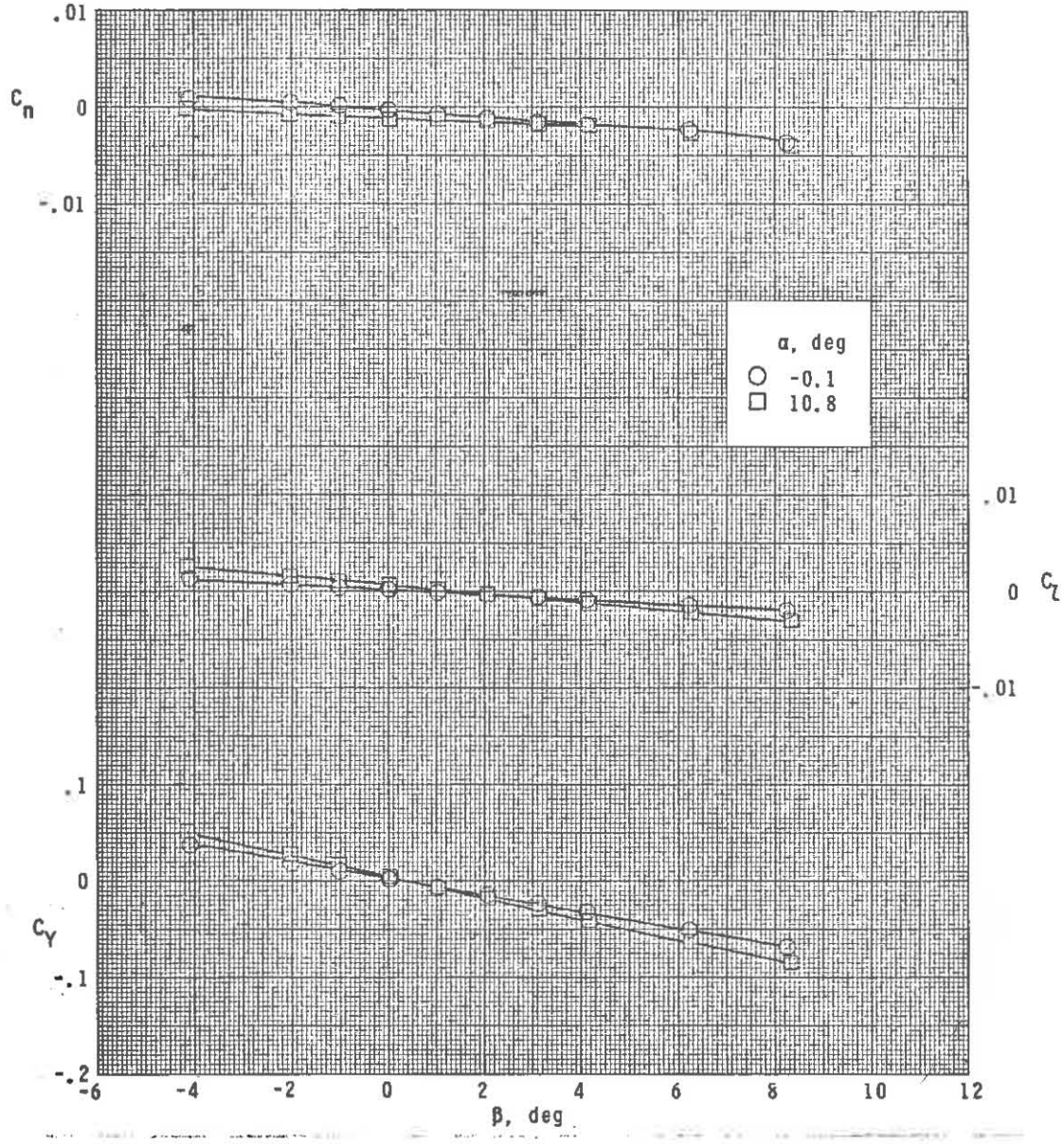

(d) M = 4.63.

Figure 19.- Concluded.

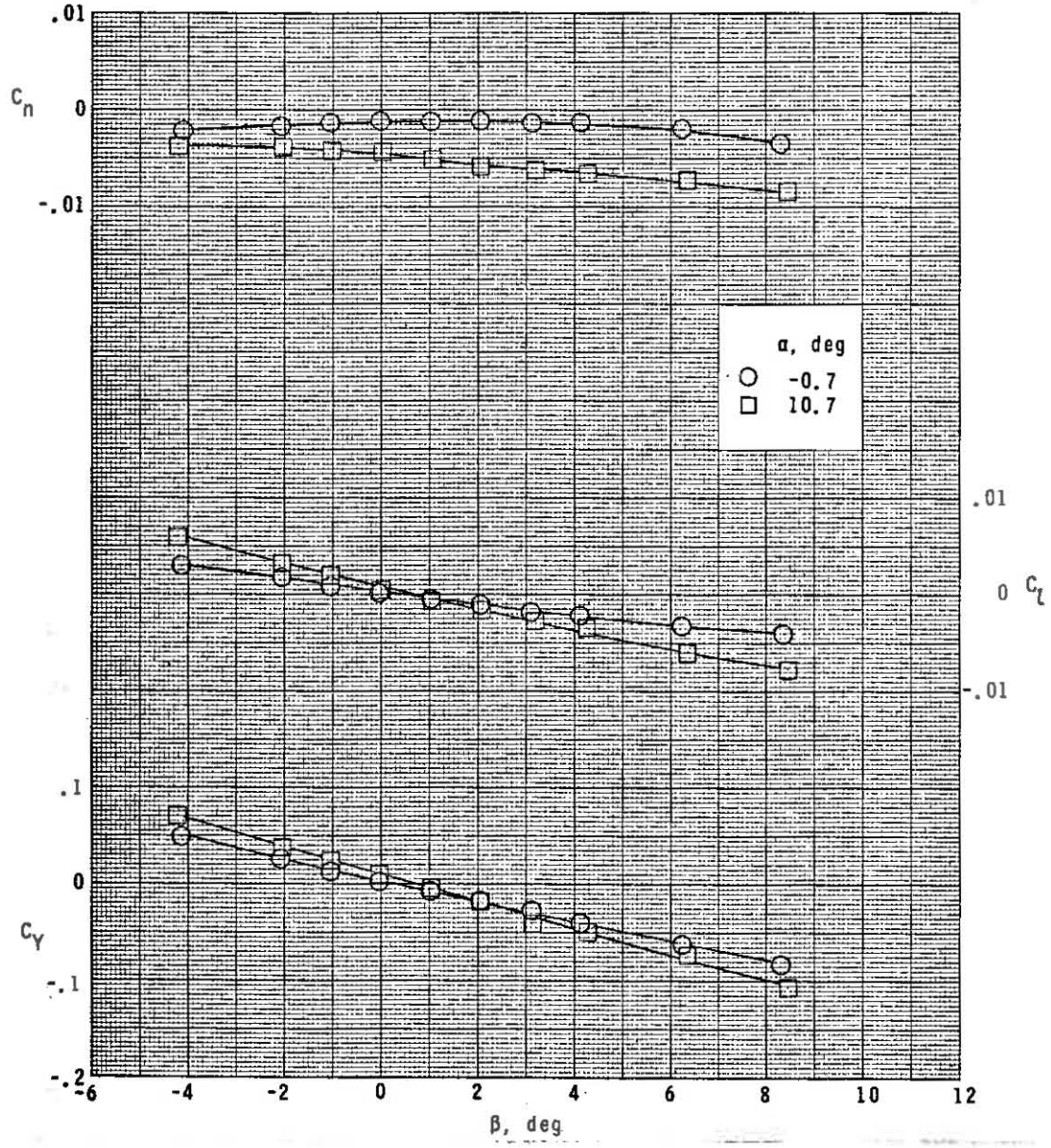

(a) M = 2.50.

Figure 20.- Sideslip characteristics at various angles of attack for right vertical tail off. $\delta_r = 15^o$.

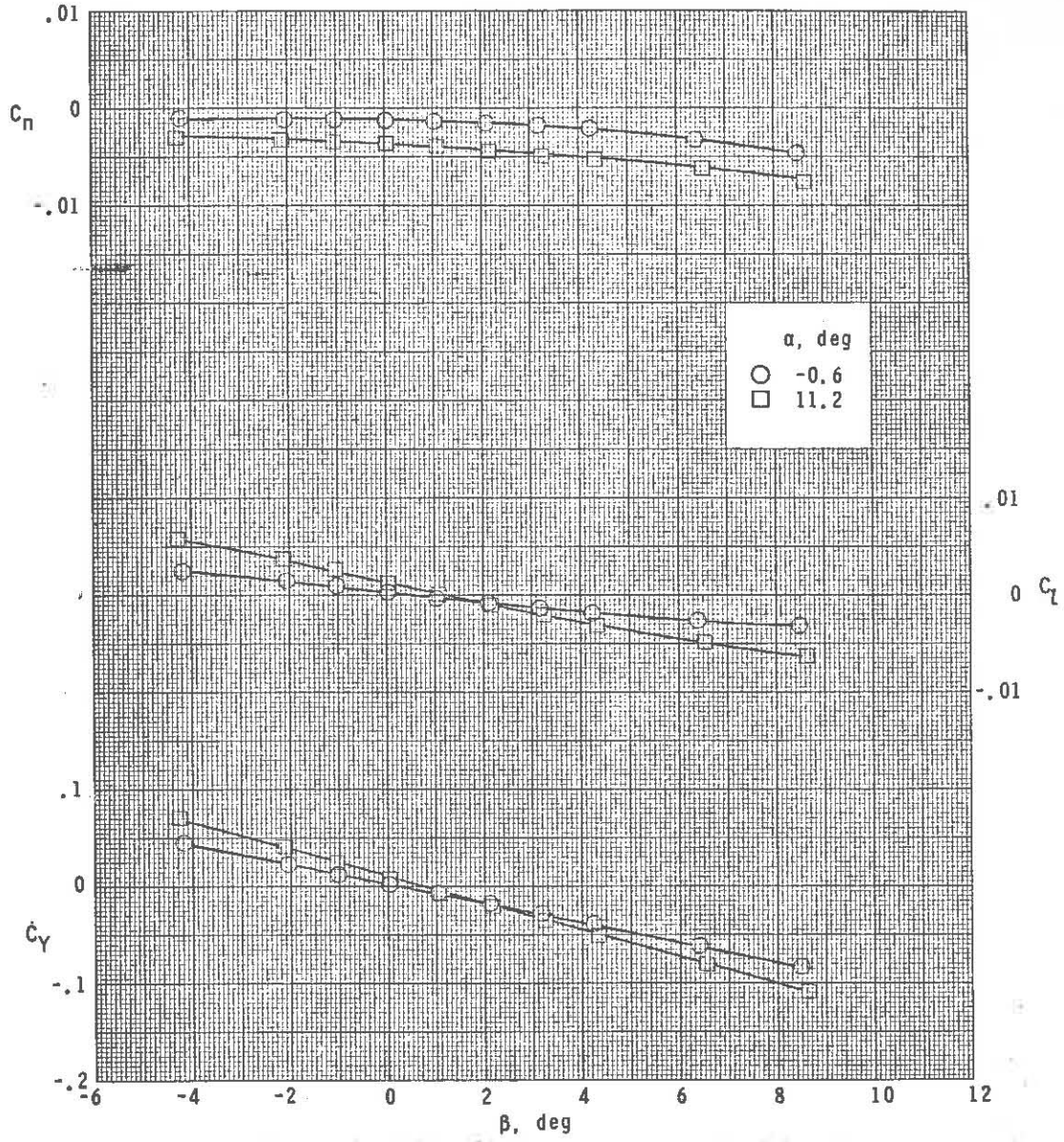

(b) M = 2.86.

Figure 20.- Continued.

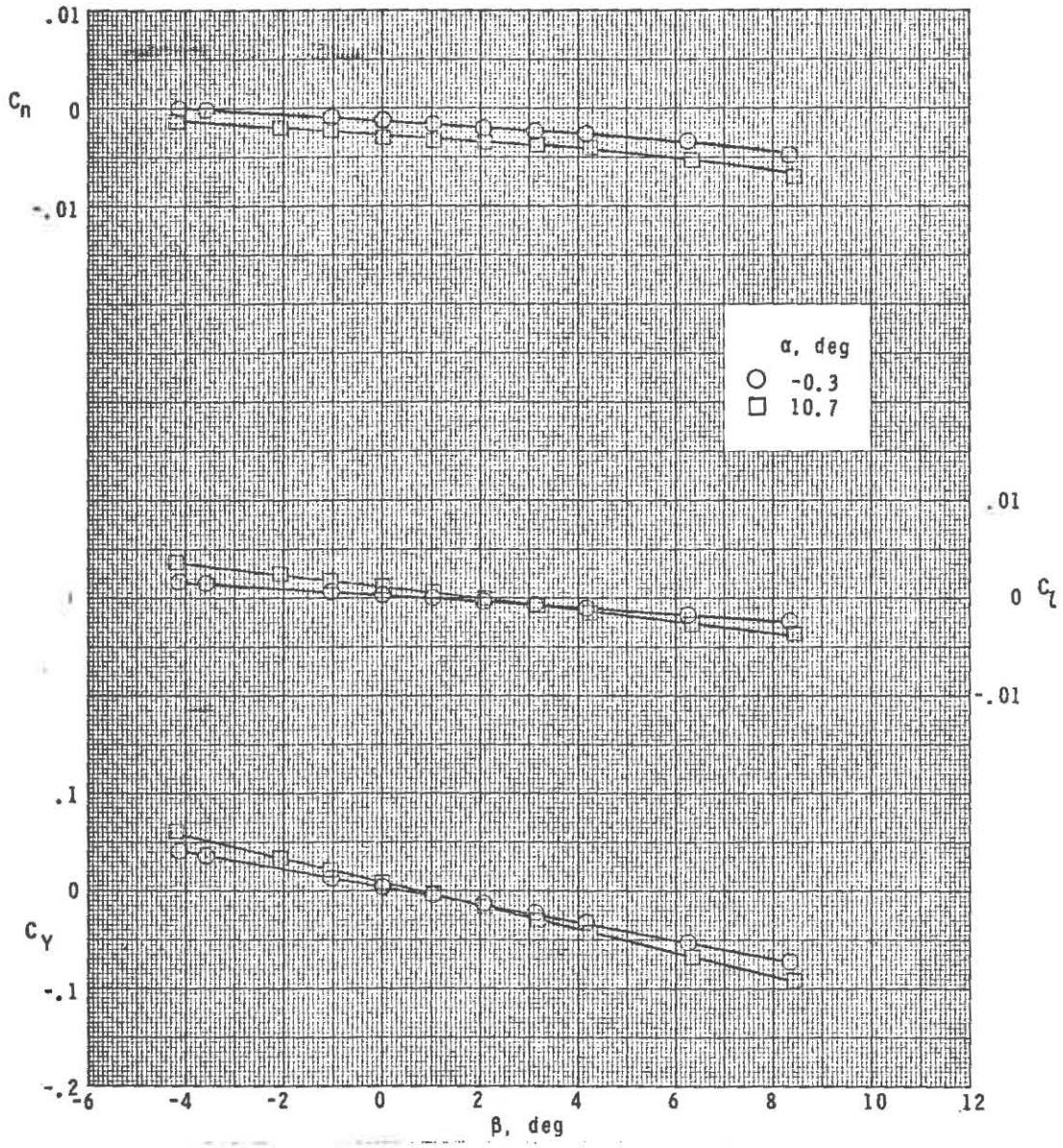

(c) M = 3.95.

Figure 20.- Continued.

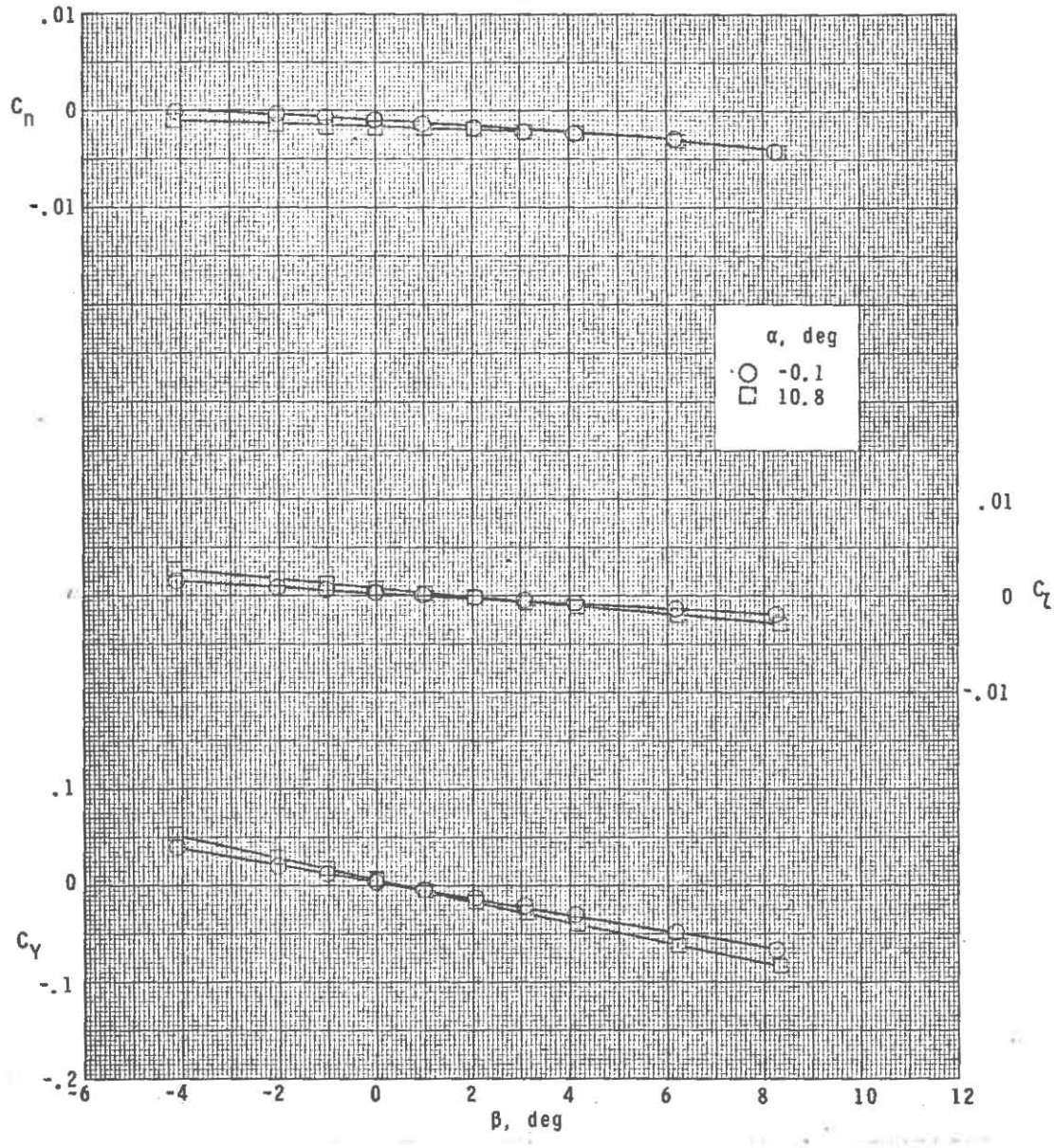

(d) M = 4.63.

Figure 20.- Concluded.

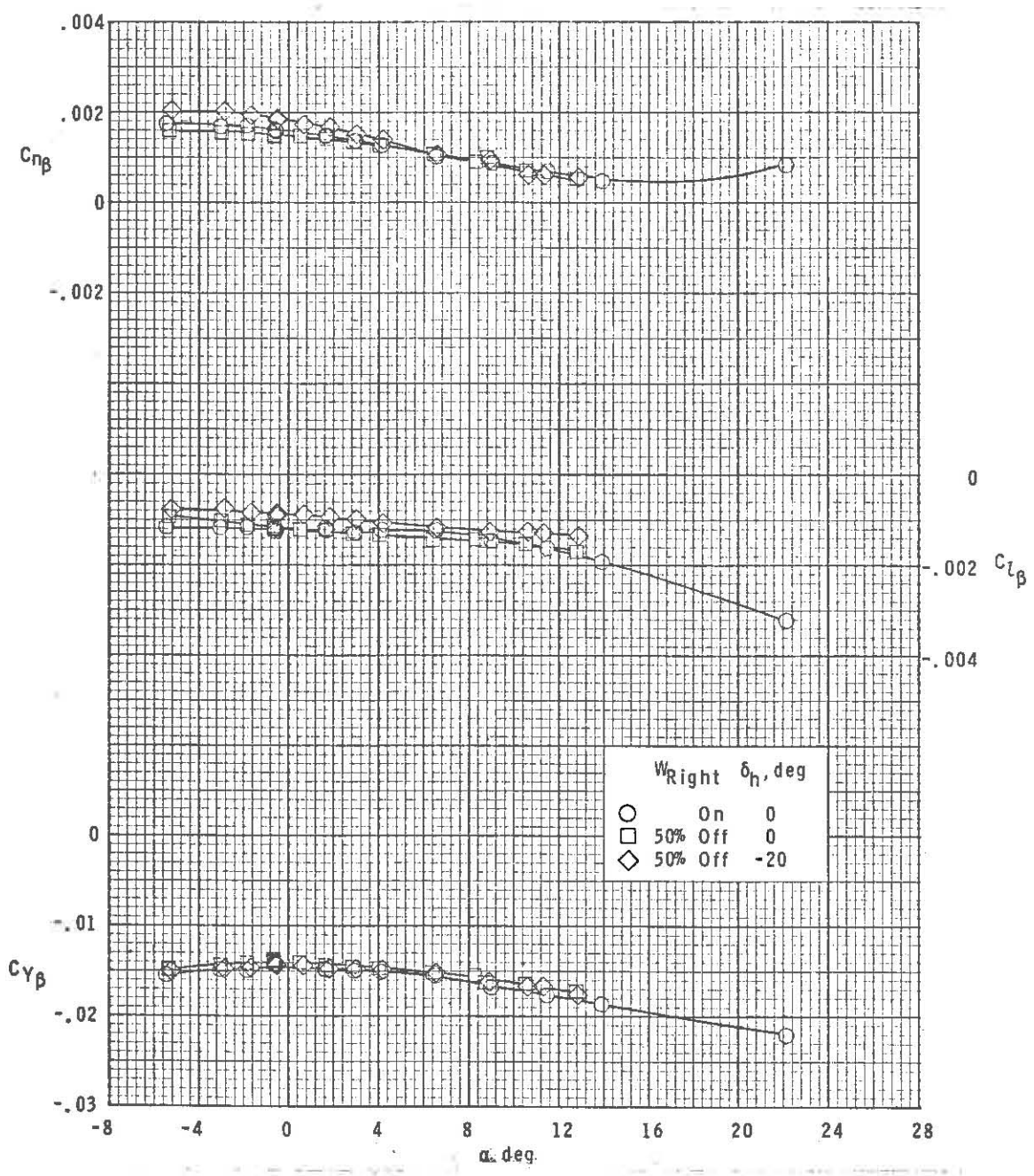

(a) M = 2.50.

Figure 21.- Sideslip parameters for asymmetric wing condition and horizontal-tail control.

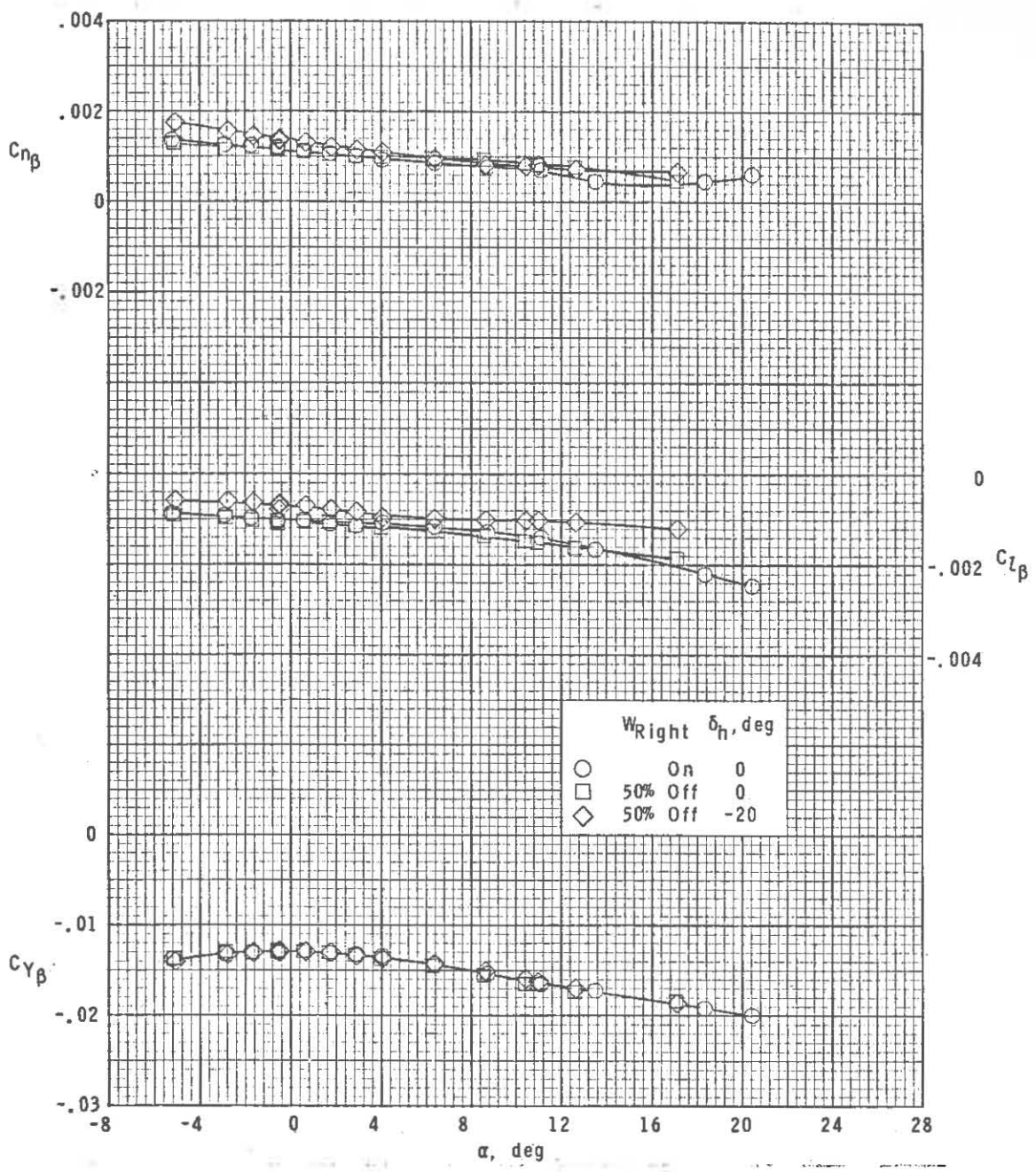

(b) M = 2.86.

Figure 21.- Continued.

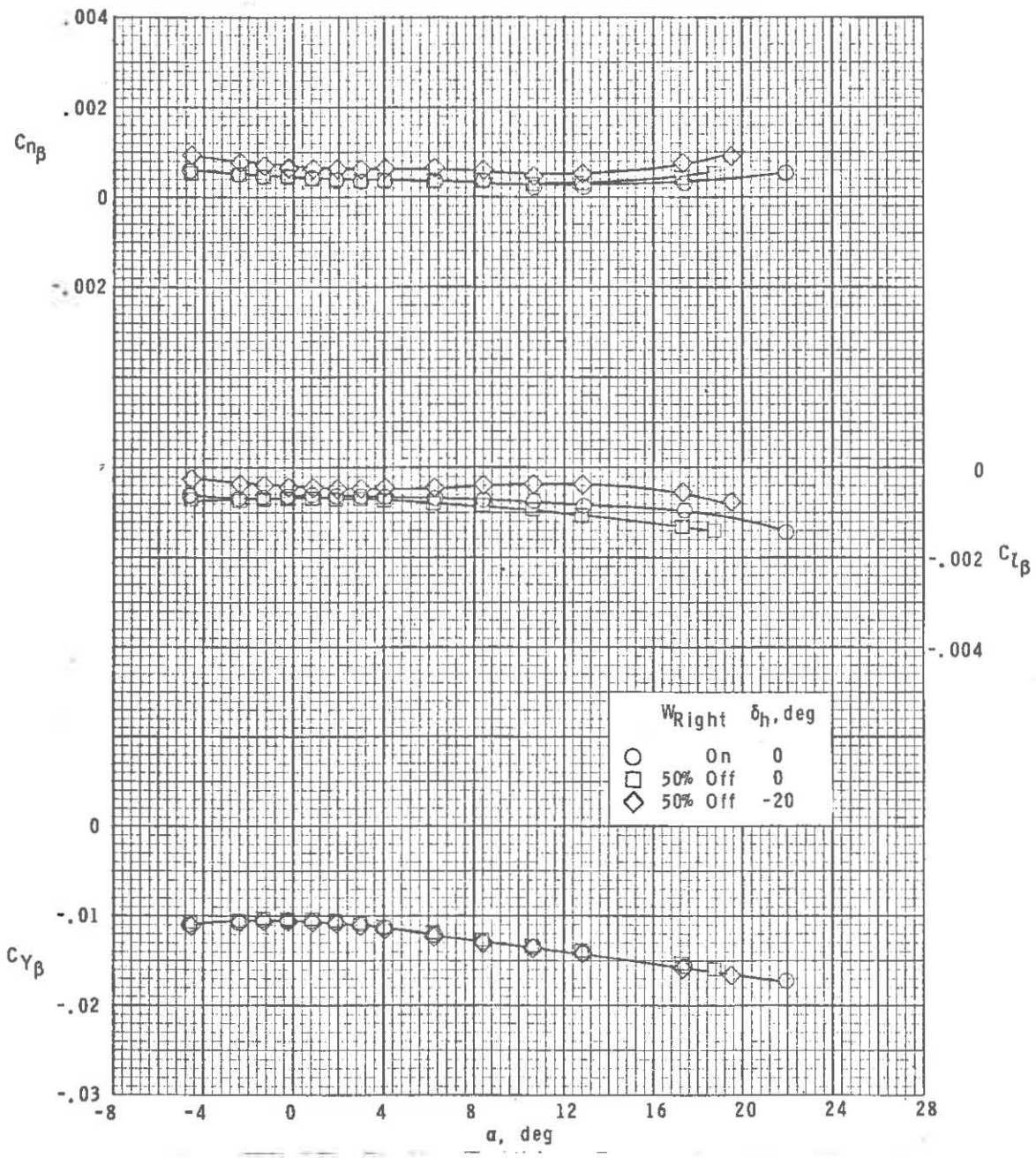

(c) M = 3.95.

Figure 21.- Continued.

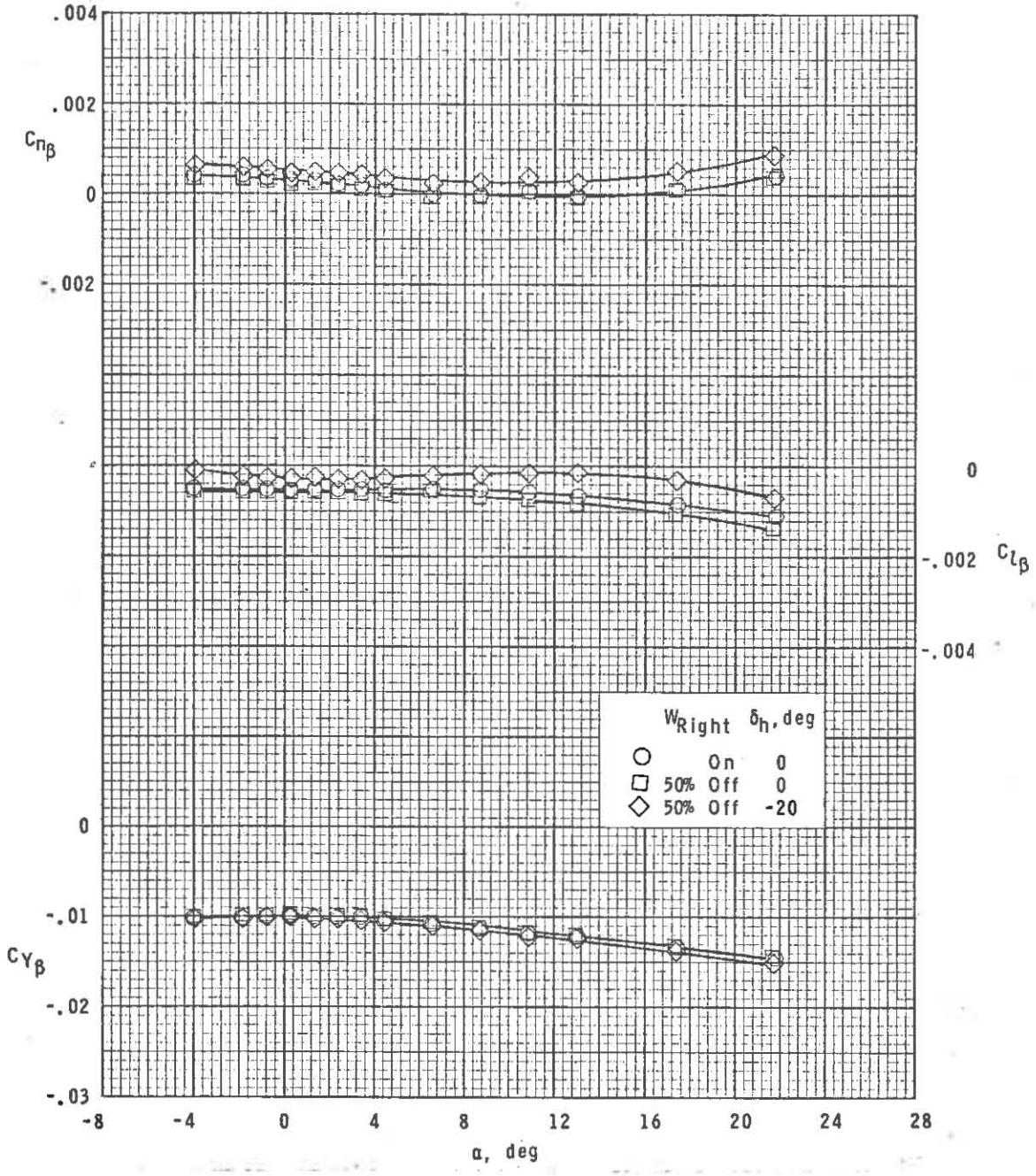

(d) M = 4.63.

Figure 21.- Concluded.

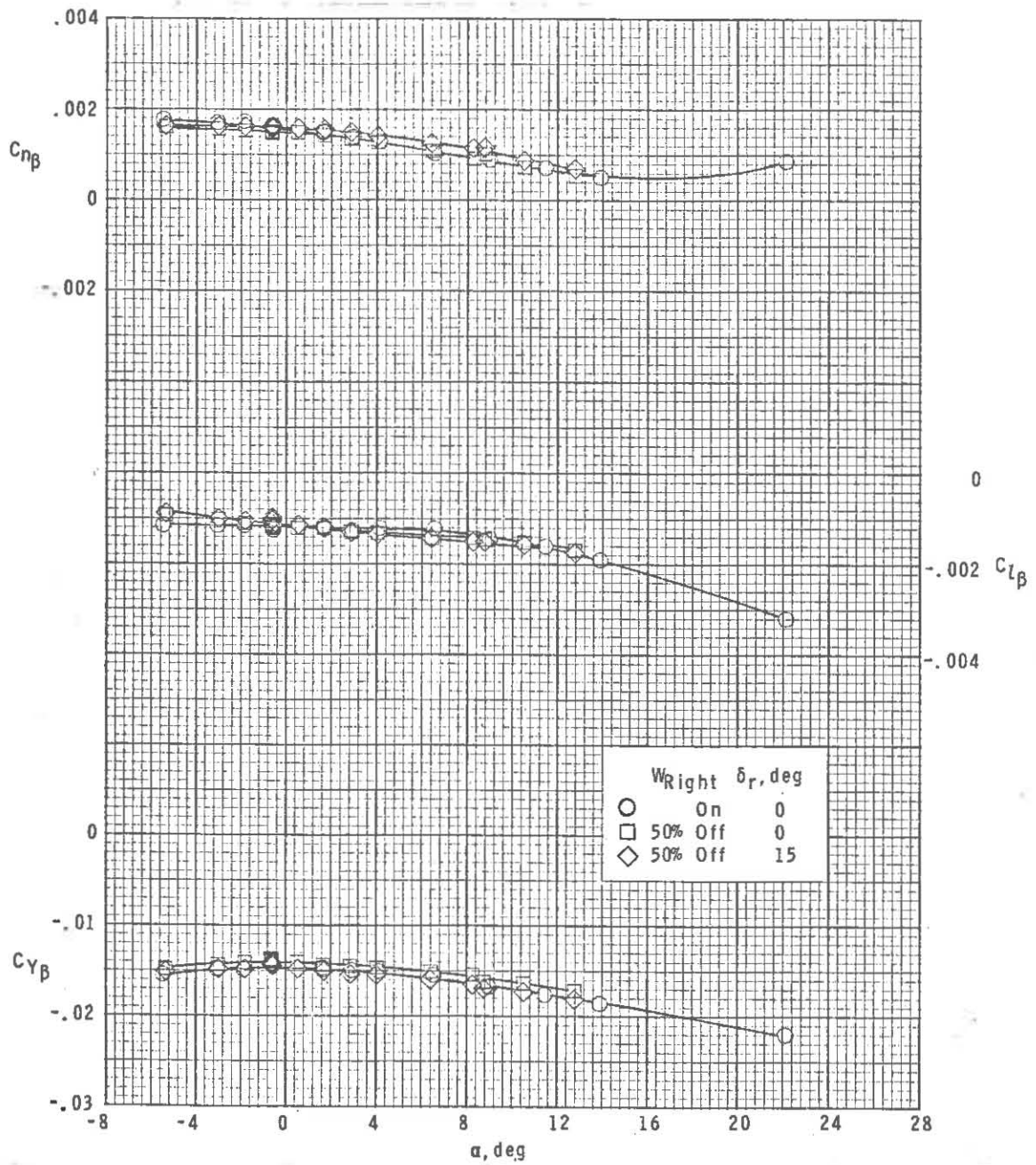

(a) M = 2.50.

Figure 22.- Sideslip parameters for asymmetric wing condition and rudder control.

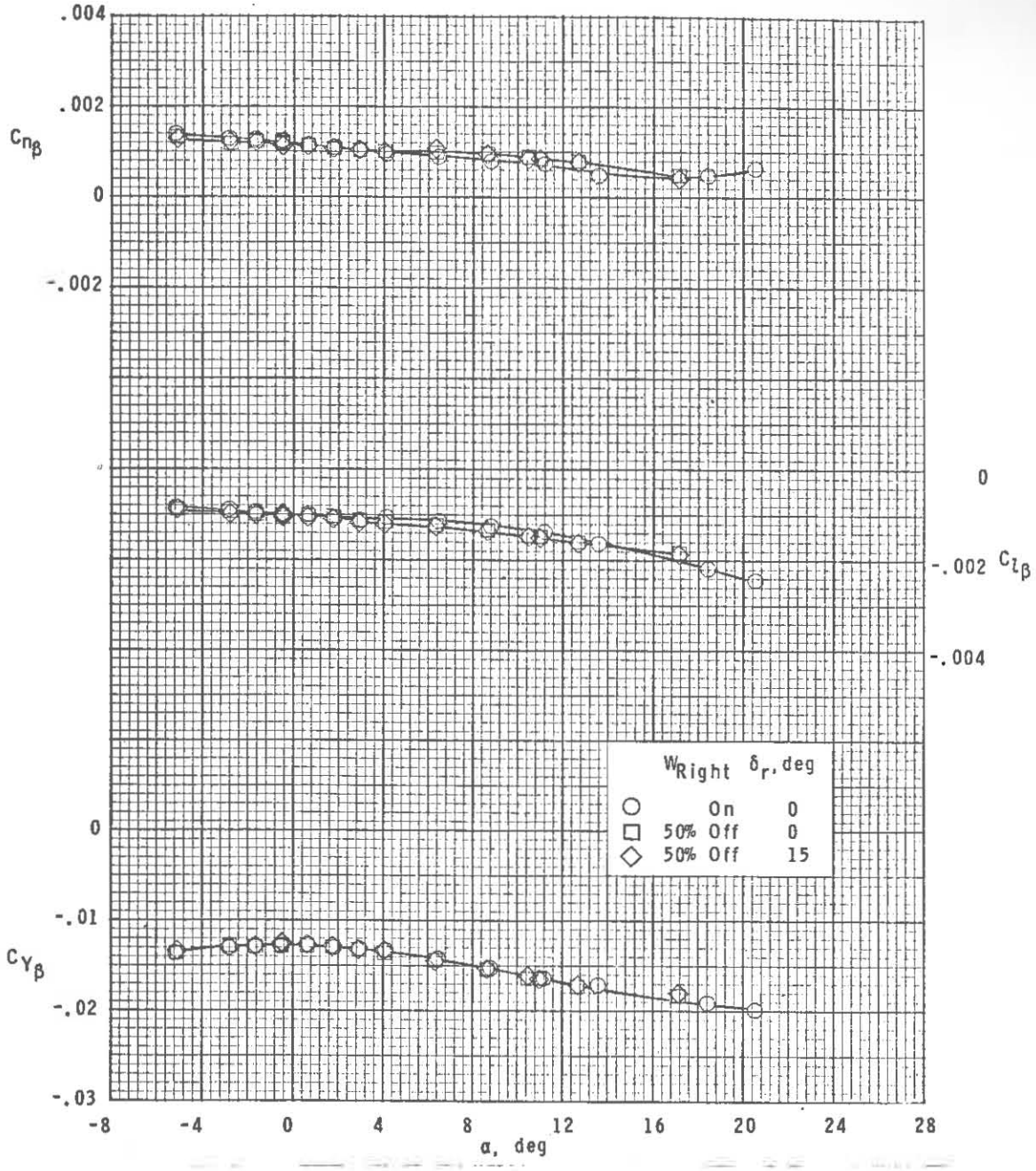

(b) M = 2.86.

Figure 22.- Continued.

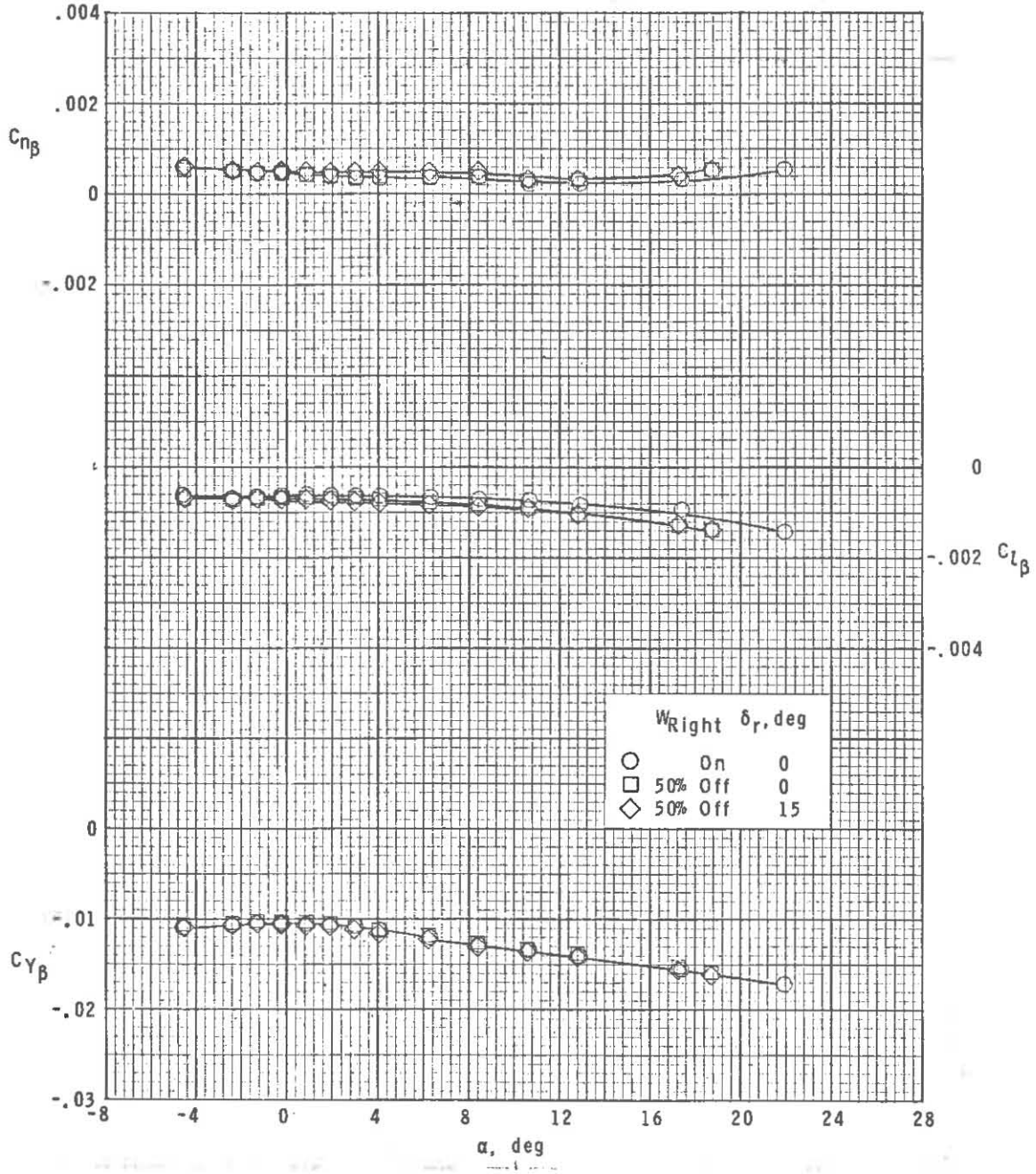

(c) M = 3.95.

Figure 22.- Continued.

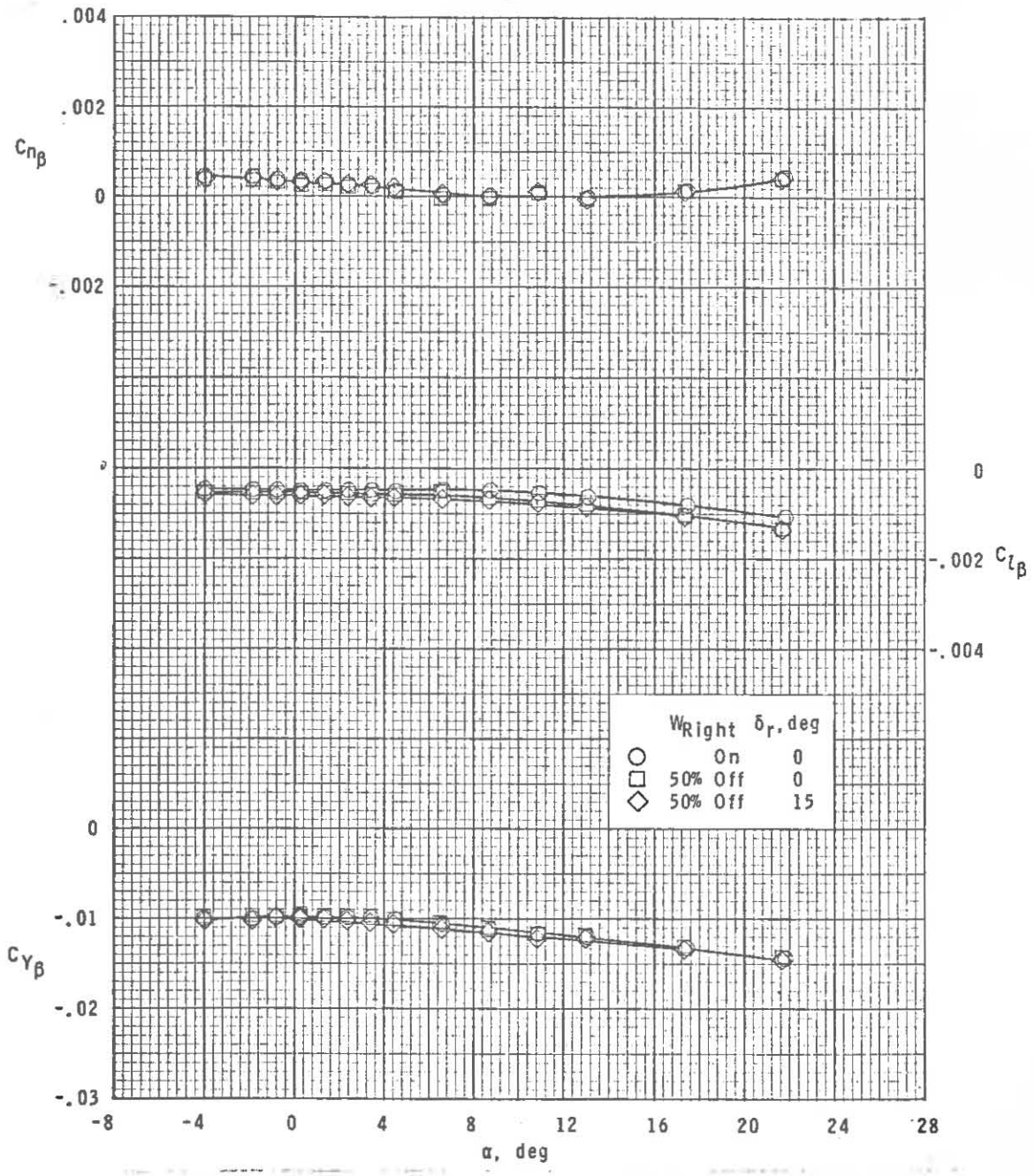

(d) M = 4.63.

Figure 22.- Concluded.

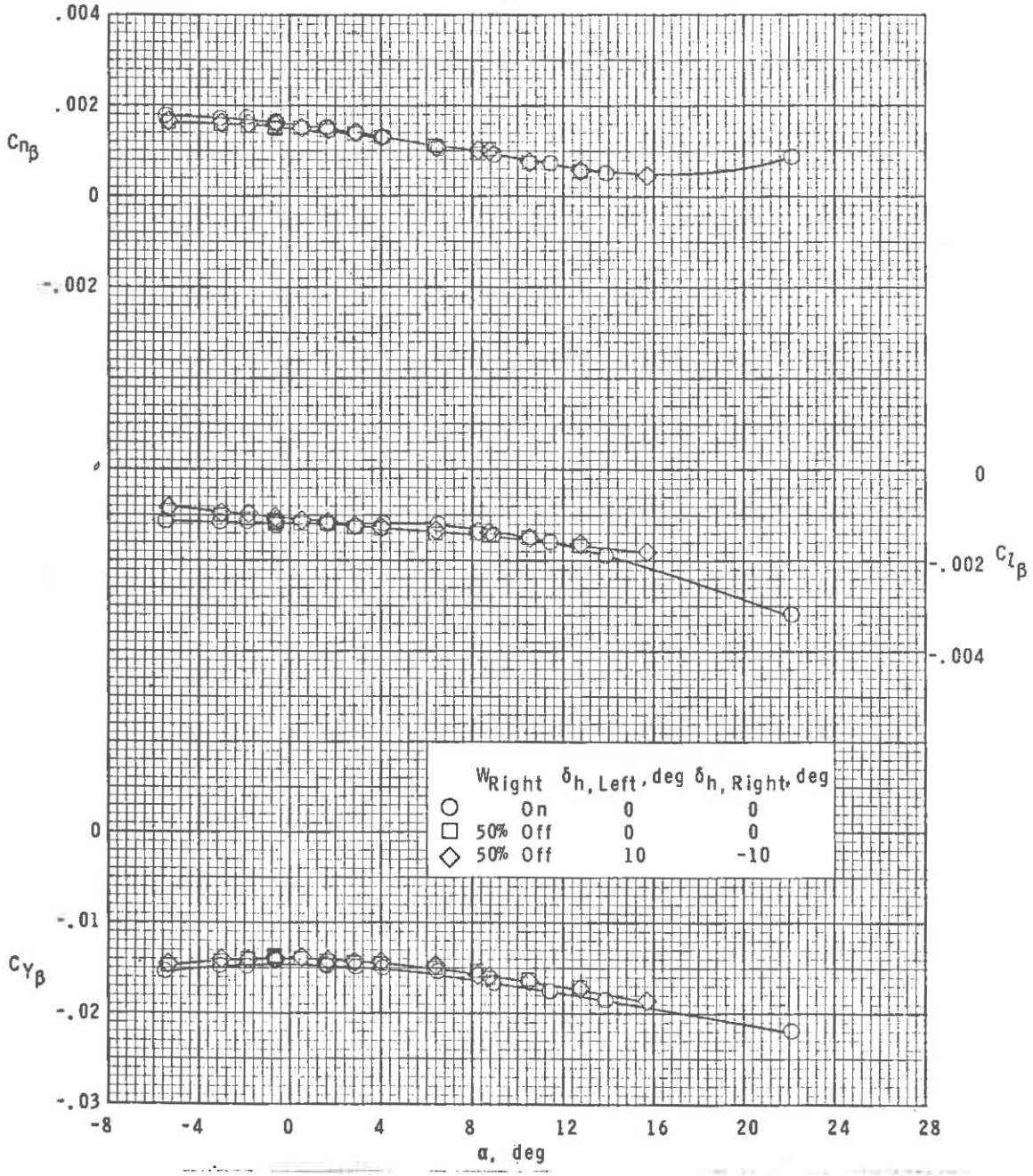

(a) M = 2.50.

Figure 23.- Sideslip parameters for asymmetric wing condition and differential horizontal-tail settings.

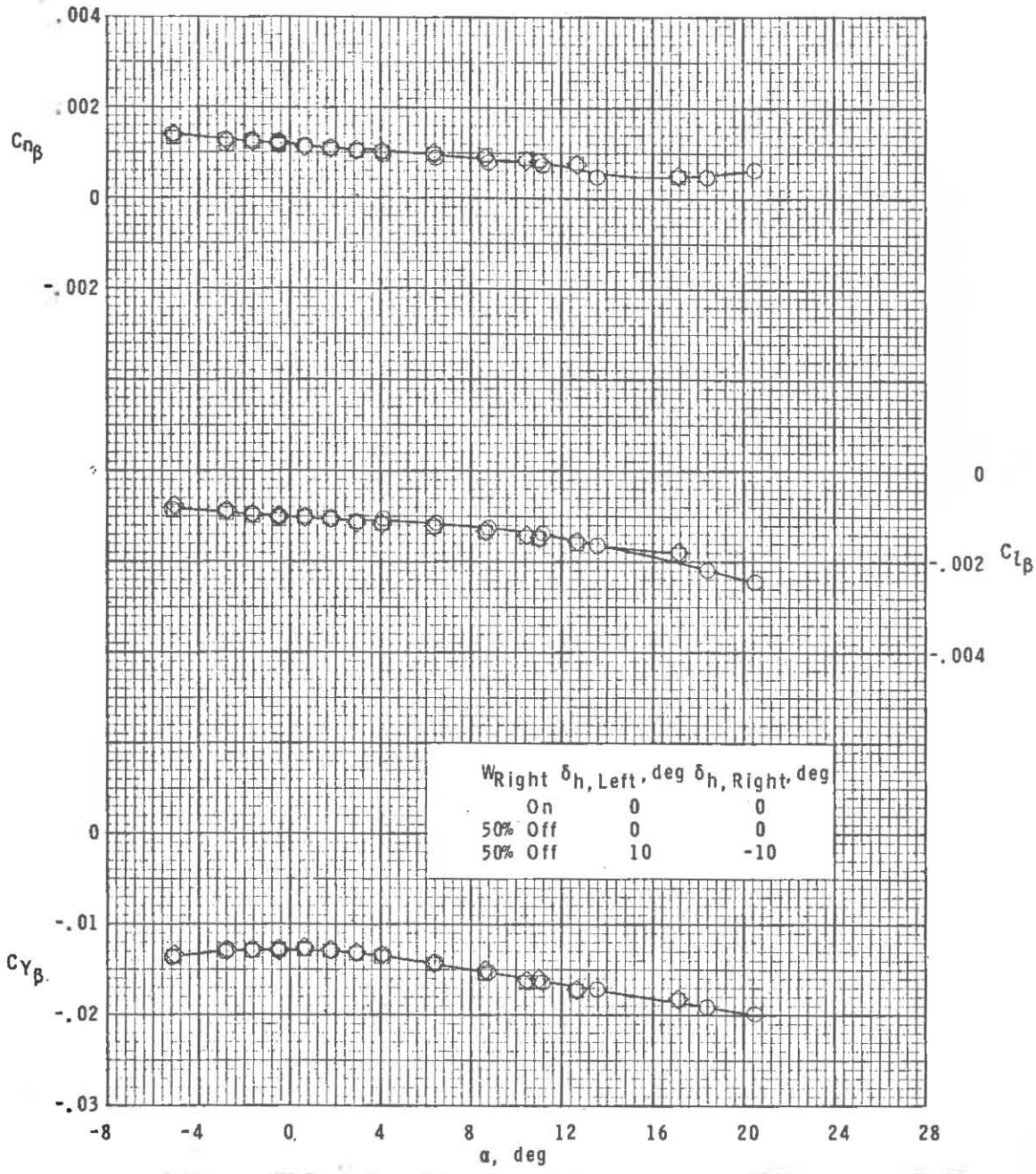

(b) M = 2.86.

Figure 23.- Continued.

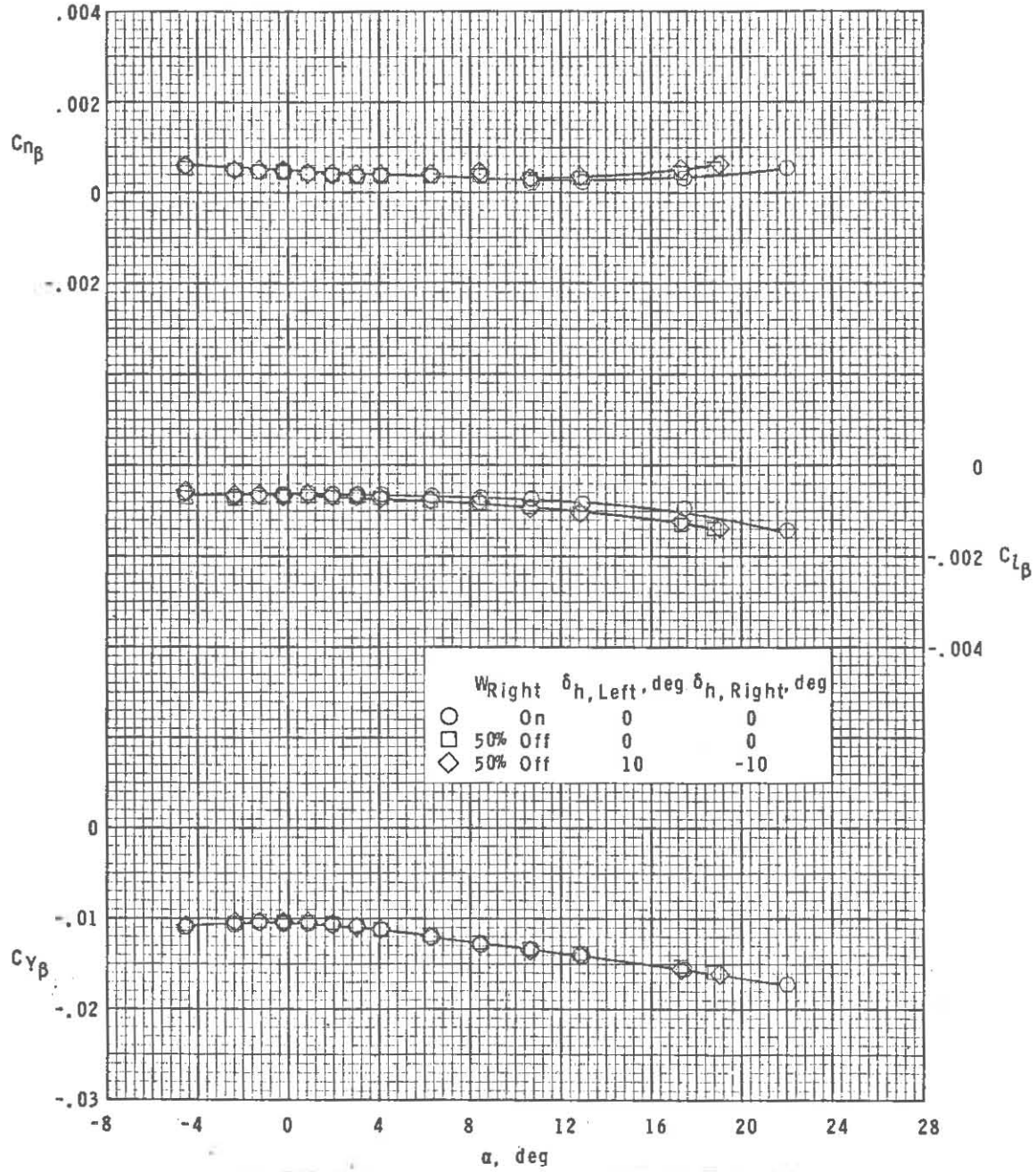

(c) M = 3.95.

Figure 23.- Continued.

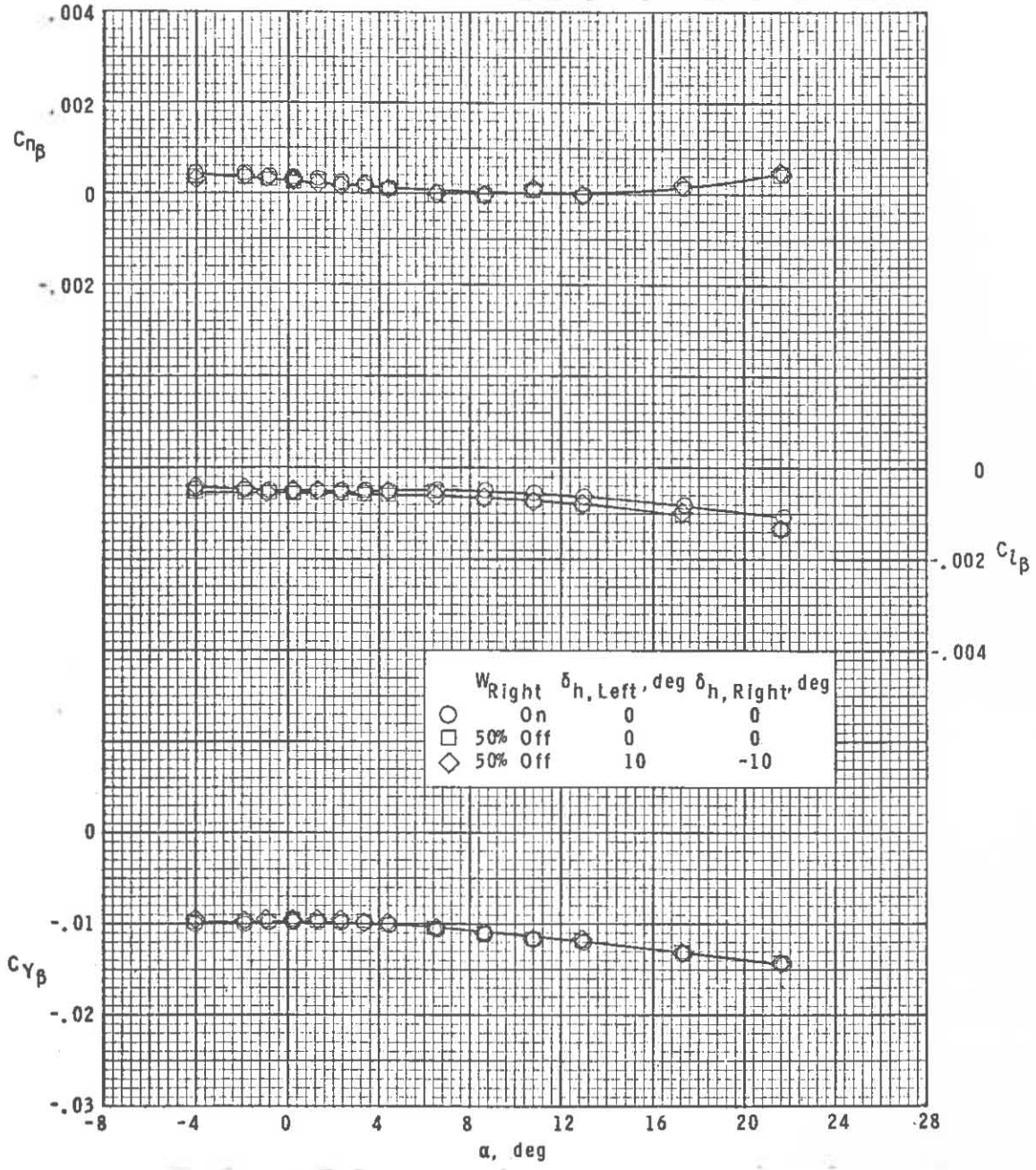

(d) M = 4.63.

Figure 23.- Concluded.

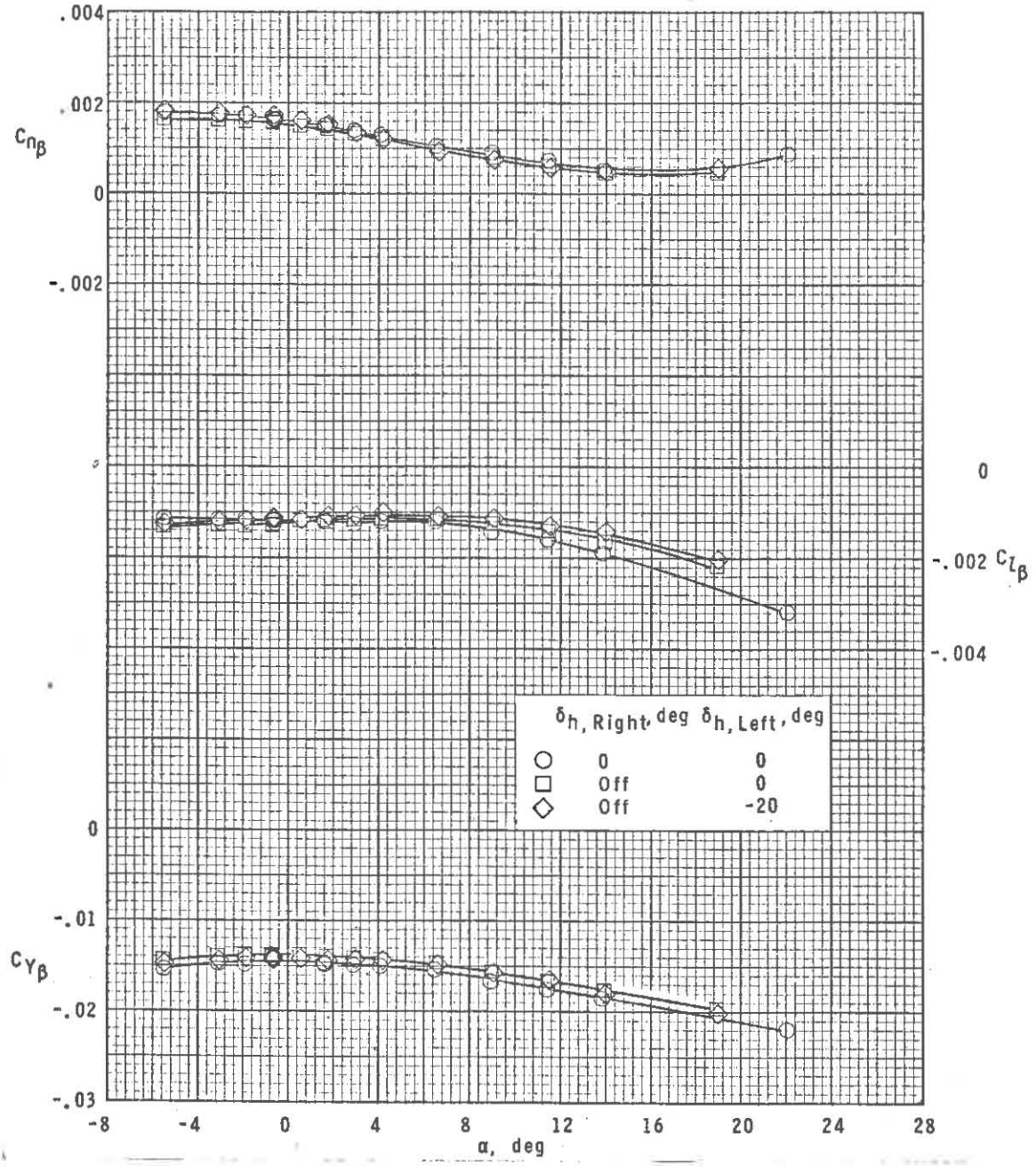

(a) M = 2.50.

Figure 24.- Sideslip parameters for asymmetric horizontal-tail condition.

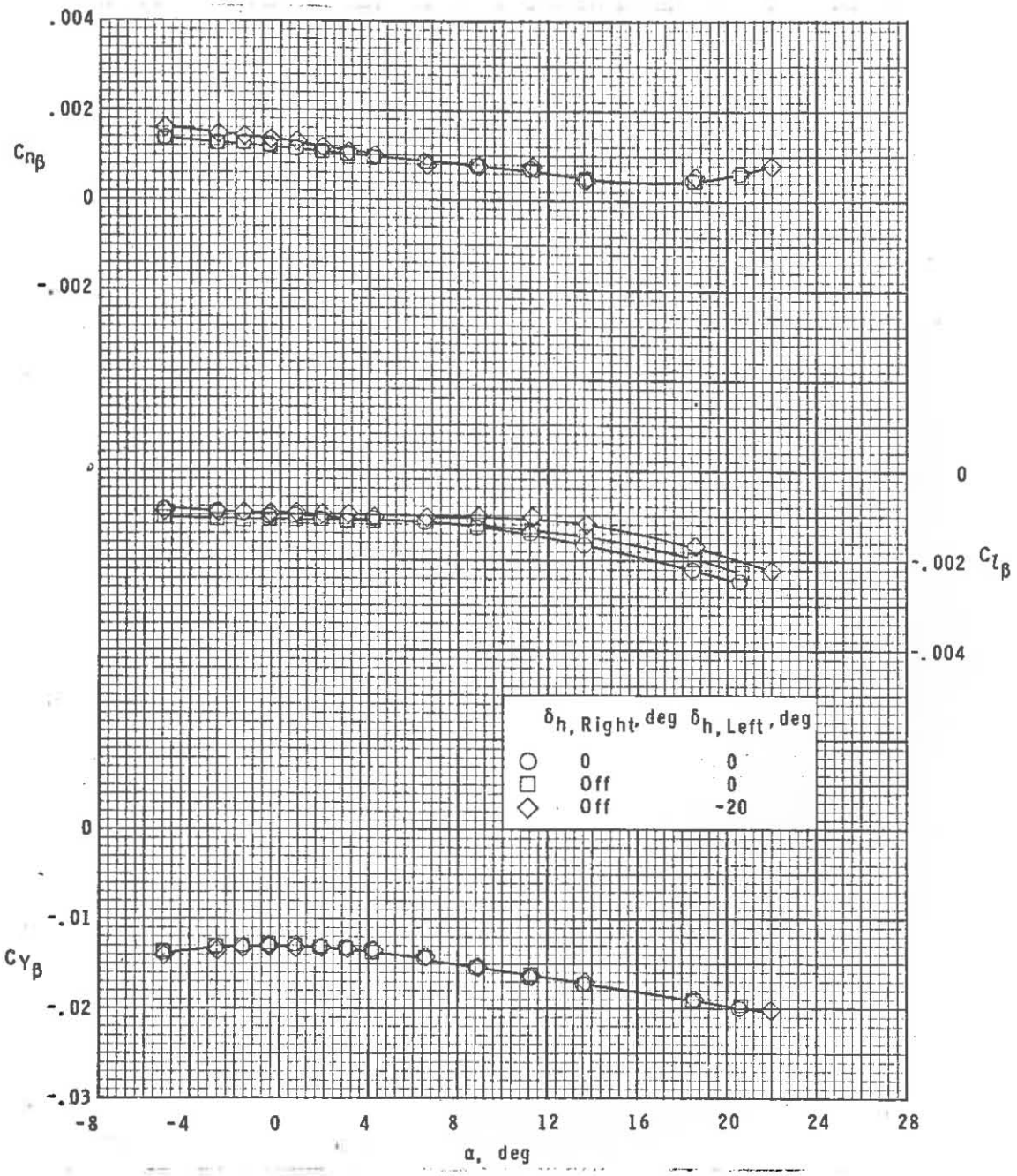

(b) M = 2.86.

Figure 24.- Continued.

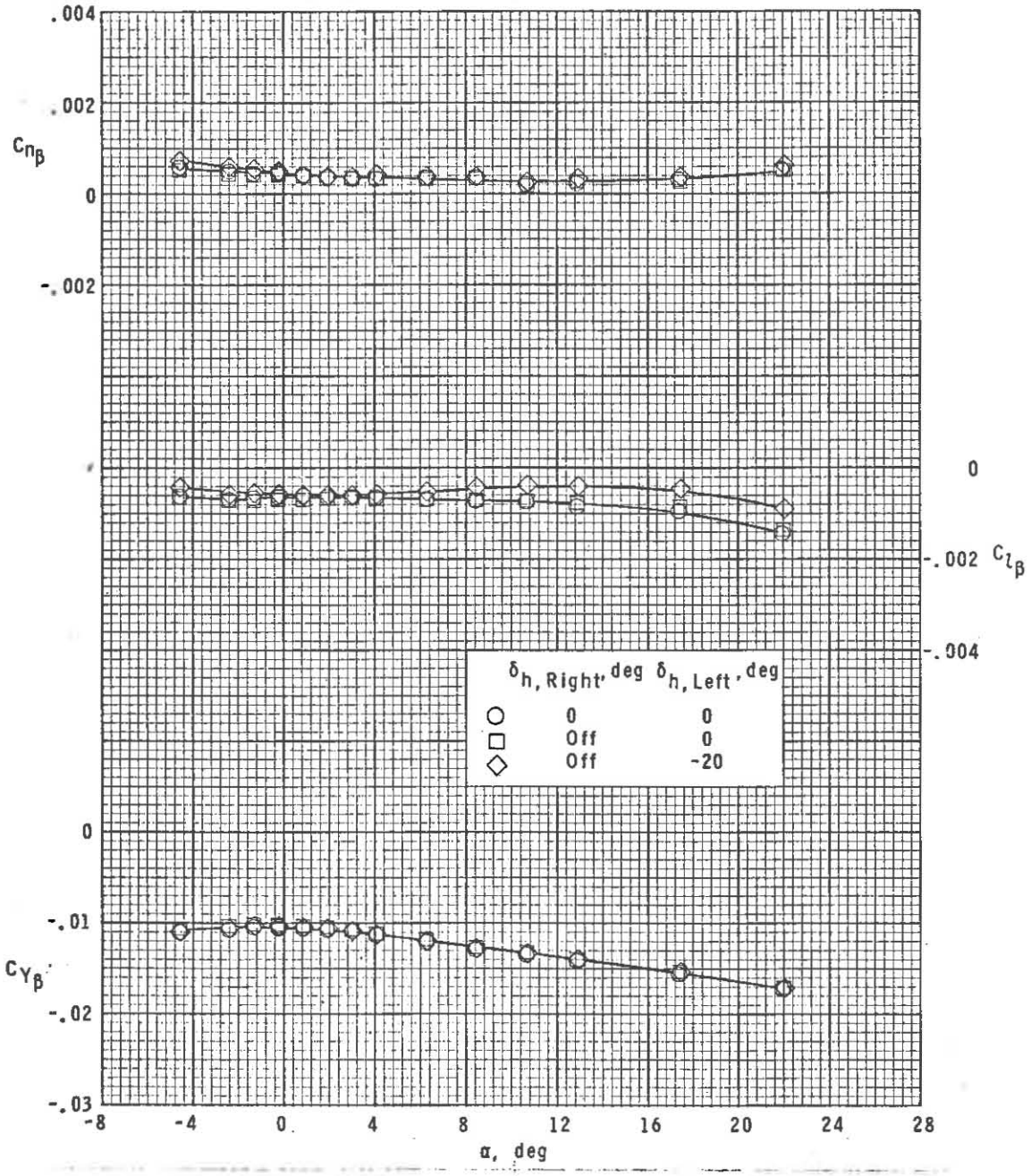

(c) M = 3.95.

Figure 24.- Continued.

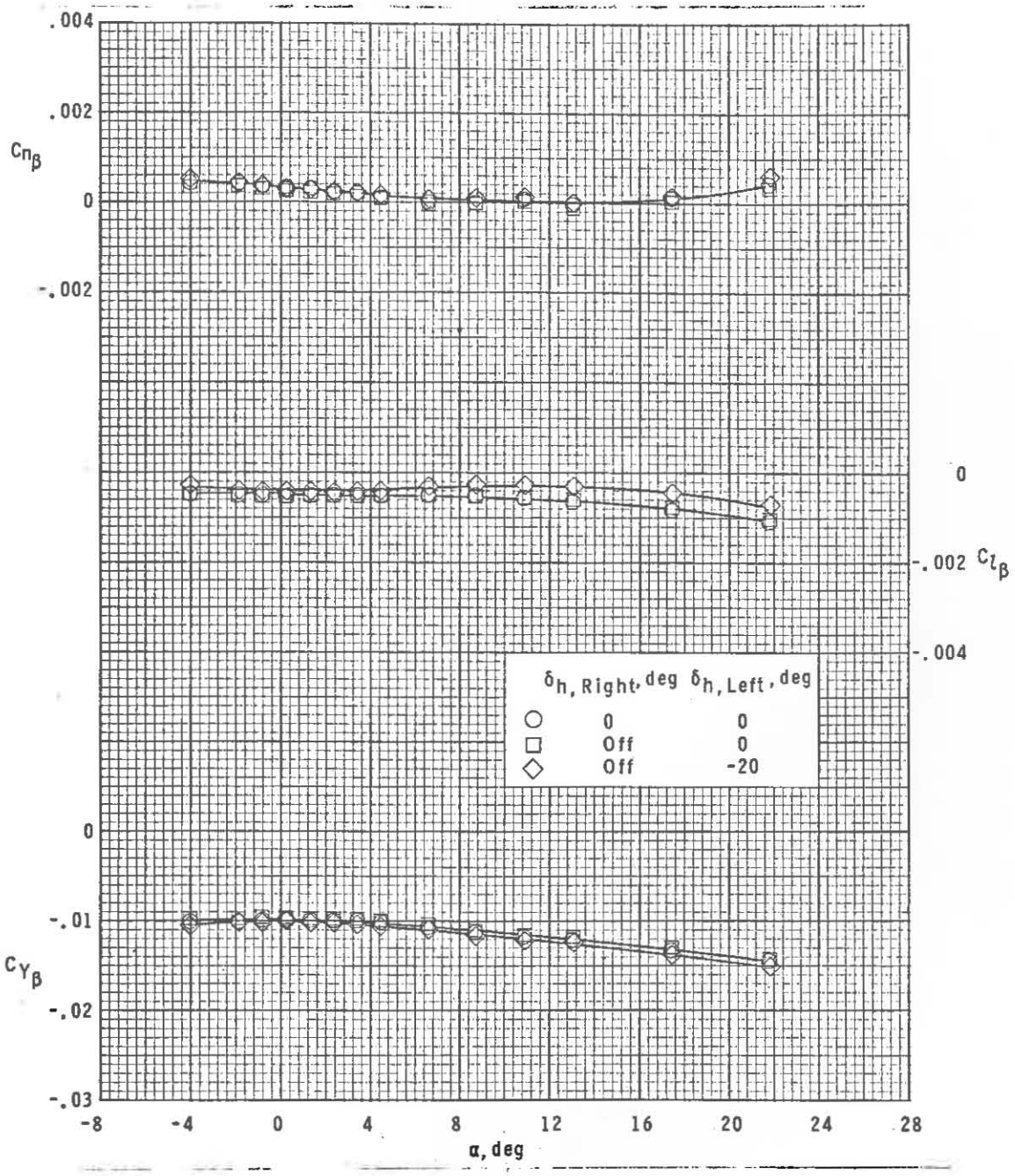

(d) M = 4.63.

Figure 24.- Concluded.

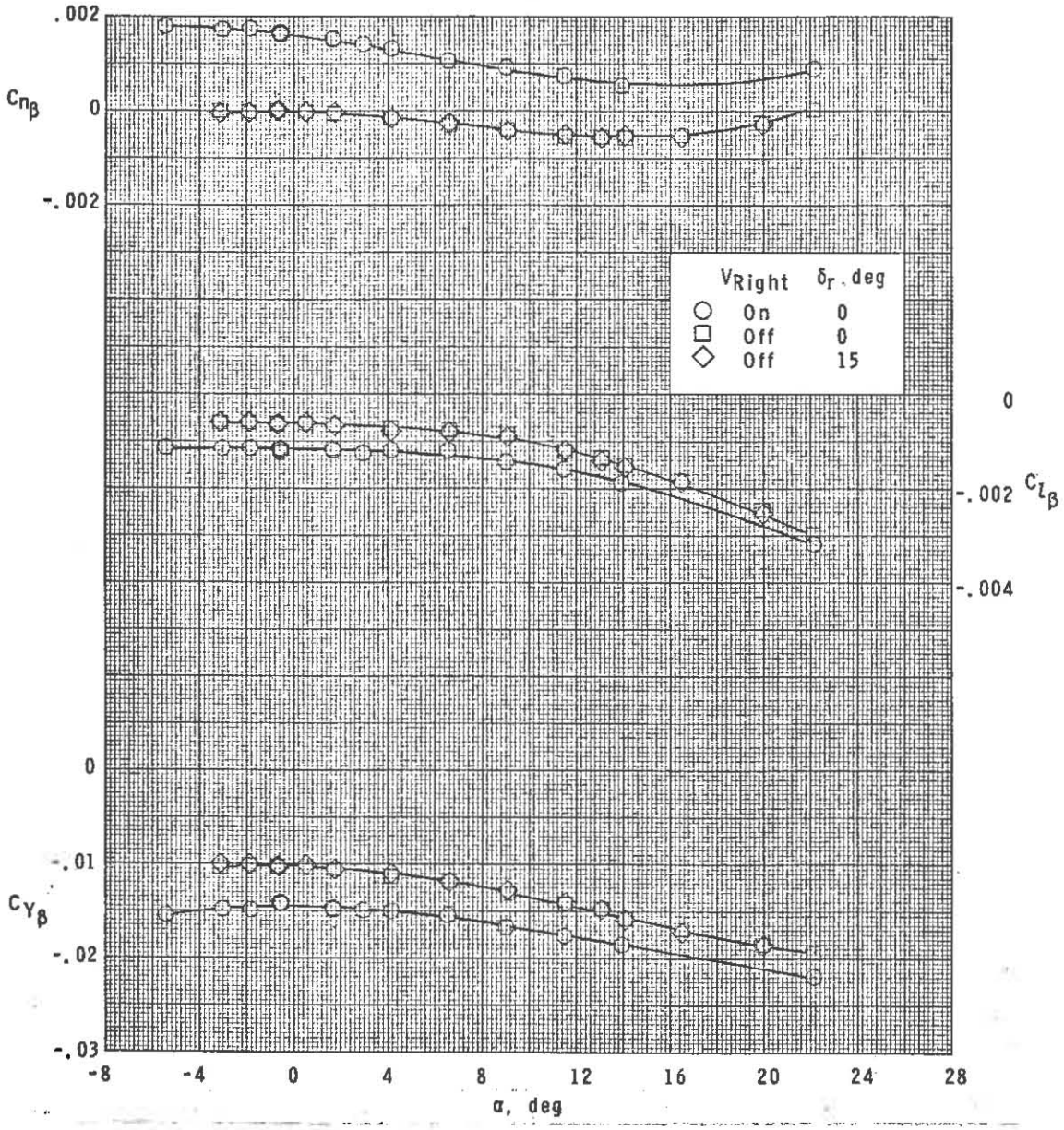

(a) M = 2.50.

Figure 25.- Sideslip parameters for asymmetric vertical-tail condition.

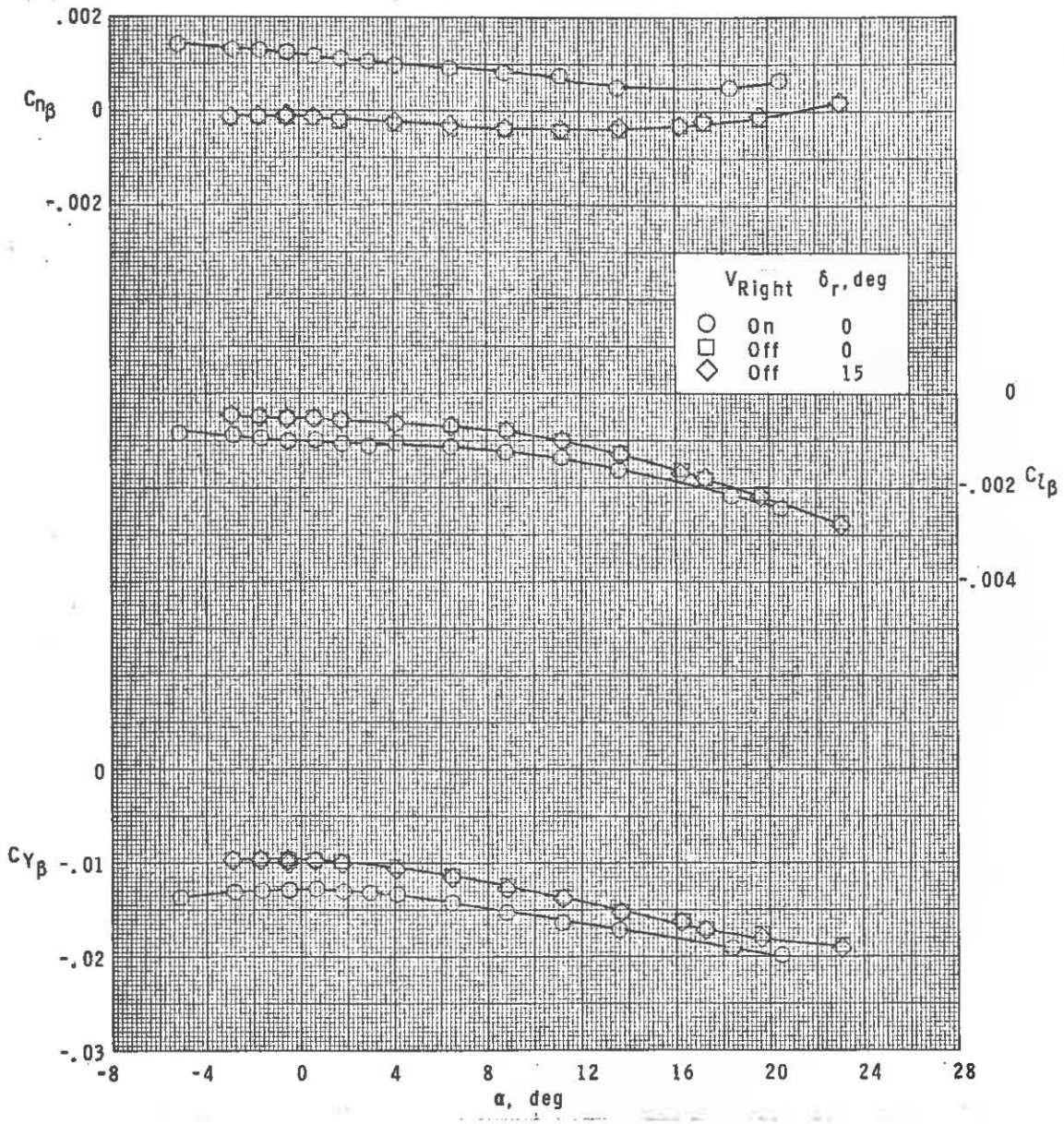

(b) M = 2.86.

Figure 25.- Continued.

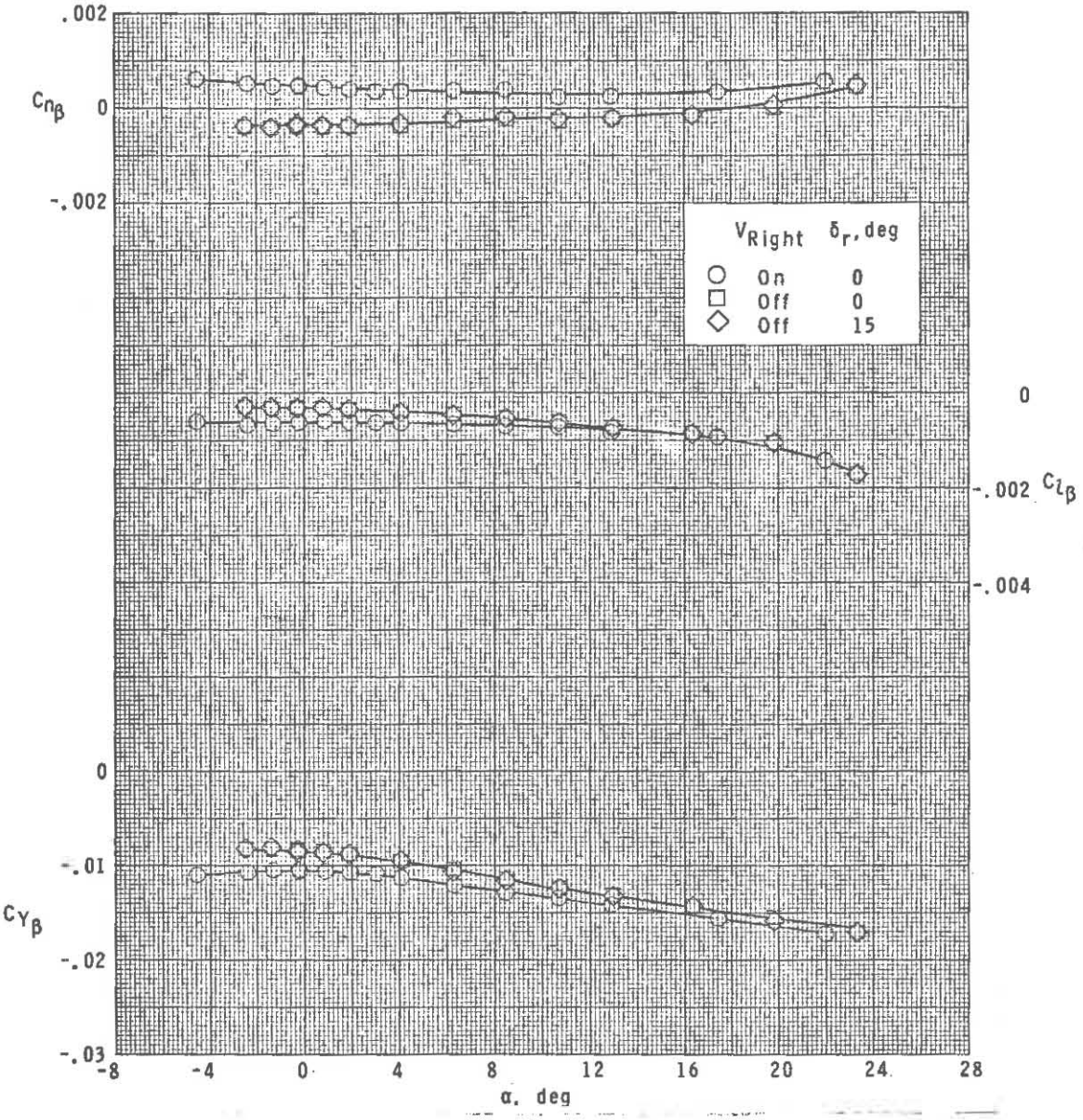

(c) M = 3.95.

Figure 25.- Continued.

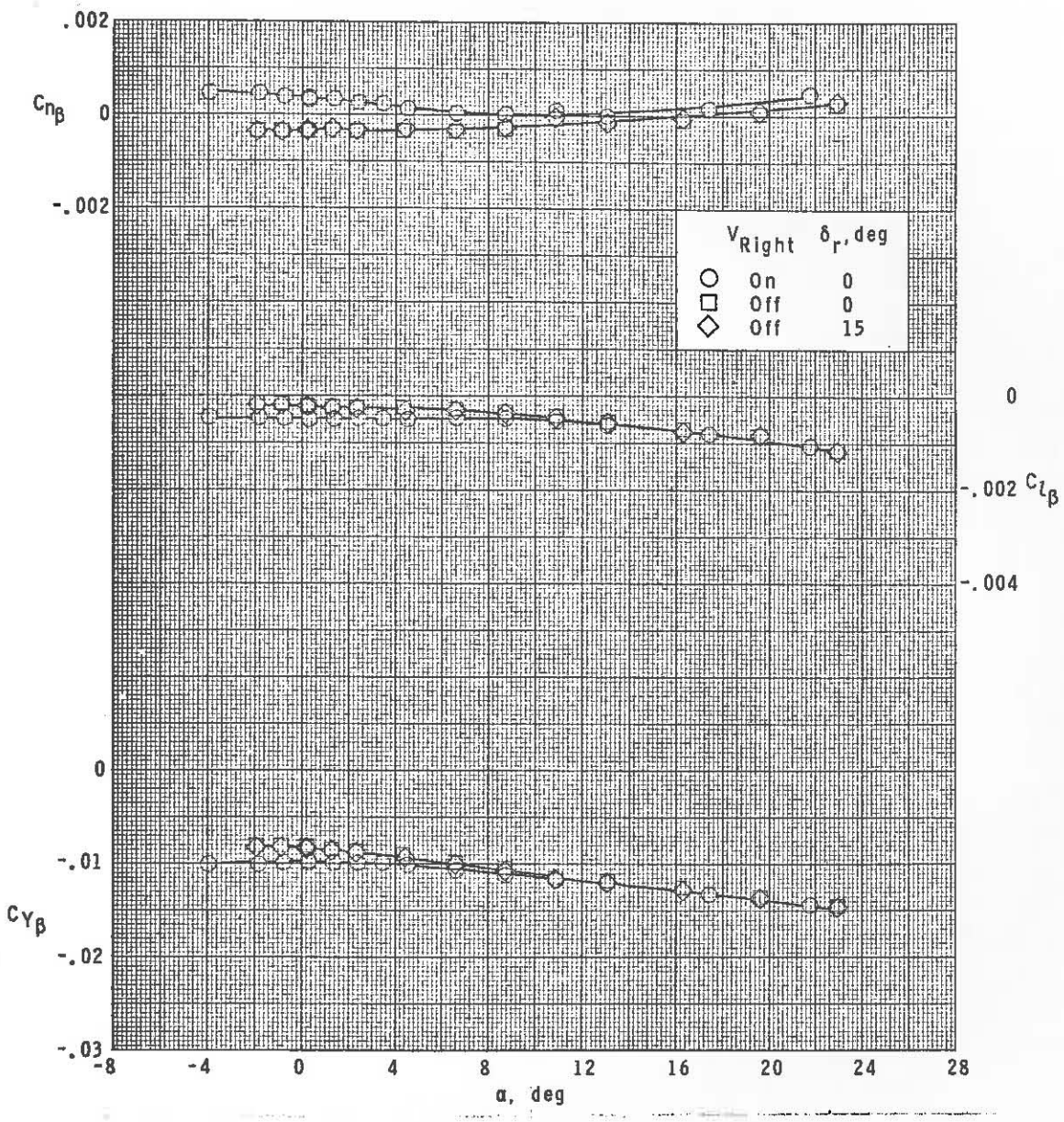

(d) M = 4.63.

Figure 25.- Concluded.